DISSERTATION

EVALUATION OF OSTEOGENIC DESIGN FACTORS IN ELECTROSPUN POLY(ε-CAPROLACTONE) NANOFIBER SCAFFOLDS

Submitted by

Timothy T. Ruckh

Graduate Degree Program in Bioengineering

In partial fulfillments of the requirements

For the degree of Doctor of Philosophy

Colorado State University

Fort Collins, Colorado

Fall 2010

COLORADO STATE UNIVERSITY

July 26, 2010

WE HEREBY RECOMMEND THAT THE DISSERTATION PREPARED UNDER OUR SUPERVISION BY TIMOTHY T. RUCKH ENTITLED “EVALUATION OF OSTEOGENIC DESIGN FACTORS IN ELECTROSPUN POLY(ε-CAPROLACTONE) NANOFIBER SCAFFOLDS” BE ACCEPTED AS FULFILLING IN PART REQUIREMENTS FOR THE DEGREE OF DOCTOR OF PHILOSOPHY.

Committee on Graduate Work

_____
Matt Kipper

_____
Susan James

_____
Stewart Ryan

_____
Advisor: Ketul Popat

_____
Director: Stuart Tobet

ABSTRACT OF DISSERTATION

EVALUATION OF OSTEOGENIC DESIGN FACTORS IN ELECTROSPUN POLY(ε-CAPROLACTONE) NANOFIBER SCAFFOLDS

Biodegradable bone tissue scaffolds have the potential to impact patients with numerous ailments. Starting with fabrication techniques that produce nano-scale features, the ability to manipulate architecture, alter surface chemistry, and deliver biological molecules allows for the design of elegant and highly effective bone scaffolds. This work aimed to develop a porous, nanofiber scaffold with osteogenic design features the capability to deliver an antibiotic molecule from within the nanofibers. Two osteogenic design factors with unique mechanisms of action were selected; hydroxyapatite nanoparticles and oleic acid. Hydroxyapatite (HAp) is the primary inorganic phase of natural bone tissue and has been used to more closely mimic the extracellular environment of synthetic bone tissue scaffolds. Oleic acid (OLA) is an ω-9 fatty acid with suspected osteogenic effects due to activation of peroxisome proliferator-activator receptors (PPARs). In separate *in vitro* evaluations, OLA significantly increased osteoblast phenotypic behaviors and led to differential expression of the three PPAR isoforms, suggesting that the OLA is activating its anticipated receptor. HAp

produced mixed results by inducing a small increase in alkaline phosphatase activity, but decreasing expression levels of bone matrix proteins. An *in vivo* evaluation of biocompatibility revealed that neither design factor increased the inflammatory response over control nanofiber scaffolds in paravertebral muscle pouches. However, both factors separately increased new osteoid production. Scaffolds with both HAp and OLA elicited the greatest osteogenic response *in vivo*, suggesting positive synergy between the two design factors. Finally, rifampicin (RIF), an antibiotic molecule was loaded into the nanofibers, and its release into static bacterial culture was effective in inhibiting bacterial population growth for both a Gram-positive and Gram-negative bacterial strain, separately. Overall, these nanofiber scaffolds were demonstrated to be effective carriers of soluble (OLA, RIF) and insoluble signals (HAp) which can modulate cell behaviors. Future work will aim to incorporate additional osteogenic features into the scaffolds and to develop multiple antibiotic release mechanisms from the nanofibers.

Timothy T. Ruckh
Graduate Degree Program in Bioengineering
Colorado State University
Fort Collins, CO 80523
Fall 2010

Acknowledgements

I would like to first thank my committee who each played a significant role in this research. Dr. Ketul Popat, my primary advisor, allowed me to formulate and conduct my research in an independent manner while providing insight and resources for the research. Dr. Matt Kapper and Dr. Susan James each played a large role in my decision to pursue a PhD in tissue engineering and they were of particular help during the troubleshooting process for electrospinning. Dr. Stuart Ryan provided much-needed clinical insight and expertise for the *in vivo* study, and also for choosing a relevant system for evaluating small-molecule release from the nanofiber scaffolds.

I also wish to acknowledge my lab mates and collaborators. Josh Porter instructed me as I was learning basic cell culture and assay techniques. Kuldeep Kumar and Derek Carroll both worked extensively on nanofiber fabrication and without their capable work I would not have been able to complete the amount of cell research as is included in this work. Our collaborators at University of Washington, Dr. Rachael Oldinski, Krissy Mirinova, and their advisor, Dr. James Bryers, contributed substantially to the bacterial culture experiments.

Finally, I would like to thank my parents, family, and close friends who have encouraged and supported me throughout the last five years.

Table of Contents

Chapter 1

1.1 Introduction

Tissue engineering is a broad field in which the principles of biology and engineering are applied in combination to develop a replacement for damaged tissue [1]. Bone tissue engineering has drawn a great deal of interest among academic and industrial researchers, in part because it represents a puzzling challenge. Bone itself is a prolific tissue and its remodeling is closely associated with a highly prolific cell source – bone marrow [2]. Despite this innate regenerative capacity, there remain several important shortcomings that clinical treatments for major orthopaedic trauma and *osteogenesis imperfecta* must overcome [3, 4]. Fundamental to solving these problems is the recognition that bone tissue functionality is highly dependent on nano-, micro-, and macro-structural tissue organization [5]. Thus, a stable fracture site and/or bone-implant interface is necessary. Complications associated with a range of diseases and injuries continue to impose their financial and lifestyle burdens on patients and health-care providers.

Several commercial and pre-clinical products have showed some degree of success for enhancing osteogenesis at implantation sites, but none of these have displaced the need for bone grafts or metallic implants in large defects [3]. Currently, the best clinical treatments for large defects are autografted or allografted bone segments. Autografted bone offers a non-immunogenic, biologically-active construct at the expense of tissue at a donor site, and thus availability and donor site pain limit this source's feasibility [6]. Allografted bone tissue is far more abundant than autografted bone, but immunogenicity and sterility are major concerns, and sterilization procedures such as irradiation or freeze-drying may alter mechanical and biochemical integrity [7, 8]. Synthetic tissue scaffolds offer an attractive option for both availability and sterility, but these are still considered an inferior clinical choice to both allografts and autografts because of inferior integration and necrosis related to stress shielding [4, 6, 9]. Thus,

synthetic tissue scaffold design strategies over the last decade and more have aimed at making substantial progress in mimicking various features of natural tissue in order to enhance osseointegration [10, 11].

As synthetic scaffolds have been developed for bone tissue engineering, techniques for *ex vivo* osteoprogenitor cell isolation and manipulation have also been developed [4, 9]. It is likely that the clinical implementation of synthetic scaffolds will integrate some of these *ex vivo* cell techniques in conjunction with scaffold design features [5]. This project focuses on the latter portion – scaffold design – as a means to attain enhanced bone tissue formation and study the efficacy of controlled molecule release for a subset of potential scaffold recipients.

1.1.1 Bone Tissue Engineering

Progress towards highly-engineered osteogenic scaffolds has been made on several tracts including scaffold architecture [12-14], growth factor incorporation [15-17], and scaffold chemical composition [18, 19]. In therapeutic applications, such a scaffold could grow an osteoprogenitor cell colony and form new bone matrix *ex vivo*, and then, ideally, be delivered as an autograft to the same patient [20]. These osteogenic scaffolds would benefit patients undergoing joint replacement [21, 22], tumor resection and endoprosthetic implantation [21, 23], maxillofacial repair [24], and skeletal tissue healing [25, 26]. An ideal synthetic bone scaffold should support osteoblast phenotypic behaviors, in particular, bone matrix deposition [27], while degrading at a rate that allows for osseointegration into the native tissue [26].

Any scaffold offered as a potential solution to this design problem requires a close examination of many factors regarding the biological response to the scaffold. One of the challenges in orthopedic tissue engineering is growing and maintaining a

viable, physiologically capable colony of cells on three-dimensional biocompatible scaffolds for delivery to patients in need of tissue replacement or regeneration. It has already been established that synthetic extracellular matrices containing a healthy population of osteoprogenitor cells will substantially increase osseous tissue formation in bone defects [5, 28, 29]. Therefore a great deal of effort has been put forth in the field of biomaterials and tissue engineering to develop scaffolds or interfaces that accelerate or improve the colonization of marrow stromal cells (MSCs) [30].

Once cell colonization is established, the scaffold must support differentiation into osteoblasts and neo-mineralization by stem cells within the marrow stromal population [31]. In order to accomplish these objectives, many current synthetic bone scaffold designs exhibit substantial porosity [27, 32-34], leading to a high surface-area-to-volume ratio and enhanced cellular adhesion, and sometimes contain additional osteogenic characteristics such as hydroxyapatite or other calcium phosphate [35-38]. Generally, investigations into the *in vitro* behavior of cells on those scaffolds examine alkaline phosphatase (ALP) activity, bone nodule formation, and cell morphology [34-36, 38]. Additional measures of osteoblast activity include the expression of genes for bone matrix proteins such as osteocalcin and/or osteopontin genes by polymerase chain reaction (PCR), or detection of those proteins by western blotting or enzyme-linked immunosorbent assay (ELISA) [32, 39]. These bone matrix proteins add detail to an analysis because they are definitive markers of the organic phase of bone matrix production rather than mineralization [40-42].

Examining levels of phenotypic expression indicate the capacity for the scaffold to support osteoblast behaviors *in vitro*, but they don't necessarily give an indication of the specific influences that a scaffold characteristic may be exerting on the cell population. For example, cellular infiltration and colonization is of concern for the

development of a 3-D scaffold so that new tissue develops through the full thickness of a scaffold [43]. Thus, scaffold porosity and pore size are two design parameters that would likely influence the cellular response. Furthermore, cellular functions for many cell phenotypes within the marrow stromal population, including mesenchymal stem cells, osteoblasts, and immune cells [2, 44, 45], are regulated in part by cytoskeletal development and organization, which depends on cell-cell and cell-substrate adhesions [46, 47]. The degree to which cells are in intimate contact with each other may depend on the ability of cells to find each other in a vast 3D scaffold if the cell population can easily infiltrate the scaffold. Thus, examining cellular infiltration, cell adhesion proteins, and cytoskeletal arrangement may be important to understanding the biological effects of scaffold design parameters.

1.1.2 Bone formation

A general understanding of the cellular events associated with new bone formation is vital to designing osteogenic scaffolds even though the exact mechanism of collagen mineralization are still unclear [42]. Within the context of nano-scaled tissue scaffolds, it is important to differentiate between the physiologic processes by which cells work in concert with each other, and the physico-chemical processes by which cells release bone matrix vesicles and these vesicle aggregate into bone nodules. The former results in the designation of whole-bone formation pathways, usually either endochondral ossification or intramembranous ossification [40]. Design of nano-scale tissue scaffolds allows for the manipulation of nano-scale processes in bone formation such as enhancing cellular adhesion [12]. However, given the complexity of both heterogeneous and homogeneous bone nucleation, relatively simple alterations to the scaffold may result in greatly potentiated bone formation.

The key difference between homogeneous and heterogeneous nucleation is whether or not there is a supersaturated calcium environments within bone matrix vesicles. Homogeneous bone formation occurs within bone matrix vesicles where the fluid within the vesicle is supersaturated with calcium [40]. Some inner leaflet phospholipids, most notably phosphatidylserine, contain functional groups, such as serine, with very high affinities for calcium [48, 49]. Heterogeneous nucleation occurs at sub-saturation concentrations when the surface-ion interaction lowers the interfacial surface energy [40]. Heterogeneous nucleation requires surface topography – collagen provides this *in vivo* – as well as non-collagenous proteins (NCPs) such as osteocalcin which have affinity for calcium [39, 50, 51]. Although the precise nature of each interaction between proteins, lipids, ions, and cells, during bone formation remains unclear, the details that are understood should be taken into account when designing an osteogenic scaffold.

1.1.3 Cell culture considerations

With the aim of designing a bone tissue scaffold for therapeutic applications, it is important to understand the differences between *in vivo* and *in vitro* conditions and how those differences might affect the process of evaluating a scaffold. For example, many previous *in vitro* investigations on nano-structured scaffold materials have used genetically engineered cell phenotypes [13, 14, 32, 43, 52]. However the cellular response may be a less accurate predictor or the *in vivo* response because of the homogenous experimental population. A more physiologically accurate approach would be to use primary marrow stromal cells to study the cellular response to a synthetic tissue scaffold.

The benefits of using a heterogeneous cell population center on capturing the interaction between cells of different lineages and with different purposes, particularly cells of mesenchymal and hematopoietic lineages [44, 45]. Mesenchymal stem cells possess the capability to differentiate into multiple cell phenotypes including osteoblasts [12, 47]. Hematopoietic stem cells are also able to differentiate into multiple cell phenotypes, but many of their phenotypic capabilities are unique to those of mesenchymal lineage, particularly immune phenotypes such as monocytes, macrophages, and osteoclasts. By using the whole marrow stromal cell population for *in vitro* studies, several stem cell phenotypes, as well as a vast range of more mature phenotypes, are able to interact to produce a more accurate representation of *in vivo* conditions [2]. Still, the best *in vitro* conditions are unlikely to match *in vivo* conditions for reasons ranging from mechanical stimulation to the ability to recruit cells from the general cell population.

"Living scaffolds" or synthetic matrices containing MSC extracts have demonstrated accelerated and enhanced bone formation within osseous defects when compared with an unpopulated matrix [28, 29]. The marrow stromal population contains a heterogeneous, pluripotent population of cells capable of differentiating along multiple mesenchymal lineages (e.g., bone [53, 54], ligament [55-57], adipose [57, 58], and muscle tissue [59]) and hematopoietic lineages [2]. Tissue culture techniques enable the isolation and *ex vivo* culture of the entire marrow stromal cell population from various sources [60], allowing these cells to serve as a model osteogenic cell source for evaluating scaffold materials. Many previous studies that utilized marrow stromal extracts cultured and passaged the cell population before seeding them on a scaffold material [27, 57, 61, 62]. However, passaging cells may alter the cell response due to aging-related changes in telomere length [63] and limit a cell's ability to differentiate into

some phenotypes [57]. Additionally, there is some evidence that chromosomal instability associated with extensive passaging may trend a mesenchymal stem cell population towards malignancy [64]. For these reasons, a direct culture of bone marrow stromal cells provides a better *in vitro* representation of a synthetic scaffold's potential to support cellular activity.

1.1.4 Architectural design considerations

The size scale of synthetic tissue scaffolds is an important scaffold design feature, and the existing literature offers a great deal of support for synthetic tissue scaffolds with micro- and/or nano-scale features based on greater cellular adhesion and phenotypic activity than untextured scaffolds [65-69]. This may be a consequence of mimicking highly-featured native tissue architecture exhibited in many natural tissues such as bone (**Figure 1.1**) [70]. In fact, nano-featured scaffolds have been shown to influence phenotypic behavior of several cell types, including neural, liver and fibroblastic cell types [32, 33, 43, 71].

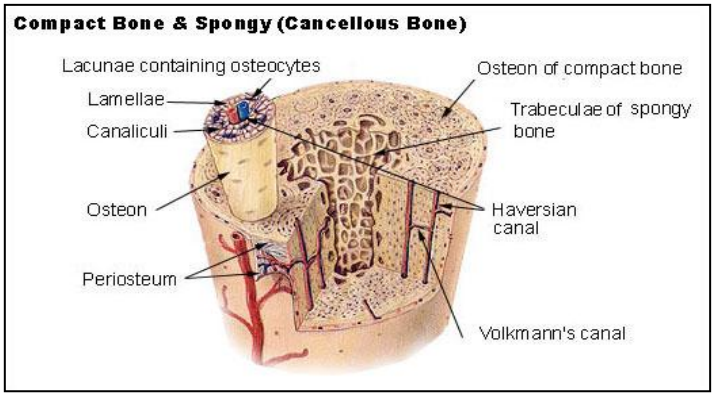

Figure 1.1 - Structure of a long-bone (National Cancer Institute)

While processes such as peptide self-assembly can produce fibers with diameters down to 10 nm, which approach that of a collagen fibril [72], other processes can produce fibers up to several microns in diameter [73-75]. Some studies have attempted to optimize fiber diameters for synthetic scaffold, but differences in the material chemistry yielded different results. For example, one study with PEOT/PBT found that a fiber diameter of 10 μm with nanopores within

the fibers was optimal for MSC adhesion and proliferation [76], while another study worked with PLGA and found decreasing cellular responses with fiber diameters below 800 nm [13], and a third study using carbon nanofibers found that some cell phenotypes such as smooth muscle cells were insensitive to fiber diameter while others such as chondrocytes have a strong dependence [77]. Perhaps the most important point is that architecture is a key design consideration for tissue scaffolds and it should be considered in parallel with scaffold chemistry and the phenotype(s) of concern.

1.1.5 Electrospinning

Electrospinning is a well-established manufacturing technique, first performed in the early 1900's for use in textiles [78]. It had been largely abandoned for years, but has seen a reemergence in popularity due, in part, to its simple and inexpensive setup [78-80]. Most publications have the same basic components to their electrospinning apparatus: a high-voltage source (up to 50kV), a syringe and syringe pump, a fine needle (18-26 gauge), and a collector (Figure 1.2) [78-82]. Additional modifications such as spinning mandrels [81] or charged collectors [83] allow for fiber alignment and patterning.

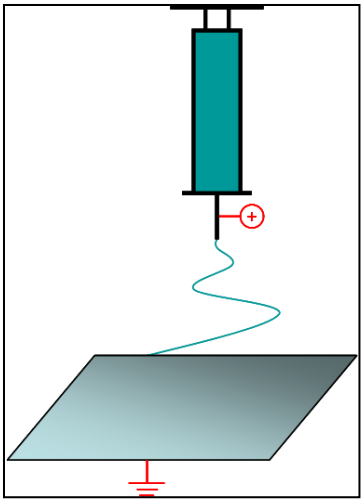

Figure 1.2 - Schematic drawing of a basic electrospinning apparatus

Electrospinning has become very popular within the tissue engineering community because it can consistently produce polymeric fibers with diameters ranging from less than 100 nanometers up to several microns [84]. Under high potential, a Taylor cone of polymer

Figure 1.3 - Illustration of a Taylor cone at the end of a catheter

solution forms at the catheter tip (Figure 1.3). Once the electrostatic forces overcome the viscosity and surface tension, a polymer jet is ejected and it travels from the catheter to a grounded collector positioned nearby (4-10 cm) with a trajectory that converges with the electric potential field lines. As the jet travels, the polymer solvent evaporates, leading to the deposition of very fine fibers on the grounded collector [75, 80, 84].

The fiber properties depend on the processing conditions as well as the nature of the polymer(s) and solvent(s). Ramakrishna *et al* (2005) describe 13 parameters which have influence the morphology of the fibers, although that is not an exhaustive description. An investigation focusing on the electrical input parameters (voltage and current) and the charge density of the solution demonstrated nonlinear behavior for each of the isolated parameters [75]. Each of these parameters contributes to observable properties such as elastic modulus, tensile strength, crystallinity, fiber diameter, fiber length, and fiber alignment [78, 81, 83]. With so many variables and interactions between variables, and the difficulty of precise control over parameters such as ambient temperature and humidity, electrospun fibers are subject to variability in some of the aforementioned characteristics. Fortunately, some parameters (input voltage, needle diameter, tip-to-collector distance, and feed rate) are easily and precisely adjustable. Adjustments to these parameters facilitate spinning for extended periods of time with reasonably consistent results for the fiber morphology and diameter (Figure 1.4).

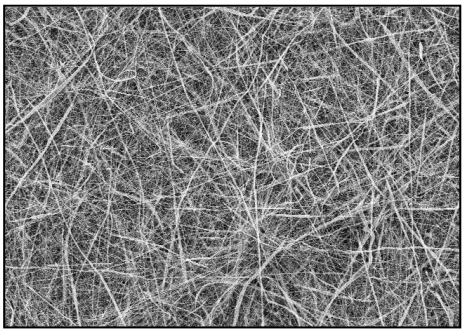

Figure 1.4 - Fibers spun without microspheres (magnification = 190x)

Since orthopaedic tissues have a micro to nano-hierarchical structure that is built up from the nanoscale [70], it is desirable to fabricate scaffolds that mimic natural tissue features. This can be done by adjusting spinning conditions; in particular by changing polymer

concentration or adding charged molecules in the spinning solution. It has been demonstrated that adding benzyl trialkylammonium chlorides (BTCs), a class of organo-soluble salts, to the spinning solutions resulted in more consistent fiber diameters [85]. However, BTCs are likely to have cytotoxic effects in cell cultures. These concerns could be addressed by adding naturally occurring, charge-carrying molecules such as fatty acid salts. Further, by changing only a few spinning parameters, notably polymer concentration, fiber diameter can be predictably increased or decreased [13, 86].

1.1.6 Synthetic tissue scaffolds in regenerative medicine

There exists a large body of support in the literature that tissue scaffolds having micro- and/or nano-scale features induce greater cellular adhesion and activity than untextured scaffolds [66, 67, 87]. Polymeric nanofibers have already been used as scaffolds for *in vitro* cultures of several distinct cell families such as orthopaedic [52], neural [71, 88, 89], and hepatic [90]. Nanofibers are attractive to tissue engineers because of the control over such parameters as the porosity of a 3D scaffold, the fiber diameter (surface-area-to-volume ratio), the choice of degradation rate, and the incorporation of bio-molecules for specific cell phenotype activity or antibiotic/antimicrobial characteristics.

Controlled release or triggered delivery of therapeutic compounds is currently a highly-active research area. There are too many approaches to summarize completely, but some of the more common strategies include encapsulation in liposomes and lipid micelles [91, 92], polymer micro- and nano-spheres or fibers [93-95], and conjugated molecules [96-98]. Drug-loaded polymers have the attractive feature of being applicable in processes, such as electrospinning, that are relatively robust, scalable, and inexpensive. Additionally, water-soluble molecules often exhibit a “burst release” effect

when encapsulated in liposomes and micelles, which can be avoided by encapsulating such a drug in polymers [94]. Designing electrospun nanofibers for drug delivery is very similar to designing nanofibers for tissue engineering. The key difference is that the polymer solution properties will change due to the added molecule. This is logical since fiber diameter and scaffold morphology are influenced by charge-carrying additives that may increase or decrease the stability of the electrospinning process [93]. This is important to keep in mind for the aforementioned cellular response as well as the changes to the release rate and duration [99, 100].

The dual-importance of fiber diameter to both the release profile and cell proliferation illustrates a technological intersection often referred to as regenerative medicine. Regenerative medicine has been described as the result of combined efforts to restore, maintain, and enhance normal cell or tissue function through combined technologies from material science, biology, and engineering [68, 101-103]. The specific mechanisms of action would strongly depend on the application for which a device is designed. For example, a "smart biomaterial" for cancer treatment might release one or more anti-cancer drugs conjugated with targeting molecules that is designed to maintain a biologically relevant time and concentration level. After the drug(s) have been completely released, the remaining biomaterial contains architecture and chemistry that promotes tissue regeneration and a return to normal cell and tissue function. Such a material does not yet exist, but a search through the current literature yields thousands of publications on developing the constitutive technologies [33, 48, 94, 104-107].

1.1.7 Poly(ε-caprolactone) as a tissue scaffold

Electrospinning can produce micro- and nano-scale fibers for any polymer that can be dissolved into a sufficiently viscous solution. As a result, the choice of polymers

for an electrospun tissue scaffold is fairly vast. Among the most common synthetic polymers used as nanofibrous tissue scaffolds are poly(lactic acid) (PLA), poly(glycolic acid) (PGA), poly(caprolactone) (PCL), and poly(ethylene glycol) (PEG) [74]. PCL is a semi-crystalline, biocompatible, aliphatic polyester [108] that has attracted increasing interest in the tissue engineering community over the past 10-15 years. It is biodegradable, with a relatively slow degradation rate [93], and readily-metabolized degradation products add to its appeal in biological applications [9, 109]. As a result, it is generally regarded as a good scaffold material for both hard and soft tissues [32, 88].

PCL degrades by hydrolysis of its ester bond. The degradation rate of a thick (>several cm) piece of PCL is on the order of years in the absence of enzymes [110]. Erosion resulting from bulk PCL hydrolysis degradation is generally regarded as surface erosion [111]. However, when the size of architectural features is decreased down to the nanoscale, degradation times for PCL *in vitro* is on the order of months rather than years, even when enzymes are excluded from the local environment. Part of the increased degradation rate may be taken as dependence on surface-area-to-volume ratio [86]. In this case of nano-featured scaffolds, erosion changes from surface to bulk erosion because water is able to move through the polymer faster than hydrolysis takes place [111].

For design cases when drug release is of concern, which is one of the appealing aspects of nano-structured degradable scaffolds [108, 112], controlled release can be predicted based on the degradation mechanisms [113, 114]. Several models have been developed that can predict the degradation behavior of a scaffold based on the polymer characteristics (molecular weight, hydrophobicity/hydrophilicity, degradation mechanisms) and scaffold morphology (fiber/sphere diameter, porosity) [100, 115, 116]. These models, particularly ones that take into account the semi-crystalline nature of

PCL, provide a means for accurately interpreting results from experimental degradation studies. PCL degradation can be divided into two stages; first a reduction in molecular weight down to ~5000 g/mol due to chain scission, followed by measurable weight loss in the second stage [108]. During the first stage, the amorphous regions preferentially undergo cleavage of the ester bond by hydrolysis, primarily because water can penetrate these regions with much greater ease than the crystalline regions [117]. Any loss of mass during this stage is unlikely to be within the limits of detection for gravimetric methods. However, as the average molecular weight of the polymer chains decreases, the shortened chains become increasingly mobile, which leads to the second stage with measurable weight loss [108]. Measured weight loss corresponds to the release of PCL chains, which are metabolized through the tricarboxylic acid cycle *in* vivo [9]. The presence of enzymes and lipases will increases the degradation rate in a concentration-dependent manner [109].

This measured weight loss, referred to as erosion, contributes to drug release by directly releasing the drug as the polymer carrier erodes as well as increasing the surface area in contact with the liquid medium into which the drug is diffusing. Thus, these release models are often referred to as diffusion-degradation-erosion [114]. Depending on the several factors including polymer crystallinity and fiber/particle size [118], the release profile may be manipulated to be linear/quasi-linear, “S” shaped, or hyperbolic [114]. In all three cases, information regarding the degradation behavior, crystallinity, and drug concentration within the polymer and liquid medium should be taken into account.

1.1.8 Antibiotic delivery

One of the complications associated with orthopaedic surgery operations is sepsis, also referred to as osteomyelitis when the infection is in bone tissue [119, 120]. Post-operative antibiotic regimens are appealing as prophylactic measures despite high sterility standards in operating rooms. This preventative measure is vital for patients undergoing surgery for highly infection-prone cases such as open fractures [121]. Antibiotic-resistant bacterial strains have reduced the numbers of effective antibiotics [120], and this has been highlighted by the much-publicized bacterial strains referred to as methacillin-resistant *staphylococcus aureus* (MRSA) [122]. The consequences of surgery-related sepsis include revision surgery, tissue debridement, and the long-term side effects of aggressive systemic antibiotic doses [123].

Some antibiotics are effective, but not effective when administered orally, such as gentamicin. Gentamicin is an aminoglycoside, a class of antibiotic drugs that do not absorb through the gut. Aminoglycosides are sometimes administered orally in order to clean out the gut from microbes, but otherwise it is administered directly to the area of interest (i.e a topical cream for skin infections) or intramuscularly/intravenously [124]. Aminoglycosides work through several mechanisms, most notably by irreversibly binding the 30s (or in a few cases the 50s) ribosomal subunit, thus arresting protein synthesis. Additionally, they also sequester ions from a biofilm, opening up cell membrane pores, which is an effective bactericidal action [125]. Other antibiotics such as rifampicin (RIF) are equally appealing for localized delivery simply to avoid systemic toxicity [126]. As an added benefit of localized delivery, multiple antibiotic release would be an effective strategy to address heterogeneous infection populations with differing resistances. For example, RIF inhibits prokaryotic RNA polymerases but has no effect on ribosomal protein translation [127-129]. By combining RIF with gentamicin, which blocks ribosomal protein translation, a microbe resistant to RIF would still be killed. It should be noted that

several substrates for localized antibiotic delivery have been developed, although only a few, such as antibiotic-loaded bone cements [130], have progressed to clinical use [131].

1.1.9 Aims of this study

This study aims to design a multifunctional bone tissue engineering scaffold that can be used to locally deliver an antibiotic agent while promoting new bone formation. The analysis will be divided into three stages:

1. Develop consistent nanofiber scaffold architecture using electrospinning and evaluate the osteogenic influence of the nanofibrous architecture
2. Incorporate and evaluate the efficacy of two osteogenic design factors – oleic acid and hydroxyapatite nanoparticles
3. Deliver a model antibiotic from the nanofibrous matrix and evaluate its bactericidal efficacy against Gram-positive and Gram-negative bacteria in static conditions.

1.2 References

1. Langer, R. and J.P. Vacanti, *Tissue engineering.* Science, 1993. **260**(5110): p. 920-6.
2. Compston, J.E., *Bone marrow and bone: a functional unit.* J Endocrinol, 2002. **173**(3): p. 387-94.
3. Drosse, I., et al., *Tissue engineering for bone defect healing: an update on a multi-component approach.* Injury, 2008. **39 Suppl 2**: p. S9-20.
4. Soucacos, P.N., E.O. Johnson, and G. Babis, *An update on recent advances in bone regeneration.* Injury, 2008. **39 Suppl 2**: p. S1-4.
5. Mistry, A.S. and A.G. Mikos, *Tissue engineering strategies for bone regeneration.* Adv Biochem Eng Biotechnol, 2005. **94**: p. 1-22.
6. Lewandrowski, K.-U., et al., *Bioresorbable bone graft substitutes of different osteoconductivities: a histologic evaluation of osteointegration of poly(propylene glycol-co-fumaric acid)-based cement implants in rats.* Biomaterials, 2000. **21**(8): p. 757-764.
7. Moreau, M.F., et al., *Gamma irradiation of human bone allografts alters medullary lipids and releases toxic compounds for osteoblast-like cells.* Biomaterials, 2000. **21**(4): p. 369-376.
8. Akkus, O. and C.M. Rimnac, *Fracture resistance of gamma radiation sterilized cortical bone allografts.* Journal of Orthopaedic Research, 2001. **19**(5): p. 927-934.
9. Salgado, A.J., O.P. Coutinho, and R.L. Reis, *Bone tissue engineering: state of the art and future trends.* Macromol Biosci, 2004. **4**(8): p. 743-65.
10. Alves, N.M., et al., *Designing biomaterials based on biomineralization of bone.* Journal of Materials Chemistry, 2010. **20**(15): p. 2911-2921.
11. Jang, J.-H., O. Castano, and H.-W. Kim, *Electrospun materials as potential platforms for bone tissue engineering.* Advanced Drug Delivery Reviews, 2009. **61**(12): p. 1065-1083.
12. Hosseinkhani, H., et al., *Osteogenic differentiation of mesenchymal stem cells in self-assembled peptide-amphiphile nanofibers.* Biomaterials, 2006. **27**(22): p. 4079-4086.
13. Bashur, C.A., L.A. Dahlgren, and A.S. Goldstein, *Effect of fiber diameter and orientation on fibroblast morphology and proliferation on electrospun poly(d,l-lactic-co-glycolic acid) meshes.* Biomaterials, 2006. **27**(33): p. 5681-5688.
14. Hu, J., X. Liu, and P.X. Ma, *Induction of osteoblast differentiation phenotype on poly(l-lactic acid) nanofibrous matrix.* Biomaterials, 2008. **29**(28): p. 3815-3821.
15. Basmanav, F., G.T. Kose, and V. Hasirci, *Sequential growth factor delivery from complexed microspheres for bone tissue engineering.* Biomaterials, 2008. **29**(31): p. 4195-204.
16. Karageorgiou, V., et al., *Porous silk fibroin 3-D scaffolds for delivery of bone morphogenetic protein-2 in vitro and in vivo.* J Biomed Mater Res A, 2006. **78**(2): p. 324-34.
17. Quaglia, F., et al., *Microspheres Made of Poly(e-caprolactone)-Based Amphiphilic Copolymers: Potential in Sustained Delivery of Proteins.* Macromolecular Bioscience, 2005. **5**(10): p. 945-954.

18. Muller, P., et al., *Calcium phosphate surfaces promote osteogenic differentiation of mesenchymal stem cells.* J Cell Mol Med, 2008. **12**(1): p. 281-91.
19. Kim, I.-Y., et al., *Chitosan and its derivatives for tissue engineering applications.* Biotechnology Advances, 2008. **26**(1): p. 1-21.
20. Shin, M., H. Yoshimoto, and J.P. Vacanti, *In vivo bone tissue engineering using mesenchymal stem cells on a novel electrospun nanofibrous scaffold.* Tissue Eng, 2004. **10**(1-2): p. 33-41.
21. Kurtz, S., et al., *Prevalence of Primary and Revision Total Hip and Knee Arthroplasty in the United States From 1990 Through 2002.* J Bone Joint Surg Am, 2005. **87**(7): p. 1487-1497.
22. Langer, R. and J.P. Vacanti, *Tissue Engineering.* Science, 1993. **260**(5110): p. 920-926.
23. Jeys, L.M., et al., *Endoprosthetic Reconstruction for the Treatment of Musculoskeletal Tumors of the Appendicular Skeleton and Pelvis.* J Bone Joint Surg Am, 2008. **90**(6): p. 1265-1271.
24. Schuckert, K.H., S. Jopp, and S.H. Teoh, *Mandibular Defect Reconstruction Using Three-Dimensional Polycaprolactone Scaffold in Combination with Platelet-Rich Plasma and Recombinant Human Bone Morphogenetic Protein-2: De Novo Synthesis of Bone in a Single Case.* Tissue Eng Part A, 2008.
25. Arthur, A., A. Zannettino, and S. Gronthos, *The therapeutic applications of multipotential mesenchymal/stromal stem cells in skeletal tissue repair.* Journal of Cellular Physiology, 2008. **9999**(9999): p. n/a.
26. Ishaug, S.L., et al., *Bone formation by three-dimensional stromal osteoblast culture in biodegradable polymer scaffolds.* Journal of Biomedical Materials Research Part A, 1997. **36**(1): p. 17-28.
27. Yoshimoto, H., et al., *A biodegradable nanofiber scaffold by electrospinning and its potential for bone tissue engineering.* Biomaterials, 2003. **24**(12): p. 2077-2082.
28. Tiedeman, J.J., et al., *The role of a composite, demineralized bone matrix and bone marrow in the treatment of osseous defects.* Orthopedics, 1995. **8**: p. 1153-1158.
29. Rougraff, B.T. and T.J. Kling, *Treatment of active unicameral bone cysts with percutaneous injection of demineralized bone matrix and autogenous bone marrow.* J Bone Joint Surg Am, 2002. **84-A**(6): p. 921-9.
30. Ban, S., et al., *Effect of electrochemically deposited apatite coating on bonding of bone to the HA-G-Ti composite and titanium.* Journal of Biomedical Materials Research Part A, 1997. **36**(1): p. 9-15.
31. Shin, H., S. Jo, and A.G. Mikos, *Biomimetic materials for tissue engineering.* Biomaterials, 2003. **24**(24): p. 4353-4364.
32. Wutticharoenmongkol, P., P. Pavasant, and P. Supaphol, *Osteoblastic Phenotype Expression of MC3T3-E1 Cultured on Electrospun Polycaprolactone Fiber Mats Filled with Hydroxyapatite Nanoparticles.* Biomacromolecules, 2007. **8**(8): p. 2602-2610.

33. Venugopal, J., et al., *Interaction of Cells and Nanofiber Scaffolds in Tissue Engineering.* Journal of Biomedical Materials Research Part B: Applied Biomaterials, 2008. **84B**(1): p. 34-48.
34. Guarino, V., et al., *Polylactic acid fibre-reinforced polycaprolactone scaffolds for bone tissue engineering.* Biomaterials, 2008. **29**(27): p. 3662-70.
35. Park, S.-H. and *e. al*, *Effect of hydroxyapatite-coated nanofibrous membrane on the responses of human periodontal ligament fibroblast.* Journal of the Ceramic Society of Japan, 2008. **116**(1349): p. 31-35.
36. Ramay, H.R. and M. Zhang, *Biphasic calcium phosphate nanocomposite porous scaffolds for load-bearing bone tissue engineering.* Biomaterials, 2004. **25**(21): p. 5171-80.
37. Zhang, P., et al., *In vivo mineralization and osteogenesis of nanocomposite scaffold of poly(lactide-co-glycolide) and hydroxyapatite surface-grafted with poly(l-lactide).* Biomaterials, 2008.
38. Kim, H.-W., H.-H. Lee, and J.C. Knowles, *Electrospinning biomedical nanocomposite fibers of hydroxyapaite/poly(lactic acid) for bone regeneration.* Journal of Biomedical Materials Research Part A, 2006. **79A**(3): p. 643-649.
39. Liu, F., L. Malaval, and J.E. Aubin, *Global amplification polymerase chain reaction reveals novel transitional stages during osteoprogenitor differentiation.* J Cell Sci, 2003. **116**(Pt 9): p. 1787-96.
40. Sikavitsas, V.I., J.S. Temenoff, and A.G. Mikos, *Biomaterials and bone mechanotransduction.* Biomaterials, 2001. **22**(19): p. 2581-93.
41. Gordon, J.A., et al., *Bone sialoprotein expression enhances osteoblast differentiation and matrix mineralization in vitro.* Bone, 2007. **41**(3): p. 462-73.
42. Baht, G.S., G.K. Hunter, and H.A. Goldberg, *Bone sialoprotein-collagen interaction promotes hydroxyapatite nucleation.* Matrix Biol, 2008. **27**(7): p. 600-8.
43. Nam, J. and *e. al*, *Improved cellular infiltration in electrospun fiber via engineered porosity.* Tissue Engineering, 2007. **13**(9): p. 2249-2257.
44. Lorenzo, J., M. Horowitz, and Y. Choi, *Osteoimmunology: interactions of the bone and immune system.* Endocr Rev, 2008. **29**(4): p. 403-40.
45. Takayanagi, H., *Osteoimmunology: shared mechanisms and crosstalk between the immune and bone systems.* Nat Rev Immunol, 2007. **7**(4): p. 292-304.
46. Ferrari, S.L., et al., *A role for N-cadherin in the development of the differentiated osteoblastic phenotype.* J Bone Miner Res, 2000. **15**(2): p. 198-208.
47. Kii, I., et al., *Cell-cell interaction mediated by cadherin-11 directly regulates the differentiation of mesenchymal cells into the cells of the osteo-lineage and the chondro-lineage.* J Bone Miner Res, 2004. **19**(11): p. 1840-9.
48. Wu, L.N., B.R. Genge, and R.E. Wuthier, *Analysis and molecular modeling of the formation, structure, and activity of the phosphatidylserine-calcium-phosphate complex associated with biomineralization.* J Biol Chem, 2008. **283**(7): p. 3827-38.

49. Genge, B.R., L.N. Wu, and R.E. Wuthier, *In vitro modeling of matrix vesicle nucleation: synergistic stimulation of mineral formation by annexin A5 and phosphatidylserine.* J Biol Chem, 2007. **282**(36): p. 26035-45.
50. Hunter, G.K. and H.A. Goldberg, *Nucleation of hydroxyapatite by bone sialoprotein.* Proc Natl Acad Sci U S A, 1993. **90**(18): p. 8562-5.
51. Taller, A., et al., *Specific adsorption of osteopontin and synthetic polypeptides to calcium oxalate monohydrate crystals.* Biophys J, 2007. **93**(5): p. 1768-77.
52. Chen, M. and *e. al*, *Role of Fiber Diameter in Adhesion and Proliferation of NIH 3T3 Fibroblast on Electrospun Polycaprolactone Scaffolds.* Tissue Engineering, 2007. **13**(3): p. 579-587.
53. Haynesworth, S., et al., *Characterization of cells with osteogenic potential from human marrow.* Bone, 1992. **13**: p. 81-88.
54. Prockop, D., *Marrow stromal cells as stem cells for nonhematopoietic tissues.* Science, 1997. **276**: p. 71-74.
55. Altman, G.H., et al., *Cell differentiation by mechanical stress.* Faseb J, 2002. **16**(2): p. 270-2.
56. Caplan, A., et al., *Mesenchymal stem cells and tissue repair. In: Jackson, D.W., ed. The Anterior Cruciate Ligament: Current and Future Concepts*. 1993, New York: Raven Press.
57. Wall, M.E., S.H. Bernacki, and E.G. Loboa, *Effects of serial passaging on the adipogenic and osteogenic differentiation potential of adipose-derived human mesenchymal stem cells.* Tissue Eng, 2007. **13**(6): p. 1291-8.
58. Beresford, J.N., et al., *Evidence for an inverse relationship between the differentiation of adipocytic and osteogenic cells in rat marrow stromal cell cultures.* J Cell Sci, 1992. **102 (Pt 2)**: p. 341-51.
59. Seshi, B., S. Kumar, and D. Sellers, *Human bone marrow stromal cell: coexpression of markers specific for multiple mesenchymal cell lineages.* Blood Cells Mol Dis, 2000. **26**(3): p. 234-46.
60. Bianco, P. and P. Gehron Robey, *Marrow stromal stem cells.* J Clin Invest, 2000. **105**(12): p. 1663-8.
61. Marletta, G., et al., *Improved osteogenic differentiation of human marrow stromal cells cultured on ion-induced chemically structured poly-[epsilon]-caprolactone.* Biomaterials, 2007. **28**(6): p. 1132-1140.
62. Li, W.-J., et al., *Multilineage differentiation of human mesenchymal stem cells in a three-dimensional nanofibrous scaffold.* Biomaterials, 2005. **26**(25): p. 5158-5166.
63. Holt, S.E., J.W. Shay, and W.E. Wright, *Refining the telomere-telomerase hypothesis of aging and cancer.* Nat Biotechnol, 1996. **14**(7): p. 836-9.
64. Miura, M., et al., *Accumulated chromosomal instability in murine bone marrow mesenchymal stem cells leads to malignant transformation.* Stem Cells, 2006. **24**(4): p. 1095-103.
65. Popat, K.C., et al., *Decreased Staphylococcus epidermis adhesion and increased osteoblast functionality on antibiotic-loaded titania nanotubes.* Biomaterials, 2007. **28**(32): p. 4880-4888.
66. Schwartz, Z. and B. Boyan, *Underlying Mechanisms at the Bone-Biomaterial Interface.* Journal of Cellular Biochemistry, 1994. **56**: p. 340-347.

67. Dee, K.C. and R. Bizios, *Mini Review: Proactive Biomaterials and Bone Tissue Engineering.* Biotechnology and Bioengineering, 1996. **50**: p. 438-442.
68. Engel, E., et al., *Nanotechnology in regenerative medicine: the materials side.* Trends in Biotechnology, 2008. **26**(1): p. 39-47.
69. Murugan, R. and S. Ramakrishna, *Design strategies of tissue engineering scaffolds with controlled fiber orientation.* Tissue Eng, 2007. **13**(8): p. 1845-66.
70. Wainwright, S., et al., *Mechanical Design in Organisms*. 2 ed. 1982: Princeton University Press.
71. Schnell, E., et al., *Guidance of glial cell migration and axonal growth on electrospun nanofibers of poly-e-caprolactone and a collagen/poly-e-caprolactone blend.* Biomaterials, 2007. **28**(19): p. 3012-3025.
72. Horii, A., et al., *Biological designer self-assembling Peptide nanofiber scaffolds significantly enhance osteoblast proliferation, differentiation and 3-D migration.* PLoS ONE, 2007. **2**(2): p. e190.
73. Dersch, R., et al., *Electrospinning of Nanofibres: Towards New Techniques, Functions, And Applications.* Australian Journal of Chemistry, 2007. **60**: p. 719-728.
74. Sill, T.J. and H.A. von Recum, *Electrospinning: Applications in drug delivery and tissue engineering.* Biomaterials, 2008. **In Press, Corrected Proof**.
75. Theron, S.A., E. Zussman, and A.L. Yarin, *Experimental investigation of the governing parameters in the electrospinning of polymer solutions.* Polymer, 2004. **45**(6): p. 2017-2030.
76. Moroni, L., et al., *Fiber diameter and texture of electrospun PEOT/PBT scaffolds influence human mesenchymal stem cell proliferation and morphology, and the release of incorporated compounds.* Biomaterials, 2006. **27**(28): p. 4911-4922.
77. Price, R.L., et al., *Selective bone cell adhesion on formulations containing carbon nanofibers.* Biomaterials, 2003. **24**(11): p. 1877-87.
78. Teo, W.E. and S. Ramakrishna, *A review on electrospinning design and nanofibre assemblies.* Nanotechnology, 2006. **17**: p. R89-R106.
79. Kim, G. and W. Kim, *Highly porous 3D nanofiber scaffold using an electrospinning technique.* Journal of Biomedical Materials Research Part B: Applied Biomaterials, 2007. **81B**(1): p. 104-110.
80. Rutledge, G.C. and S.V. Fridrikh, *Formation of fibers by electrospinning.* Advanced Drug Delivery Reviews, 2007. **59**(14): p. 1384-1391.
81. Thomas, V., et al., *Mechano-morphological studies of aligned nanofibrous scaffolds of polycaprolactone fabricated by electrospinning.* Journal of Biomaterials Science -- Polymer Edition, 2006. **17**(9): p. 969-984.
82. Chen, J.-P., G.-Y. Chang, and J.-K. Chen, *Electrospun collagen/chitosan nanofibrous membrane as wound dressing.* Colloids and Surfaces A, 2008. **313-314**: p. 183-188.
83. Zhang, D. and J. Chang, *Patterning of Electrospun Fibers Using Electroconductive Templates.* Advanced Materials, 2007. **19**(21): p. 3664-3667.

84. Ramakrishna, S., et al., *An Introduction to Electrospinning and Nanofibers*. 2005, Singapore: World Scientific Publishing Co. Pte. Ltd. 382.
85. Choi, J.S., et al., *Effect of organosoluble salts on the nanofibrous structure of electrospun poly(3-hydroxybutyrate-co-3-hydroxyvalerate).* International Journal of Biological Macromolecules, 2004. **34**(4): p. 249-256.
86. Bolgen, N., et al., *In vitro and in vivo degradation of non-woven materials made of poly(e-caprolactone) nanofibers prepared by electrospinning under different conditions.* Journal of Biomaterials Science -- Polymer Edition, 2005. **16**(12): p. 1537-1555.
87. Popat, K.C., et al., *Osteogenic differentiation of marrow stromal cells cultured on nanoporous alumina surfaces.* Journal of Biomedical Materials Research Part A, 2007. **80A**(4): p. 955-964.
88. Sangsanoh, P., et al., *In Vitro Biocompatibility of Schwann Cells on Surfaces of Biocompatible Polymeric Electrospun Fibrous and Solution-Cast Film Scaffolds.* Biomacromolecules, 2007. **8**(5): p. 1587-1594.
89. Corey, J.M. and *e. al*, *Aligned electrospun nanofibers specify the direction of dorsal root ganglia neurite growth.* Journal of Biomedical Materials Research Part A, 2007. **83a**(3): p. 636-645.
90. Chua, K.-N., et al., *Stable immobilization of rat hepatocyte spheroids on galactosylated nanofiber scaffold.* Biomaterials, 2005. **26**(15): p. 2537-2547.
91. Farokhzad, O.C. and R. Langer, *Impact of nanotechnology on drug delivery.* ACS Nano, 2009. **3**(1): p. 16-20.
92. Youan, B.B., *Impact of nanoscience and nanotechnology on controlled drug delivery.* Nanomed, 2008. **3**(4): p. 401-6.
93. Zeng, J., et al., *Biodegradable electrospun fibers for drug delivery.* Journal of Controlled Release, 2003. **92**(3): p. 227-231.
94. Xie, J., R.S. Tan, and C.-H. Wang, *Biodegradable microparticles and fiber fabrics for sustained delivery of cisplatin to treat C6 glioma in vitro.* Journal of Biomedical Materials Research Part A, 2008. **85A**(4): p. 897-908.
95. Fujiyama, J., et al., *Cisplatin incorporated in microspheres: development and fundamental studies for its clinical application.* Journal of Controlled Release, 2003. **89**: p. 397-408.
96. Farokhzad, O.C., J.M. Karp, and R. Langer, *Nanoparticle-aptamer bioconjugates for cancer targeting.* Expert Opin Drug Deliv, 2006. **3**(3): p. 311-24.
97. Sharman, W.M., J.E. van Lier, and C.M. Allen, *Targeted photodynamic therapy via receptor mediated delivery systems.* Adv Drug Deliv Rev, 2004. **56**(1): p. 53-76.
98. Luo, Y. and G.D. Prestwich, *Cancer-targeted polymeric drugs.* Curr Cancer Drug Targets, 2002. **2**(3): p. 209-26.
99. Arifin, D.Y., L.Y. Lee, and C.H. Wang, *Mathematical modeling and simulation of drug release from microspheres: Implications to drug delivery systems.* Adv Drug Deliv Rev, 2006. **58**(12-13): p. 1274-325.
100. Tzafriri, A.R., *Mathematical modeling of diffusion-mediated release from bulk degrading matrices.* J Control Release, 2000. **63**(1-2): p. 69-79.

101. Anderson, D.G., J.A. Burdick, and R. Langer, *Materials science. Smart biomaterials.* Science, 2004. **305**(5692): p. 1923-4.
102. Kopecek, J., *Smart and genetically engineered biomaterials and drug delivery systems.* Eur J Pharm Sci, 2003. **20**(1): p. 1-16.
103. Furth, M.E., A. Atala, and M.E. Van Dyke, *Smart biomaterials design for tissue engineering and regenerative medicine.* Biomaterials, 2007. **28**(34): p. 5068-73.
104. Whang, K., T.K. Goldstick, and K.E. Healy, *A biodegradable polymer scaffold for delivery of osteotropic factors.* Biomaterials, 2000. **21**(24): p. 2545-2551.
105. Ma, P.X., *Biomimetic materials for tissue engineering.* Advanced Drug Delivery Reviews, 2008. **60**(2): p. 184-198.
106. Bolgen, N. and *e. al*, *In vivo performance of antibiotic embedded electrospun PCL membranes for prevention of abdominal adhesions.* Journal of Biomedical Materials Research Part B: Applied Biomaterials, 2007. **81b**(2): p. 530-543.
107. Tauro, J.R. and R.A. Gemeinhart, *Matrix Metalloprotease Triggered Delivery of Cancer Chemotherapeutics from Hydrogel Matrixes.* Bioconjugate Chem., 2005. **16**(5): p. 1133-1139.
108. Sinha, V.R., et al., *Poly-e-caprolactone microspheres and nanospheres: an overview.* International Journal of Pharmaceutics, 2004. **278**(1): p. 1-23.
109. Pulkkinen, M., et al., *Effects of block length on the enzymatic degradation and erosion of oxazoline linked poly-ε-caprolactone.* European Journal of Pharmaceutical Sciences, 2007. **31**(2): p. 119-128.
110. Kulkarni, A., et al., *Enzymatic Chain Scission Kinetics of Poly(ε-caprolactone) Monolayers.* Langmuir, 2007. **23**(24): p. 12202-12207.
111. von Burkersroda, F., L. Schedl, and A. Gopferich, *Why degradable polymers undergo surface erosion or bulk erosion.* Biomaterials, 2002. **23**(21): p. 4221-31.
112. Biondi, M., et al., *Controlled drug delivery in tissue engineering.* Advanced Drug Delivery Reviews, 2008. **60**(2): p. 229-242.
113. Charlier, A., B. Leclerc, and G. Couarraze, *Release of mifepristone from biodegradable matrices: experimental and theoretical evaluations.* Int J Pharm, 2000. **200**(1): p. 115-20.
114. Berchane, N.S., et al., *Effect of mean diameter and polydispersity of PLG microspheres on drug release: experiment and theory.* Int J Pharm, 2007. **337**(1-2): p. 118-26.
115. Arifin, D.Y., L.Y. Lee, and C.-H. Wang, *Mathematical modeling and simulation of drug release from microspheres: Implications to drug delivery systems.* Advanced Drug Delivery Reviews, 2006. **58**(12-13): p. 1274-1325.
116. Higuchi, T., *Mechanism of Sustained-Action Medication.* Journal of Pharmaceutical Sciences, 1963. **52**(12): p. 1145-1149.
117. Coccoli, V., et al., *Engineering of poly(epsilon-caprolactone) microcarriers to modulate protein encapsulation capability and release kinetic.* J Mater Sci Mater Med, 2008. **19**(4): p. 1703-11.

118. Berkland, C., K. Kim, and D.W. Pack, *PLG microsphere size controls drug release rate through several competing factors.* Pharm Res, 2003. **20**(7): p. 1055-62.
119. Zilberman, M. and J.J. Elsner, *Antibiotic-eluting medical devices for various applications.* J Control Release, 2008. **130**(3): p. 202-15.
120. Coviello, V. and M.R. Stevens, *Contemporary concepts in the treatment of chronic osteomyelitis.* Oral Maxillofac Surg Clin North Am, 2007. **19**(4): p. 523-34, vi.
121. Schmidmaier, G., et al., *Prophylaxis and treatment of implant-related infections by antibiotic-coated implants: a review.* Injury, 2006. **37 Suppl 2**: p. S105-12.
122. Klevens, R.M., et al., *Invasive methicillin-resistant Staphylococcus aureus infections in the United States.* JAMA, 2007. **298**(15): p. 1763-71.
123. Lucke, M., et al., *Systemic versus local application of gentamicin in prophylaxis of implant-related osteomyelitis in a rat model.* Bone, 2005. **36**(5): p. 770-8.
124. Rohrbaugh, T.M., et al., *Absorption of oral aminoglycosides following bone marrow transplantation.* Cancer, 1984. **53**(7): p. 1502-6.
125. Shakil, S., et al., *Aminoglycosides versus bacteria – a description of the action, resistance mechanism, and nosocomial battleground.* J. Biomed. Sci., 2005. **15**: p. 5-14.
126. Saad, E.I., et al., *Role of oxidative stress and nitric oxide in the protective effects of alpha-lipoic acid and aminoguanidine against isoniazid-rifampicin-induced hepatotoxicity in rats.* Food Chem Toxicol, 2010.
127. Frippiat, F., F. Meunier, and G. Derue, *Place of newer quinolones and rifampicin in the treatment of Gram-positive bone and joint infections.* J Antimicrob Chemother, 2004. **54**(6): p. 1158; author reply 1159.
128. Pohlod, D.J., L.D. Saravolatz, and M.M. Somerville, *In-vitro susceptibility of gram-positive cocci to LY146032 teicoplanin, sodium fusidate, vancomycin, and rifampicin.* J Antimicrob Chemother, 1987. **20**(2): p. 197-202.
129. Tupin, A., et al., *Resistance to rifampicin: at the crossroads between ecological, genomic and medical concerns.* Int J Antimicrob Agents, 2010. **35**(6): p. 519-23.
130. Mont, M., B. Waldman, and D.S. Hungerford, *Evaluation of preoperative cultures before second-stage reimplantation of a total knee prosthesis complicated by infection: A comparison-group study.* Journal of Bone and Joint Surgery, 2000. **82**: p. 1552-1557.
131. Smith, A.W., *Biofilms and antibiotic therapy: is there a role for combating bacterial resistance by the use of novel drug delivery systems?* Adv Drug Deliv Rev, 2005. **57**(10): p. 1539-50.

Chapter 2

2.1 Chapter summary

This research section provided the basis for the research contained in chapters three and four. Previous investigations had examined *in vitro* and *in vivo* cytocompatibility for nanofiber scaffolds fabricated from a wide range of polymers, but none had performed a direct comparison of nanofiber scaffolds against smooth surfaces in osteogenic conditions. In order to demonstrate that nanofiber scaffolds would increase cell responses in maintenance and osteogenic conditions, nanofiber poly(ε-caprolactone) (PCL) scaffolds were fabricated by electrospinning along with smooth PCL discs. Marrow stromal cells (MSCs) were isolated from rats and cultured *in vitro* on either material to assess short-term cytocompatibility and long-term osteoblast phenotypic behaviors. The short-term cytocompatibility results indicated that nanofiber scaffolds supported greater cell adhesion and viability compared with smooth surfaces. In osteogenic conditions, MSCs cultured on nanofiber scaffolds also displayed increased levels of alkaline phosphatase activity for 3 weeks of culture. Calcium phosphate mineralization was substantially accelerated on nanofiber scaffolds compared to control surfaces as indicated through von Kossa and calcium staining, scanning electron microscopy and energy-dispersive X-ray spectroscopy. Increased levels of intra- and extracellular levels of osteocalcin and osteopontin were observed on nanofiber scaffolds using immunofluorescence techniques after 3 weeks of culture. This section demonstrated the enhanced tissue regeneration property of nanofiber scaffolds over smooth surfaces. Furthermore, research into chemical and biological design factors on nanofiber scaffolds should control or account for the effects of nanofibrous architecture.

2.2 Motivations and aims

Progress towards highly engineered osteogenic scaffolds was described in the introduction section. One of the challenges in orthopedic tissue engineering is growing

and maintaining a viable, physiologically capable colony of cells on three-dimensional biocompatible scaffolds for delivery to patients in need of tissue replacement or regeneration. It has already been established that the use of synthetic extracellular matrices containing a healthy population of osteoprogenitor cells will substantially increase osseous tissue formation in bone defects [5, 28, 29]. Therefore a great deal of effort has been made in the field of biomaterials and tissue engineering to develop scaffolds or interfaces that accelerate or improve the colonization of marrow stromal cells (MSCs) [30]. Existing literature offers a great deal of support for tissue scaffolds with micro- and/or nanoscale features because of greater cellular adhesion and phenotypic activity than non-textured scaffolds [65-69]. These improvements may a result of mimicking the highly featured native tissue architecture exhibited in many natural tissues.

‘‘Living scaffolds” or synthetic matrices containing bone MSC extracts have demonstrated accelerated and enhanced bone formation within osseous defects when compared with an unpopulated matrix [28, 29]. The marrow stromal population contains a heterogeneous, pluripotent population of cells capable of differentiating along multiple mesenchymal lineages (e.g. bone [53, 132], ligament [55, 57, 133], adipose [57, 58] and muscle tissue [59]) as well as along immune and hematopoietic cell lineages [2]. Tissue culture techniques enable the isolation and ex vivo culture of the entire marrow stromal cell population from various sources [134], allowing these cells to serve as a model osteogenic cell source for evaluating scaffold properties.

Previous studies that utilized MSCs, cultured and passaged these cells before seeding them on a scaffold material [57, 61, 62, 135]. However, passaging cells may alter the cell response due to aging-related changes in telomere length [63] and limit a

cell's ability to differentiate into some phenotypes [57]. Furthermore, passaged cell populations do not represent the cellular diversity

of the bone marrow stromal population because of the elimination of non-adherent cells. Osteo-immuno cross-talk may play an important role in how osteoprogenitor cells and immature osteoblasts behave on the scaffold [2, 44, 45, 136]. For these reasons, a direct culture of bone MSCs would provide a better in vitro representation of a synthetic scaffold's potential to support cellular activity.

In this chapter, poly(ε-caprolactone) (PCL) nanofiber scaffolds were evaluated against control surfaces for their support of osteogenic differentiation of MSCs. PCL scaffolds were fabricated by electrospinning to produce nanofiber architecture, and these scaffolds were characterized in terms of their architectural feature size. Then cell responses to the scaffolds and control surfaces were measured in maintenance and osteogenic conditions separately.

2.3. Materials and methods

This section provides the details for experimental methods used in each section. It includes the conditions and procedures for manufacturing nanofiber scaffolds, harvesting bone marrow stromal cells from rats, sterilizing scaffolds and seeding cells onto the scaffolds, and analyzing the cell responses to the scaffolds.

2.3.1. PCL nanofiber scaffold fabrication

PCL nanofiber scaffolds were fabricated using an electrospinning technique. The electrospinning apparatus consisted of a syringe pump (Harvard Apparatus), a glass syringe (Hamilton, model 1010), Teflon fluidic tubing (Hamilton, model 86510), a 20-gauge blunt-tip catheter (Hamilton, model 7746-04), and a male luer lock adapter

(Hamilton, model 86511). A high-voltage power source (Gamma High Voltage Research, model ES30P-10W/DAM) was

connected to the catheter tip with a standard alligator clamp. The collector consisted of an aluminum foil fastened onto a 0.5 in. thick copper plate (McMaster Carr, Robbinsville, NJ) with electrical tape and positioned horizontally below the catheter.

Polymer solution was prepared by dissolving oleic acid sodium salt (OLA) (Sigma) in methanol. PCL pellets (Mw = 80,000, Sigma) were dissolved in chloroform and the polymer solution was mixed with OLA in methanol on a magnetic stir plate to produce a homogeneous mixture with a 4:1 chloroform:methanol volume ratio. The final solution was 12% solid w/w and the PCL:OLA ratio of the solid weight was 97:3. The volumetric flow rate was 2.8 ml/h, applied voltage 21 kV and tip-to-collector distance 10 cm. Scaffolds were sputter-coated with 10 nm of gold and imaged under a scanning electron microscope to evaluate the nanofiber architecture. Fiber diameters were computed using the image analysis system built into the scanning electron microscope. Smooth PCL (control) surfaces were fabricated by sintering PCL pellets (Mw = 80,000, Sigma) on a glass plate in a 10 mm Teflon washer. The resulting discs were then allowed to air-cool before being removed from the glass surface.

2.3.2. Isolation of bone marrow stromal cells

MSCs were isolated from male Wistar rats (Rattus norvegicus) supplied by Harlan Sprague Dawley, Inc. (separate time points, unmixed cell populations). The animal protocol was approved by the Colorado State University Animal Care and Use Committee. This Committee is in compliance with the NIH Guide for Care and Use of Laboratory Animals. Limbs were aseptically removed from recently killed animals, and soft tissue was removed from the bones. Metaphyseal ends of the bones were removed

to expose the bone marrow cavity. In a 50 ml conical tube, marrow was repeatedly flushed with culture medium (α-Minimum Essential Medium (α-MEM) with 10% fetal bovine serum (FBS, Sigma) and 1% penicillin/streptomycin (pen/strep, Sigma)) using 10 ml syringes with 18 and 25 gauge needles. Media containing cells and debris was filtered with a 70 μm nylon filter into a clean tube, and the cells were counted using a hemocytometer before seeding. Control (smooth PCL) and nanofiber scaffold (both discs with area 0.7 cm^2) were sterilized by exposing them to UV light for 60 min followed by soaking in 70% ethanol for 60 min. The substrates were then washed twice with warm PBS followed by warm culture media prior to MSC seeding. Cells were seeded on scaffolds in a 24-well plate at a density of 1 million cells per well. Cultures were incubated at 37 ^oC under 5% CO_2 for the duration of the study. Half of the media was changed at day 4. On day seven, the media was replaced with osteogenic differentiation media (α-MEM with 10% FBS, 1% pen/strep, 10^{-8} M dexamethasone, 50 μg/ml ascorbic acid, 8 mM β-glycerolphosphate). All test and control surfaces were cultured and assayed in triplicate at each time point specified (i.e. one, two or three weeks post-differentiation). Media was changed every two days for up to three weeks. MSC response was investigated in two phases:

(a) Cell adhesion, proliferation and viability up to seven days of initial culture (short-term). This time point is in conjunction with the time required for adherent progenitor cells in the bone marrow to adhere and proliferate on the scaffold surface.

(b) Cell osteogenic differentiation and matrix production for up to three weeks after differentiation media was supplied (long-term). This time point is far enough into the

differentiation phase to see significant changes in the expression of bone marker proteins as well as mineralization on the scaffold surfaces.

2.3.3. Short-term MSC response on nanofiber scaffolds

After one, four, and seven days of culture, cell responses to the scaffolds were investigated through cell adhesion, viability (metabolic activity) and morphology. Live cell adhesion was investigated using calcein AM (Invitrogen) (excitation 485 nm, emission 530 nm). Calcein AM can penetrate live cell membranes, where the AM is cleaved and the resulting calcein molecule fluoresces green. The cells were incubated in 2 μM of calcein AM in PBS for 45 min and then imaged with a fluorescence microscope (Zeiss) with appropriate filters. Images were analyzed (ImageJ, NIH) to compute the per cent area covered by live cells for comparison with the cell viability assay.

Cell viability was measured after 1 and 4 days of culture (log-phase growth) using a commercially available MTT assay kit (Sigma). Adhered cells were incubated at 37 ^{o}C for 3 h in a 3-[4,5-dimethylthiazol-2-yl]-2,5-diphenyl tetrazolium bromide (MTT) solution. Mitochondrial dehydrogenases of viable cells cleave the tetrazolium ring, yielding purple formazan crystals. Formazan crystals were then dissolved in the MTT solvent with 10 vol.% Triton-X. The optical density (OD) of the solvent is proportional to the mitochondrial activity of the cells on the surface. OD was measured at 570 nm using a spectrophotometer (FLUOstar Omega, BMGLabtech, Durham, NC). Background absorbance at 690 nm was subtracted from the measured absorbance.

Cell morphology on control surfaces and nanofiber scaffolds was evaluated after 1, 2 and 7 days of culture using field emission scanning electron microscopy (SEM, JEOL JSM-6500F). The scaffolds were gently removed from the culture media and immersed in PBS for 5 min to remove un-adhered cells and proteins. The cells were then fixed in a

fixing solution (3% glutaraldehyde with 0.1 M sucrose and 0.1 M sodium cacodylate in deionized water) for 45 min, rinsed in a buffer solution (fixing solution without glutaraldehyde) and then dehydrated in increasing concentrations of ethanol (30%, 50%, 70%, 90% and 100%) for 10 min each. After dehydration, the scaffolds were immersed in hexamethyldisilazane for 10 min and were air-dried. The scaffolds were stored in a desiccator until further characterization. They were then sputter-coated with 10 nm of gold and imaged by SEM. Particular attention was paid to the shape of adhered cells, the location of cells on the scaffold and any characteristics of filopodia adhesions to scaffold features.

2.3.4. Long-term MSC response on nanofiber scaffolds

MSC responses to the nanofiber scaffolds were investigated 1, 2 and 3 weeks after providing the cells with osteogenic differentiation media. Alkaline phosphatase (ALP) activity, calcium and phosphate deposition, and extracellular matrix (ECM) protein production were used to assess the osteoconductivity of the nanofiber scaffolds. Nanofiber and control scaffolds were removed from the culture media and rinsed twice in PBS prior to analysis.

To determine the ALP activity, the adhered cells were lysed with Cell Lytic™ solution (Sigma) for 1 h. A commercially available ALP colorimetric assay kit (Quantichrome™, BioAssay Systems) was used to quantify ALP concentration in the lysate. Briefly, ALP catalyzes the reaction of *p*-nitrophenolphosphate to *p*-nitrophenol and phosphate. *p*-Nitrophenol was measured using a plate reader (yellow, 405 nm) at 1 and 4 min in order to determine the concentration of ALP in the lysate. ALP was calculated using the guidelines provided by the manufacturer. Further, the total protein content of the lysate was measured using a commercially available BCA assay and the absorbance of the

solution was measured using a plate reader at a wavelength of 570 nm. The absorbance was then converted to protein content using an albumin standard curve to determine the amount of intracellular protein. All the ALP data was normalized with total protein content to account for changes in number of cells present on each surface.

In order to stain the scaffolds for phosphate, they were rinsed twice with cacodylate buffer and then immersed in 4% paraformaldehyde (w/v) in cacodylate buffer for 10 min. They were then rinsed with deionized water and a solution of silver nitrate in deionized water was then added for 20 min, allowing the phosphate and silver nitrate to react to form a brown precipitate. The reaction was spontaneously stopped by rinsing three times with deionized water. Scaffolds were dried in a desiccator and digital images of stained surfaces were captured using a Canon PowerShot SD1000.

In order to stain the scaffolds for calcium, they were rinsed twice in cold (4 ^{o}C) Ringer's solution. They were then immersed in cold 4% paraformaldehyde (w/v) in PBS solution for 10 min, rinsed in cold deionized water, and submerged in cold Alizarin red solution (2 wt%) in sodium hydroxide for 10 min. The scaffolds were rinsed three times with cold deionized water and allowed to dry in a desiccator. Calcium forms a complex with Alizarin red S via a chelation process and the end-product is birefringent. Digital images of stained surfaces were captured using a Canon PowerShot SD1000.

Cell morphology was investigated using SEM as described earlier. Samples prepared for SEM were also examined for surface elemental composition using an energy-dispersive X-ray spectroscopy (EDS) probe (Thermo Electron, Noran System) attached to the JEOL JSM-6500F electron microscope. EDS was used to detect mineralization (calcium and phosphorus) on the samples. Instrument aperture and probe current were adjusted to give a dead time of 15–20%. Surfaces were analyzed for 5 min at 5–15 kV and a magnification of 100–5000x to provide a complete profile of the

different elements present. Spatial element mapping was performed by grouping pixels with similar atomic spectra.

After 3 weeks in osteogenic media, scaffolds were removed and immunolabeled for osteopontin (OC) and osteocalcin (OP). Cells were fixed by immersing in 3.7% paraformaldehyde (w/v) in PBS for 10 min followed by permeabilization in a 1% Triton-X in PBS solution for 10 min. A blocking serum with 40 μg/mL trypan blue (Sigma) and 100 μg/mL bovine serum albumin in PBS was used to prevent non-specific antibody binding. After rinsing the scaffolds with PBS, they were incubated in either osteopontin primary antibody (1:100 in PBS, V-19 purified goat polyclonal antibody of human origin, Santa Cruz Biotechnology) or osteocalcin primary antibody (1:100 in PBS, P-18 purified goat polyclonal antibody of mouse origin, Santa Cruz Biotechnology) for 1 h. After an additional blocking step and PBS wash, samples were then incubated in FITC-conjugated secondary antibodies for osteocalcin and osteopontin (1:200 donkey antigoat IgG, Santa Cruz Biotechnology) for 45 min. Samples were rinsed once more before imaging with 470 nm excitation wavelength using a fluorescence microscope (Zeiss).

2.3.5. Statistical analysis

All scaffolds were cultured and assayed in triplicate at each time point specified. All the studies were conducted in triplicate using different animals as the MSC source for each study. The data was pooled from the studies using different cell sources (n = 6). All the statistics presented here as a mean ± standard deviation. A two-tailed, unpaired t-test was performed to determine the statistical significance, defined as a p-value less than 0.05.

2.4. Results

2.4.1. Fabrication of nanofiber scaffolds

In this study, nanofiber scaffolds were fabricated using electrospinning to be bead-free, and characterized using SEM in terms of their mean fiber diameters (**Figure 2.1(a–c)**). Fiber diameters for the scaffolds used in this study were consistent, with a mean fiber diameter of 372 nm and standard deviation of 179 nm (**Figure 2.1(c)**). Approximately 90% of fiber diameters were between 200 and 500 nm, although occasional extreme outliers were observed up to nearly 2 μm and were included in the statistical analysis (n_{min} = 12).

2.4.2. Short-term MSC response on nanofiber scaffolds

The ability of nanofiber scaffolds to support MSC adhesion and proliferation was evaluated using live cell fluorescence staining and MTT assay. Cells were stained with the live cell stain calcein AM. Figure 2.2 shows fluorescence microscopy images of live cells on control and nanofiber scaffolds.

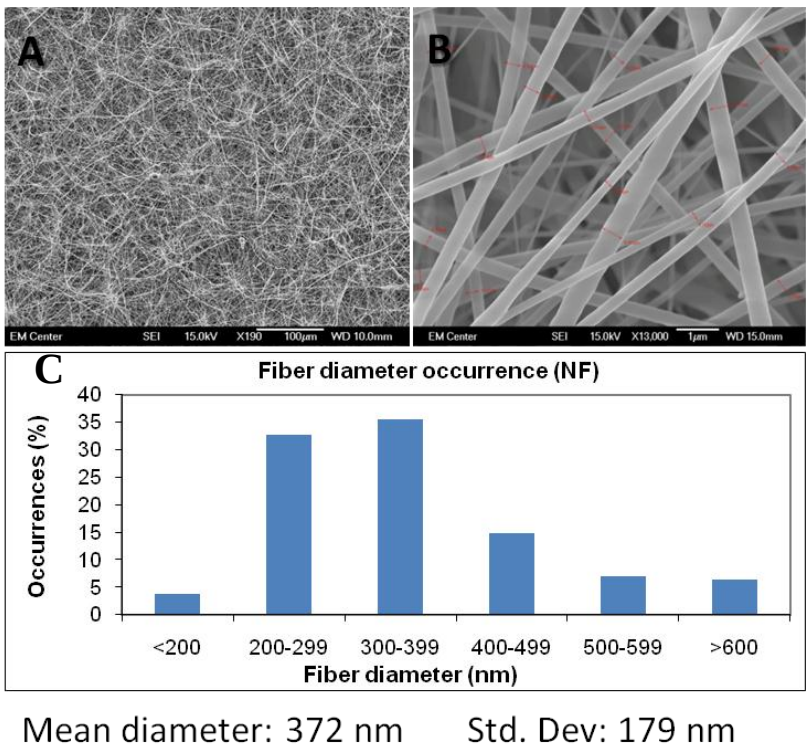

Figure 2.1 – SEM images of nanofiber scaffolds at 150x (A) and 13,000x (B) magnification. Fiber diameter histogram with mean and standard deviation are also presented

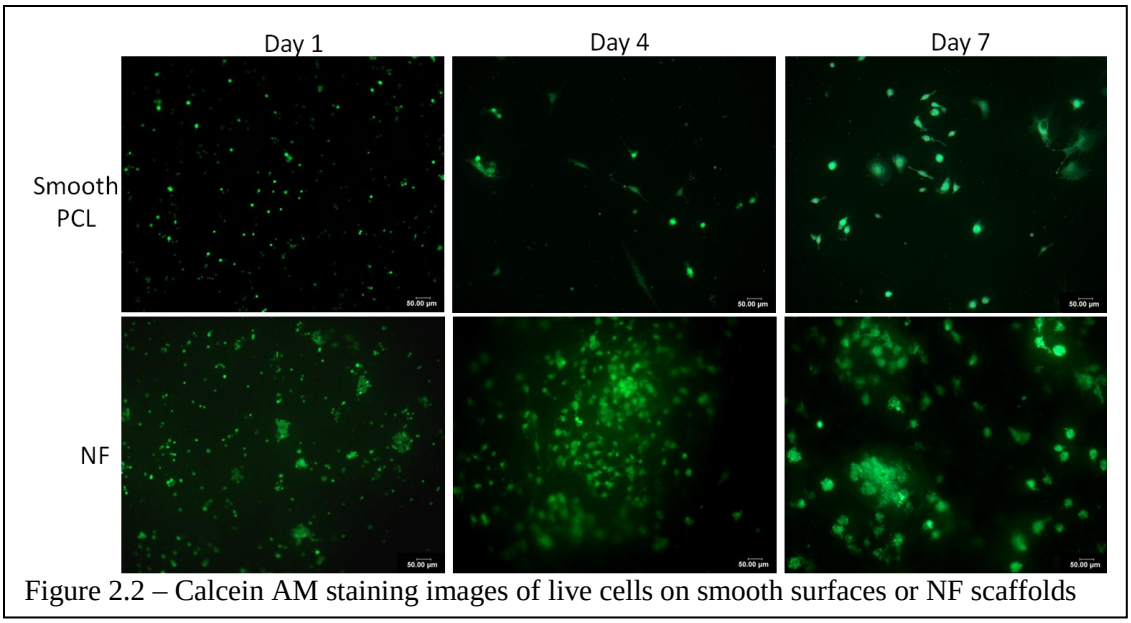

Figure 2.2 – Calcein AM staining images of live cells on smooth surfaces or NF scaffolds

ImageJ software was used to calculate the cell coverage on control and nanofiber scaffolds (**Figure 2.3(a)**).

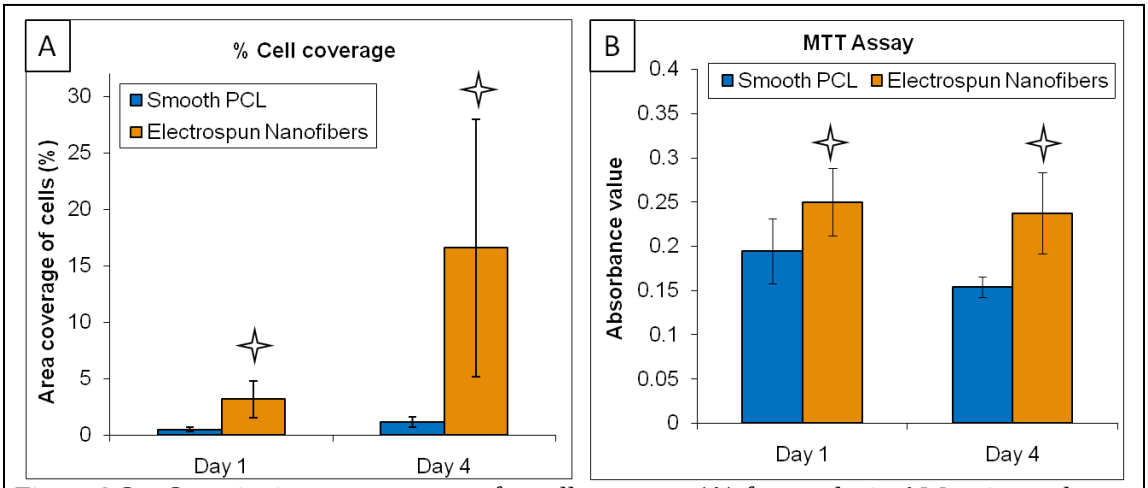

Figure 2.3 – Quantitative measurements for cell coverage (A) from calcein AM stains and metabolic activity (B) measured by MTT assay

Cell viability was investigated using a commercially available MTT assay. The measurements were taken after 1 and 4 days of culture since this time period is associated with the log-phase growth of the cell population. Our results suggested that MSCs are viable on both nanofiber scaffolds and control surfaces for up to 4 days in culture (**Figure 2.3(b)**). Further, the cell viability on nanofiber scaffolds was significantly

greater than control surfaces at both time points. To visualize morphological changes in MSCs, SEM images were taken after 1, 4 and 7 days of culture (**Figure 2.4**). SEM analysis supported the fluorescence microscopy results that the MSCs preferentially adhere, spread and colonize on nanofiber scaffold as compared to control surfaces.

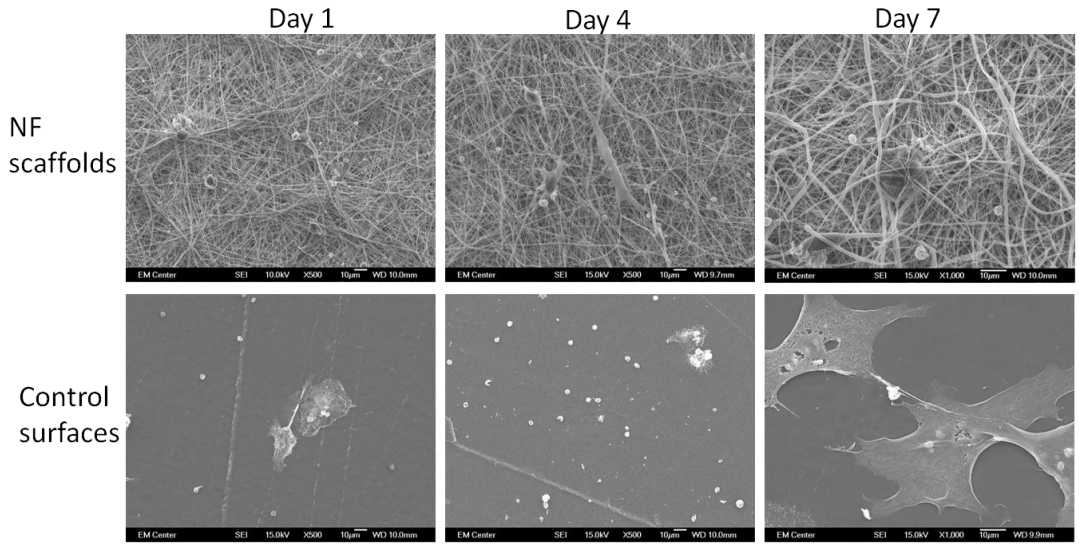

Figure 2.4 – SEM images of cells on NF scaffolds or smooth control surfaces at 1, 4, or 7 days post-seeding

2.4.3. Long-term MSC response on nanofiber scaffolds

The ability of nanofiber scaffolds to support osteogenic differentiation was evaluated using biochemical assays and immunofluorescence imaging for bone matrix proteins. ALP cleaves organic phosphate esters and is a key component of bone matrix vesicles. The ALP patterns observed over the 3 week experimental period (4 week total culture time) for nanofiber scaffolds demonstrated elevated ALP levels after 3 weeks of

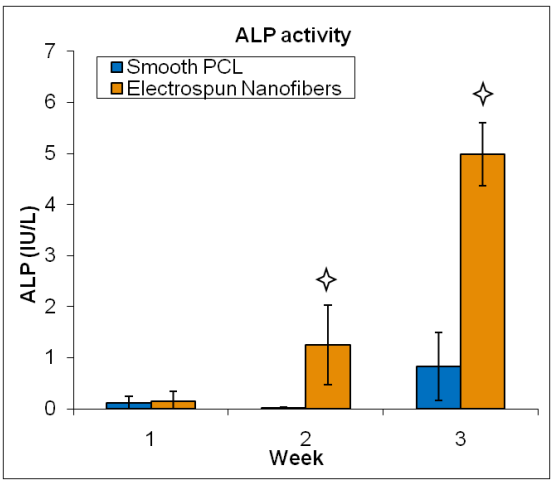

Figure 2.5 – Intracellular ALP measured by colorimetric assay. Star denotes statistically significant ($p \leq 0.05$) difference within a time point

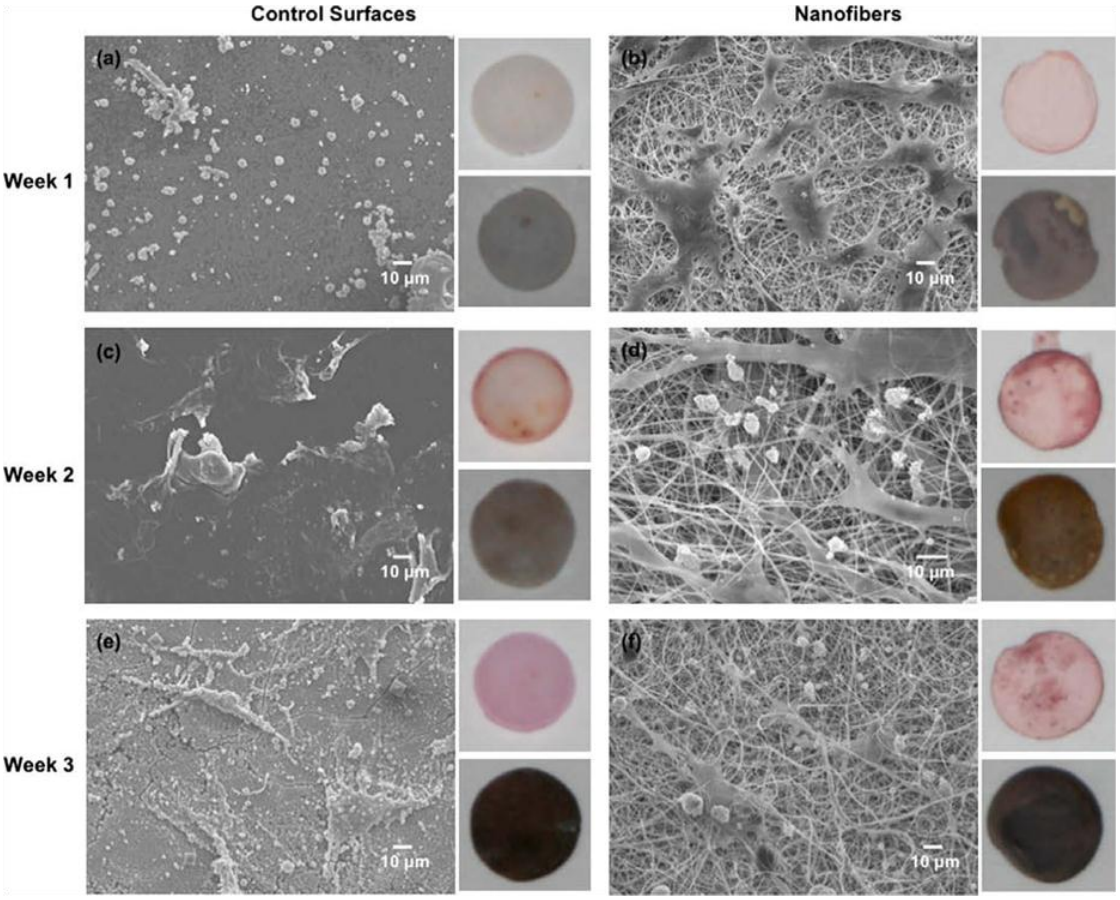

Figure 2.6 – SEM images of smooth control surfaces (a, c, e) and nanofiber scaffolds (b, d, f) after 1, 2, and 3 weeks in osteogenic media. Alizarin calcium staining (red) and von Kossa phosphate staining (brown) digital images also pictured

culture compared to the control surfaces (**Figure 2.5**) [87, 137, 138]. Mineralization patterns were examined qualitatively by SEM/EDS, Alizarin calcium staining and von Kossa staining. Figure 1.6 shows digital images of the stained surfaces (calcium (red) on top; phosphate (brown) stain on bottom) along with SEM images after 3 weeks of culture on both nanofiber scaffolds and control surfaces. SEM images and staining results indicated that cells seeded on nanofiber scaffolds display accelerated mineralization compared to control (smooth) surfaces. EDS scans (**Figure 2.7**) also showed greater calcium and phosphorous peaks for mineral deposits on nanofiber scaffolds than on control surfaces, indicative of greater amounts of both elements. An EDS mapping tool grouped pixels with similar atomic spectra, thus confirming that the observed mineral

deposits were Ca–P. OP and OC were imaged using immunofluorescent staining after 3 weeks in osteogenic medium. Immunofluorescent staining for OP and OC revealed different deposition patterns between the nanofiber scaffolds and control surfaces. Greater amounts of both bone matrix proteins were evident on the nanofiber scaffolds, with many rough-shaped (mineral deposits) and cell-shaped objects visible (**Figure 2.8 (c and d)**) compared to that on control surfaces (**Figure 2.8 (a and b)**). One particularly interesting finding from the nanofiber scaffolds was that both stains were observed within the scaffold because of strong backlighting of nanofiber features, strongly suggesting that osteoblasts had migrated to the scaffold interior and were actively producing organic bone matrix components (**Figure 2.8 (e and f)**).

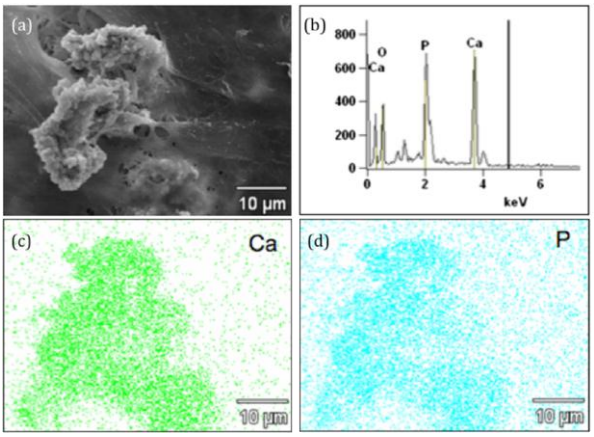

Figure 2.7 – Combined SEM (a) and EDX spectrum (b) with atomic imaging (c & d)

2.5. Discussion

Nanofiber scaffolds fabricated by electrospinning have been shown to be excellent tissue scaffolds for several unique cell phenotypes [32, 71, 88, 139]. In this study, nanofiber scaffolds were fabricated to be bead-free and were characterized using SEM in terms of their mean fiber diameters (**Figure 2.1 (a–c)**). Fiber diameter has been shown to influence the cellular response to multiple nanofiber materials in a manner that is co-dependent on the fiber material [76, 139-141].

Fiber diameters for the scaffolds used in this study were consistent, with a mean fiber diameter of 372 nm and standard deviation of 179 nm (**Figure 2.1(c)**).

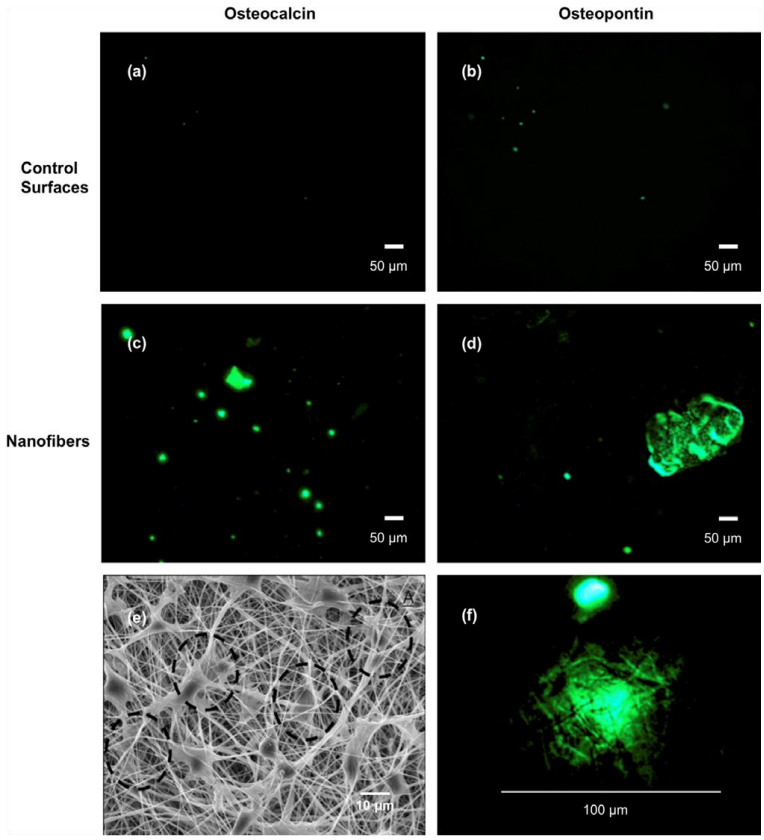

Figure 2.8 – Immunofluorescent images (a-d, f) and SEM image (e) after 3 weeks in osteogenic media. Magnification for a-d is 10x, scale bar is 50 µm. Magnification for f is 40x, scale bar is 100 µm.

Approximately 90% of fiber diameters were between 200 and 500 nm, although occasional extreme outliers were observed up to nearly 2 µm and were included in the statistical analysis. In order to increase the fiber diameter consistency, OLA was included at 3% of the total solid weight, which stabilized the process by adding charge to the solution [85]. The result was fibers with an estimated standard deviation of approximately half the mean fiber diameter. Additionally, nearly all SEM images showed bead-free nanofiber morphology, indicating relatively good polymer stream stability (**Figure 2.1 (a and b)**). As shown in the SEM images, the fibers appeared to be smooth, and while there were some small changes in diameter, the fiber morphology was generally consistent along the length of the sampled fibers. The quantitative and qualitative observations were indicative of stable electrospinning conditions.

It has been reported that free OLA may influence pre-osteoblast functionality when present at higher concentrations and in serum-free conditions [142]. However, the concentrations of OLA used in this study were relatively low, and it seems unlikely that

OLA would influence the behavior of entire cell population in the culture because of the presence of a range of fatty acids in the serum used with the culture medium. However, it should be acknowledged that some MSCs, particularly osteoblasts and osteoprogenitors, may be influenced by OLA via peroxisome proliferator activated receptors (PPARs) [136, 143]. There is evidence that activation of PPARα and possibly PPARδ may direct differentiation of mature progenitor cells towards osteoblasts rather than adipocytes [142-144]. Furthermore, several other studies have shown the role of PPARγ in directing osteoprogenitor cells into adipocytes rather than osteogenic lineages [145, 146]. Our current research results are insufficient to draw any conclusions about the effects of OLA, but its potential for influence should be noted. Moreover, this may present additional possibilities for adding osteoconductive design features into nanofiber scaffolds, and studies in our laboratory are now directed towards evaluating the effects of OLA on MSC differentiation.

Synthetic bone tissue scaffolds have the capacity to regenerate functional bone tissue at the site of serious injury (i.e. critical-sized defects or non-union fractures). Marrow stromal cells migrate to the injury site in a carefully orchestrated manner, controlled by chemokines, growth factors and ECM proteins [147, 148]. Initial attachment of MSC is especially critical for long-term stability and differentiation of the cells; thus, the capacity for nanofiber scaffolds to support MSC adhesion and proliferation was evaluated using live cell fluorescence staining and an MTT assay.

Cells on nanofiber scaffolds formed noticeably more colonies than on control surfaces after 1 and 4 days of initial culture, which was reflected in the significant differences in cell coverage (**Figure 2.2 (a and b)**; **Figure 2.3 (a)**, and **Figure 2.2 (c and d)**; **Figure 2.3 (a)**). It is worth noting that these measured differences in cell coverage were observed in a corresponding manner in the cell viability assay after 1 and 4 days of

culture (as discussed later in this section). After 7 days, cells on control surfaces had spread out individually, but there were still only small clusters of a few cells rather than the more highly populated colonies observed on nanofiber scaffolds (**Figure 2.2 (e and f)**). The cell coverage was not calculated after 4 days since differences on nanofiber scaffolds and control surfaces were visually very clear, and cells on nanofiber scaffolds were near confluence at many locations.

Cell viability was investigated using a commercially available MTT assay, which measures the total intracellular mitochondrial activity in the cell population. A measurement of cell viability is important in evaluating the capacity for a scaffold to support initial cell proliferation. In order to deliver a scaffold containing cells with therapeutic potential, the colony must demonstrate good viability. As expected, our results suggest that cells are viable on both nanofiber scaffolds and control surfaces for up to 4 days in culture (**Figure 2.3 (b)**). Further, the cell viability on nanofiber scaffolds was significantly greater than on control surfaces at both time points.

Cell viability, as assessed by the MTT assay, was measured after 1 and 4 days of culture since this time period is associated with the log-phase growth of the cell population. MTT provides complimentary information to calcein-AM staining because the MTT assay differentiates between levels of metabolic activity of a cell population rather than a snapshot of cells that retain the activated calcein AM molecule. A visual inspection of colonization, as well as a measurement of cellular metabolism and spreading provided information on the ability of cells to populate these nanofiber scaffolds. Based on these two analyses, the nanofiber scaffolds demonstrated a greater ability to support MSC populations than the control surfaces.

In order to visualize morphological changes in MSCs, SEM images were taken after 1, 4 and 7 days of culture. SEM analysis supported fluorescence microscopy results

indicating that the MSCs preferentially adhere, spread and aggregate on nanofiber scaffolds as compared to control surfaces (**Figure 2.4**). After 1 day of culture, the cells on both control surfaces and nanofiber scaffolds were relatively spherical in morphology (**Figure 2.4 (a and b)**). However, some cells on nanofiber scaffolds showed a small degree of spreading. After 4 days of culture, most of the cells maintained a spherical appearance on control surfaces, whereas on nanofiber scaffolds the cells have spread out and show filopodia extending towards adjacent cells (**Figure 2.4 (c and d)**). While there were a few tightly clustered colonies on nanofiber scaffolds, it was more common to see few cells in close proximity to other cells without tight clustering. After 7 days of culture, most cells have spread out on both control and nanofiber scaffolds, but the overall cell population was noticeably less dense on control than on nanofiber scaffolds (**Figure 2.4 (e and f)**). No infiltrated cells were observed under SEM after 1 and 4 days of culture, though several cells were observed to be beneath the top layer of fibers after 7 days in culture.

A successful bone scaffold must demonstrate support for enhanced bone formation, including organic and inorganic components of natural tissue. ALP is a key component of bone matrix vesicles because of its role in the formation of apatitic calcium phosphate [149], and it is an early indicator of immature osteoblast activity [39]. Although cells in several tissues—liver, kidney, placenta, etc.—generate the enzyme, elevated levels of ALP in bone tissue typically are observed several days prior to neo-mineralization and during the initial phase of bone matrix deposition [39, 150]. The ALP patterns observed over the 3 week experimental period for nanofiber scaffolds were consistent with the previously established patterns in osteoblast-like populations cultured on other nano-structured materials [87, 137, 138]. Figure 5 shows ALP activity normalized to total protein content to account for difference in number of cells present on each surface. The

colorimetric ALP assay results at 1 week of culture showed no statistical difference between nanofiber scaffolds and control surfaces, and standard deviations for both the nanofibers and smooth surfaces were nearly equal to the value of the mean, indicating large inter-specimen variability. After 2 weeks, significant differences were evident between the nanofiber scaffolds and control surfaces; and after 3 weeks, cells on nanofiber scaffolds produced considerably increased levels of ALP, with statistical significance over the control surfaces.

Mineralization patterns were qualitatively examined by SEM/EDS, Alizarin calcium staining and von Kossa staining. Figure 2.6 shows digital images of the stained surfaces (calcium (red) on top, phosphate (brown) stain on bottom) along with SEM images after 3 weeks of culture on both nanofiber and control surfaces. SEM images showed surface mineralization in the form of discrete nodules in greater abundance than control surfaces. Calcium and phosphate minerals were stained in the form of Alizarin red (calcium) and von Kossa (phosphate), respectively, and nanofiber scaffolds showed greater speckled patterns, indicative of mineral nodule formation, than the control surfaces which were much more homogeneous (**Figure 2.6 (a and b)**). SEM images show that the cells on nanofiber scaffolds had colonized and the surface is covered with dense cell populations. In these cell colonies, filopodia were observed to be in direct contact with neighboring cells as well as with nanofiber architecture. On nanofiber scaffolds, cells were frequently and clearly visible underneath the top layer of nanofibers.

After 2 weeks of culture in osteogenic media, nanofiber scaffolds exhibited frequent mineralization in the form of spherulites (**Figure 2.6 (d)**), and while there was evidence of some mineralization on smooth PCL surfaces, it was less noticeable and there were very few spherulites (**Figure 2.6 (c)**). Further, cells on nanofiber scaffolds were interacting with spherulites and mineral aggregates. Similar to the results after 1 week,

the cells were more widely spread and formed colonies on nanofiber scaffolds as compared to control surfaces. After 3 weeks in osteogenic media, mineralization on nanofiber scaffolds had further increased (**Figure 2.6 (f)**). Notable amounts of calcium and phosphate were observed on control surfaces, though the SEM images revealed a lower amount of cell spreading and mineralization (**Figure 2.6 (e)**). Nanofiber scaffolds had substantial calcium phosphate deposition and cells were frequently observed in intimate contact with the deposited mineral. As with the 2 week culture, there was greater cell density on the nanofiber scaffold surface than on the control surface, and quite a few cells were observed beneath the top layer of fibers. EDS scans detected Ca:P mineral deposits on nanofiber scaffolds with greater abundance than on control surfaces. Figure 2.7 shows an elemental compositional map of mineral deposit on nanofiber scaffolds after 3 weeks of culture. EDS is not ideal for making precise about the stoichiometry of calcium phosphates on gold-coated samples since gold will confound the phosphorus K-line signal, but these atomic spectra are clear indicators that cells have deposited calcium phosphates on the surface.

OP and OC were imaged using immunofluorescent staining. OP is a non-collagenous bone matrix protein that is believed to be an important factor in cell adhesion to mineralized tissue, as well as playing a role in regulating bone remodeling in a manner dependent on its degree of phosphorylation and sulfation [151, 152]. It has a region rich in aspartic acid with high affinity for mineralization as well as several integrin-binding sequences [153-155]. OC is highly specific to bone tissue and generally produced towards the end of new bone matrix deposition [156]. It is also thought to play a role in modulating mineralization as it has glutamic acid-rich regions with strong binding affinities to both Ca2+ and hydroxyapatite [154, 155]. Immunofluorescence staining was performed on nanofiber scaffolds and control surfaces using commercially

available OP and OC primary antibodies and a FITC-conjugated secondary antibody after 3 weeks in osteogenic media.

Several differences were apparent between the nanofiber and control surfaces. Immunofluorescent labeling demonstrated greater amounts of both bone matrix proteins, OP and OC, on the nanofiber scaffold surface (**Figure 2. (8c and d)**) compared to that on control surfaces (**Figure 2.8 (a and b)**). One particularly interesting finding on the nanofiber scaffolds was that both stains were observed within the scaffold because of strong backlighting of nanofiber features, indicating not only infiltration into the scaffold, but also active production of bone matrix protein by the infiltrated cells (**Figure 2.8 (e and f)**). Since we are using an immunofluorescent staining technique, our results suggest that the backlighting is not due to fluorescent residues, but due to marker proteins secreted by the differentiated cells. The microscope used for this study was not ideal for quantifying infiltration depth, but combined with repeated observations of infiltrated cells by SEM, there is clear evidence supporting the potential of these scaffolds for three-dimensional bone tissue formation. From an architectural standpoint, the nanofiber scaffolds are more desirable than the control surfaces for several reasons, including increased cell adhesion, proliferation, differentiation and ECM production [68, 69, 157, 158]. Bulk PCL has a very slow degradation rate [109], but with the very large surface-area-to-volume ratio characteristic of nanofibers, the degradation rate for the nanofiber scaffolds could be tuned to approximate more closely the remodeling rate of bone. The porosity of nanofiber scaffolds also allow for cell infiltration and three-dimensional mineralization.

Evidence suggesting cellular infiltration was observed via SEM, and immunofluorescent images showed strong signals of bone matrix protein synthesis from the scaffold interior as well as on the surface. More rigorous studies are now being

conducted in vitro as well as in vivo to evaluate the ability of nanofiber scaffolds to entrap cells and integrate with the bone.

2.6. Conclusions

Given the wide range of potential bone graft recipients, a synthetic source of bone tissue scaffolds that enhances bone formation holds the potential for a substantial positive clinical impact. This work demonstrated the ability to produce consistent nanofibers by incorporating an organosoluble, non-toxic fatty acid salt using an electrospinning process. In addition, nanofiber scaffolds supported greater adhesion and proliferation by MSCs as compared to control surfaces. In osteogenic conditions, ALP activity, mineralization, and osteocalcin and osteopontin production were also greater compared to control surfaces. The performance of these nanofiber scaffolds demonstrates that studies examining osteogenic design factors must control for architecture independently of any soluble or insoluble design factor.

2.7 References

1. Langer, R. and J.P. Vacanti, *Tissue engineering.* Science, 1993. **260**(5110): p. 920-6.
2. Compston, J.E., *Bone marrow and bone: a functional unit.* J Endocrinol, 2002. **173**(3): p. 387-94.
3. Drosse, I., et al., *Tissue engineering for bone defect healing: an update on a multi-component approach.* Injury, 2008. **39 Suppl 2**: p. S9-20.
4. Soucacos, P.N., E.O. Johnson, and G. Babis, *An update on recent advances in bone regeneration.* Injury, 2008. **39 Suppl 2**: p. S1-4.
5. Mistry, A.S. and A.G. Mikos, *Tissue engineering strategies for bone regeneration.* Adv Biochem Eng Biotechnol, 2005. **94**: p. 1-22.
6. Lewandrowski, K.-U., et al., *Bioresorbable bone graft substitutes of different osteoconductivities: a histologic evaluation of osteointegration of poly(propylene glycol-co-fumaric acid)-based cement implants in rats.* Biomaterials, 2000. **21**(8): p. 757-764.
7. Moreau, M.F., et al., *Gamma irradiation of human bone allografts alters medullary lipids and releases toxic compounds for osteoblast-like cells.* Biomaterials, 2000. **21**(4): p. 369-376.

8. Akkus, O. and C.M. Rimnac, *Fracture resistance of gamma radiation sterilized cortical bone allografts.* Journal of Orthopaedic Research, 2001. **19**(5): p. 927-934.
9. Salgado, A.J., O.P. Coutinho, and R.L. Reis, *Bone tissue engineering: state of the art and future trends.* Macromol Biosci, 2004. **4**(8): p. 743-65.
10. Alves, N.M., et al., *Designing biomaterials based on biomineralization of bone.* Journal of Materials Chemistry, 2010. **20**(15): p. 2911-2921.
11. Jang, J.-H., O. Castano, and H.-W. Kim, *Electrospun materials as potential platforms for bone tissue engineering.* Advanced Drug Delivery Reviews, 2009. **61**(12): p. 1065-1083.
12. Hosseinkhani, H., et al., *Osteogenic differentiation of mesenchymal stem cells in self-assembled peptide-amphiphile nanofibers.* Biomaterials, 2006. **27**(22): p. 4079-4086.
13. Bashur, C.A., L.A. Dahlgren, and A.S. Goldstein, *Effect of fiber diameter and orientation on fibroblast morphology and proliferation on electrospun poly(d,l-lactic-co-glycolic acid) meshes.* Biomaterials, 2006. **27**(33): p. 5681-5688.
14. Hu, J., X. Liu, and P.X. Ma, *Induction of osteoblast differentiation phenotype on poly(l-lactic acid) nanofibrous matrix.* Biomaterials, 2008. **29**(28): p. 3815-3821.
15. Basmanav, F., G.T. Kose, and V. Hasirci, *Sequential growth factor delivery from complexed microspheres for bone tissue engineering.* Biomaterials, 2008. **29**(31): p. 4195-204.
16. Karageorgiou, V., et al., *Porous silk fibroin 3-D scaffolds for delivery of bone morphogenetic protein-2 in vitro and in vivo.* J Biomed Mater Res A, 2006. **78**(2): p. 324-34.
17. Quaglia, F., et al., *Microspheres Made of Poly(e-caprolactone)-Based Amphiphilic Copolymers: Potential in Sustained Delivery of Proteins.* Macromolecular Bioscience, 2005. **5**(10): p. 945-954.
18. Muller, P., et al., *Calcium phosphate surfaces promote osteogenic differentiation of mesenchymal stem cells.* J Cell Mol Med, 2008. **12**(1): p. 281-91.
19. Kim, I.-Y., et al., *Chitosan and its derivatives for tissue engineering applications.* Biotechnology Advances, 2008. **26**(1): p. 1-21.
20. Shin, M., H. Yoshimoto, and J.P. Vacanti, *In vivo bone tissue engineering using mesenchymal stem cells on a novel electrospun nanofibrous scaffold.* Tissue Eng, 2004. **10**(1-2): p. 33-41.
21. Kurtz, S., et al., *Prevalence of Primary and Revision Total Hip and Knee Arthroplasty in the United States From 1990 Through 2002.* J Bone Joint Surg Am, 2005. **87**(7): p. 1487-1497.
22. Langer, R. and J.P. Vacanti, *Tissue Engineering.* Science, 1993. **260**(5110): p. 920-926.
23. Jeys, L.M., et al., *Endoprosthetic Reconstruction for the Treatment of Musculoskeletal Tumors of the Appendicular Skeleton and Pelvis.* J Bone Joint Surg Am, 2008. **90**(6): p. 1265-1271.
24. Schuckert, K.H., S. Jopp, and S.H. Teoh, *Mandibular Defect Reconstruction Using Three-Dimensional Polycaprolactone Scaffold in Combination with*

Platelet-Rich Plasma and Recombinant Human Bone Morphogenetic Protein-2: De Novo Synthesis of Bone in a Single Case. Tissue Eng Part A, 2008.
25. Arthur, A., A. Zannettino, and S. Gronthos, *The therapeutic applications of multipotential mesenchymal/stromal stem cells in skeletal tissue repair.* Journal of Cellular Physiology, 2008. **9999**(9999): p. n/a.
26. Ishaug, S.L., et al., *Bone formation by three-dimensional stromal osteoblast culture in biodegradable polymer scaffolds.* Journal of Biomedical Materials Research Part A, 1997. **36**(1): p. 17-28.
27. Yoshimoto, H., et al., *A biodegradable nanofiber scaffold by electrospinning and its potential for bone tissue engineering.* Biomaterials, 2003. **24**(12): p. 2077-2082.
28. Tiedeman, J.J., et al., *The role of a composite, demineralized bone matrix and bone marrow in the treatment of osseous defects.* Orthopedics, 1995. **8**: p. 1153-1158.
29. Rougraff, B.T. and T.J. Kling, *Treatment of active unicameral bone cysts with percutaneous injection of demineralized bone matrix and autogenous bone marrow.* J Bone Joint Surg Am, 2002. **84-A**(6): p. 921-9.
30. Ban, S., et al., *Effect of electrochemically deposited apatite coating on bonding of bone to the HA-G-Ti composite and titanium.* Journal of Biomedical Materials Research Part A, 1997. **36**(1): p. 9-15.
31. Shin, H., S. Jo, and A.G. Mikos, *Biomimetic materials for tissue engineering.* Biomaterials, 2003. **24**(24): p. 4353-4364.
32. Wutticharoenmongkol, P., P. Pavasant, and P. Supaphol, *Osteoblastic Phenotype Expression of MC3T3-E1 Cultured on Electrospun Polycaprolactone Fiber Mats Filled with Hydroxyapatite Nanoparticles.* Biomacromolecules, 2007. **8**(8): p. 2602-2610.
33. Venugopal, J., et al., *Interaction of Cells and Nanofiber Scaffolds in Tissue Engineering.* Journal of Biomedical Materials Research Part B: Applied Biomaterials, 2008. **84B**(1): p. 34-48.
34. Guarino, V., et al., *Polylactic acid fibre-reinforced polycaprolactone scaffolds for bone tissue engineering.* Biomaterials, 2008. **29**(27): p. 3662-70.
35. Park, S.-H. and *e. al*, *Effect of hydroxyapatite-coated nanofibrous membrane on the responses of human periodontal ligament fibroblast.* Journal of the Ceramic Society of Japan, 2008. **116**(1349): p. 31-35.
36. Ramay, H.R. and M. Zhang, *Biphasic calcium phosphate nanocomposite porous scaffolds for load-bearing bone tissue engineering.* Biomaterials, 2004. **25**(21): p. 5171-80.
37. Zhang, P., et al., *In vivo mineralization and osteogenesis of nanocomposite scaffold of poly(lactide-co-glycolide) and hydroxyapatite surface-grafted with poly(l-lactide).* Biomaterials, 2008.
38. Kim, H.-W., H.-H. Lee, and J.C. Knowles, *Electrospinning biomedical nanocomposite fibers of hydroxyapaite/poly(lactic acid) for bone regeneration.* Journal of Biomedical Materials Research Part A, 2006. **79A**(3): p. 643-649.
39. Liu, F., L. Malaval, and J.E. Aubin, *Global amplification polymerase chain reaction reveals novel transitional stages during osteoprogenitor differentiation.* J Cell Sci, 2003. **116**(Pt 9): p. 1787-96.

40. Sikavitsas, V.I., J.S. Temenoff, and A.G. Mikos, *Biomaterials and bone mechanotransduction.* Biomaterials, 2001. **22**(19): p. 2581-93.
41. Gordon, J.A., et al., *Bone sialoprotein expression enhances osteoblast differentiation and matrix mineralization in vitro.* Bone, 2007. **41**(3): p. 462-73.
42. Baht, G.S., G.K. Hunter, and H.A. Goldberg, *Bone sialoprotein-collagen interaction promotes hydroxyapatite nucleation.* Matrix Biol, 2008. **27**(7): p. 600-8.
43. Nam, J. and *e. al*, *Improved cellular infiltration in electrospun fiber via engineered porosity.* Tissue Engineering, 2007. **13**(9): p. 2249-2257.
44. Lorenzo, J., M. Horowitz, and Y. Choi, *Osteoimmunology: interactions of the bone and immune system.* Endocr Rev, 2008. **29**(4): p. 403-40.
45. Takayanagi, H., *Osteoimmunology: shared mechanisms and crosstalk between the immune and bone systems.* Nat Rev Immunol, 2007. **7**(4): p. 292-304.
46. Ferrari, S.L., et al., *A role for N-cadherin in the development of the differentiated osteoblastic phenotype.* J Bone Miner Res, 2000. **15**(2): p. 198-208.
47. Kii, I., et al., *Cell-cell interaction mediated by cadherin-11 directly regulates the differentiation of mesenchymal cells into the cells of the osteo-lineage and the chondro-lineage.* J Bone Miner Res, 2004. **19**(11): p. 1840-9.
48. Wu, L.N., B.R. Genge, and R.E. Wuthier, *Analysis and molecular modeling of the formation, structure, and activity of the phosphatidylserine-calcium-phosphate complex associated with biomineralization.* J Biol Chem, 2008. **283**(7): p. 3827-38.
49. Genge, B.R., L.N. Wu, and R.E. Wuthier, *In vitro modeling of matrix vesicle nucleation: synergistic stimulation of mineral formation by annexin A5 and phosphatidylserine.* J Biol Chem, 2007. **282**(36): p. 26035-45.
50. Hunter, G.K. and H.A. Goldberg, *Nucleation of hydroxyapatite by bone sialoprotein.* Proc Natl Acad Sci U S A, 1993. **90**(18): p. 8562-5.
51. Taller, A., et al., *Specific adsorption of osteopontin and synthetic polypeptides to calcium oxalate monohydrate crystals.* Biophys J, 2007. **93**(5): p. 1768-77.
52. Chen, M. and *e. al*, *Role of Fiber Diameter in Adhesion and Proliferation of NIH 3T3 Fibroblast on Electrospun Polycaprolactone Scaffolds.* Tissue Engineering, 2007. **13**(3): p. 579-587.
53. Haynesworth, S., et al., *Characterization of cells with osteogenic potential from human marrow.* Bone, 1992. **13**: p. 81-88.
54. Prockop, D., *Marrow stromal cells as stem cells for nonhematopoietic tissues.* Science, 1997. **276**: p. 71-74.
55. Altman, G.H., et al., *Cell differentiation by mechanical stress.* Faseb J, 2002. **16**(2): p. 270-2.
56. Caplan, A., et al., *Mesenchymal stem cells and tissue repair. In: Jackson, D.W., ed. The Anterior Cruciate Ligament: Current and Future Concepts*. 1993, New York: Raven Press.
57. Wall, M.E., S.H. Bernacki, and E.G. Loboa, *Effects of serial passaging on the adipogenic and osteogenic differentiation potential of adipose-derived human mesenchymal stem cells.* Tissue Eng, 2007. **13**(6): p. 1291-8.

58. Beresford, J.N., et al., *Evidence for an inverse relationship between the differentiation of adipocytic and osteogenic cells in rat marrow stromal cell cultures.* J Cell Sci, 1992. **102 (Pt 2)**: p. 341-51.
59. Seshi, B., S. Kumar, and D. Sellers, *Human bone marrow stromal cell: coexpression of markers specific for multiple mesenchymal cell lineages.* Blood Cells Mol Dis, 2000. **26**(3): p. 234-46.
60. Bianco, P. and P. Gehron Robey, *Marrow stromal stem cells.* J Clin Invest, 2000. **105**(12): p. 1663-8.
61. Marletta, G., et al., *Improved osteogenic differentiation of human marrow stromal cells cultured on ion-induced chemically structured poly-[epsilon]-caprolactone.* Biomaterials, 2007. **28**(6): p. 1132-1140.
62. Li, W.-J., et al., *Multilineage differentiation of human mesenchymal stem cells in a three-dimensional nanofibrous scaffold.* Biomaterials, 2005. **26**(25): p. 5158-5166.
63. Holt, S.E., J.W. Shay, and W.E. Wright, *Refining the telomere-telomerase hypothesis of aging and cancer.* Nat Biotechnol, 1996. **14**(7): p. 836-9.
64. Miura, M., et al., *Accumulated chromosomal instability in murine bone marrow mesenchymal stem cells leads to malignant transformation.* Stem Cells, 2006. **24**(4): p. 1095-103.
65. Popat, K.C., et al., *Decreased Staphylococcus epidermis adhesion and increased osteoblast functionality on antibiotic-loaded titania nanotubes.* Biomaterials, 2007. **28**(32): p. 4880-4888.
66. Schwartz, Z. and B. Boyan, *Underlying Mechanisms at the Bone-Biomaterial Interface.* Journal of Cellular Biochemistry, 1994. **56**: p. 340-347.
67. Dee, K.C. and R. Bizios, *Mini Review: Proactive Biomaterials and Bone Tissue Engineering.* Biotechnology and Bioengineering, 1996. **50**: p. 438-442.
68. Engel, E., et al., *Nanotechnology in regenerative medicine: the materials side.* Trends in Biotechnology, 2008. **26**(1): p. 39-47.
69. Murugan, R. and S. Ramakrishna, *Design strategies of tissue engineering scaffolds with controlled fiber orientation.* Tissue Eng, 2007. **13**(8): p. 1845-66.
70. Wainwright, S., et al., *Mechanical Design in Organisms*. 2 ed. 1982: Princeton University Press.
71. Schnell, E., et al., *Guidance of glial cell migration and axonal growth on electrospun nanofibers of poly-e-caprolactone and a collagen/poly-e-caprolactone blend.* Biomaterials, 2007. **28**(19): p. 3012-3025.
72. Horii, A., et al., *Biological designer self-assembling Peptide nanofiber scaffolds significantly enhance osteoblast proliferation, differentiation and 3-D migration.* PLoS ONE, 2007. **2**(2): p. e190.
73. Dersch, R., et al., *Electrospinning of Nanofibres: Towards New Techniques, Functions, And Applications.* Australian Journal of Chemistry, 2007. **60**: p. 719-728.
74. Sill, T.J. and H.A. von Recum, *Electrospinning: Applications in drug delivery and tissue engineering.* Biomaterials, 2008. **In Press, Corrected Proof**.

75. Theron, S.A., E. Zussman, and A.L. Yarin, *Experimental investigation of the governing parameters in the electrospinning of polymer solutions.* Polymer, 2004. **45**(6): p. 2017-2030.
76. Moroni, L., et al., *Fiber diameter and texture of electrospun PEOT/PBT scaffolds influence human mesenchymal stem cell proliferation and morphology, and the release of incorporated compounds.* Biomaterials, 2006. **27**(28): p. 4911-4922.
77. Price, R.L., et al., *Selective bone cell adhesion on formulations containing carbon nanofibers.* Biomaterials, 2003. **24**(11): p. 1877-87.
78. Teo, W.E. and S. Ramakrishna, *A review on electrospinning design and nanofibre assemblies.* Nanotechnology, 2006. **17**: p. R89-R106.
79. Kim, G. and W. Kim, *Highly porous 3D nanofiber scaffold using an electrospinning technique.* Journal of Biomedical Materials Research Part B: Applied Biomaterials, 2007. **81B**(1): p. 104-110.
80. Rutledge, G.C. and S.V. Fridrikh, *Formation of fibers by electrospinning.* Advanced Drug Delivery Reviews, 2007. **59**(14): p. 1384-1391.
81. Thomas, V., et al., *Mechano-morphological studies of aligned nanofibrous scaffolds of polycaprolactone fabricated by electrospinning.* Journal of Biomaterials Science -- Polymer Edition, 2006. **17**(9): p. 969-984.
82. Chen, J.-P., G.-Y. Chang, and J.-K. Chen, *Electrospun collagen/chitosan nanofibrous membrane as wound dressing.* Colloids and Surfaces A, 2008. **313-314**: p. 183-188.
83. Zhang, D. and J. Chang, *Patterning of Electrospun Fibers Using Electroconductive Templates.* Advanced Materials, 2007. **19**(21): p. 3664-3667.
84. Ramakrishna, S., et al., *An Introduction to Electrospinning and Nanofibers*. 2005, Singapore: World Scientific Publishing Co. Pte. Ltd. 382.
85. Choi, J.S., et al., *Effect of organosoluble salts on the nanofibrous structure of electrospun poly(3-hydroxybutyrate-co-3-hydroxyvalerate).* International Journal of Biological Macromolecules, 2004. **34**(4): p. 249-256.
86. Bolgen, N., et al., *In vitro and in vivo degradation of non-woven materials made of poly(e-caprolactone) nanofibers prepared by electrospinning under different conditions.* Journal of Biomaterials Science -- Polymer Edition, 2005. **16**(12): p. 1537-1555.
87. Popat, K.C., et al., *Osteogenic differentiation of marrow stromal cells cultured on nanoporous alumina surfaces.* Journal of Biomedical Materials Research Part A, 2007. **80A**(4): p. 955-964.
88. Sangsanoh, P., et al., *In Vitro Biocompatibility of Schwann Cells on Surfaces of Biocompatible Polymeric Electrospun Fibrous and Solution-Cast Film Scaffolds.* Biomacromolecules, 2007. **8**(5): p. 1587-1594.
89. Corey, J.M. and *e. al*, *Aligned electrospun nanofibers specify the direction of dorsal root ganglia neurite growth.* Journal of Biomedical Materials Research Part A, 2007. **83a**(3): p. 636-645.
90. Chua, K.-N., et al., *Stable immobilization of rat hepatocyte spheroids on galactosylated nanofiber scaffold.* Biomaterials, 2005. **26**(15): p. 2537-2547.

91. Farokhzad, O.C. and R. Langer, *Impact of nanotechnology on drug delivery.* ACS Nano, 2009. **3**(1): p. 16-20.
92. Youan, B.B., *Impact of nanoscience and nanotechnology on controlled drug delivery.* Nanomed, 2008. **3**(4): p. 401-6.
93. Zeng, J., et al., *Biodegradable electrospun fibers for drug delivery.* Journal of Controlled Release, 2003. **92**(3): p. 227-231.
94. Xie, J., R.S. Tan, and C.-H. Wang, *Biodegradable microparticles and fiber fabrics for sustained delivery of cisplatin to treat C6 glioma in vitro.* Journal of Biomedical Materials Research Part A, 2008. **85A**(4): p. 897-908.
95. Fujiyama, J., et al., *Cisplatin incorporated in microspheres: development and fundamental studies for its clinical application.* Journal of Controlled Release, 2003. **89**: p. 397-408.
96. Farokhzad, O.C., J.M. Karp, and R. Langer, *Nanoparticle-aptamer bioconjugates for cancer targeting.* Expert Opin Drug Deliv, 2006. **3**(3): p. 311-24.
97. Sharman, W.M., J.E. van Lier, and C.M. Allen, *Targeted photodynamic therapy via receptor mediated delivery systems.* Adv Drug Deliv Rev, 2004. **56**(1): p. 53-76.
98. Luo, Y. and G.D. Prestwich, *Cancer-targeted polymeric drugs.* Curr Cancer Drug Targets, 2002. **2**(3): p. 209-26.
99. Arifin, D.Y., L.Y. Lee, and C.H. Wang, *Mathematical modeling and simulation of drug release from microspheres: Implications to drug delivery systems.* Adv Drug Deliv Rev, 2006. **58**(12-13): p. 1274-325.
100. Tzafriri, A.R., *Mathematical modeling of diffusion-mediated release from bulk degrading matrices.* J Control Release, 2000. **63**(1-2): p. 69-79.
101. Anderson, D.G., J.A. Burdick, and R. Langer, *Materials science. Smart biomaterials.* Science, 2004. **305**(5692): p. 1923-4.
102. Kopecek, J., *Smart and genetically engineered biomaterials and drug delivery systems.* Eur J Pharm Sci, 2003. **20**(1): p. 1-16.
103. Furth, M.E., A. Atala, and M.E. Van Dyke, *Smart biomaterials design for tissue engineering and regenerative medicine.* Biomaterials, 2007. **28**(34): p. 5068-73.
104. Whang, K., T.K. Goldstick, and K.E. Healy, *A biodegradable polymer scaffold for delivery of osteotropic factors.* Biomaterials, 2000. **21**(24): p. 2545-2551.
105. Ma, P.X., *Biomimetic materials for tissue engineering.* Advanced Drug Delivery Reviews, 2008. **60**(2): p. 184-198.
106. Bolgen, N. and *e. al*, *In vivo performance of antibiotic embedded electrospun PCL membranes for prevention of abdominal adhesions.* Journal of Biomedical Materials Research Part B: Applied Biomaterials, 2007. **81b**(2): p. 530-543.
107. Tauro, J.R. and R.A. Gemeinhart, *Matrix Metalloprotease Triggered Delivery of Cancer Chemotherapeutics from Hydrogel Matrixes.* Bioconjugate Chem., 2005. **16**(5): p. 1133-1139.
108. Sinha, V.R., et al., *Poly-e-caprolactone microspheres and nanospheres: an overview.* International Journal of Pharmaceutics, 2004. **278**(1): p. 1-23.

109. Pulkkinen, M., et al., *Effects of block length on the enzymatic degradation and erosion of oxazoline linked poly-e-caprolactone.* European Journal of Pharmaceutical Sciences, 2007. **31**(2): p. 119-128.
110. Kulkarni, A., et al., *Enzymatic Chain Scission Kinetics of Poly(e-caprolactone) Monolayers.* Langmuir, 2007. **23**(24): p. 12202-12207.
111. von Burkersroda, F., L. Schedl, and A. Gopferich, *Why degradable polymers undergo surface erosion or bulk erosion.* Biomaterials, 2002. **23**(21): p. 4221-31.
112. Biondi, M., et al., *Controlled drug delivery in tissue engineering.* Advanced Drug Delivery Reviews, 2008. **60**(2): p. 229-242.
113. Charlier, A., B. Leclerc, and G. Couarraze, *Release of mifepristone from biodegradable matrices: experimental and theoretical evaluations.* Int J Pharm, 2000. **200**(1): p. 115-20.
114. Berchane, N.S., et al., *Effect of mean diameter and polydispersity of PLG microspheres on drug release: experiment and theory.* Int J Pharm, 2007. **337**(1-2): p. 118-26.
115. Arifin, D.Y., L.Y. Lee, and C.-H. Wang, *Mathematical modeling and simulation of drug release from microspheres: Implications to drug delivery systems.* Advanced Drug Delivery Reviews, 2006. **58**(12-13): p. 1274-1325.
116. Higuchi, T., *Mechanism of Sustained-Action Medication.* Journal of Pharmaceutical Sciences, 1963. **52**(12): p. 1145-1149.
117. Coccoli, V., et al., *Engineering of poly(epsilon-caprolactone) microcarriers to modulate protein encapsulation capability and release kinetic.* J Mater Sci Mater Med, 2008. **19**(4): p. 1703-11.
118. Berkland, C., K. Kim, and D.W. Pack, *PLG microsphere size controls drug release rate through several competing factors.* Pharm Res, 2003. **20**(7): p. 1055-62.
119. Zilberman, M. and J.J. Elsner, *Antibiotic-eluting medical devices for various applications.* J Control Release, 2008. **130**(3): p. 202-15.
120. Coviello, V. and M.R. Stevens, *Contemporary concepts in the treatment of chronic osteomyelitis.* Oral Maxillofac Surg Clin North Am, 2007. **19**(4): p. 523-34, vi.
121. Schmidmaier, G., et al., *Prophylaxis and treatment of implant-related infections by antibiotic-coated implants: a review.* Injury, 2006. **37 Suppl 2**: p. S105-12.
122. Klevens, R.M., et al., *Invasive methicillin-resistant Staphylococcus aureus infections in the United States.* JAMA, 2007. **298**(15): p. 1763-71.
123. Lucke, M., et al., *Systemic versus local application of gentamicin in prophylaxis of implant-related osteomyelitis in a rat model.* Bone, 2005. **36**(5): p. 770-8.
124. Rohrbaugh, T.M., et al., *Absorption of oral aminoglycosides following bone marrow transplantation.* Cancer, 1984. **53**(7): p. 1502-6.
125. Shakil, S., et al., *Aminoglycosides versus bacteria – a description of the action, resistance mechanism, and nosocomial battleground.* J. Biomed. Sci., 2005. **15**: p. 5-14.

126. Saad, E.I., et al., *Role of oxidative stress and nitric oxide in the protective effects of alpha-lipoic acid and aminoguanidine against isoniazid-rifampicin-induced hepatotoxicity in rats.* Food Chem Toxicol, 2010.
127. Frippiat, F., F. Meunier, and G. Derue, *Place of newer quinolones and rifampicin in the treatment of Gram-positive bone and joint infections.* J Antimicrob Chemother, 2004. **54**(6): p. 1158; author reply 1159.
128. Pohlod, D.J., L.D. Saravolatz, and M.M. Somerville, *In-vitro susceptibility of gram-positive cocci to LY146032 teicoplanin, sodium fusidate, vancomycin, and rifampicin.* J Antimicrob Chemother, 1987. **20**(2): p. 197-202.
129. Tupin, A., et al., *Resistance to rifampicin: at the crossroads between ecological, genomic and medical concerns.* Int J Antimicrob Agents, 2010. **35**(6): p. 519-23.
130. Mont, M., B. Waldman, and D.S. Hungerford, *Evaluation of preoperative cultures before second-stage reimplantation of a total knee prosthesis complicated by infection: A comparison-group study.* Journal of Bone and Joint Surgery, 2000. **82**: p. 1552-1557.
131. Smith, A.W., *Biofilms and antibiotic therapy: is there a role for combating bacterial resistance by the use of novel drug delivery systems?* Adv Drug Deliv Rev, 2005. **57**(10): p. 1539-50.
132. Prockop, D.J., *Marrow stromal cells as stem cells for nonhematopoietic tissues.* Science, 1997. **276**(5309): p. 71-4.
133. Young, R.G., et al., *Use of mesenchymal stem cells in a collagen matrix for Achilles tendon repair.* J Orthop Res, 1998. **16**(4): p. 406-13.
134. Bianco, P., et al., *Bone marrow stromal stem cells: nature, biology, and potential applications.* Stem Cells, 2001. **19**(3): p. 180-92.
135. Yoshimoto, H., et al., *A biodegradable nanofiber scaffold by electrospinning and its potential for bone tissue engineering.* Biomaterials, 2003. **24**(12): p. 2077-82.
136. Michalik, L. and W. Wahli, *Peroxisome proliferator-activated receptors: three isotypes for a multitude of functions.* Curr Opin Biotechnol, 1999. **10**(6): p. 564-70.
137. Shin, H., et al., *Modulation of differentiation and mineralization of marrow stromal cells cultured on biomimetic hydrogels modified with Arg-Gly-Asp containing peptides.* J Biomed Mater Res A, 2004. **69**(3): p. 535-43.
138. Bancroft, G.N., et al., *Fluid flow increases mineralized matrix deposition in 3D perfusion culture of marrow stromal osteoblasts in a dose-dependent manner.* Proc Natl Acad Sci U S A, 2002. **99**(20): p. 12600-5.
139. Chen, M., et al., *Role of fiber diameter in adhesion and proliferation of NIH 3T3 fibroblast on electrospun polycaprolactone scaffolds.* Tissue Eng, 2007. **13**(3): p. 579-87.
140. Bashur, C.A., L.A. Dahlgren, and A.S. Goldstein, *Effect of fiber diameter and orientation on fibroblast morphology and proliferation on electrospun poly(D,L-lactic-co-glycolic acid) meshes.* Biomaterials, 2006. **27**(33): p. 5681-8.

141. Bashur, C.A., et al., *Effect of fiber diameter and alignment of electrospun polyurethane meshes on mesenchymal progenitor cells.* Tissue Eng Part A, 2009. **15**(9): p. 2435-45.
142. Jackson, S. and L. Demer, *Peroxisome proliferator-activated receptor activators modulate the osteoblastic maturation of MC3T3-E1 preosteoblasts.* FEBS Lett, 2000. **471**(1): p. 119 - 124.
143. Still, K., et al., *The Peroxisome Proliferator Activator Receptor Alpha/Delta Agonists Linoleic Acid and Bezafibrate Upregulate Osteoblast Differentiation and Induce Periosteal Bone Formation In Vivo.* Calcif Tissue Int, 2008.
144. Kawaguchi, H., et al., *Distinct effects of PPARgamma insufficiency on bone marrow cells, osteoblasts, and osteoclastic cells.* J Bone Miner Metab, 2005. **23**(4): p. 275-9.
145. Lin, T.-H., et al., *PPARg inhibits osteogenesis via the down-regulation of the expression of COX-2 and iNOS in rats.* Bone, 2007. **41**: p. 562-574.
146. Moerman, E., et al., *Aging activates adipogenic and suppresses osteogenic programs in mesenchymal marrow stroma/stem cells: the role of PPAR-gamma2 transcription factor and TGF-beta/BMP signaling pathways.* Aging Cell, 2004. **3**: p. 379.
147. Brooke, G., et al., *Molecular trafficking mechanisms of multipotent mesenchymal stem cells derived from human bone marrow and placenta.* Stem Cells Dev, 2008. **17**(5): p. 929-40.
148. Ponte, A.L., et al., *The in vitro migration capacity of human bone marrow mesenchymal stem cells: comparison of chemokine and growth factor chemotactic activities.* Stem Cells, 2007. **25**(7): p. 1737-45.
149. Anderson, H.C., et al., *Impaired calcification around matrix vesicles of growth plate and bone in alkaline phosphatase-deficient mice.* Am J Pathol, 2004. **164**(3): p. 841-7.
150. Heinemann, C., et al., *Novel textile chitosan scaffolds promote spreading, proliferation, and differentiation of osteoblasts.* Biomacromolecules, 2008. **9**(10): p. 2913-20.
151. Damsky, C.H., *Extracellular matrix-integrin interactions in osteoblast function and tissue remodeling.* Bone, 1999. **25**(1): p. 95-6.
152. Sodek, J., et al., *Novel functions of the matricellular proteins osteopontin and osteonectin/SPARC.* Connect Tissue Res, 2002. **43**(2-3): p. 308-19.
153. McKee, M.D. and A. Nanci, *Osteopontin: an interfacial extracellular matrix protein in mineralized tissues.* Connect Tissue Res, 1996. **35**(1-4): p. 197-205.
154. Young, M.F., *Bone matrix proteins: their function, regulation, and relationship to osteoporosis.* Osteoporos Int, 2003. **14 Suppl 3**: p. S35-42.
155. Young, M.F., et al., *Structure, expression, and regulation of the major noncollagenous matrix proteins of bone.* Clin Orthop Relat Res, 1992(281): p. 275-94.
156. Robey, P.G., et al., *Structure and molecular regulation of bone matrix proteins.* J Bone Miner Res, 1993. **8 Suppl 2**: p. S483-7.
157. Koh, H.S., et al., *Enhancement of neurite outgrowth using nano-structured scaffolds coupled with laminin.* Biomaterials, 2008. **29**(26): p. 3574-82.

158. Sill, T.J. and H.A. von Recum, *Electrospinning: applications in drug delivery and tissue engineering.* Biomaterials, 2008. **29**(13): p. 1989-2006.
159. Johnson, M.R., et al., *Sustained release of BMP-2 in a lipid-based microtube vehicle.* Acta Biomater, 2009. **5**(1): p. 23-8.
160. Laflamme, C. and M. Rouabhia, *Effect of BMP-2 and BMP-7 homodimers and a mixture of BMP-2/BMP-7 homodimers on osteoblast adhesion and growth following culture on a collagen scaffold.* Biomed Mater, 2008. **3**(1): p. 15008.
161. Laurencin, C.T., et al., *Poly(lactide-co-glycolide)/hydroxyapatite delivery of BMP-2-producing cells: a regional gene therapy approach to bone regeneration.* Biomaterials, 2001. **22**(11): p. 1271-7.
162. Lee, J.Y., et al., *Osteoblastic differentiation of human bone marrow stromal cells in self-assembled BMP-2 receptor-binding peptide-amphiphiles.* Biomaterials, 2009. **30**(21): p. 3532-41.
163. Olivares-Navarrete, R., et al., *Integrin alpha2beta1 plays a critical role in osteoblast response to micron-scale surface structure and surface energy of titanium substrates.* Proc Natl Acad Sci U S A, 2008. **105**(41): p. 15767-72.
164. Marletta, G., et al., *The effect of irradiation modification and RGD sequence adsorption on the response of human osteoblasts to polycaprolactone.* Biomaterials, 2005. **26**(23): p. 4793-804.
165. Palmer, L.C., et al., *Biomimetic systems for hydroxyapatite mineralization inspired by bone and enamel.* Chem Rev, 2008. **108**(11): p. 4754-83.
166. Nikolov, S. and D. Raabe, *Hierarchical modeling of the elastic properties of bone at submicron scales: the role of extrafibrillar mineralization.* Biophys J, 2008. **94**(11): p. 4220-32.
167. Norman, J., et al., *Micromechanical properties of human trabecular bone: a hierarchical investigation using nanoindentation.* J Biomed Mater Res A, 2008. **87**(1): p. 196-202.
168. McCreadie, B.R., et al., *Hierarchical structure of bone and micro-computed tomography.* Adv Exp Med Biol, 2001. **496**: p. 67-83.
169. White, D.J., et al., *The collagen receptor subfamily of the integrins.* Int J Biochem Cell Biol, 2004. **36**(8): p. 1405-10.
170. Denhardt, D.T. and M. Noda, *Osteopontin expression and function: role in bone remodeling.* J Cell Biochem Suppl, 1998. **30-31**: p. 92-102.
171. Kazanecki, C.C., D.J. Uzwiak, and D.T. Denhardt, *Control of osteopontin signaling and function by post-translational phosphorylation and protein folding.* J Cell Biochem, 2007. **102**(4): p. 912-24.
172. Cui, W. and *e. al*, *In situ growth of hydroxyapatite within electrospun poly(DL-lactide) fibers.* Journal of Biomedical Materials Research Part A, 2007. **82A**(4): p. 831-841.
173. Fang, B., et al., *Proliferation and osteoblastic differentiation of human bone marrow stromal cells on hydroxyapatite/bacterial cellulose nanocomposite scaffolds.* Tissue Eng Part A, 2009. **15**(5): p. 1091-8.
174. Guarino, V., et al., *The Influence of Hydroxyapatite Particles on in Vitro Degradation Behaviour of Pcl Based Composite Scaffolds.* Tissue Eng Part A, 2009.

175. Lee, J.H., et al., *Control of osteogenic differentiation and mineralization of human mesenchymal stem cells on composite nanofibers containing poly[lactic-co-(glycolic acid)] and hydroxyapatite.* Macromol Biosci, 2010. **10**(2): p. 173-82.
176. Mei, F., et al., *Improved Biological Characteristics of Poly(L-Lactic Acid) Electrospun Membrane by Incorporation of Multiwalled Carbon Nanotubes/Hydroxyapatite Nanoparticles.* Biomacromolecules, 2007. **8**(12): p. 3729-3735.
177. Xu, H.E., et al., *Molecular recognition of fatty acids by peroxisome proliferator-activated receptors.* Mol Cell, 1999. **3**(3): p. 397-403.
178. Berger, J. and D. Moller, *The mechanisms of action of PPARs.* Annu Rev Med, 2002. **53**: p. 409 - 435.
179. Lecka-Czernik, B. and L.J. Suva, *Resolving the Two "Bony" Faces of PPAR-gamma.* PPAR Res, 2006. **2006**: p. 27489.
180. Syversen, U., et al., *PPAR-Alpha Agonists Increase Bone Mineral Density in Female Rats.* Abstract at ASBMR 25th Annual Meeting, 2003.
181. Ruckh, T.T., et al., *Osteogenic Differentiation of Bone Marrow Stromal Cells on Poly(epsilon-caprolactone) Nanofiber Scaffolds.* Acta Biomater, 2010.
182. Fregel, R., A. Gonzalez, and V.M. Cabrera, *Improved ethanol precipitation of DNA.* Electrophoresis, 2010. **31**(8): p. 1350-2.
183. Khatiwala, C.B., et al., *ECM compliance regulates osteogenesis by influencing MAPK signaling downstream of RhoA and ROCK.* J Bone Miner Res, 2009. **24**(5): p. 886-98.
184. McBeath, R., et al., *Cell shape, cytoskeletal tension, and RhoA regulate stem cell lineage commitment.* Dev Cell, 2004. **6**(4): p. 483-95.
185. Meyers, V.E., et al., *RhoA and cytoskeletal disruption mediate reduced osteoblastogenesis and enhanced adipogenesis of human mesenchymal stem cells in modeled microgravity.* J Bone Miner Res, 2005. **20**(10): p. 1858-66.
186. Salih, E., et al., *Protein kinases of cultured osteoblasts: selectivity for the extracellular matrix proteins of bone and their catalytic competence for osteopontin.* J Bone Miner Res, 1996. **11**(10): p. 1461-73.
187. Katayama, Y., et al., *Casein kinase 2 phosphorylation of recombinant rat osteopontin enhances adhesion of osteoclasts but not osteoblasts.* J Cell Physiol, 1998. **176**(1): p. 179-87.
188. Wang, J., et al., *Expression of bone microsomal casein kinase II, bone sialoprotein, and osteopontin during the repair of calvarial defects.* Bone, 1998. **22**(6): p. 621-8.
189. Bellows, C.G., S.M. Reimers, and J.N. Heersche, *Expression of mRNAs for type-I collagen, bone sialoprotein, osteocalcin, and osteopontin at different stages of osteoblastic differentiation and their regulation by 1,25 dihydroxyvitamin D3.* Cell Tissue Res, 1999. **297**(2): p. 249-59.
190. Gupta, D., et al., *Nanostructured biocomposite substrates by electrospinning and electrospraying for the mineralization of osteoblasts.* Biomaterials, 2009. **30**(11): p. 2085-94.

191. Jackson, S.M. and L.L. Demer, *Peroxisome proliferator-activated receptor activators modulate the osteoblastic maturation of MC3T3-E1 preosteoblasts.* FEBS Lett, 2000. **471**(1): p. 119-24.
192. de Jong, D.S., et al., *Identification of novel regulators associated with early-phase osteoblast differentiation.* J Bone Miner Res, 2004. **19**(6): p. 947-58.
193. Badami, A.S., et al., *Effect of fiber diameter on spreading, proliferation, and differentiation of osteoblastic cells on electrospun poly(lactic acid) substrates.* Biomaterials, 2006. **27**(4): p. 596-606.
194. Tsiridis, E., N. Upadhyay, and P. Giannoudis, *Molecular aspects of fracture healing: which are the important molecules?* Injury, 2007. **38 Suppl 1**: p. S11-25.
195. Chen, L., et al., *Insulin-like growth factor 2 (IGF2) potentiates BMP9-induced osteogenic differentiation and bone formation.* J Bone Miner Res, 2010.
196. Sundelacruz, S. and D.L. Kaplan, *Stem cell- and scaffold-based tissue engineering approaches to osteochondral regenerative medicine.* Semin Cell Dev Biol, 2009. **20**(6): p. 646-55.
197. Ekholm, E.C., et al., *Expression of extracellular matrix genes: transforming growth factor (TGF)-beta1 and ras in tibial fracture healing of lathyritic rats.* Bone, 2000. **27**(4): p. 551-7.
198. Hirakawa, K., et al., *Localization of the mRNA for bone matrix proteins during fracture healing as determined by in situ hybridization.* J Bone Miner Res, 1994. **9**(10): p. 1551-7.
199. Schuckert, K.H., S. Jopp, and S.H. Teoh, *Mandibular defect reconstruction using three-dimensional polycaprolactone scaffold in combination with platelet-rich plasma and recombinant human bone morphogenetic protein-2: de novo synthesis of bone in a single case.* Tissue Eng Part A, 2009. **15**(3): p. 493-9.
200. Thorwarth, M., et al., *Expression of bone matrix proteins during de novo bone formation using a bovine collagen and platelet-rich plasma (prp)--an immunohistochemical analysis.* Biomaterials, 2005. **26**(15): p. 2575-84.
201. Kosaki, N., et al., *Impaired bone fracture healing in matrix metalloproteinase-13 deficient mice.* Biochem Biophys Res Commun, 2007. **354**(4): p. 846-51.
202. Weiss, S., et al., *Systemic regulation of angiogenesis and matrix degradation in bone regeneration--distraction osteogenesis compared to rigid fracture healing.* Bone, 2005. **37**(6): p. 781-90.
203. Henle, P., G. Zimmermann, and S. Weiss, *Matrix metalloproteinases and failed fracture healing.* Bone, 2005. **37**(6): p. 791-8.
204. Coleman, J.E., *Structure and mechanism of alkaline phosphatase.* Annu Rev Biophys Biomol Struct, 1992. **21**: p. 441-83.
205. Orimo, H. and T. Shimada, *The role of tissue-nonspecific alkaline phosphatase in the phosphate-induced activation of alkaline phosphatase and mineralization in SaOS-2 human osteoblast-like cells.* Mol Cell Biochem, 2008. **315**(1-2): p. 51-60.

206. Kulterer, B., et al., *Gene expression profiling of human mesenchymal stem cells derived from bone marrow during expansion and osteoblast differentiation.* BMC Genomics, 2007. **8**: p. 70.
207. Venugopal, J., et al., *Electrospun-modified nanofibrous scaffolds for the mineralization of osteoblast cells.* Journal of Biomedical Materials Research Part A, 2007. **85**(2): p. 408-417.
208. Qin, C., O. Baba, and W.T. Butler, *Post-translational modifications of sibling proteins and their roles in osteogenesis and dentinogenesis.* Crit Rev Oral Biol Med, 2004. **15**(3): p. 126-36.
209. Keykhosravani, M., et al., *Comprehensive identification of post-translational modifications of rat bone osteopontin by mass spectrometry.* Biochemistry, 2005. **44**(18): p. 6990-7003.
210. Yoshida, T., M.F. Clark, and P.H. Stern, *The small GTPase RhoA is crucial for MC3T3-E1 osteoblastic cell survival.* J Cell Biochem, 2009. **106**(5): p. 896-902.
211. Chan, M.C., et al., *A novel regulatory mechanism of the bone morphogenetic protein (BMP) signaling pathway involving the carboxyl-terminal tail domain of BMP type II receptor.* Mol Cell Biol, 2007. **27**(16): p. 5776-89.
212. Zambuzzi, W.F., et al., *On the road to understanding of the osteoblast adhesion: cytoskeleton organization is rearranged by distinct signaling pathways.* J Cell Biochem, 2009. **108**(1): p. 134-44.
213. Fromigue, O., et al., *RhoA GTPase inactivation by statins induces osteosarcoma cell apoptosis by inhibiting p42/p44-MAPKs-Bcl-2 signaling independently of BMP-2 and cell differentiation.* Cell Death Differ, 2006. **13**(11): p. 1845-56.
214. Oest, M.E., et al., *Quantitative assessment of scaffold and growth factor-mediated repair of critically sized bone defects.* J Orthop Res, 2007. **25**(7): p. 941-50.
215. Hartman, O., et al., *Biofunctionalization of electrospun PCL-based scaffolds with perlecan domain IV peptide to create a 3-D pharmacokinetic cancer model.* Biomaterials, 2010. **31**(21): p. 5700-18.
216. Basmanav, F., G. Kose, and V. Hasirci, *Sequential growth factor delivery from complexed microspheres for bone tissue engineering.* Biomaterials, 2008. **29**: p. 4195.
217. Hamada, K., et al., *Spatial distribution of mineralized bone matrix produced by marrow mesenchymal stem cells in self-assembling peptide hydrogel scaffold.* J Biomed Mater Res A, 2008. **84**(1): p. 128-36.
218. Hosseinkhani, H., et al., *Bone regeneration on a collagen sponge self-assembled peptide-amphiphile nanofiber hybrid scaffold.* Tissue Eng, 2007. **13**(1): p. 11-9.
219. Zhang, F., et al., *Sustained BMP signaling in osteoblasts stimulates bone formation by promoting angiogenesis and osteoblast differentiation.* J Bone Miner Res, 2009. **24**(7): p. 1224-33.

220. Zadravec, D., et al., *Ablation of the very-long-chain fatty acid elongase ELOVL3 in mice leads to constrained lipid storage and resistance to diet-induced obesity.* Faseb J, 2010.
221. Mahe, G., et al., *An unfavorable dietary pattern is associated with symptomatic ischemic stroke and carotid atherosclerosis.* J Vasc Surg, 2010.
222. Smit, L.A., A. Baylin, and H. Campos, *Conjugated linoleic acid in adipose tissue and risk of myocardial infarction.* Am J Clin Nutr, 2010. **92**(1): p. 34-40.
223. MacLean, C.H., et al., *Effects of omega-3 fatty acids on cancer risk: a systematic review.* JAMA, 2006. **295**(4): p. 403-15.
224. Leitzmann, M.F., et al., *Dietary intake of n-3 and n-6 fatty acids and the risk of prostate cancer.* Am J Clin Nutr, 2004. **80**(1): p. 204-16.
225. Holmes, M.D., et al., *Association of dietary intake of fat and fatty acids with risk of breast cancer.* JAMA, 1999. **281**(10): p. 914-20.
226. Willson, T., et al., *The PPARs: From Orphan Receptors to Drug Discovery.* Journal of Medicinal Chemistry, 2000. **43**(4): p. 527-550.
227. Jeninga, E.H., et al., *PPARγ regulates expression of the anti-lipolytic G-protein-coupled receptor 81 (GPR81/Gpr81).* J Biol Chem, 2009.
228. Kliewer, S., et al., *Peroxisome proliferator-activated receptors: from genes to physiology.* Recent Prog Horm Res, 2001. **56**: p. 239 - 263.
229. Chan, B., et al., *PPAR agonists modulate human osteoclast formation and activity in vitro.* Bone, 2007. **40**(1): p. 149 - 159.
230. Maurin, A.C., et al., *Role of polyunsaturated fatty acids in the inhibitory effect of human adipocytes on osteoblastic proliferation.* Bone, 2002. **31**(1): p. 260-6.
231. Pirih, F.Q., et al., *Nuclear receptor profile in calvarial bone cells undergoing osteogenic versus adipogenic differentiation.* Journal of Cellular Biochemistry, 2008. **105**(5): p. 1316-1326.
232. Grey, A., et al., *The peroxisome proliferator-activated receptor-gamma agonist rosiglitazone decreases bone formation and bone mineral density in healthy postmenopausal women: a randomized, controlled trial.* J Clin Endocrinol Metab, 2007. **92**(4): p. 1305 - 1310.
233. Lemberger, T., et al., *PPAR tissue distribution and interactions with other hormone-signaling pathways.* Ann N Y Acad Sci, 1996. **804**: p. 231 - 251.
234. Dang, Z. and C.W. Lowik, *The balance between concurrent activation of ERs and PPARs determines daidzein-induced osteogenesis and adipogenesis.* J Bone Miner Res, 2004. **19**(5): p. 853-61.
235. Takada, I. and S. Kato, *[Molecular mechanism of switching adipocyte / osteoblast differentiation through regulation of PPAR-gamma function.].* Clin Calcium, 2008. **18**(5): p. 656-61.
236. Takada, I., et al., *Suppression of PPAR transactivation switches cell fate of bone marrow stem cells from adipocytes into osteoblasts.* Ann N Y Acad Sci, 2007. **1116**: p. 182-95.
237. Hoshino, A. and Y. Isono, *Degradation of aliphatic polyester films by commercially available lipases with special reference to rapid and complete degradation of poly(L-lactide) film by lipase PL derived from Alcaligenes sp.* Biodegradation, 2002. **13**(2): p. 141-7.

238. Gerardo-Nava, J., et al., *Human neural cell interactions with orientated electrospun nanofibers in vitro.* Nanomedicine (Lond), 2009. **4**(1): p. 11-30.
239. Kumbar, S.G., et al., *Electrospun poly(lactic acid-co-glycolic acid) scaffolds for skin tissue engineering.* Biomaterials, 2008. **29**(30): p. 4100-7.
240. Nam, J., et al., *Novel electrospun scaffolds for the molecular analysis of chondrocytes under dynamic compression.* Tissue Eng Part A, 2009. **15**(3): p. 513-23.
241. Grasl, C., et al., *Electrospun polyurethane vascular grafts: In vitro mechanical behavior and endothelial adhesion molecule expression.* J Biomed Mater Res A, 2010. **93**(2): p. 716-23.
242. Persenaire, O., et al., *Mechanisms and kinetics of thermal degradation of poly(epsilon-caprolactone).* Biomacromolecules, 2001. **2**(1): p. 288-94.
243. Zeng, J., et al., *Enzymatic degradation of poly(L-lactide) and poly(epsilon-caprolactone) electrospun fibers.* Macromol Biosci, 2004. **4**(12): p. 1118-25.
244. Pitt, C., et al., *Aliphatic polyesters II. The degradation of poly (DL-lactide), poly (epsilon-caprolactone), and their copolymers in vivo.* Biomaterials, 1981. **2**(4): p. 215-220.
245. Prakash, A., et al., *Bilayers as phase transfer agents for nanocrystals prepared in nonpolar solvents.* ACS Nano, 2009. **3**(8): p. 2139-46.
246. Wang, H.B., et al., *Focal adhesion kinase is involved in mechanosensing during fibroblast migration.* Proc Natl Acad Sci U S A, 2001. **98**(20): p. 11295-300.
247. Chen, C.S., et al., *Geometric control of cell life and death.* Science, 1997. **276**(5317): p. 1425-8.
248. Xie, J. and C.-H. Wang, *Electrospun Micro- and Nanofibers for Sustained Delivery of Paclitaxel to Treat C6 Glioma in Vitro.* Pharmaceutical Research, 2003. **23**(8): p. 1817-1826.
249. Musacchio, E., et al., *Effects of unsaturated free fatty acids on adhesion and gene expression of extracellular matrix macromolecules in human osteoblast-like cultures.* Connective Tissue Research, 2007. **48**: p. 34-38.
250. Berger, J. and D. Moller, *The Mechanisms of Action of PPARs.* Annual Review of Medicine, 2002. **53**: p. 409-435.
251. Beertsen, W. and T. van den Bos, *Alkaline phosphatase induces the mineralization of sheets of collagen implanted subcutaneously in the rat.* J Clin Invest, 1992. **89**(6): p. 1974-80.
252. Gundberg, C.M., *Matrix proteins.* Osteoporos Int, 2003. **14 Suppl 5**: p. S37-40; discussion S40-2.
253. Hasegawa, T., et al., *The PPARgamma-selective ligand BRL-49653 differentially regulates the fate choices of rat calvaria versus rat bone marrow stromal cell populations.* BMC Dev Biol, 2008. **8**: p. 71.
254. Valmeseda, A., et al., *Opposite regulation of PPAR-α and -γ gene expression by both their ligands and retinoic acid in brown adipocytes.* Mol Cell Endocrinol, 1999. **154**: p. 101-109.
255. Kliewer, S.A., et al., *Fatty acids and eicosanoids regulate gene expression through direct interactions with peroxisome proliferator-activated receptors α*

and γ. Proceedings of the National Academy of Sciences of the United States of America, 1997. **94**(9): p. 4318-4323.
256. Syversen, U., et al., *Different skeletal effects of the peroxisome proliferator activated receptor (PPAR)alpha agonist fenofibrate and the PPARgamma agonist pioglitazone.* BMC Endocrine Disorders, 2009. **9**(1): p. 10.
257. Wang, X., H. Zhao, and R. Andersson, *Proteomics and leukocytes: an approach to understanding potential molecular mechanisms of inflammatory responses.* J Proteome Res, 2004. **3**(5): p. 921-9.
258. Tachimoto, H., M. Ebisawa, and B.S. Bochner, *Cross-talk between integrins and chemokines that influences eosinophil adhesion and migration.* Int Arch Allergy Immunol, 2002. **128 Suppl 1**: p. 18-20.
259. Komatsu, D.E. and S.J. Warden, *The control of fracture healing and its therapeutic targeting: Improving upon nature.* Journal of Cellular Biochemistry, 2010. **109**(2): p. 302-311.
260. Robling, A.G., A.B. Castillo, and C.H. Turner, *Biomechanical and molecular regulation of bone remodeling.* Annu Rev Biomed Eng, 2006. **8**: p. 455-98.
261. Kim, H.J., et al., *Dexamethsone suppresses bone formation via the osteoclast.* Adv Exp Med Biol, 2007. **602**: p. 43-6.
262. Kondo, T., et al., *Dexamethasone promotes osteoclastogenesis by inhibiting osteoprotegerin through multiple levels.* J Cell Biochem, 2008. **103**(1): p. 335-45.
263. Karsenty, G., H.M. Kronenberg, and C. Settembre, *Genetic Control of Bone Formation.* Annu Rev Cell Dev Biol, 2009. **25**: p. 629-648.
264. Liu, C.H., et al., *Noninvasive delivery of gene targeting probes to live brains for transcription MRI.* Faseb J, 2008. **22**(4): p. 1193-203.
265. Liu, P.K., et al., *Transcription MRI: a new view of the living brain.* Neuroscientist, 2008. **14**(5): p. 503-20.
266. Bozic, K.J. and M.D. Ries, *The impact of infection after total hip arthroplasty on hospital and surgeon resource utilization.* J Bone Joint Surg Am, 2005. **87**(8): p. 1746-51.
267. Shi, Z., et al., *Antibacterial and mechanical properties of bone cement impregnated with chitosan nanoparticles.* Biomaterials, 2006. **27**(11): p. 2440-9.
268. Nablo, B.J., et al., *Inhibition of implant-associated infections via nitric oxide release.* Biomaterials, 2005. **26**(34): p. 6984-90.
269. Choi, J.S., K.W. Leong, and H.S. Yoo, *In vivo wound healing of diabetic ulcers using electrospun nanofibers immobilized with human epidermal growth factor (EGF).* Biomaterials, 2008. **29**(5): p. 587-96.
270. Schneider, A., et al., *Biofunctionalized electrospun silk mats as a topical bioactive dressing for accelerated wound healing.* Acta Biomater, 2009. **5**(7): p. 2570-8.
271. Kim, K., et al., *Incorporation and controlled release of a hydrophilic antibiotic using poly(lactide-co-glycolide)-based electrospun nanofibrous scaffolds.* J Control Release, 2004. **98**(1): p. 47-56.

272. Lee, J.H., et al., *Microfluidic Approach to Create 3D Tissue Models for Biofilm-Related Infection of Orthopaedic Implants.* Tissue Eng Part C Methods, 2010.
273. Campoccia, D., L. Montanaro, and C.R. Arciola, *The significance of infection related to orthopedic devices and issues of antibiotic resistance.* Biomaterials, 2006. **27**(11): p. 2331-9.
274. Harris, L.G. and R.G. Richards, *Staphylococci and implant surfaces: a review.* Injury, 2006. **37 Suppl 2**: p. S3-14.
275. Gillespie, W.J. and G.H. Walenkamp, *Antibiotic prophylaxis for surgery for proximal femoral and other closed long bone fractures.* Cochrane Database Syst Rev, 2010. **3**: p. CD000244.
276. Chu, V.H., et al., *Staphylococcus aureus bacteremia in patients with prosthetic devices: costs and outcomes.* Am J Med, 2005. **118**(12): p. 1416.
277. Ritger, P. and N.A. Peppas, *A simple equation for description of solute release I. Fickian and non-Fickian release from non-swellable devices in the form of slabs, spheres, and cylinders or discs.* Journal of Controlled Release, 1987. **5**: p. 23-36.
278. Sinclair, G. and N. Peppas, *Analysis of non-Fickian transport in polymers using simplified exponential expressions.* Journal of Membrane Science, 1984. **17**: p. 329-331.
279. Lavicky, J., et al., *The effects of peptidoglycan, a pyrogenic constituent of gram-positive microorganisms, on the pharmacokinetics of rifampicin.* Toxicon, 1988. **26**(3): p. 293-300.
280. Ma, J., X. He, and E. Jabbari, *Osteogenic Differentiation of Marrow Stromal Cells on Random and Aligned Electrospun Poly(L: -lactide) Nanofibers.* Ann Biomed Eng, 2010.
281. Ishaug, S.L., et al., *Bone formation by three-dimensional stromal osteoblast culture in biodegradable polymer scaffolds.* J Biomed Mater Res, 1997. **36**(1): p. 17-28.
282. Venugopal, J., et al., *Continuous nanostructures for the controlled release of drugs.* Curr Pharm Des, 2009. **15**(15): p. 1799-808.
283. Liu, L., et al., *Radiosynthesis and bioimaging of the tuberculosis chemotherapeutics isoniazid, rifampicin and pyrazinamide in baboons.* J Med Chem, 2010. **53**(7): p. 2882-91.

Chapter 3

3.1 Chapter Summary

Incorporation of biomimetic hydroxyapatite nanoparticles into polymer nanofibers can be accomplished with electrospinning. In this work, hydroxyapatite (HAp) nanoparticles, were incorporated into poly(ε-caprolactone) (PCL) nanofibers at two concentrations – 1% and 10% of the solid weight. Rat bone marrow stromal cells were seeded on the scaffolds and their initial response was evaluated for 7 days in maintenance media, and then for the 3 following weeks in osteogenic media. Results showed differences in metabolic activity and cell coverage at days 1 and 4 while in maintenance media. However, by day 7, cell coverage values and live cell images showed very similar colonies on all three scaffolds. In osteogenic conditions, the 10% HAp scaffolds exhibited significantly increased ALP assay levels at week 3, though not at weeks 1 and 2. Osteopontin and Osteocalcin immunofluorescent microscopy revealed a trend that both mineralized scaffolds had greater amounts of both proteins though qPCR and results indicated the opposite trend for osteopontin. Additionally, type I collagen expression was decreased on HAp scaffolds. These results indicate that cells are clearly interpreting the mineralization in the nanofibers, even at just 1% w/w, and the sensing mechanism may be important in understanding scaffold design and bone tissue maintenance.

3.2 Motivation and Aims

Synthetic tissue scaffolds for bone regeneration have taken several design approaches with the intent of enhancing bone formation by marrow stromal cells (MSCs). In order to enhance progenitor cell differentiation, biomimetic designs have been explored that enhance cell functionality once progenitors are differentiated into specialized phenotypes such as osteoblasts. Soluble signals such as growth factors or cytokines have been shown to enhance osteoblastogenesis [159-162] by activating cell surface receptors. Additionally, immobilizing and presenting whole extracellular matrix (ECM) proteins such as fibronectin or short adhesion peptides such as RGS have both been shown to enhance proliferation and phenotypic behaviors [163, 164]. Previous studies have shown modestly-enhanced osteoblast phenotypic behaviors by incorporating hydroxyapatite (HAp) or other calcium phosphate phases to bulk of the scaffolds as an immobilized signal [32, 37], but unlike growth factor delivery, the mechanisms which induce changes in the cell phenotypic behaviors have yet to be clarified. The goal of this chapter is to fabricate HAp/PCL composite nanofibers by electrospinning, and then examine changes to key osteoblast behaviors.

Hydroxyapatite ($Ca_5(PO_4)_3OH$) (HAp) is the primary inorganic phase of bone tissue, and in Haversian bone it resides in gaps at the ends of type I collagen fibrils with a well-controlled crystallographic orientation [165]. As new bone is forming and existing bone is remodeled, osteoblasts secrete bone matrix vesicles (BMVs) containing Ca-rich fluid and phosphatases such as alkaline phosphatase (ALP) [49, 149] that release phosphates. HAp integration into type I collagen comprises a bone subunit, and mature bone tissue is further strengthened by its hierarchical architecture [166-168]. Cells are capable of binding to collagen through several integrin heterodimers [169], but binding to HAp crystals is believed to require adaptive proteins, notably osteopontin [153, 170,

171]. Because HAp is an important component of natural bone tissue, it is an attractive design feature for synthetic bone tissue scaffolds as a means of more closely mimicking the natural tissue composition [37, 172-176]. Thus we aim to produce HAp/PCL composite nanofibers by embedding HAp nanoparticles in PCL nanofibers.

HAp is a substantially more hydrophilic molecule than PCL. To prevent agglomeration of HAp nanoparticles during electrospinning process, one previous study included 12-hydroxystearic acid into the polymer solution as a surfactant.[38] Adding a surfactant allowed HAp to be more homogenously distributed throughout the PCL nanofibers, which in turn avoided disruptions to the fiber scaffold morphology (i.e. microbeads). In this study, we have used oleic acid (OLA) sodium salt to prevent agglomeration of HAp nanoparticles. OLA is an organosoluble fatty acid salt that is non-toxic to cells. It is a known agonist to peroxisome proliferator–activator receptors (PPARs), a class of nuclear receptors [177]. PPARs have been associated with a wide range of cellular functions and processes [145, 178-180]. In order to account for possible effects of PPAR, the concentration as held constant for all scaffolds

In this chapter, PCL scaffolds with two different concentrations of HAp were fabricated using electrospinning process. In order to account for any potential effects of OLA on PPARs, the concentration was kept constant for all scaffolds. The effects of modulating HAp concentration were examined on marrow stromal cells cultured in maintenance media through seven days, and then in osteogenic media for three weeks. The effect of increasing the concentration of HAp in PCL scaffolds was investigated in terms of marrow stromal cell adhesion and proliferation in maintenance conditions and expression of osteoblast phenotypic genes in osteogenic conditions.

3.3 Methods

3.3.1 Fabrication and characterization of HAp-PCL nanofiber scaffolds

Nanofiber scaffolds were fabricated using electrospinning process. A polymer solution was prepared by dissolving of 12% w/w PCL (Sigma) with 3% oleic acid sodium salt in a solvent mixture of 3:1 chloroform and methanol (Sigma), and 0%, 1% and 10% w/v of hydroxyapatite (HAp) nanoparticles (size≤200 nm, Sigma) were homogeneously mixed into this solution to achieve different concentrations of HAp in the scaffolds. A high-voltage power supply (Gamma High Voltage) was applied between 18-21 kV on a blunt-tip catheter positioned 4-4.5" from a grounded collector. The polymer solution was fed to the catheter tip by a syringe pump (Kent Scientific) at 1.8-2.1 mL/hr and the scaffolds were deposited on the grounded collector.

In order to examine the morphology of the nanofiber scaffolds, they were sputter-coated with 10 nm of gold and imaged under high magnification using a field-emission scanning electron microscope (SEM, JEOL JSM-6500F) followed by an EDX spatial elemental mapping examination. Instrument aperture and probe current were adjusted to give a dead time of 15–20%. Surfaces were analyzed for 5 min at 5–15 kV and a magnification of 100–5000x to provide a complete profile of the different elements present. Spatial element mapping was performed by grouping pixels with similar atomic spectra. Fiber diameters were measured using SEM image analysis software. Ten measurements were made on each scaffold with n_{min} = 30 and size distribution histogram was plotted.

Thermal characterization of the nanofiber scaffolds was performed to determine the effect of electrospinning process on polymer crystallinity and thermal stability. Digital scanning calorimetry (DSC, TA Instruments DSC 2920) was used to determine the polymer crystallinity in different nanofiber scaffolds. The scaffolds were heated from 5^{o}C

to 120°C at 5°C/min and the crystallinity of a sampled was calculated by the following equation:

$$X_c\% = 100 \times \frac{\Delta H_{m,sample}}{\Delta H_{m,std}}$$

where $\Delta H_{m,sample}$ is the enthalpy of melting of the nanofiber scaffold and $\Delta H_{m,std}$ is the enthalpy of melting of 100% crystalline PCL ($\Delta H_{m,std}$ = 139 J/g) [174]. Thermogravimetric analysis (TGA, TA Instruments TGA 2950) was used to measure the change in mass as a function of temperature. The nanofiber scaffolds were heated from 25°C to 700°C at 10°C/min and the weight loss was measured. In both the thermal analysis techniques, polymer pellets that had not been subjected to electrospinning process were used as controls, and are noted as "Source PCL".

3.3.2 Rat marrow stromal cell culture

Marrow stromal cells (MSC) were isolated from male Wistar rats (*Rattus norvegicus*) supplied by Harlan Sprague Dawley, Inc (separate time points, unmixed cell populations). Limbs were aseptically removed from recently euthanized animals. Soft tissue was removed and the bones were briefly stored in cold PBS before isolating cells. Metaphyseal ends of the bones were removed to expose the bone marrow cavity. In a 50 mL conical tube, marrow was repeatedly flushed with maintenance media (α-MEM with 10 % fetal bovine serum (FBS, Sigma) and 1 % penicillin/streptomycin (pen/strep, Sigma)) using 10 mL syringes with 18 and 25 gauge needles. Media containing cells and debris was filtered with a 70μm nylon filter into a clean tube. Cells were counted using a hemocytometer before seeding. Control (smooth PCL) and electrospun scaffolds (NF and MN) (surface area approximately 0.7 cm^2) were sterilized by exposing them to UV light for 60 min followed by soaking in 70 % ethanol for 60 min. The

substrates were then washed twice with warm PBS followed by warm culture media prior to MSC seeding. Cells were seeded on scaffolds in a 24-well plate at a density of 1 million per well. Cultures were incubated at 37.0 °C and 5 % CO_2 for the duration of the study. Half of the media was changed at day 4. On Day 7, the media was replaced with osteogenic differentiation media (α-MEM with 10% fetal bovine serum, 1% penicillin-streptomycin, 10^{-8} M dexamethosone, 50 μg/mL ascorbic acid, 8 mM β-glycerolphosphate). Media was changed every 2 days for up to 3 weeks of culture. All scaffolds were cultured and assayed in triplicate at each time point specified (i.e. 1, 2, or 3 weeks post-differentiation, n=6).

3.3.3 MSC adhesion and proliferation on HAp-PCL nanofiber scaffolds

After 1, 4, and 7 days of culture in maintenance media, cell responses to the scaffolds were investigated through cell adhesion, and viability (mitochondrial activity) viability was examined after 1 and 4 days. Cells adhesion was investigated using the live cell stain calcein AM (Invitrogen) (ex: 485 nm, em: 530 nm). Calcein AM can penetrate live cell membranes, where the AM is cleaved and the resulting calcein molecule fluoresces green. The cells were incubated in 2 mM of calcein AM in PBS for 45 min and were imaged with a fluorescence microscope (Zeiss) with appropriate filters. Images were analyzed (ImageJ, NIH) to compute the percent area covered by live cells for comparison with the cell viability assay.

Cell viability was measured after 1 and 4 days of culture (log phase growth) using a commercially available MTT assay kit (Sigma). Adhered cells were incubated at 37 °C for 3 hours in a (3-[4,5-dimethylthiazol-2-yl]-2,5-diphenyl tetrazolium bromide (MTT) solution. Mitochondrial dehydrogenases of viable cells cleave the tetrazolium ring, yielding purple formazan crystals. Formazan crystals were then dissolved in the MTT

solvent with 10% (volume) Triton-X. The optical density (OD) of the solvent is proportional to the mitochondrial activity of the cells on the surface. OD was measured at 570 nm using a spectrophotometer (FLUOstar Omega; BMG Labtech, Durham NC). Background absorbance at 690 nm was subtracted from the measured absorbance.

3.3.4 MSC differentiation on HAp-PCL nanofiber scaffolds

MSC responses to the electrospun scaffolds were investigated 1, 2, and 3 weeks after providing the cells with osteogenic differentiation media. A colorimetric alkaline phosphatase (ALP) assay, total protein assay, quantitative polymerase chain reaction (qPCR), and immunofluorescent staining were used to evaluate the cell responses to nanofibrous architecture with varying concentrations of HAp nanoparticles.

In order to quantify intracellular ALP production at weeks 1, 2, and 3, cells were lysed by incubation in CellLytic® (Sigma) at room temperature, and the lysate was used for ALP and BCA total protein assay. ALP activity was measured using a commercially-available colorimetric assay kit (Quantichrome™ BioAssay Systems), and the manufacturer's protocol was followed[181]. Briefly, ALP catalyzes the reaction removing the phosphate from *p*-nitrophenolphosphate (*p*-NPP), thus yielding *p*-nitrophenol, and the p-nitrophenol concentration is measured by the absorbance at 405 nm. The same lysate was also used to determine the total intracellular protein content using a commercially available BCA (bicinchoninic acid) assay (Pierce Biotechnology). The absorbance of the solution was measured using a plate reader at a wavelength of 570 nm and was converted to protein content using an albumin standard curve. All of the ALP data was normalized with the total protein content to account for changes in number of cells present on each surface.

The expression levels of several key bone-related genes were measured with qPCR after 1, 2 and 3 weeks of culture. Messenger RNA (mRNA) was purified from other nucleic acids (rRNA, tRNA, DNA) using an RNeasy extraction kit (Qiagen). Genomic DNA (gDNA) contamination was avoided by degrading any remaining gDNA with DNaseI (Fermentas). Complimentary DNA (cDNA) template was generated from mRNA with a first-strand synthesis kit (Fermentas), and both the DNaseI and reverse transcriptase enzymes were thermally inactivated after their respective steps according to the manufacturer's protocols. cDNA was stored in at -80^{o}C until further use. For PCR reactions, primers were either designed as documented below, or were purchased as a forward-reverse primer mix (Qiagen). Custom-designed primers (**Table 3.1**) were validated by running gel electrophoresis with the product to ensure that the amplicon length matched the predicted length, and by performing a melt curve step at the end of real-time quantitative PCR (qPCR) to verify the presence of a single amplicon.

Table 3.1 - Custom primers used for qPCR

Osteopontin: *Forward:* atcaggacagcaacgggaagac *Reverse:* gagttccaaagccagcctggaa *Amplicon length*: 224 bp Collagen IαI: *Forward:* acagaggcataaagggtcatcg *Reverse:* cctggcaaagatggactcaacg *Amplicon length:* 159 bp

The amplicon from successful reactions was purified using the ethanol precipitation method [182]. Finally, purified amplicon concentrations were measured with a spectrophotometer (Nanodrop, Thermo Scientific), and standards were then diluted with DNase-free water for use in calculating the copy number from test qPCR reactions.

After three weeks in osteogenic media, scaffolds were removed and immuno-labeled for osteopontin and osteocalcin. Cells were fixed with 3.7% paraformaldehyde in PBS solution and permeabilized with a 1% Triton-X in PBS solution. Blocking serum of 40 μg/mL of trypan blue (Sigma) and 100 μg/mL of bovine serum albumin in PBS was used to reduce non-specific antibody binding. After rinsing and blocking, the scaffolds were incubated in either an osteopontin primary antibody (1:100 in PBS, V-19 purified goat polyclonal antibody of mouse origin, Santa Cruz Biotechnology) or an osteocalcin primary antibody (P-18 purified goat polyclonal antibody of mouse origin, Santa Cruz Biotechnology) for one hour. After an additional blocking step and PBS wash, the scaffolds were then incubated in a FITC-conjugated secondary antibody (1:200 donkey anti-goat IgG, Santa Cruz Biotechnology) for 45 minutes in the dark. The scaffolds were rinsed once more before being imaged under 470 nm excitation wavelength using a fluorescence microscope (Zeiss).

3.3.5 Statistical analysis

All test and control substrates were cultured and assayed in triplicate at each time point specified. The experiments were conducted in duplicate using different animals as the MSC source for each study. The data was pooled from the studies using different cell sources. All the statistics presented here as a mean +/- standard deviation. A general linear model of ANOVA with a Tukey adjustment for multiple comparisons was used to determine the effects of treatment (HAp concentration), time (days or weeks where noted), and the interaction of treatment by time. Any data point with a student residual value greater than 3 was deemed an outlier, and the ANOVA was re-calculated with that point removed. Any effect (HAp, time, or HAp*time) with a p-value less than

0.05 was considered significant. For significant effects, assay values at each were compared using a two-way t-test and p-values were reported.

3.4 Results

3.4.1 Fabrication and characterization of HAp-PCL nanofiber scaffolds

In this study, PCL nanofiber scaffolds were fabricated with 0%, 1%, and 10% HAp nanoparticles embedded within the nanofibers. The scaffolds were examined under SEM to examine the scaffold morphology and fiber diameters. The results here showed continuous nanofibers for all three scaffolds with no observable nanoparticle agglomeration or fiber distortion due to the presence of HAp (**Figure 3.1 (A, B)**). There was a measurable, though small decrease in the mean fiber diameter for scaffolds with

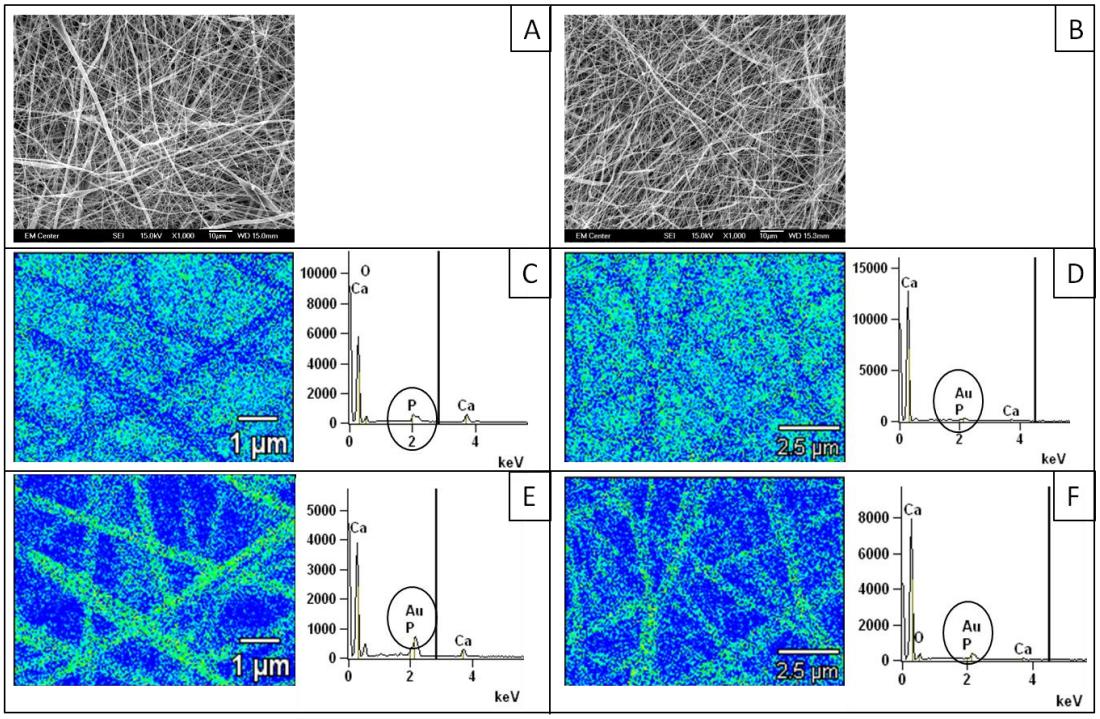

Figure 3.1 – SEM (A and B) and EDX (C-F) images of 10% (A, C, E) and 1% (B, D, F) HAp scaffolds. Atomic spectra showed next to the corresponding EDX images

10% HAp (**Figure 3.2 (A)**), from 360 nm to 290 nm. However, for all three scaffold types, >80% of the fibers measured within 200-500 nm in diameter (**Figure 3.2 (B)**). HAp-free scaffolds were examined in Chapter 2 and SEM images may be viewed in that chapter.

Further, EDX was used demonstrate the distribution of HAp nanoparticles in the PCL nanofibers. The two spectral images for each scaffold type show a difference between the gold-coated surface (**Figures 3.1 (E and F)**) and the signal from the

uncoated interior (**Figures 3.1 (C and D)**). Both show the presence of calcium and phosphorus, but only the surface spectra show gold. Additionally, the homogenous appearance of spectral maps strongly suggests that HAp nanoparticles are relatively evenly distributed throughout the polymer nanofibers.

Thermal gravimetric analysis (TGA) and digital scanning calorimetry (DSC), were used to measure the composition and crystallinity of the PCL/HAp nanofiber scaffolds.

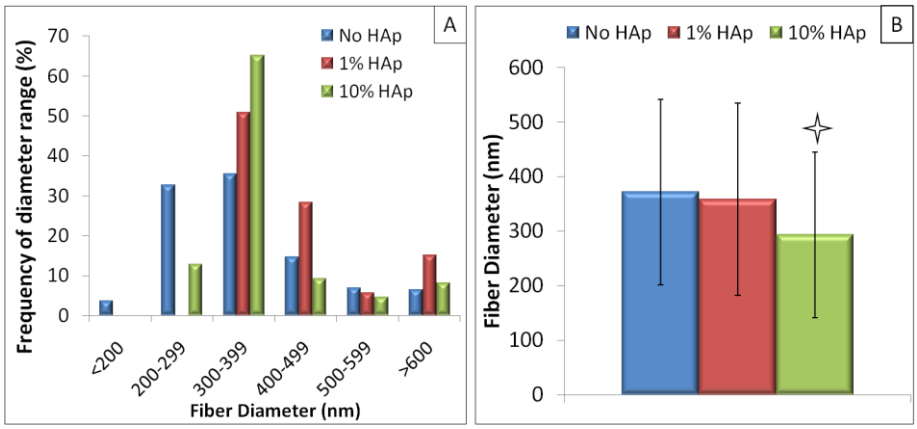

Figure 3.2 – Fiber diameter histogram (A) and mean fiber diameters (B) for all three scaffolds.

TGA was analyzed over a range of temperatures associated with PCL mass loss, but not HAp loss [174], and the mass lost during analysis was PCL. Source PCL was included to describe any changes to the polymer due to electrospinning process and HAp nanoparticles. DSC did not measure any significant difference between the three scaffolds (HAp-free, 1% HAp, and 10% HAp) as well as the source PCL (**Figure 3.3 (A)**). However, TGA showed significant differences in mass loss between 10% HAp all other

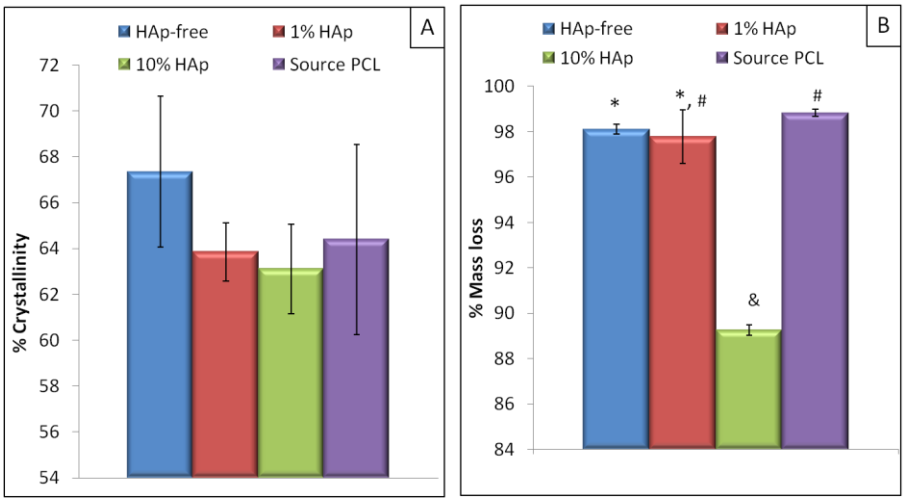

Figure 3.3 - % crystallinity (A) and mass loss (B) measured by DSC and TGA respectively.

samples (**Figure 3 (B)**). All three scaffolds and the source PCL showed slightly lower mass losses than anticipated, and there was no significant difference between 1% and HAp-free scaffolds. However, each material was displaced from its anticipated value by 1-2%, which may have simply been due to measurement uncertainty. Overall, between the SEM and EDX images, there is strong evidence that HAp nanoparticles are relatively homogenously distributed throughout the nanofibers, and TGA provides strong evidence that the desired amounts of 1% and 10% wt HAp nanoparticles were incorporated into PCL nanofibers.

3.4.2 MSC adhesion and proliferation on HAp-PCL nanofiber scaffolds

Fresh marrow stromal cells were harvested from rat long bones and seeded onto scaffolds at a density of $1x10^6$ cells/scaffold. The cells cultured in maintenance media free of differentiation factors, and the metabolic activity was measured after 1 and 4 days of culture using MTT assay, and live cells were stained with calcein AM after 1, 4, and 7 days of culture. The metabolic activity was measured using a commercially-available MTT assay kit, and days 1 and 4 were chosen because this period is associated with log-phase population growth. The MTT results (**Figure 3.4**) show that HAp-free scaffolds supported the greatest overall metabolic activity, followed by 10% HAp and then 1% HAp,

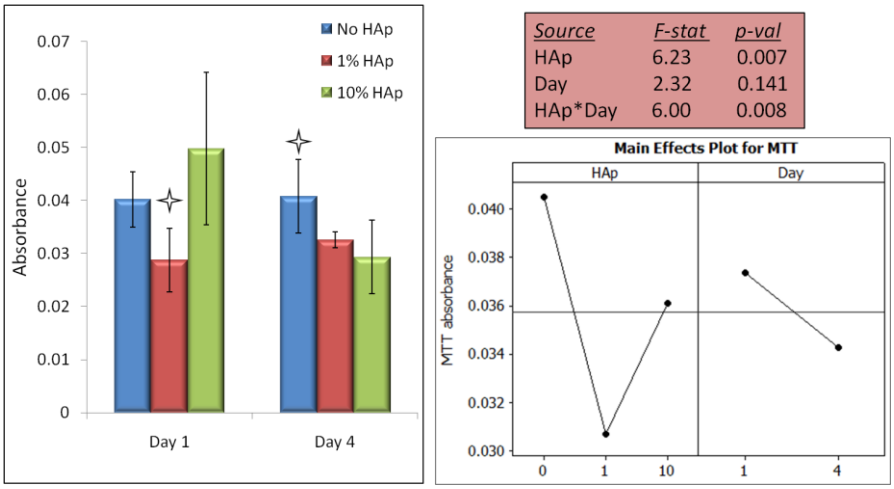

Figure 3.4 – Metabolic activity levels measured by an MTT assay

and the effect of HAp was significant (p=0.007)

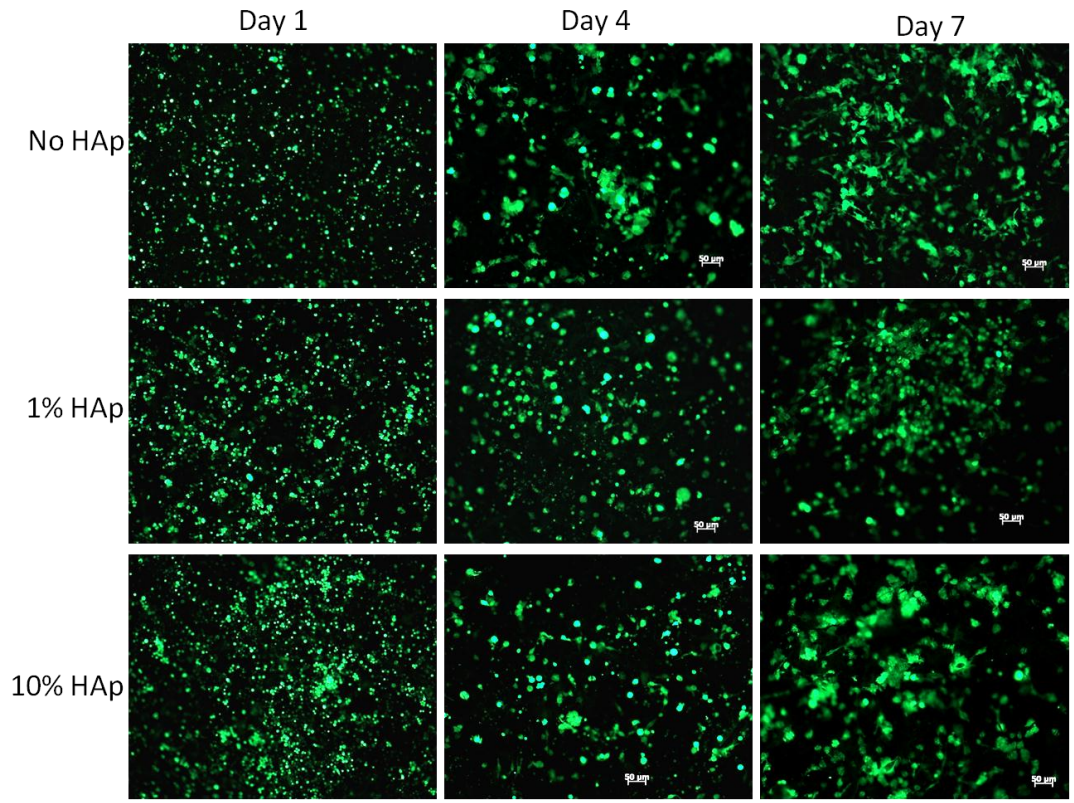

Figure 3.5 – Fluorescent images of live cells stained by calcein AM on HAp-free, 1% HAp, and 10% HAp scaffolds at days 1, 4, and 7

Calcein AM was used to image live adhered cells on the scaffold surfaces. The fluorescence microscopy images were used to calculate the scaffold surface area covered by live cells. The images (**Figure 3.5**) show similarities for cells on the different scaffolds. At day one, cells on all three scaffolds clearly had adhered in large numbers, but they were very small

Cell coverage

Source	*F-stat*	*p-val*
HAp	2.08	0.154
Day	3.54	0.051
HAp*Day	2.27	0.102

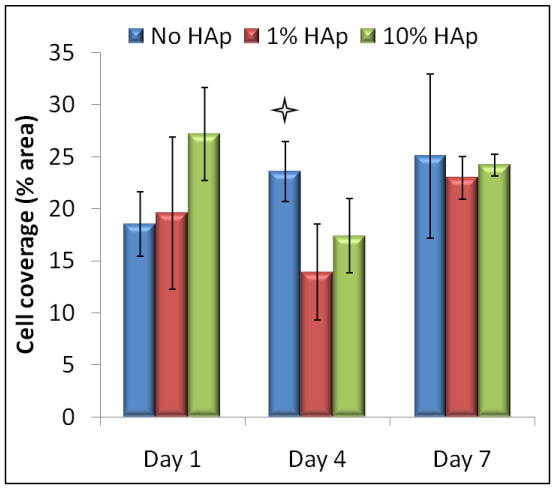

Figure 3.6 – Live cell coverage of scaffold surfaces measured at days 1, 4, and 7

compared to later days. By day four, cells were larger though possibly less densely populated. At this point, a measurable difference between cells on HAp-free scaffolds and 1% and 10% scaffolds was apparent (**Figure 3.6**). However, by day 7 the cells were large and densely populated on all scaffolds and there was no significant difference in cell coverage and the fluorescent images showed strong similarities between scaffolds.

3.4.3 MSC differentiation on HAp-PCL nanofiber scaffolds

In order to evaluate differences in the osteogenic capacity of HAp-PCL scaffolds, the cells were differentiated with glucocorticoids at day seven. After 1, 2, and 3 weeks in osteogenic media, intracellular ALP was measured by colorimetric assay and the expression level for several key genes were measured by quantitative polymerase chain reaction (qPCR). Alkaline phosphatase (ALP) activity and total protein were measured using commercially-available, colorimetric assay kits and ALP was normalized with the amount of total protein. ALP activity was very low on all three scaffolds after week one (**Figure 3.7**). At week two, all three scaffolds supported marked increases in ALP, although there were no significant differences. By week three, cells on 10% HAp produced significantly more ALP than cells on HAp-free scaffolds, and neither level was

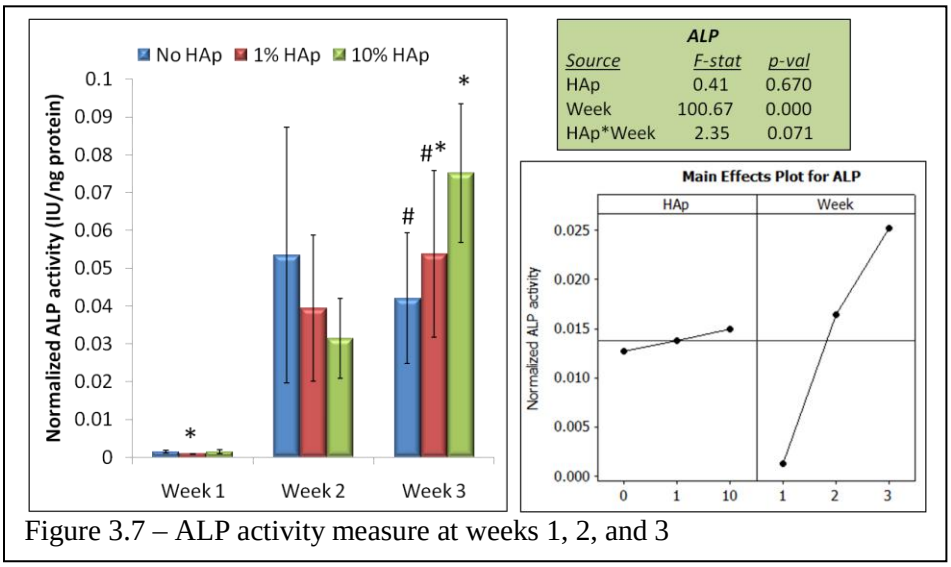

Figure 3.7 – ALP activity measure at weeks 1, 2, and 3

significantly different from 1% HAp scaffolds. Overall, the effect of time (weeks) was highly significant and the interaction of HAp and week was nearly significant (p=0.07).

Quantitative polymerase chain reaction (qPCR) was used to precisely measure the levels of gene expression for several key genes related to osteoblast behaviors. The expression level for each gene was normalized with respect to RPL13A, a housekeeping gene that encodes for the 60s ribosomal subunit protein, L13A. The $\log_{10}$, normalized expression levels were then used for an ANOVA with an adjustment for multiple comparisons.

RhoA is a small GTPase associated with actin cytoskeletal reorganization and it has shown to be key for osteoblast behaviors [183-185]. RhoA expression levels were significantly affected by HAp concentration, week, and the interaction of HAp with week (**Figure 3.8**). Overall, HAp-free scaffolds supported the greatest levels of RhoA expression, followed by 10% HAp and then 1% HAp. It is important to note that the expression levels only show statistical significance within a time-point at week three. At week three, cells on 1% and 10% HAp scaffolds had down-regulated RhoA expression whereas cells on HAp-free scaffolds maintained expression levels consistent with the previous two weeks

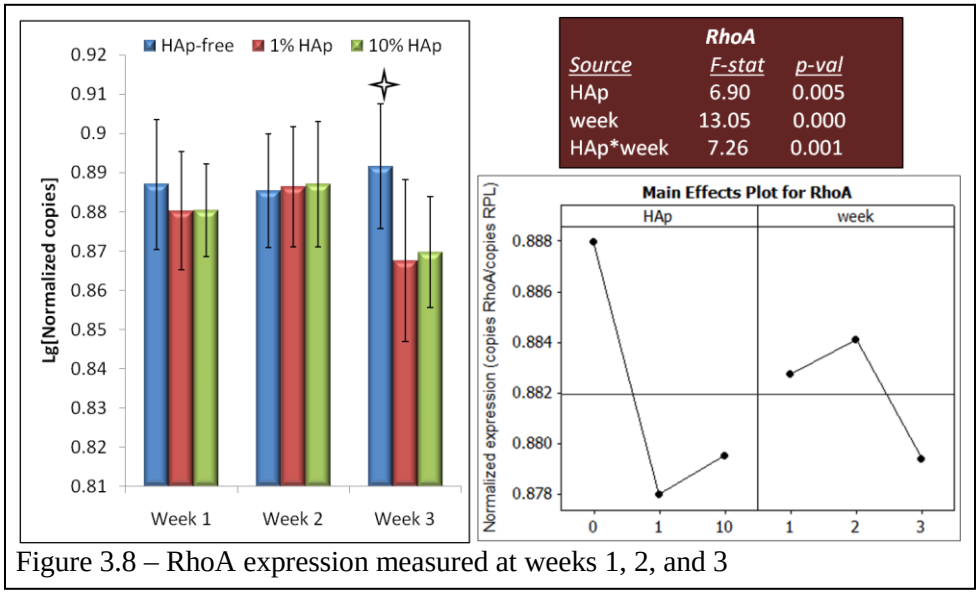

Figure 3.8 – RhoA expression measured at weeks 1, 2, and 3

Casein Kinase II (CKII) is a serine/threonine kinase that has been shown to be the major relevant kinase of bone phosphoproteins such as osteopontin [186-188]. The effects of HAp, week, and the interaction of HAp and week were all significant, though the effects were over a relatively narrow range of normalized expression levels (**Figure 3.9**). Both HAp and week had the effect of decreasing the expression levels, but it should be noted that in week one, 10% HAp supported the greatest expression of CKII which was significant relative to cells 1% HAp scaffolds. At week two, expression levels were very similar, and then at week three, cells on HAp-free scaffolds expressed CKII at levels significantly greater than cells on either HAP scaffold.

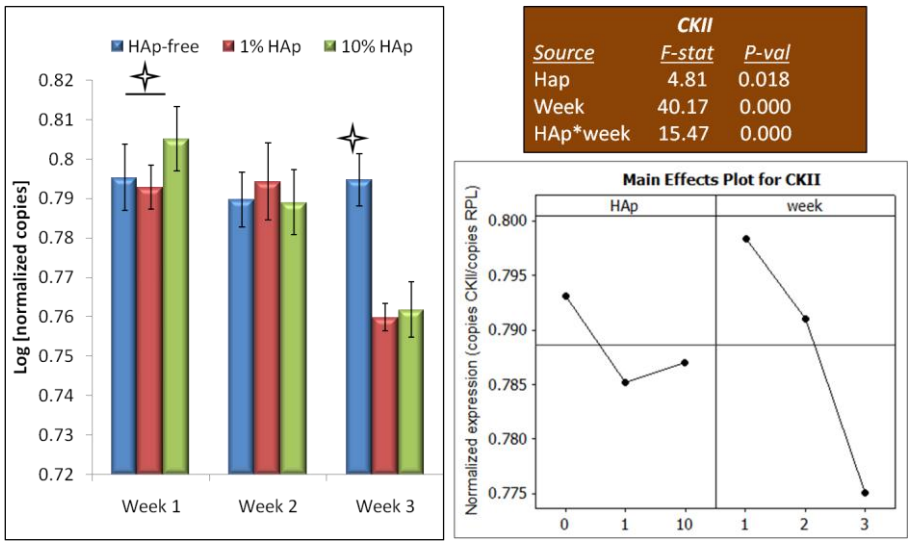

Figure 3.9 – Casein Kinase II expression measured at weeks 1, 2, and 3

Osteopontin (OP) is a bone matrix phosphoprotein secreted by both osteoblasts and osteoclasts [170, 187, 189]. Both main effects (HAp and week) and the interaction effect were all significant within a narrow range (**Figure 3.10**). At week one, cells on 10% HAp expressed greater levels than cells on 1% HAp scaffolds, and at week three, cells on HAp-free scaffolds expressed significantly greater levels of OP than cells on either HAp scaffold. Overall, cells on HAp-free scaffolds expressed the greatest amount of OP, followed by cells on 10% HAp and then 1% HAp scaffolds.

Collagen I is the major organic phase of bone matrix, and is secreted by

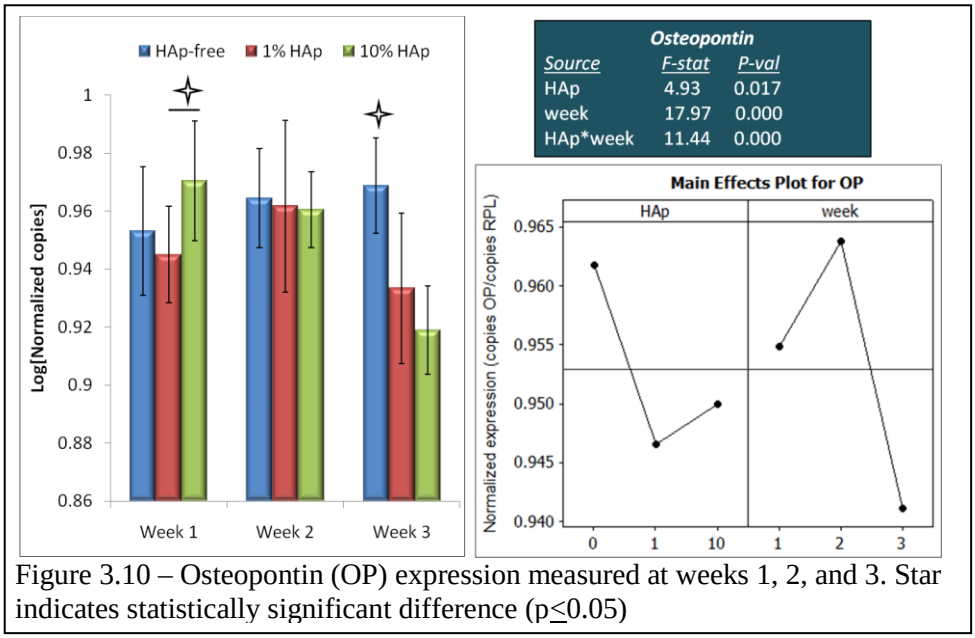

Figure 3.10 – Osteopontin (OP) expression measured at weeks 1, 2, and 3. Star indicates statistically significant difference ($p \leq 0.05$)

osteoblasts during bone synthesis. As with other genes, both main effects and the interaction effect were significant though the differences were over a small range of expression levels (**Figure 3.11**). Overall, cells on HAp-free scaffolds expressed the greatest amounts of collagen I, followed by cells on 1% HAp and then 10% HAp scaffolds. Cells on HAp-free scaffolds also had sustained gene expression through three weeks whereas cells on both HAp scaffolds displayed a marked decrease in collagen expression at week three.

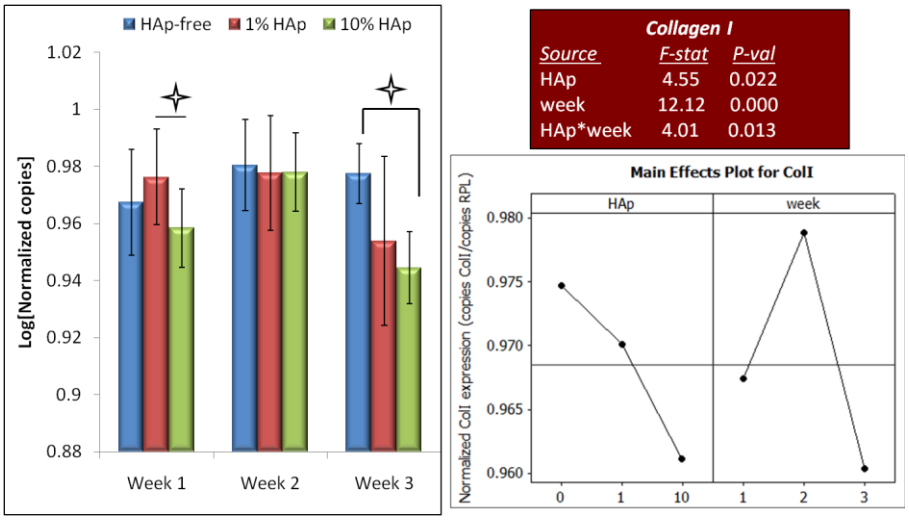

Figure 3.11 – Type I collagen expression at weeks 1, 2, and 3. Star indicates statistically-significant difference ($p \leq 0.05$)

At week 3, cells were immunolabeled for either osteopontin or osteocalcin and then viewed under a fluorescence microscope. The images revealed presence of both bone matrix proteins on all the scaffolds (**Figure 3.12**). Many small depositions were visible on scaffold surfaces, and larger aggregates (>50 μm) were also observed, more so on 10% HAp scaffolds. In general, greater amounts of both bone matrix proteins were evident on the 10% HAp scaffolds as compared to 1% and HAp-free scaffolds.

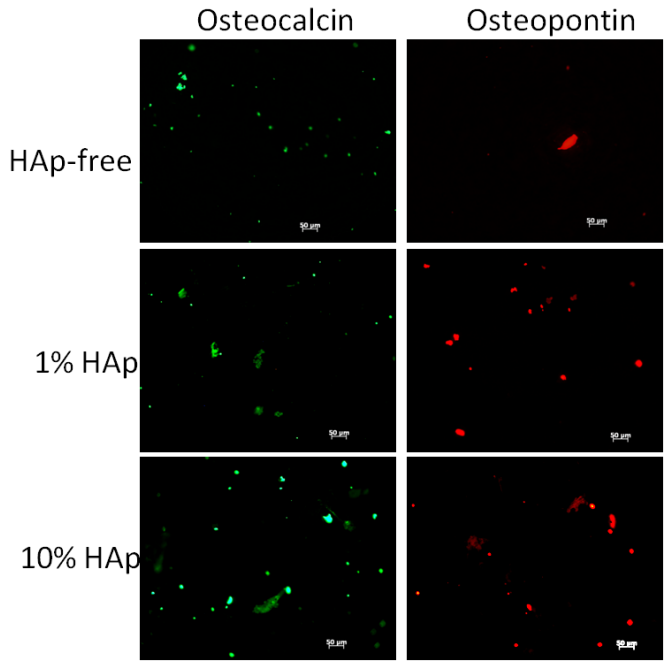

Figure 3.12 – Immunolabeled OP and OC after 3 weeks in osteogenic media. Scale bars are 50 μm

3.5 Discussion

The aim of this study was to determine the effects of including and varying the amount of HAp nanoparticles in polymer nanofibers would affect cell adhesion and proliferation as well as osteoblast phenotypic behaviors. In order to assess these cell responses, HAp-free scaffolds were fabricated along with scaffolds with 1% w/w HAp or 10% w/w HAp nanoparticles. To prevent agglomeration of hydrophilic HAp nanoparticles in a solution with organic solvents and hydrophobic PCL, a surfactant was included in the electrospinning solution. Incorporation of HAp nanoparticles in polymer nanofibers has been successfully demonstrated in prior research studies[190] with similar scaffolds, but they did not use a surfactant and they reported some particle

agglomeration [190]. By contrast, these nanofibers were fabricated with oleic acid (OLA), an 18-carbon, w-9 monounsaturated fatty acid. Kim *et al* (2006) used a different fatty with the sole function being fabricating mineralized nanofibers without agglomeration,[38] but OLA may enhance bone formation through activation of fatty acid receptors [143, 191]. Thus, the concentration of OLA was kept as a constant level for all scaffolds used in this study

Scaffold characterization by SEM showed that differences between HAp-free and 1% HAp scaffolds were nominal while both scaffolds were statistically different from 10% HAp scaffolds. It is important to note that the mean fiber value shifted from ~360 nm for HAp-free scaffolds to 290 nm for 10% HAp scaffolds (**Figure 3.2 (B)**). However, looking at the fiber diameter histogram (**Figure 3.2 (A)**), all three scaffolds have their median value in the same diameter range (300-399 nm), and >80% of the fiber diameters fall within 200-500 nm. Furthermore, differences over this low range of fiber diameters have been shown to be of negligible importance for osteoblasts and fibroblasts, a phenotype sharing a very similar transcriptome to that of osteoblasts [192], on similar nanostructured materials [140, 193]. Given that additional variables in the system here include surface chemistry and mechanical stiffness due to HAp nanoparticles, it is reasonable to conclude that the differences in fiber diameter are not important to the cellular responses.

Fracture repair involves multiple overlapping healing phases involving wide range of processes for cell recruitment and signaling [194-196], ECM production [197-200], and then ECM remodeling [201-203]. Fundamental to each of these processes is the ability for cells to adhere and proliferate in the repair area. By imaging live cells with a calcein AM fluorescent stain, measuring their coverage area, and measuring metabolic activity with an MTT assay, cell adhesion and colonization can be evaluated. The correlation

between cell coverage and MTT was strong; with the measured cell coverage values closely matching MTT absorbance values at days one and four (**Figures 3.4 & 3.6**). The initial days after cell seeded are associated with log phase population growth and proliferation on tissue scaffolds, and MTT absorbance values are used as relative measures of overall metabolic activity for the cell population. Metabolic expenditures during this time are likely to go towards proliferation, though it is clear from the fluorescent stain that substantial cell spreading occurred (cytoskeletal formation and reorganization) during the first week. It should be noted that by day seven, cell coverage values were very similar, which is important because osteogenic differentiation factors were added to the cell media at that point. This finding is consistent with recent literature examining nanofiber scaffolds containing HAp nanoparticles [175].

In order to evaluate the effects of HAp on bone matrix production for each of the three weeks in osteogenic media, a colorimetric ALP assay along with qPCR for five genes. After three weeks in osteogenic media cells were also immunolabeled for two bone matrix proteins, OP and OC. Of the five genes, two bone matrix genes (OP, Col1) were selected to determine changes in bone matrix production along with the ALP colorimetric assay, two genes (CKII and RhoA) were selected that would illustrate cell adaptations due to HAp nanoparticles, and one housekeeping gene (RPL13A) was used to normalize expression values.

Alkaline phosphatase (ALP) is a key enzyme in bone matrix vesicles that cleaves organic phosphate esters, thus supplying mineral nucleation sites with phosphate ions [149, 204, 205]. Its expression profile is typically associated with a peak during early differentiation of progenitor cells into immature osteoblast phenotypes, and then production tapers off as osteoblast cells either mature into osteocytes or undergo apoptosis [206]. The results show that while HAp is not significant overall (while not

separating the effects of weeks), the effect of weeks is significant and the interaction of HAp and weeks is borderline significant (p=0.07). Due to the large temporal changes in ALP expression, it is valuable important to look at the interaction of HAp and weeks than it is to look at HAp on its own. The final time point, week three, shows that ALP is most abundant on 10% HAp scaffolds, and the t-test at that time point is significant over HAp-free scaffolds. Previous studies examining ALP expression on polymer-mineral composite scaffolds used more homogeneous cell populations and also found a similar trend of small increases in ALP activity on mineralized scaffolds [35, 37, 175, 207]. Since these studies used several different polymers and demonstrated similar results, this nominal overall increase in ALP activity through three weeks on synthetic polymer-HAp scaffolds can be considered to be a predictable result.

Collagen I (Col1) and osteopontin (OP) are organic components of bone tissue. OP is part of the family of non-collagenous proteins (NCPs) referred to as SIBLING (Small Integrin-Binding LIgand, N-Linked Glycoprotein) proteins [208]. Col1 is the major organic phase of bone and makes up ~30% of bone mass. Both proteins are expressed by osteoprogenitors, pre-osteoblasts and osteoblasts, though OP is expressed in greater levels across multiple phenotypic phases while Col1 is expressed highest by matrix-producing osteoblasts and then is down-regulated in a similar manner as ALP [39]. The expression levels for both Col1 and OP were similar with HAp-free scaffolds supporting the greatest overall expression levels, followed by 10% and then 1% scaffolds (**Figures 3.10 & 3.11**). Down-regulation of Col1 has been identified as an indicator that matrix-producing osteoblasts are continuing on their maturation path. This is somewhat in contradiction to ALP activity levels which may be expected to approximate Col1 expression levels [39]. However, the overall expression level of Col1 was still very high and ALP levels generally decrease between the third and fourth week.

By examining expression levels for two enzymes, casein kinase II (CKII) and RhoA, that play important roles in regulating bone formation and osteoblast behaviors, potential mechanisms influencing differences in cell responses to PCL-HAp scaffolds may be identified. CKII is a serine/threonine kinase that is believed to be responsible for most of the physiologically-relevant phosphorylation for bone phosphoproteins such as OP [186]. It phosphorylates the side-group on serine residues, and the degree of phosphorylation of bone matrix proteins such as OP is believed to up or down-regulate local bone remodeling behavior by osteoblasts and osteoclasts [171, 209]. RhoA, a small GTPase associated with key osteoblast behaviors as well as actin cytoskeletal remodeling. Recent findings have identified RhoA as not only a regulator or osteoblastogenesis[184, 185], but also of mechanotransduction [183] and apoptotic regulation specifically for osteoblasts [210].

The qPCR results show only nominally higher RhoA expression levels by cells on HAp-free scaffolds at week one, then equal expression levels at week two before significantly greater expression levels by cells on HAp-free scaffolds at week three (**Figure 3.8**). Similarly, CKII expression levels were differentially regulated with statistically significance overall. At week one, 10% HAp scaffolds supported the highest expression, while week two levels were highly similar on all scaffolds, and week three levels were highest on HAp-free scaffolds (**Figure 3.9**). The overall effect of HAp was significant for both proteins, and HAp-free scaffolds supported the greatest overall expression. Since both RhoA and CKII are dependent on phosphorylation for to switch between active and inactive states [183], further studies focused on changes in activation of both enzymes will be necessary. However, RhoA is subject to proteosomal degradation through ubiquitination [211], and osteoblasts have been shown to completely eliminate cytosolic RhoA in as little as 18 hours [212]. Therefore, significant

differential RhoA expression levels are a strong indicator that RhoA should be explored as a means to explain differential osteoblast behaviors in response to PCL-HAp nanofiber scaffolds.

The qPCR data for these four genes points to several important conclusion regarding mineralized polymer scaffold design. Most notably, the greatest expression levels for OP, CKII, and RhoA occurred on HAp-free scaffolds, followed by 10% HAP, and then 1% HAp (**Figures 3.8, 3.9, and 3.10**). Col1 deviated from this trend with HAp-free scaffolds supporting the greatest expression, followed by 1% HAp and then 10% HAp (**Figure 3.11**). This demonstrates that cells are very sensitive to changes in extracellular mineralization, and bone-related gene expression may be moderately suppressed with low HAp concentrations within the nanofibers, as evidenced on 1% scaffolds. Aside from Col1, gene expression moderately increased between cells on 1% and 10% HAp concentration. However, the expression levels supported by 10% HAp scaffolds were still less than HAp-free scaffolds and closer in value to 1% scaffolds.

This is the first study to report Col1 and CKII expression levels by qPCR, and one of only two that have examined gene expression for bone matrix proteins [175]. However, the similarity of ALP activity levels between this and previous studies indicates that these gene expression values can be received with confidence [37, 207]. Overall, the data indicates that the cells sense mineralized, fibrous architecture in their extracellular environment. This chemistry and architecture causes the cells to reduce their bone matrix production, as indicated by the Col1 and OP expression levels. Additionally, the similar expression patterns for CKII and OP suggest that it is unlikely that OP would be phosphorylated to different degrees between treatments. Thus, the mineralization within the polymer nanofibers is the main cause of differential bone matrix production.

3.6 Conclusion

PCL nanofiber scaffolds were fabricated to be HAp-free, or have either 1% or 10% HAp nanoparticles within the PCL nanofibers. Material characterization methods verified that the desired nanofibrous morphology and compositions were achieved, and a difference in mean fiber diameter was unlikely to significantly affect the cell population. There were difference in the initial levels of metabolic activity, but by day seven, the cell populations, as measured by coverage, were very similar. Once in osteogenic media, cells on 10% HAp scaffolds supporting the greatest ALP levels at week three, though there were no differences at weeks one or two. qPCR data demonstrated that key genes were differentially regulated. Type I Collagen (Col1) expression levels decreased in a manner dependent on HAp concentration, while OP, CKII, and RhoA depended more on the presence than concentration of HAp. The presence of HAp in these PCL nanofiber scaffolds caused a decrease in OP, CKII and Col1 expression. These results show that cells are highly sensitive to changes in extracellular mineralization, and understanding how cells sense this change would be highly beneficial to synthetic scaffold design. Future studies will investigate activation for RhoA and CKII and also evaluate these scaffolds *in vivo* to validate the results in the absence of glucocorticoids.

3.9 Future Work

This chapter showed that incorporating HAp into PCL nanofibers causes an increase in ALP activity at one time-point and a decrease in type I collagen expression. These results were consistent with several previous studies examining polymer-HAp nanofibers for osteogenesis. Chapter 5 addresses the *in vivo* work that was performed to evaluate the efficacy of incorporating HAp into nanofibers as a means of increasing osteogenesis, and those results indicate that HAp increases *in vivo* osteogenesis. This,

combined with the observation that cells are sensitive to HAp nanoparticles in nanofibers even at only 1% w/w suggests that the cells have a sensitive mechanism by which they sense mineralization in their extracellular surroundings. Much of the literature pertaining to cell adhesion in bone tissue has focused on OP, OC, and osteonectin (ON), but changes in integrin expression have not yet been examined. Integrin expression has been shown to change with changes between polymer and metallic substrates [163], and these changes should be investigated with PCL-HAp nanofiber constructs. Understanding the molecular tools by which cells sense this mineralization may be important to future scaffold designs, and also for understanding bone tissue maintenance.

The inclusion of 10% HAp in nanofiber scaffolds is likely to change the mechanical properties of the scaffold. Recently, the signaling pathway with through which mechanical stiffness is sensed in cells was linked with activating RhoA [183]. This is a significant finding because activating RhoA has been shown to be necessary for osteoblastogenesis [184, 185] and RhoA activity can regulate pro-survival or apoptosis pathways [210, 213]. An investigation into the change in PCL-HAp scaffold stiffness, and the effects on RhoA activity and downstream substrates would be a significant contribution to synthetic scaffold design.

3.8 References

1. Johnson, M.R., et al., *Sustained release of BMP-2 in a lipid-based microtube vehicle.* Acta Biomater, 2009. **5**(1): p. 23-8.
2. Laflamme, C. and M. Rouabhia, *Effect of BMP-2 and BMP-7 homodimers and a mixture of BMP-2/BMP-7 homodimers on osteoblast adhesion and growth following culture on a collagen scaffold.* Biomed Mater, 2008. **3**(1): p. 15008.
3. Laurencin, C.T., et al., *Poly(lactide-co-glycolide)/hydroxyapatite delivery of BMP-2-producing cells: a regional gene therapy approach to bone regeneration.* Biomaterials, 2001. **22**(11): p. 1271-7.
4. Lee, J.Y., et al., *Osteoblastic differentiation of human bone marrow stromal cells in self-assembled BMP-2 receptor-binding peptide-amphiphiles.* Biomaterials, 2009. **30**(21): p. 3532-41.
5. Olivares-Navarrete, R., et al., *Integrin alpha2beta1 plays a critical role in osteoblast response to micron-scale surface structure and surface energy of titanium substrates.* Proc Natl Acad Sci U S A, 2008. **105**(41): p. 15767-72.
6. Marletta, G., et al., *The effect of irradiation modification and RGD sequence adsorption on the response of human osteoblasts to polycaprolactone.* Biomaterials, 2005. **26**(23): p. 4793-804.
7. Wutticharoenmongkol, P., P. Pavasant, and P. Supaphol, *Osteoblastic Phenotype Expression of MC3T3-E1 Cultured on Electrospun Polycaprolactone Fiber Mats Filled with Hydroxyapatite Nanoparticles.* Biomacromolecules, 2007. **8**(8): p. 2602-2610.
8. Zhang, P., et al., *In vivo mineralization and osteogenesis of nanocomposite scaffold of poly(lactide-co-glycolide) and hydroxyapatite surface-grafted with poly(l-lactide).* Biomaterials, 2008.
9. Palmer, L.C., et al., *Biomimetic systems for hydroxyapatite mineralization inspired by bone and enamel.* Chem Rev, 2008. **108**(11): p. 4754-83.
10. Anderson, H.C., et al., *Impaired calcification around matrix vesicles of growth plate and bone in alkaline phosphatase-deficient mice.* Am J Pathol, 2004. **164**(3): p. 841-7.
11. Genge, B.R., L.N. Wu, and R.E. Wuthier, *In vitro modeling of matrix vesicle nucleation: synergistic stimulation of mineral formation by annexin A5 and phosphatidylserine.* J Biol Chem, 2007. **282**(36): p. 26035-45.
12. Nikolov, S. and D. Raabe, *Hierarchical modeling of the elastic properties of bone at submicron scales: the role of extrafibrillar mineralization.* Biophys J, 2008. **94**(11): p. 4220-32.
13. Norman, J., et al., *Micromechanical properties of human trabecular bone: a hierarchical investigation using nanoindentation.* J Biomed Mater Res A, 2008. **87**(1): p. 196-202.
14. McCreadie, B.R., et al., *Hierarchical structure of bone and micro-computed tomography.* Adv Exp Med Biol, 2001. **496**: p. 67-83.
15. White, D.J., et al., *The collagen receptor subfamily of the integrins.* Int J Biochem Cell Biol, 2004. **36**(8): p. 1405-10.
16. Denhardt, D.T. and M. Noda, *Osteopontin expression and function: role in bone remodeling.* J Cell Biochem Suppl, 1998. **30-31**: p. 92-102.

17. Kazanecki, C.C., D.J. Uzwiak, and D.T. Denhardt, *Control of osteopontin signaling and function by post-translational phosphorylation and protein folding.* J Cell Biochem, 2007. **102**(4): p. 912-24.
18. McKee, M.D. and A. Nanci, *Osteopontin: an interfacial extracellular matrix protein in mineralized tissues.* Connect Tissue Res, 1996. **35**(1-4): p. 197-205.
19. Cui, W. and *e. al*, *In situ growth of hydroxyapatite within electrospun poly(DL-lactide) fibers.* Journal of Biomedical Materials Research Part A, 2007. **82A**(4): p. 831-841.
20. Fang, B., et al., *Proliferation and osteoblastic differentiation of human bone marrow stromal cells on hydroxyapatite/bacterial cellulose nanocomposite scaffolds.* Tissue Eng Part A, 2009. **15**(5): p. 1091-8.
21. Guarino, V., et al., *The Influence of Hydroxyapatite Particles on in Vitro Degradation Behaviour of Pcl Based Composite Scaffolds.* Tissue Eng Part A, 2009.
22. Lee, J.H., et al., *Control of osteogenic differentiation and mineralization of human mesenchymal stem cells on composite nanofibers containing poly[lactic-co-(glycolic acid)] and hydroxyapatite.* Macromol Biosci, 2010. **10**(2): p. 173-82.
23. Mei, F., et al., *Improved Biological Characteristics of Poly(L-Lactic Acid) Electrospun Membrane by Incorporation of Multiwalled Carbon Nanotubes/Hydroxyapatite Nanoparticles.* Biomacromolecules, 2007. **8**(12): p. 3729-3735.
24. Kim, H.-W., H.-H. Lee, and J.C. Knowles, *Electrospinning biomedical nanocomposite fibers of hydroxyapaite/poly(lactic acid) for bone regeneration.* Journal of Biomedical Materials Research Part A, 2006. **79A**(3): p. 643-649.
25. Xu, H.E., et al., *Molecular recognition of fatty acids by peroxisome proliferator-activated receptors.* Mol Cell, 1999. **3**(3): p. 397-403.
26. Berger, J. and D. Moller, *The mechanisms of action of PPARs.* Annu Rev Med, 2002. **53**: p. 409 - 435.
27. Lecka-Czernik, B. and L.J. Suva, *Resolving the Two "Bony" Faces of PPAR-gamma.* PPAR Res, 2006. **2006**: p. 27489.
28. Lin, T.-H., et al., *PPARg inhibits osteogenesis via the down-regulation of the expression of COX-2 and iNOS in rats.* Bone, 2007. **41**: p. 562-574.
29. Syversen, U., et al., *PPAR-Alpha Agonists Increase Bone Mineral Density in Female Rats.* Abstract at ASBMR 25th Annual Meeting, 2003.
30. Ruckh, T.T., et al., *Osteogenic Differentiation of Bone Marrow Stromal Cells on Poly(epsilon-caprolactone) Nanofiber Scaffolds.* Acta Biomater, 2010.
31. Fregel, R., A. Gonzalez, and V.M. Cabrera, *Improved ethanol precipitation of DNA.* Electrophoresis, 2010. **31**(8): p. 1350-2.
32. Khatiwala, C.B., et al., *ECM compliance regulates osteogenesis by influencing MAPK signaling downstream of RhoA and ROCK.* J Bone Miner Res, 2009. **24**(5): p. 886-98.
33. McBeath, R., et al., *Cell shape, cytoskeletal tension, and RhoA regulate stem cell lineage commitment.* Dev Cell, 2004. **6**(4): p. 483-95.

34. Meyers, V.E., et al., *RhoA and cytoskeletal disruption mediate reduced osteoblastogenesis and enhanced adipogenesis of human mesenchymal stem cells in modeled microgravity.* J Bone Miner Res, 2005. **20**(10): p. 1858-66.
35. Salih, E., et al., *Protein kinases of cultured osteoblasts: selectivity for the extracellular matrix proteins of bone and their catalytic competence for osteopontin.* J Bone Miner Res, 1996. **11**(10): p. 1461-73.
36. Katayama, Y., et al., *Casein kinase 2 phosphorylation of recombinant rat osteopontin enhances adhesion of osteoclasts but not osteoblasts.* J Cell Physiol, 1998. **176**(1): p. 179-87.
37. Wang, J., et al., *Expression of bone microsomal casein kinase II, bone sialoprotein, and osteopontin during the repair of calvarial defects.* Bone, 1998. **22**(6): p. 621-8.
38. Bellows, C.G., S.M. Reimers, and J.N. Heersche, *Expression of mRNAs for type-I collagen, bone sialoprotein, osteocalcin, and osteopontin at different stages of osteoblastic differentiation and their regulation by 1,25 dihydroxyvitamin D3.* Cell Tissue Res, 1999. **297**(2): p. 249-59.
39. Gupta, D., et al., *Nanostructured biocomposite substrates by electrospinning and electrospraying for the mineralization of osteoblasts.* Biomaterials, 2009. **30**(11): p. 2085-94.
40. Jackson, S.M. and L.L. Demer, *Peroxisome proliferator-activated receptor activators modulate the osteoblastic maturation of MC3T3-E1 preosteoblasts.* FEBS Lett, 2000. **471**(1): p. 119-24.
41. Still, K., et al., *The Peroxisome Proliferator Activator Receptor Alpha/Delta Agonists Linoleic Acid and Bezafibrate Upregulate Osteoblast Differentiation and Induce Periosteal Bone Formation In Vivo.* Calcif Tissue Int, 2008.
42. de Jong, D.S., et al., *Identification of novel regulators associated with early-phase osteoblast differentiation.* J Bone Miner Res, 2004. **19**(6): p. 947-58.
43. Badami, A.S., et al., *Effect of fiber diameter on spreading, proliferation, and differentiation of osteoblastic cells on electrospun poly(lactic acid) substrates.* Biomaterials, 2006. **27**(4): p. 596-606.
44. Bashur, C.A., L.A. Dahlgren, and A.S. Goldstein, *Effect of fiber diameter and orientation on fibroblast morphology and proliferation on electrospun poly(D,L-lactic-co-glycolic acid) meshes.* Biomaterials, 2006. **27**(33): p. 5681-8.
45. Tsiridis, E., N. Upadhyay, and P. Giannoudis, *Molecular aspects of fracture healing: which are the important molecules?* Injury, 2007. **38 Suppl 1**: p. S11-25.
46. Chen, L., et al., *Insulin-like growth factor 2 (IGF2) potentiates BMP9-induced osteogenic differentiation and bone formation.* J Bone Miner Res, 2010.
47. Sundelacruz, S. and D.L. Kaplan, *Stem cell- and scaffold-based tissue engineering approaches to osteochondral regenerative medicine.* Semin Cell Dev Biol, 2009. **20**(6): p. 646-55.
48. Ekholm, E.C., et al., *Expression of extracellular matrix genes: transforming growth factor (TGF)-beta1 and ras in tibial fracture healing of lathyritic rats.* Bone, 2000. **27**(4): p. 551-7.

49. Hirakawa, K., et al., *Localization of the mRNA for bone matrix proteins during fracture healing as determined by in situ hybridization.* J Bone Miner Res, 1994. **9**(10): p. 1551-7.
50. Schuckert, K.H., S. Jopp, and S.H. Teoh, *Mandibular defect reconstruction using three-dimensional polycaprolactone scaffold in combination with platelet-rich plasma and recombinant human bone morphogenetic protein-2: de novo synthesis of bone in a single case.* Tissue Eng Part A, 2009. **15**(3): p. 493-9.
51. Thorwarth, M., et al., *Expression of bone matrix proteins during de novo bone formation using a bovine collagen and platelet-rich plasma (prp)--an immunohistochemical analysis.* Biomaterials, 2005. **26**(15): p. 2575-84.
52. Kosaki, N., et al., *Impaired bone fracture healing in matrix metalloproteinase-13 deficient mice.* Biochem Biophys Res Commun, 2007. **354**(4): p. 846-51.
53. Weiss, S., et al., *Systemic regulation of angiogenesis and matrix degradation in bone regeneration--distraction osteogenesis compared to rigid fracture healing.* Bone, 2005. **37**(6): p. 781-90.
54. Henle, P., G. Zimmermann, and S. Weiss, *Matrix metalloproteinases and failed fracture healing.* Bone, 2005. **37**(6): p. 791-8.
55. Coleman, J.E., *Structure and mechanism of alkaline phosphatase.* Annu Rev Biophys Biomol Struct, 1992. **21**: p. 441-83.
56. Orimo, H. and T. Shimada, *The role of tissue-nonspecific alkaline phosphatase in the phosphate-induced activation of alkaline phosphatase and mineralization in SaOS-2 human osteoblast-like cells.* Mol Cell Biochem, 2008. **315**(1-2): p. 51-60.
57. Kulterer, B., et al., *Gene expression profiling of human mesenchymal stem cells derived from bone marrow during expansion and osteoblast differentiation.* BMC Genomics, 2007. **8**: p. 70.
58. Park, S.-H. and *e. al*, *Effect of hydroxyapatite-coated nanofibrous membrane on the responses of human periodontal ligament fibroblast.* Journal of the Ceramic Society of Japan, 2008. **116**(1349): p. 31-35.
59. Venugopal, J., et al., *Electrospun-modified nanofibrous scaffolds for the mineralization of osteoblast cells.* Journal of Biomedical Materials Research Part A, 2007. **85**(2): p. 408-417.
60. Qin, C., O. Baba, and W.T. Butler, *Post-translational modifications of sibling proteins and their roles in osteogenesis and dentinogenesis.* Crit Rev Oral Biol Med, 2004. **15**(3): p. 126-36.
61. Liu, F., L. Malaval, and J.E. Aubin, *Global amplification polymerase chain reaction reveals novel transitional stages during osteoprogenitor differentiation.* J Cell Sci, 2003. **116**(Pt 9): p. 1787-96.
62. Keykhosravani, M., et al., *Comprehensive identification of post-translational modifications of rat bone osteopontin by mass spectrometry.* Biochemistry, 2005. **44**(18): p. 6990-7003.
63. Yoshida, T., M.F. Clark, and P.H. Stern, *The small GTPase RhoA is crucial for MC3T3-E1 osteoblastic cell survival.* J Cell Biochem, 2009. **106**(5): p. 896-902.

64. Chan, M.C., et al., *A novel regulatory mechanism of the bone morphogenetic protein (BMP) signaling pathway involving the carboxyl-terminal tail domain of BMP type II receptor.* Mol Cell Biol, 2007. **27**(16): p. 5776-89.
65. Zambuzzi, W.F., et al., *On the road to understanding of the osteoblast adhesion: cytoskeleton organization is rearranged by distinct signaling pathways.* J Cell Biochem, 2009. **108**(1): p. 134-44.
66. Fromigue, O., et al., *RhoA GTPase inactivation by statins induces osteosarcoma cell apoptosis by inhibiting p42/p44-MAPKs-Bcl-2 signaling independently of BMP-2 and cell differentiation.* Cell Death Differ, 2006. **13**(11): p. 1845-56.

Chapter 4

4.1 Chapter summary

In this chapter, the effects of oleic acid (OLA) released from PCL nanofiber scaffolds on cell behaviors was investigated. PCL-OLA scaffolds were fabricated to contain either 1% or 5% w/w OLA, and OLA-free scaffolds were produced by incubating 1% OLA in methanol for 24 hours. The scaffolds were characterized in terms of their fiber diameter, and changes in composition and crystallinity were measured by thermogravimetric analysis (TGA) and differential scanning calorimetry (DSC). Additionally, scaffold mass loss due to the presence of an esterase was measured. In order to evaluate the response of marrow stromal cells (MSCs), fresh marrow stromal extracts were seeded onto the scaffolds, and cell adhesion and metabolic activity were measured during the initial week after seeding. After one week, cells were provided with osteogenic media. Intracellular alkaline phosphatase (ALP) activity and calcium deposition were measured colorimetrically, and gene expression levels for osteopontin (OP), RhoA, and three peroxisome proliferator-activator receptor isoforms were measured with quantitative polymerase chain reaction (qPCR). After three weeks, OP and osteocalcin (OC) were immunolabeled for fluorescent microscopy. Scaffold characterization results showed that the three scaffolds contained similar fiber diameter distributions, and the crystallinity of the materials were all similar to source PCL. TGA measured a significantly different composition for 5%, but not 1% OLA scaffolds. OLA had a significant effect on both metabolic activity and cell coverage, decreasing both measures in significant manners. However, in osteogenic conditions, cells on 5% OLA scaffolds showed significantly greater ALP activity, calcium deposition, and OP accumulation throughout three weeks in osteogenic media. QPCR expression data showed that cells differentially expressed OP with moderate significance. RhoA was not differentially expressed, and only PPARα and δ, not γ, were expressed with significant differences. These results indicate that

cells on 5% OLA scaffolds showed the greatest levels of osteoblast phenotypic behaviors, and the OLA is likely acting through PPARs on the 5% scaffolds.

4.2 Motivation and Aims

Designing bone tissue scaffolds with soluble design factors remains a very active area, with the greatest attention paid to growth factors and short peptides [160, 214-218]. When these signals are presented to progenitor cells, they will activate endocrine signaling pathways [160, 162, 219], thus directing the progenitor cells towards osteoblastogenesis. One area that has not yet received significant attention is the role of fatty acids in osteoblastogenesis. Fatty acids are an abundant part of the normal human diet, and variations in fatty acid species within particular tissues have been linked to diseases such as obesity [220], atherosclerosis [221], heart disease [222], and cancer [223-225]. Many fatty acids are agonists for peroxisome proliferator-activator receptors (PPAR), a class nuclear membrane receptors that has been associated with a wide range of cellular functions [136]. Cells express three isoforms of PPARs; α, δ, and γ, and each isoforms contains a DNA-binding domain so that the activated PPAR (as a heterodimer with a retinoic acid receptor) can bind to gene promoter regions [226]. Many cellular fate processes including differentiation of progenitor cells into adipocytes rather than osteoblasts have been positively correlated to differential PPAR expression and activation [143, 145, 191, 227-229].

Oleic acid (OLA) is an organosoluble, ω-9, monounsaturated fatty acid that has been shown to increase osteoblast phenotypic behaviors such as ALP expression in serum-free conditions [143]. It has also been shown to permit immortalized osteoblast cell proliferation in serum-supplemented conditions [230]. Fatty acids such as OLA are found in diverse range in bone marrow and they are likely processed and secreted from

medullary adipocytes [230]. OLA has been shown to have the greatest affinity for PPARα and lowest for PPARγ, a phenotypic marker for adipocytes [177]. In fact, steroid hormones used to treat non-skeletal endocrine diseases have been scrutinized for their potential inhibitory effects on osteoblasts due to cross-talk between PPARs and other families nuclear receptors [231-234]. Whereas PPARγ activation has been widely accepted as an effective pathway for adipocytogenesis, PPARα activation continues to be studied as a *suspected* mechanism for osteoblastogenesis [144, 235, 236]. The aim of this chapter is to demonstrate that OLA, a fatty acid with strong preferential binding to PPARα, will enhance osteoblast phenotypic behaviors and induce differential expression of PPARs.

4.3 Materials and methods

4.3.1 Fabrication & Characterization of Nanofiber Scaffolds

Nanofiber scaffolds were fabricated by electrospinning 80,000 molecular weight PCL polymer (Sigma) solution (12% w/w) with either 1% or 5% w/w of OLA-sodium salt (Sigma). PCL and OLA were dissolved in a solvent mixture of 3:1 (volume ratio) chloroform:methanol (Sigma) and loaded into a glass syringe (Hamilton, Gastight 1010). The polymer solution was fed to a blunt-tip catheter by a syringe pump (Harvard Apparatus) at a rate of 1.8-2.1 mL/hr. A high-voltage power supply (Gamma High Voltage Research, model ES30P-10W/DAM) was used to apply voltage in the range of 18-21 kV to the blunt-tip catheter that was positioned 4-4.5” from the grounded collector plate.

In order to fabricate control (OLA-free) nanofiber scaffolds, 1% OLA scaffolds were incubated in methanol for 24 hrs to leach out the OLA-sodium salt. 1% OLA scaffolds and OLA-free scaffolds were examined under X-ray photon spectroscopy (XPS) to

detect the presence or absence of sodium which characteristic to OLA. XPS was performed with a PHI-5800 spectrometer using a monochromatic Al Kα X-ray source (1486.6 eV). The measurements were taken at an electron takeoff angle of 45^{o} from the normal sampling surface. The binding energy scale was calibrated prior to analysis by the Au4f$_{7/2}$ peak at 83.9 eV, and the linearity was verified by the Cu3p$_{1/2}$ and Cu2p$_{3/2}$ peaks at 76.5 and 932.5 eV respectively. Survey scans were performed between 10 eV and 1100 eV with pass energy of 187.5 eV. All spectra were referenced by setting the C1s peak to 285.0 eV to compensate for residual charging effects.

In order to examine the morphology of the nanofiber scaffolds and determine the fiber diameter, they were sputter-coated with 10 nm of gold and imaged under high magnification using a field-emission scanning electron microscope (SEM, JEOL JSM-6500F). Fiber diameters were measured using SEM image analysis software. Ten measurements were made on each scaffold with n_{min}=30 and size distribution histogram was plotted.

Thermal characterization of the nanofiber scaffolds was performed to determine the effect of electrospinning process on polymer crystallinity and thermal stability. Digital scanning calorimetry (DSC, TA Instruments DSC 2920) was used to determine the polymer crystallinity in different nanofiber scaffolds. The scaffolds were heated from 5^{o}C to 120^{o}C at 5^{o}C/min and the crystallinity of a sampled was calculated by the following equation:

$$X_c\% = 100 \times \frac{\Delta H_{m,sample}}{\Delta H_{m,std}} \quad \text{(Equation 1)}$$

where $\Delta H_{m,sample}$ is the enthalpy of melting of the nanofiber scaffold and $\Delta H_{m,std}$ is the enthalpy of melting of 100% crystalline PCL ($\Delta H_{m,std}$ = 139 J/g) [174]. Thermogravimetric analysis (TGA, TA Instruments TGA 2950) was used to measure the change in mass as

a function of temperature. The nanofiber scaffolds were heated from 25°C to 700°C at 10°C/min and the weight loss was measured. In both the thermal analysis techniques, polymer pellets that had not been subjected to electrospinning were used as controls.

4.3.2 PCL/OLA scaffold mass loss due to esterase activity

Changes in the mass of the PCL/OLA nanofiber scaffolds was investigated in conditions with and without an esterase. 10 mm discs of OLA-free, 1% OLA, and 5% OLA scaffolds were cut using a sterile biopsy punch, weighed, and then the scaffolds were sterilized by washing in ultra-pure H_2O (R=18.2 MΩ) and PBS, with 10 min UV exposure during each wash. Scaffolds were then incubated at 37°C and 100% humidity in 1 mL of either PBS or PBS with 8 IU of lipase from *pseudomonas capacia* [110, 237]. At days 1, 4, and 7, scaffolds were removed from PBS, rinsed with diH_2O and dried in a desiccator overnight. Their masses were weighed again and the percent of mass lost was calculated. The number of scaffolds at each time point in PBS-enzyme was N=3, whereas the number of scaffolds in PBS at each time point was N=2.

4.3.3 Isolation and Culture of Marrow Stromal Cells

Marrow stromal cells (MSC) were isolated from male Wistar rats (*Rattus norvegicus*) supplied by Harlan Sprague Dawley, Inc. Animal protocol was approved by Colorado State University Animal Care and Use Committee. This committee is in compliance with the NIH Guide for Care and Use of Laboratory Animals. Limbs were aseptically removed from the recently euthanized animals. Soft tissue was removed and the bones were briefly stored in cold PBS before isolating cells. Metaphyseal ends of the bones were removed to expose the bone marrow cavity. In a 50 mL conical tube, marrow was repeatedly flushed with culture maintenance media (α-MEM (Hyclone) with 10 % fetal bovine serum (FBS, Sigma) and 1 % penicillin/streptomycin (PS, Sigma))

using 10 mL syringe with 18 and 25 gauge needles. Media containing cells and debris was filtered with a 70μm nylon filter into a clean conical tube. Cells were counted using a hemocytometer before seeding on nanofiber scaffolds.

Prior to cell seeding, nanofiber scaffolds, denoted as OLA-free, 1% OLA, and 5% OLA, (surface area approximately 0.7 cm^2) were sterilized under uv light for 60 min while in DI water. The substrates were then washed twice with warm PBS followed by warm culture media. The cells were seeded on the nanofiber scaffolds in a 24-well plate at a density of 1 X 10^6 cells per well. The cultures were incubated at 37^{o}C and 5 % CO_2 for the duration of the study. Half of the media was changed after 4 days of culture. After 7 days of culture, the media was replaced with osteogenic differentiation media (maintenance media plus 10^{-8} M dexamethosone (Sigma), 50 μg/mL ascorbic acid (Sigma), 8 mM β-glycerophosphate (Sigma)). Subsequent media changes were done every 2 days for up to 3 weeks of culture.

4.3.4 MSC Adhesion and Proliferation on PCL/OLA Nanofiber Scaffolds

MSC response to the nanofiber scaffolds was investigated through cell adhesion, viability (mitochondrial activity), and morphology after 1, 4, and 7 days of culture. The scaffolds were removed from the culture media and rinsed twice in PBS prior to further analysis.

Cells adhesion was investigated using a live cell stain, Calcein AM (Invitrogen) (ex: 485 nm, em: 530 nm). Calcein AM can penetrate live cell membranes, where the AM is cleaved and the resulting calcein molecule fluoresces green. The cells were incubated in 2 μM of calcein AM in PBS for 45 min and were imaged with a fluorescence microscope with a 470 nm filter. Images were analyzed using ImageJ (NIH) software to compute the percent area covered by live cells on different nanofiber scaffolds.

MSC viability on nanofiber scaffolds was measured after 1 and 4 days of culture (log phase growth) using a commercially available MTT assay kit (Sigma). The adhered cells were incubated at 37^{o}C for 3 hrs in a (3-(4,5-dimethylthiazol-2-yl)-2,5-diphenyl tetrazolium bromide (MTT) solution. Mitochondrial dehydrogenases of viable cells cleave the tetrazolium ring, yielding purple formazan crystals. Formazan crystals were then dissolved in the MTT solvent containing 10% (volume) Triton-X (Sigma). The optical density (OD) was measured at 570 nm using a plate reader (BMG Labtech, FLUOStar Omega). The background absorbance at 690 nm was subtracted from the measured absorbance. The OD is proportional to the mitochondrial activity of the live proliferative cells on the scaffold surface.

4.3.5 MSC Differentiation on PCL/OLA Nanofiber Scaffolds

MSC differentiation on nanofiber scaffolds was investigated after 1, 2 and 3 weeks of providing the cells with osteogenic differentiation media (i.e. after 1 week in maintenance media). Alkaline phosphatase (ALP) activity, calcium deposition, surface phosphate deposition, and non-collagenous bone matrix protein deposition were used to assess the differences in cell phenotypic behavior due to the presence of OLA in the nanofiber scaffolds. The scaffolds were removed from the culture media and rinsed twice in PBS prior to further analysis.

To determine the alkaline phosphatase (ALP) activity on nanofiber scaffolds, the adhered cells were lysed with Cell Lytic™ (Sigma) solution for 1 hr. A commercially available ALP colorimetric assay kit (Quantichrome™ BioAssay Systems) was used to quantify ALP concentration in the lysate. Briefly, ALP catalyzes the reaction of *p*-nitrophenolphosphate (*p*-NPP) to *p*-nitrophenol and phosphate. *p*-nitrophenol was measured using a plate reader at 405 nm after 1 and 4 mins in order to determine the

concentration of ALP in the lysate. ALP concentration was calculated using the guidelines provided by the manufacturer. Further, the same lysate was also used to determine the total intracellular protein content using a commercially available BCA (bicinchoninic acid) assay (Pierce Biotechnology). The absorbance of the solution was measured using a plate reader at a wavelength of 570 nm and was converted to protein content using an albumin standard curve. All the ALP data was normalized with the total protein content to account for changes in number of cells present on each surface.

In order to visualize the phosphate deposition on the nanofiber scaffold surface, von Kossa staining technique was used. The scaffolds were rinsed twice with cacodylate buffer and then immersed in 2% paraformaldehyde (Sigma) (w/v) in cacodylate buffer for 10 min. They were then rinsed with de-ionized water and then a 1% silver nitrate solution (Sigma) in DI water was added. The scaffolds were incubated at room temperature for 20 mins, allowing the phosphate and silver nitrate to react to form a brown precipitate. The reaction was spontaneously stopped by rinsing the scaffolds three times with DI water. Scaffolds were dried in a desiccator and digital images of stained surfaces were captured.

Cell morphology on nanofiber scaffolds was investigated using SEM. The cells were immersed in a fixing solution (3% glutaraldehyde (Sigma) with 0.1 M sucrose (Sigma) and 0.1 M sodium cacodylate (Polysciences) in DI water) for 45 min, rinsed in a buffer solution (fixing solution without glutaraldehyde), and then dehydrated in increasing concentrations of ethanol (30, 50, 70, 90, and 100 %) for 10 min each. After dehydration the scaffolds were immersed in hexamethyldisilazane (HDMS, Alfa) for 10 min and were air-dried. The scaffolds were stored in a desiccator until further SEM characterization. Prior to SEM imaging, the scaffolds were sputter-coated with 10 nm layer of gold. The scaffolds were also examined for surface elemental composition using an attached

energy-dispersive X-ray spectroscopy (EDX) probe (Thermo Electron, Noran system) to the SEM. EDX was used to detect mineralization (presence of calcium and phosphorus) on the scaffold surfaces. Instrument aperture and probe current were adjusted to give a dead time between 15 – 20 %. Scaffold surfaces were analyzed for 20 mins at 10 – 15 kV and a magnification of 1000 to 5000x to provide a complete profile of different elements present. Spatial element mapping was performed by grouping pixels with similar atomic spectra.

Gene expression for osteopontin, RhoA, PPARα, PPARδ, and PPARγ were investigated 1, 2 and 3 weeks after providing the cells with osteogenic differentiation media (i.e. after 1 week in maintenance media). The scaffolds were removed from the culture media and gently rinsed twice in PBS prior to lysate incubation. Messenger RNA (mRNA) was purified from using an mRNA purification kit (RNeasy, Qiagen). Genomic DNA (gDNA) contamination was avoided by degrading any remaining gDNA with DNaseI (Fermentas). Complimentary DNA (cDNA) template was generated from mRNA with a first-strand synthesis kit (Fermentas), and both the DNaseI and reverse transcriptase enzymes were thermally inactivated after their respective steps according to the manufacturer's protocols. cDNA was then stored at -80^{o}C until further use. For PCR reactions, primers for OP were designed as documented below, and all others were purchased as a forward-reverse primer mix (Qiagen) where noted. Custom-designed primers (**Table 4.1**) were validated by running gel electrophoresis with the product to ensure that the amplicon length matched the predicted length, and by performing a melt curve step at the end of real-time quantitative PCR (qPCR) to verify the presence of a single amplicon.

Table 4.2 - OP primers used for qPCR

Osteopontin:
Forward: atcaggacagcaacgggaagac
Reverse: gagttccaaagccagcctggaa
Amplicon length: 224 bp

The amplicon from successful reactions was purified using the ethanol precipitation method [182]. Finally, purified amplicon concentrations were measured with a spectrophotometer (Nanodrop, Thermo Scientific), and standards were then diluted with DNase-free water for use in calculating the copy number from test qPCR reactions.

After 3 weeks in osteogenic media, the cells on scaffolds were immuno-labeled for osteopontin (OP) or osteocalcin (OC). The cells were fixed by immersing in 3.7% paraformaldehyde (w/v) in PBS for 10 mins followed by permeabilization in a 1% Triton-X in PBS solution for 10 mins. A blocking serum of 40 μg/mL of trypan blue (Sigma) and 100 μg/mL of bovine serum albumin (Sigma) in PBS was used to reduce non-specific antibody binding. After rinsing and blocking, scaffolds were incubated in either an OP primary antibody (1:100 in PBS, V-19 purified goat polyclonal antibody of human origin, Santa Cruz Biotechnology) or OC primary antibody (1:100 in PBS, P-18 purified goat polyclonal antibody of mouse origin, Santa Cruz Biotechnology) for 1 hr. After an additional blocking step and PBS wash, scaffolds were then incubated in FITC-conjugated donkey anti-goat IgG (1:100 dilution, Santa Cruz Biotechnology) for 45 minutes in the dark. The scaffolds were rinsed once more before imaging under 470 nm excitation wavelength using a fluorescence microscope.

4.3.6 Statistical analysis

All nanofiber scaffolds (OLA-free, 1% OLA, and 5% OLA) were cultured and assayed in triplicate at each time point specified. The experiments were conducted in duplicate using different animals as the MSC source for each study. For the analysis of

mass-loss, a one-way ANOVA examining the effects of day, OLA, and enzyme was performed. For cell studies, a one-way ANOVA with a Tukey adjustment for multiple comparisons was performed to determine the significance of OLA (concentration within the polymer nanofibers), time (weeks or days as indicated), and the interaction of OLA and time (the effects of time on a measurement, separated by treatment). Statistical significance was defined as $p \leq 0.05$. Values with a student residual >3 were deemed outliers and removed, and the statistical analysis was performed again. For treatments which were found to be significant, statistical groupings for t-tests within the same time-point are reported, with different symbols indicative of a p-value < 0.05. All statistics are presented here as a mean +/- standard deviation.

4.4 RESULTS

4.4.1 Fabrication & Characterization of Nanofiber Scaffolds

In this study, PCL nanofiber scaffolds were fabricated with either 1% or 5% OLA in PCL polymer solution using electrospinning technique and the scaffolds were characterized using SEM to evaluate their nano-architecture (**Figure 4.1 (a, b)**). OLA-free scaffolds were confirmed to be free of the OLA-sodium salt molecule by XPS (data not shown). The nanofiber scaffolds with different OLA concentrations have insignificant differences in their mean fiber diameters (**Figure 4.1 (c)**), and the fiber diameter distribution histogram revealed a possible mild positive skew for both OLA concentrations (**Figure 4.1 (d)**). Further, all the scaffolds occasional had very large diameter nanofibers, up to and sometimes exceeding 1 μm in diameter, however, > 85% of the fibers were in the range of 150-350 nm. Since OLA-free scaffolds were fabricated by leaching out the salt from 1% OLA scaffolds, their fiber diameters were represented by those of the 1% OLA scaffolds.

Thermal characterization of the nanofiber scaffolds was performed to determine the effect of electrospinning process on polymer crystallinity and thermal stability. DSC revealed no significant differences in the crystallinity of the polymer between scaffolds containing different concentrations of OLA. For nanofiber scaffolds (OLA-free, 1% OLA and 5% OLA), the PCL crystallinity was similar to that of source PCL pellets (not-electrospun; control samples) that had not been subjected to electrospinning. The methanol treatment used to produce OLA-free scaffolds also had no significant effect on the crystallinity of the polymer (**Figure 4.2 (a)**). However, TGA revealed significant differences in mass loss for 5% OLA scaffolds as compared to other scaffolds and control substrate (**Figure 4.2 (b)**). Further, there were insignificant differences in mass loss for OLA-free scaffolds, 1% OLA scaffolds and control substrate.

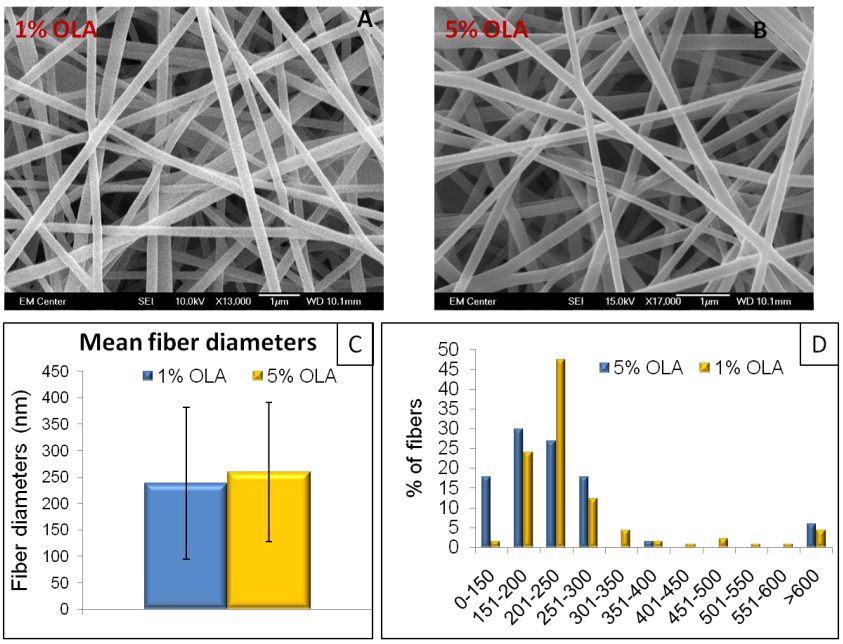

Figure 4.1 – SEM images of 1% OLA (A) and 5% OLA (B) scaffolds with the fiber diameter characteristics (C and D)

4.4.2 PCL/OLA scaffold mass lost due to esterase activity

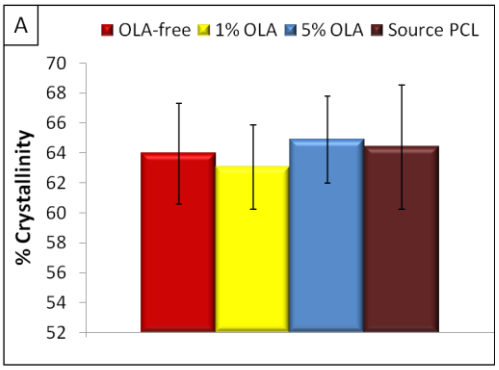

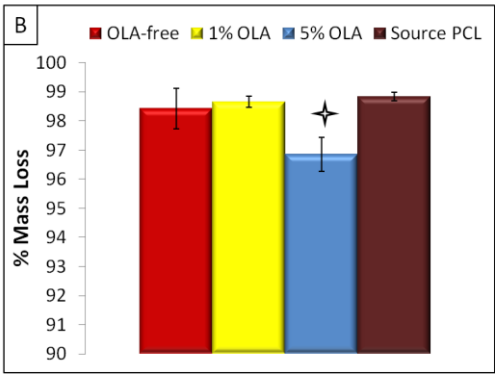

Figure 4.2 – Scaffold characterization of % crystallinity by DSC (A) and % mass loss by TGA (B). Star indicates significant difference ($p \leq 0.05$)

In order to evaluate the effects of an esterase on the degradation behavior of PCL/OLA nanofibers scaffolds, the scaffolds were weighed and placed in either PBS or PBS with lipase of *pseudomonas capecia* an enzyme with esterase activity. After 1, 4, or 7 days the scaffolds were removed, rinsed, dried, and weighed again to calculate the mass loss. The presence of the enzyme had a clear effect on mass loss, which resulted in a highly significant ($p<0.0001$) overall main effect (**Figure 4.3**). Neither the effect of day nor OLA were significant at the 95% level, though the effect of day ($p=0.09$) would be significant at the 90% confidence level. Within each time point, there were several statistically-significant differences, though only at day 1 was there a difference in mass loss between scaffolds – OLA-free and 5% OLA – in PBS without enzyme. All other comparisons were insignificant. Generally the mean value of mass loss for scaffolds in the enzyme was lowest for OLA-free scaffolds, but this trend was not observed for scaffolds in PBS

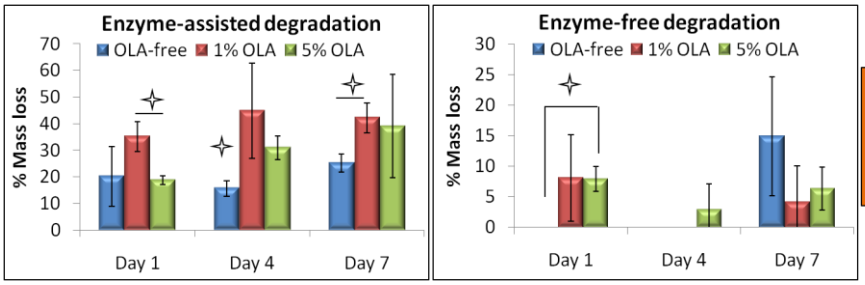

Figure 4.3 – Mass loss of PCL/OLA scaffolds after 1, 4, and 7 days. Star indicates statistically-significant difference ($p \leq 0.05$)

with no enzyme. Thus there may have been loss due to OLA elution which was accelerated due to bulk erosion, but the differences in mass loss between scaffolds in the enzyme were likely driven by a loss of PCL mass.

4.4.3 MSC Adhesion and Proliferation on Nanofiber Scaffolds

MSCs were seeded on different nanofiber scaffolds in a 24 well plate at a density of 1 X 10^6 cells/well and their response was investigated through cell adhesion, viability (mitochondrial activity), and morphology after 1, 4, and 7 days of culture. A commercially available MTT assay was used to measure the overall metabolic activity for the cell population on different nanofiber scaffolds after 1 and 4 days of culture since this is the time-period associated with log-phase growth of cells (**Figure 4.4**).

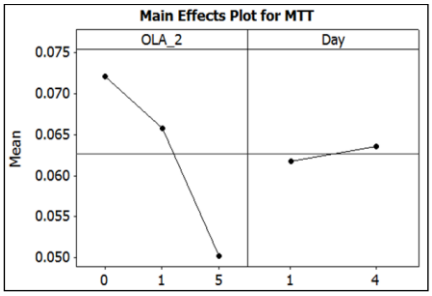

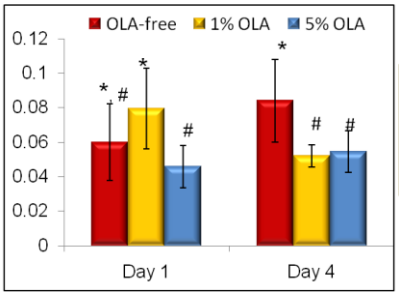

MTT		
Source	F-stat	p-val
OLA	6.24	0.004
Day	0.12	0.732
*OLA*Day*	8.57	0.001

Figure 4 – MTT assay results for days 1 and 4. Symbols indicate statistically-like grouping ($p \geq 0.05$)

The results show that the cells are viable on all the scaffolds after 4 days of culture. Statistically, both OLA and the interaction of OLA by day were highly significant, but the effect of day was not significant. The main effect of OLA was a clear decrease in metabolic activity with an increase in OLA concentration within the polymer nanofibers. T-tests revealed significant differences in cell viability after 1 day of culture between 1% and 5% OLA scaffolds, while neither scaffold had a significant difference from the OLA-free (control) scaffolds. However by day 4, OLA-free scaffolds supported the greatest levels of metabolic activity and both 1% and 5% OLA scaffolds supported similar, reduced levels.

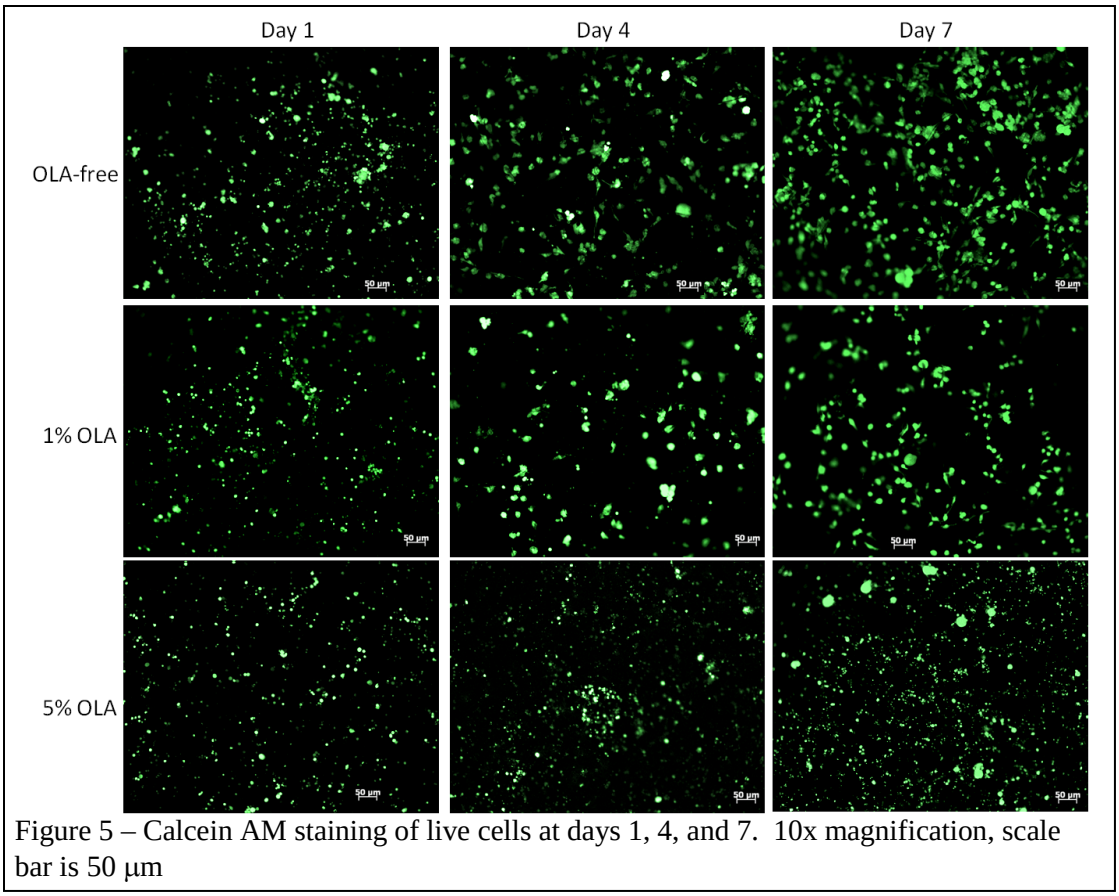

Figure 5 – Calcein AM staining of live cells at days 1, 4, and 7. 10x magnification, scale bar is 50 µm

The live, adhered cells were stained with calcein AM and imaged using a fluorescence microscope after 1, 4 and 7 days of culture (**Figure 4.5**). The images show a clear trend of decrease in cell coverage with increases in OLA concentration within the polymer nanofibers, and this trend is more prominent with the progression of time. Across the three time points, cells on 5% OLA scaffolds were much less spread out than those on OLA-free scaffolds. By contrast the cells on 1% OLA scaffolds appear to be spreading in a similar way as those on OLA-free scaffolds, however there appear to be fewer cells compared to both the 5% OLA and OLA-free scaffolds.

In order to quantify this trend and calculate the percentage of scaffold area covered by live cells, the fluorescence microscopy images were analyzed using ImageJ software. The cell coverage data confirms the visual observation that increasing OLA concentration within the polymer nanofibers decreases the cell coverage area (**Figure**

4.6). Statistically, the effects of OLA, day, and OLA*day (interaction effect) were all highly significant. The interaction plot reveals clear differences in the trends of cell coverage between different nanofiber scaffolds. The cells on OLA-free scaffolds showed a dramatic increase in the coverage after 7 days of culture, whereas the cells on 1% OLA scaffolds had moderate increases in coverage followed by the cells on 5% OLA scaffolds had effectively no increase in cell coverage for up to 7 days of culture.

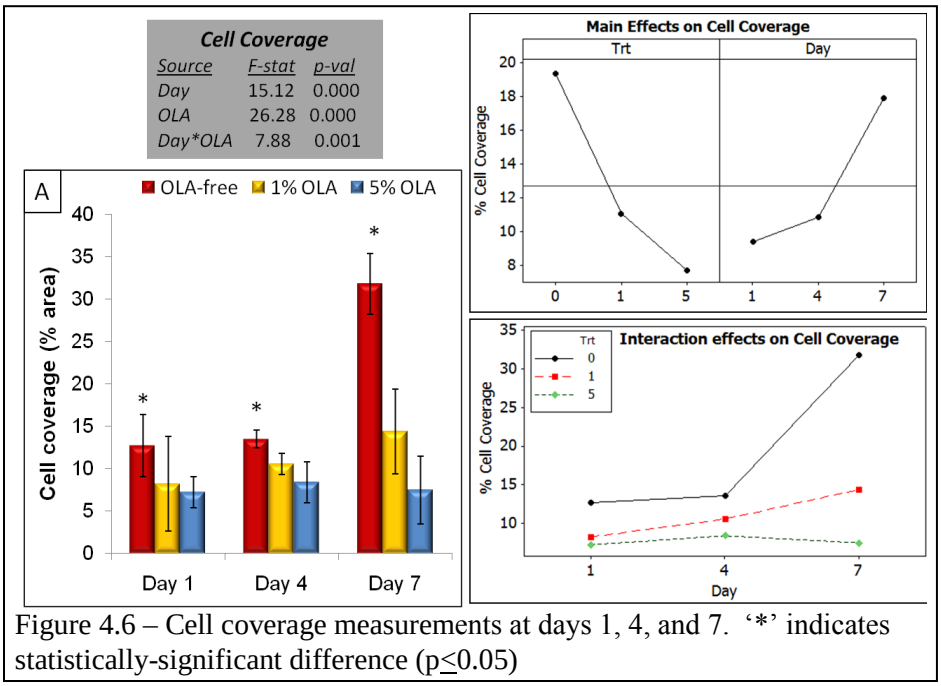

Figure 4.6 – Cell coverage measurements at days 1, 4, and 7. '*' indicates statistically-significant difference ($p \leq 0.05$)

4.4.4 MSC Differentiation on PCL/OLA Nanofiber Scaffolds

MSC differentiation into osteoblasts on nanofiber scaffolds was investigated after 1, 2 and 3 weeks of providing the cells with osteogenic differentiation media (i.e. after 1 week in maintenance media). ALP activity was measured using a colorimetric assay and the results were normalized with total intracellular protein content measured using a BCA assay. The normalized results show significantly higher ALP activity on 5% OLA scaffolds as compared to 1% OLA and OLA-free scaffolds (**Figure 4.7**), with OLA, week, and the interaction of OLA by week all at highly significant p-values. Not only did the cells on 5% OLA scaffolds display the greatest ALP levels, but the trend observed

through culture period of three weeks shows a sustained increase in the activity from week to week that neither 1% OLA nor OLA-free scaffolds supported.

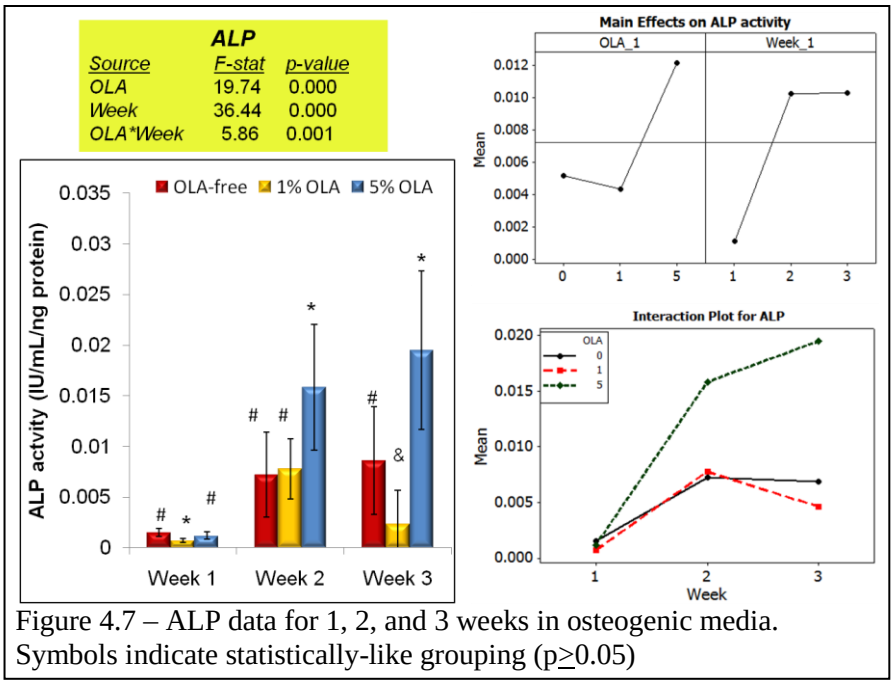

Figure 4.7 – ALP data for 1, 2, and 3 weeks in osteogenic media. Symbols indicate statistically-like grouping ($p \geq 0.05$)

Calcium deposition due to mineralization by osteoblasts was quantified using a colorimetric assay. The results show increased calcium deposition on 5% OLA scaffolds as compared to 1% OLA and OLA-free scaffolds (**Figure 4.8**) The effects of OLA, week, and the interaction of OLA by week were all significant. However, similar to ALP activity after 3 weeks of culture, the cells on 5% OLA scaffolds also

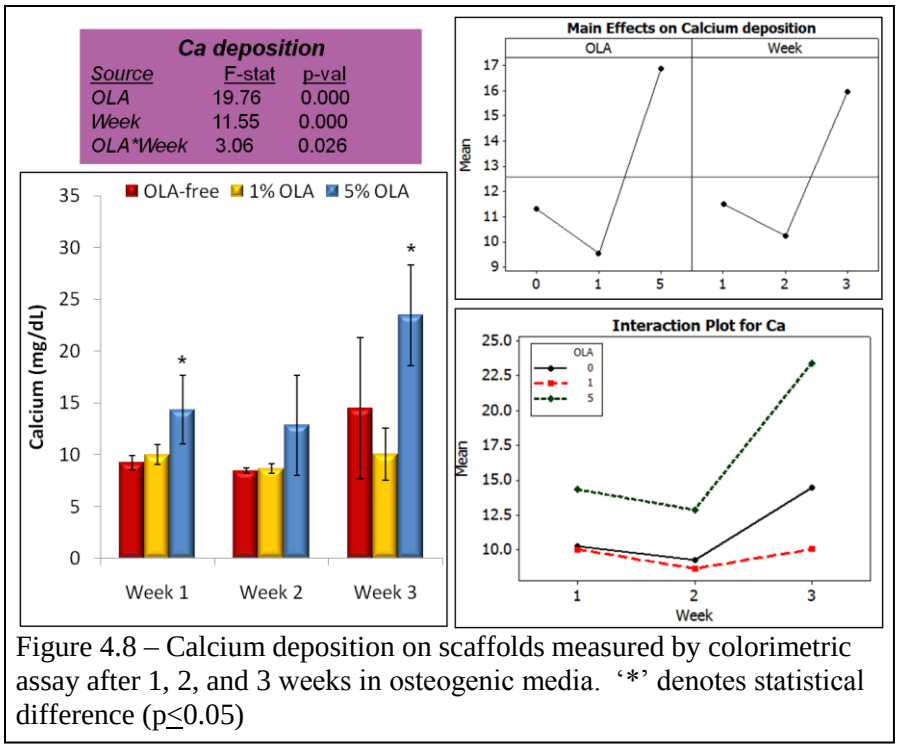

Figure 4.8 – Calcium deposition on scaffolds measured by colorimetric assay after 1, 2, and 3 weeks in osteogenic media. '*' denotes statistical difference ($p \leq 0.05$)

had greatest levels of calcium deposition followed by OLA-free and 1% OLA scaffolds.

SEM imaging coupled with EDX and von Kossa (phosphate) staining was used to examine the MSC differentiation and bone matrix mineral deposition on scaffold surfaces (**Figure 4.9**). All three scaffolds supported cell adhesion and Ca-P mineralization for up to 3 weeks of culture in osteogenic media. The scaffolds showed an inhomogeneous pattern of cell adhesion with certain regions without any cells (**Figure 4.9 (g)**) while others nearly completely covered with dense cell colonies (**Figure 4.9 (f)**). Generally,

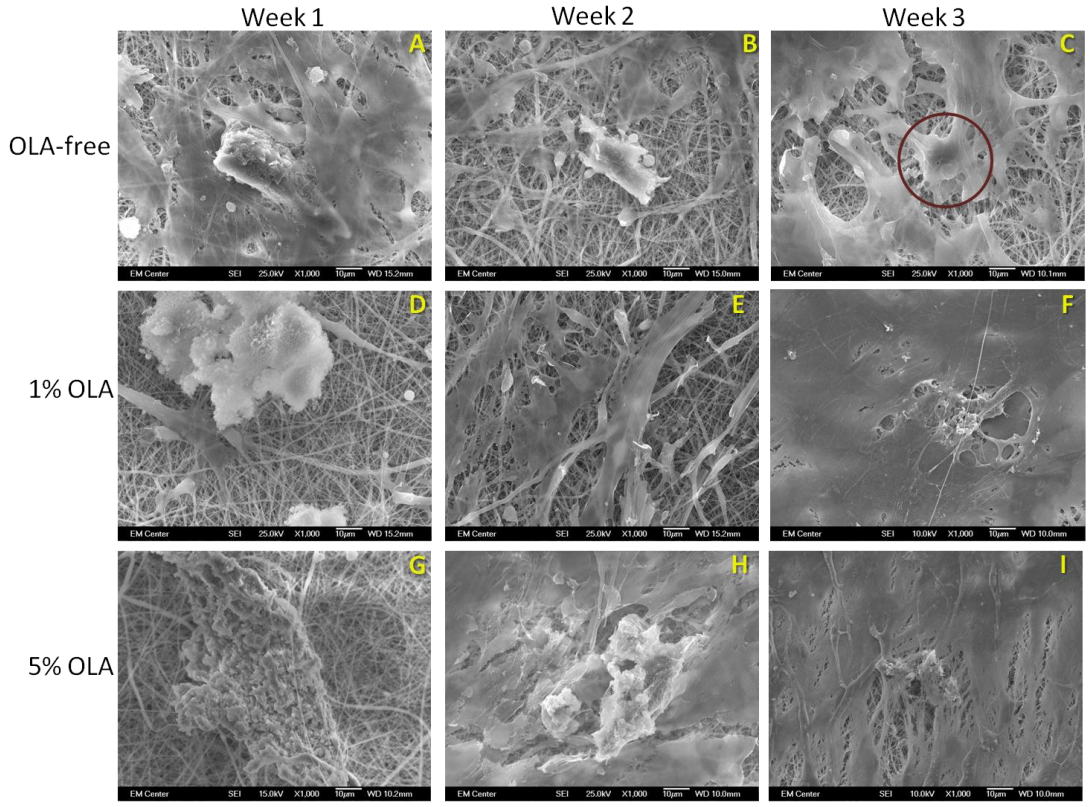

Figure 9 – SEM images of cells and/or mineralization on OLA-free (A-C), 1% OLA (D-F), and 5% OLA (G-I) scaffolds.

1% OLA scaffolds appeared to contain less mineralization than the OLA-free and 5% OLA scaffolds, as evaluated by SEM and EDX. This was particularly evident at weeks 1 and 2 (**Figures 4.9 (a, b, d, e, g, h)**). Long, very thin fibrils were visible only in the cases of large (greater than ~10 μm) mineral deposits (**Figure 4.9 (d) and 4.10)**). These fibrils were not observed with very small spherulites (**Figure 4.10 (a)**).

Phosphate staining for scaffolds revealed dark, heterogeneously distributed pattern throughout the scaffold surfaces (**Figure 4.11**). It was difficult to observe any qualitative differences between scaffolds since the staining showed up quite dark, though this dark stain is indicative of substantive mineralization on all scaffolds. EDX confirmed that the mineral deposits observed under SEM were Ca-P, and these deposits were abundantly distributed on scaffold surfaces. The size of Ca-P deposits varied over a very large size range; some were 10-50 μm in their largest axis (**Figure 4.10 (b)**), while other Ca-P appeared as small spherulites <1μm (**Figure 4.10 (a)**). SEM images revealed that the cells appear to be in intimate contact with mineral deposits on the scaffold surface (**Figure 4.10 (a, c, f, h)**). It should be noted that Ca-P mineralization was evident even in regions without any cells (e.g **Figure 4.9 (g)**). Further, EDX also detected mineral deposits immediately underneath the dense cell colonies suggesting infiltration of the cells in the scaffold porous architecture. The atomic spectra obtained from the EDX data was used to determine the stoichiometric atomic ratio of Ca:P, which varied between 1.6-1.7 for on all scaffolds.

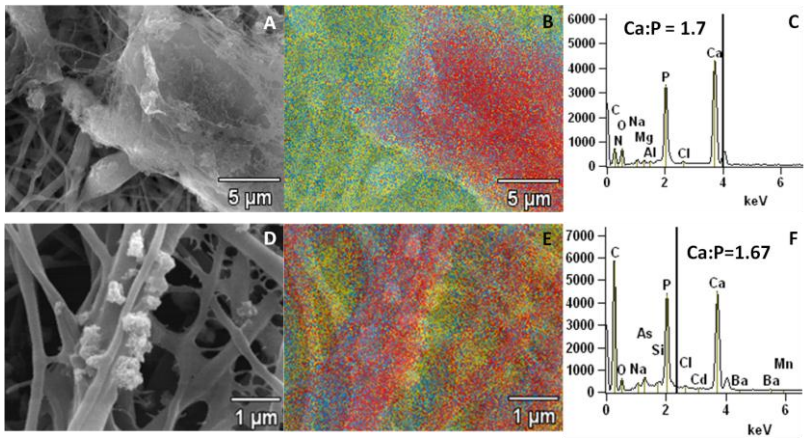

Figure 10 –SEM (A and D) and EDX (B and E) images of mineralization at 2000x (A and B) or 15,000x (D and E) magnification. Atomic spectrum of red phase from EDX images also picture (C and F)

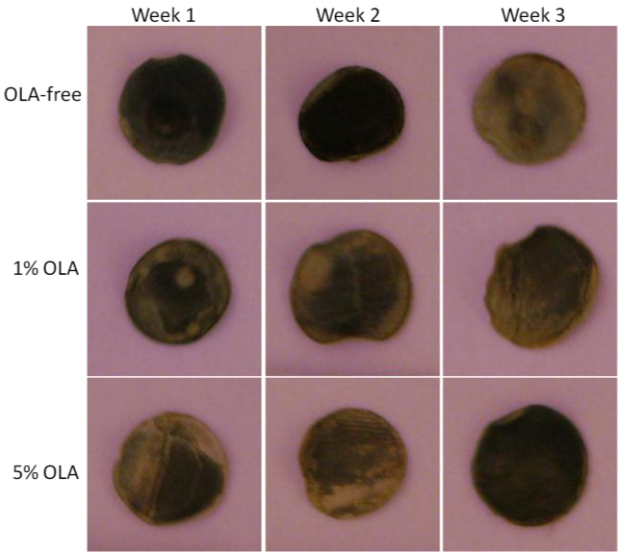

Figure 4.11 – Digital images of phosphate (von Kossa) stains

Osteopontin is an important component of bone ECM, and it is secreted by both osteoblasts and osteoclasts [170, 187, 189]. The expression profile of OP by cells on all three scaffolds was fairly dynamic, with an expression peak at week two (**Figure 4.12**). The main effect of OLA was moderately significant (p=0.09), and the trend suggests that overall expression levels increase as OLA increases. The interaction effect of OLA by week was highly significant (p=0.001), and mean expression values by cells on OLA scaffolds were greater than those on OLA-free scaffolds for weeks one and two. In individual t-tests, there was a significant difference at week one between expression levels on OLA-free and 5% OLA scaffolds. Overall this suggests that differences in expression levels suggested in the ANOVA model were due to cumulative expression throughout the three-week period.

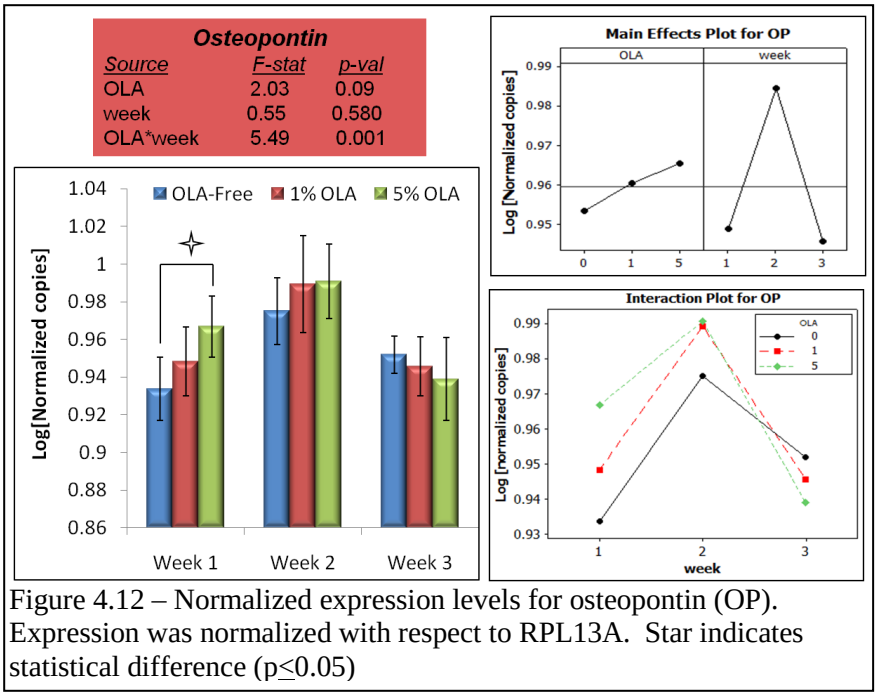

Figure 4.12 – Normalized expression levels for osteopontin (OP). Expression was normalized with respect to RPL13A. Star indicates statistical difference ($p \leq 0.05$)

OP and osteocalcin (OC) deposition on scaffolds were visualized using immunofluorescent staining **(Figure 4.13**) The immunofluorescent images revealed that OP appeared in the greatest abundance on 5% OLA scaffolds after 3 weeks of culture, and OC appeared in relatively equal abundance across all three scaffolds. The images revealed presence of both bone matrix proteins on all the scaffolds with similar patterns as that of mineralization.

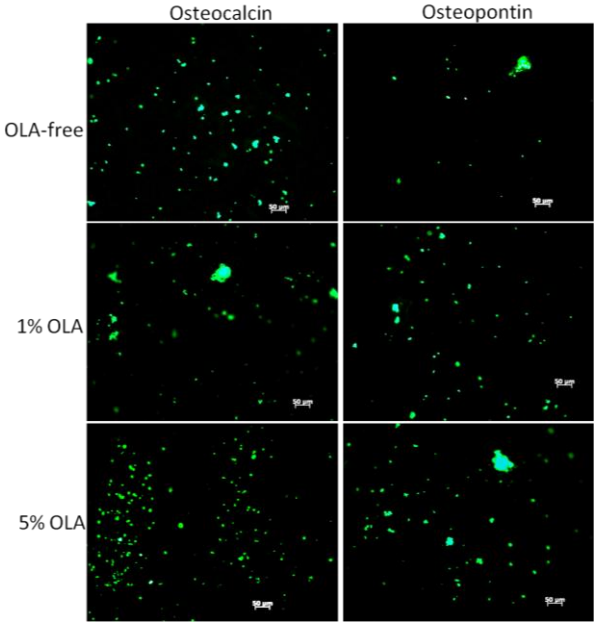

Figure 4.13 – Immunofluorescent stains of OP and OC. Magnification is 10x, scale bar is 50 μm

RhoA is a small GTPase associated with actin cytoskeletal reorganization, and several studies have demonstrated crucial roles for RhoA in osteoblast behaviors, including osteoblastogenesis [183-185]. Expression levels were relatively consistent across all three weeks (**Figure 4.14**), and the ANOVA showed no significant difference due to the main effect of OLA and the interaction of OLA by week. The effect of week

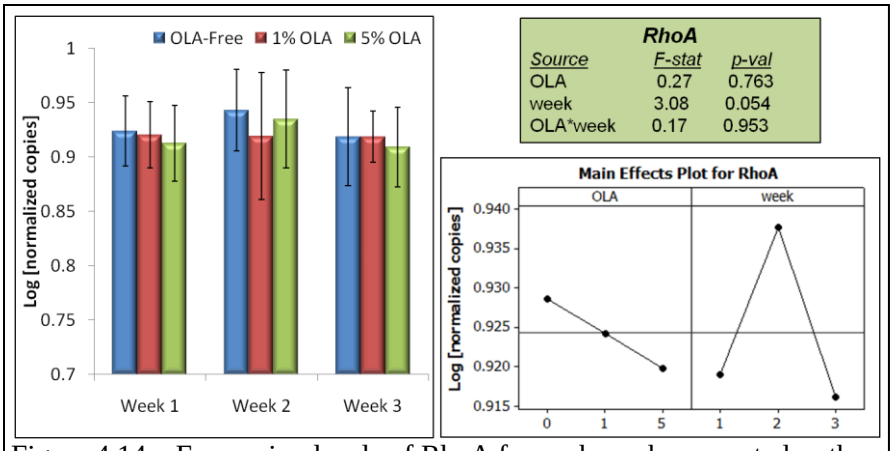

Figure 4.14 – Expression levels of RhoA for each week, presented as the log of normalized values

was significant and expression peaked at week two, which was evident in the main effects plot. Most importantly, OLA had no significant effect on RhoA expression by cells in osteogenic media.

Expression levels for the three isoforms of PPARs were examined at each week. PPARα expression showed highly significant ($p \leq 0.001$) changes due to OLA, with a clear decreasing trend with increase in OLA concentration (**Figure 4.15**). Additionally, the interaction effect of OLA by week was also significant, indicating that changes in expression levels from week to week were different depending on the OLA content of the scaffolds. The interaction plot shows that for weeks one and two, expression levels on both OLA scaffolds change in similar manners. Further, between weeks two and three, cells 1% OLA and OLA-free showed a similar change in expression levels. Interestingly, t-tests showed that statistically significant ($p \leq 0.05$) differences existed between expression levels on OLA-free and 1% OLA scaffolds at weeks one and two, while expression levels on 5% OLA scaffolds were different from the other two at week three. It should be noted that a t-test between OLA-free and 5% OLA scaffolds was borderline yielded a p-value of 0.1, though this is not significant at 95% confidence. Most importantly here, there is a clear trend showing that

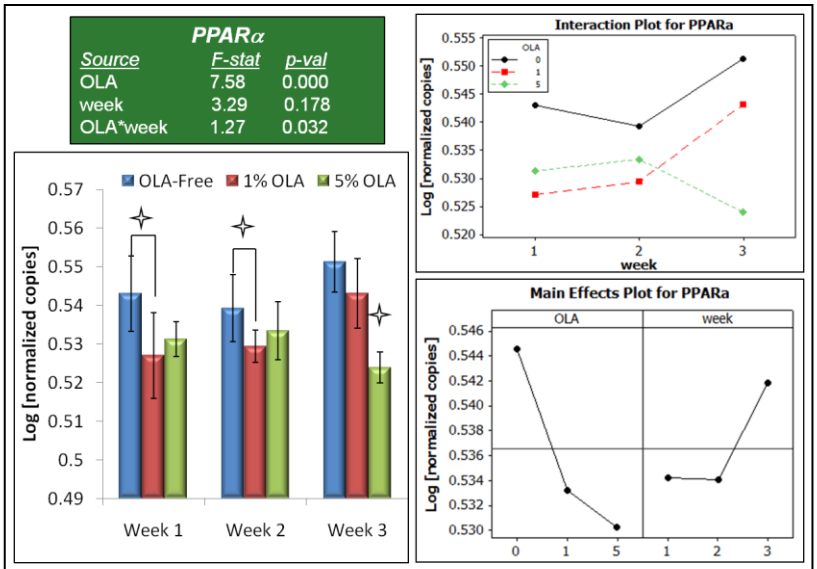

Figure 4.15 – Expression levels of PPARα for each week. Data presented as the log of normalized expression. Star indicates statistically significant difference ($p \leq 0.05$)

changes in OLA concentration within the nanofiber scaffolds has a significant effect on PPARα expression levels.

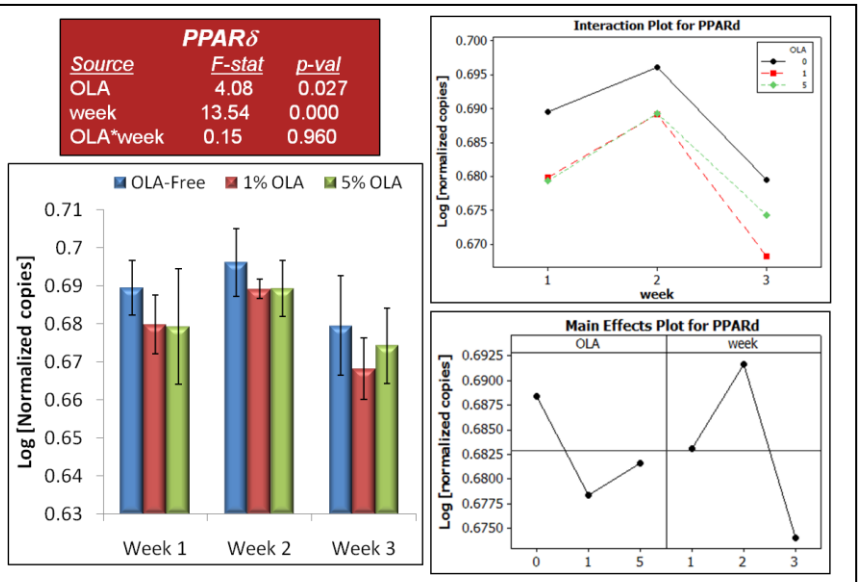

Figure 4.16 – Expression levels of PPARδ for each week. Data presented as the log of normalized expression

Expression levels for PPARδ were also affected by OLA in the nanofibers.. Both main effects, OLA and week, were significant, but the interaction effect was not significant (**Figure 4.16**). Unlike PPARα, there were no significant differences within each time point. This indicates that the significant differences observed in the main effect of OLA were due to sustained higher normalized expression levels on OLA-free scaffolds throughout the three week period. Interestingly, the main effect of week showed an expression profile with a peak at week two, which was also seen with RhoA and OP expression levels. Overall, the key result for PPARδ expression is that, like PPARα, expression levels were greatest on OLA-free scaffolds.

Unlike the α and δ isoforms, the main effect of OLA did not have a significant effect on PPARγ expression (p=0.56) (**Figure 4.17**). Both the main effect of week and the interaction effect were significant, likely due to substantial up-regulations on all three scaffolds at week three. Individual t-tests also showed no significant differences between treatments, though a test between OLA-free and 5% OLA scaffolds at weeks

two and three both measured p=0.1, which is moderately significant. Overall, PPARγ was not differentially expressed due to OLA release.

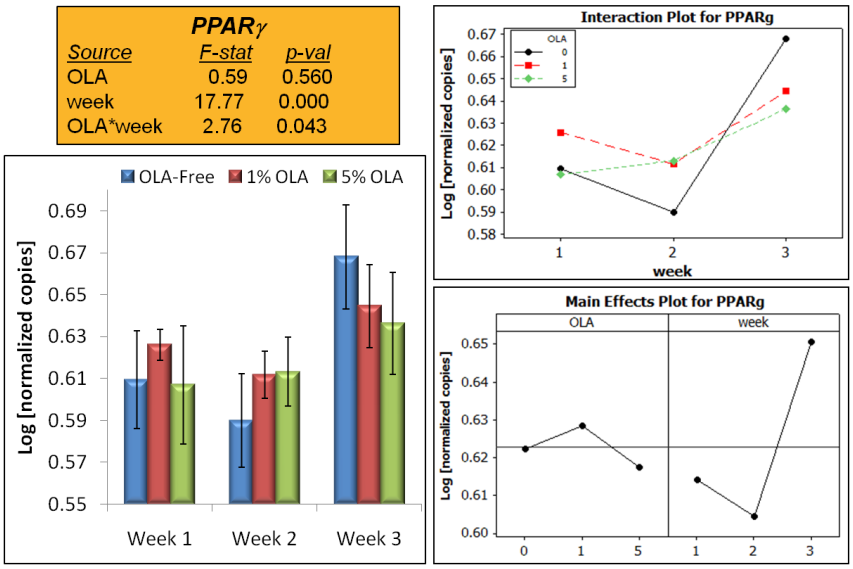

Figure 4.17 - Expression levels of PPARγ for each week. Data presented as the log of normalized expression

In order to further analyze the effects of OLA on PPARs, ratios of expression levels were calculated for ANOVA. First looking at α/γ, the main effect of OLA shows that the *presence* of OLA leads to lesser expression of PPARα with respect to PPARγ. The expression ratios for cells on 1% and 5% OLA scaffolds were nearly identical. Both main effects were significant, and the interaction effect was borderline significant (**Figure 4.18**). The interaction plot shows that the expression profiles for cells on all three scaffolds move similarly between weeks one and two. Then, due to a dramatic increase in PPARγ expression, the expression ratio drops on OLA-free scaffolds. At week one, a t-test of expression ratios was significant between OLA-free and 1% OLA scaffolds, and only borderline significant (p=0.07) between OLA-free and 5% OLA scaffolds. Similarly at week two, t-tests between both OLA scaffolds and OLA-free scaffolds were only borderline significant (p=0.09 for both). Overall, the results show a very strong difference in the ratio of expression levels for PPARα and PPARγ.

The expression ratio of α/δ also showed highly significant changes due to OLA concentration, week, and the interaction of OLA by week (**Figure 4.19**). The main effect

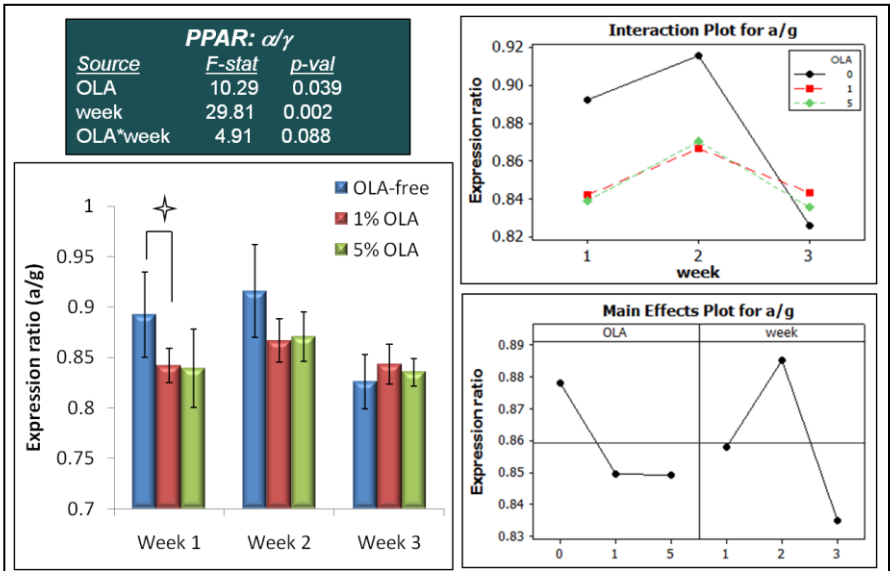

Figure 4.18 – Expression ratio of the α and γ isoforms of PPARs. Star indicates statistically-significant difference ($p \leq 0.05$)

of OLA was a clear decrease in the ratio of α/δ expression with increase in OLA concentration within the scaffold. This decreasing trend was very small between cells on OLA-free and 1% OLA scaffolds, and larger for 5% scaffolds. As shown on the interaction plot, the expression ratio for cells on 5% OLA scaffolds increased by a very small margin each week. At individual time points, the α/δ ratio was significantly different between OLA-free and 5% OLA scaffolds at week one, and then between 5% OLA and the other two scaffolds at week three.

The expression ratio of δ/γ showed the greatest similarities between the three scaffolds (**Figure 4.20**). The effect of OLA was not significant while the effect of week and the interaction effect of OLA by week were both significant. The large changes in expression between weeks was apparent, and the interaction plot for the δ/γ ratio on each scaffold shows a peak at week two and then a decrease, which is likely due to PPARγ up-regulation at week three for each scaffold. Because the effect of OLA was not significant for the δ/γ ratio, it will not be included in the discussion.

4.5 DISCUSSION

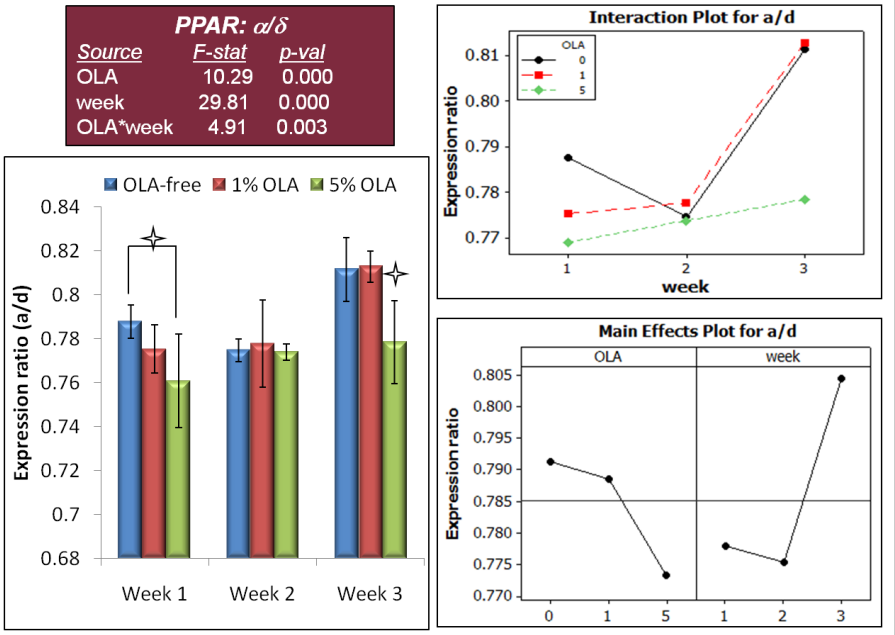

Figure 4.19 – Expression ratio of the α and δ isoforms of PPARs. Star indicates statistically-significant difference ($p \leq 0.05$)

Polymer nanofibers have been shown to support phenotypic behaviors by multiple cell types including neural [238], dermal fibroblasts [239], chondrocytes [240], and vascular endothelial [241]. In this study PCL scaffolds infused with oleic acid were fabricated to produce consistent nanofiber architecture. Characterization by SEM revealed insignificant differences (p=0.3) between the nanofiber architecture for 1% and 5% OLA scaffolds (OLA-free scaffolds were produced from 1% OLA scaffolds), with the mean fiber diameter values being within 20 nm of each other (**Figure 4.1 (a-c)**). The fiber diameter histogram for the two OLA concentrations shows only a slight shift in the scaffolds' fiber diameter characteristics (**Figure 4.1 (d)**). Large variations in fiber diameter are known to affect cellular functionality [139-141, 193]. By verifying that the differences between the fiber diameters are nominal assures that the differences in cell responses observed in this study are not due to the differences scaffold architecture.

Thermal analysis techniques were used to evaluate the differences in crystallinity and composition of different nanofiber scaffolds. DSC was used to determine the % crystallinity of PCL in nanofiber scaffolds (**Figure 4.2 (a)**). The % crystallinity is an

important parameter that governs the degradation of semi-crystalline polymers such as PCL [111, 242, 243]. PCL degrades through hydrolysis of its ester bonds, and amorphous regions are more susceptible to hydrolysis than crystalline regions. Thus, a scaffold with greater PCL crystallinity would likely degrade more slowly than a scaffold with substantially lower PCL crystallinity [237, 244]. As a caveat, enzymatic degradation of PCL does not preferentially target amorphous regions; enzymes may hydrolyze ester bonds in either crystalline or amorphous regions of the polymer [109, 110, 243].

DSC showed insignificant differences between the PCL crystallinity for OLA-free, 1% and 5% OLA scaffolds, and PCL pellets. This would suggest that none of the scaffolds are more or less susceptible to degradation. In the case of enzyme-free conditions, the mass loss data corroborates that hypothesis (**Figure 4.3**) by showing similarly low mass losses. Clearly, enzymatic degradation was much more rapid than degradation mediated by water molecules diffusing through the polymer and hydrolyzing ester bonds. With the large mass loss values in enzyme-assisted samples, bulk erosion certainly took place and that would permit more rapid OLA release. However, both OLA scaffolds were only 1% and 5% OLA, and most of the mass lost was PCL. Overall, these results indicate that the

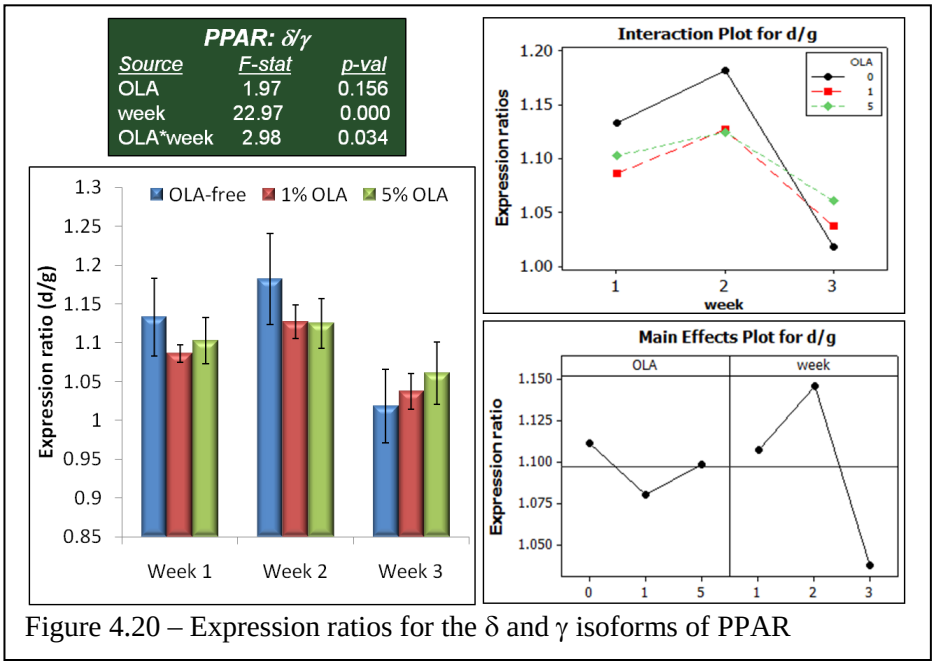

Figure 4.20 – Expression ratios for the δ and γ isoforms of PPAR

electrospinning process as well as inclusion on OLA in the polymer had a negligible effect on its crystallinity. Further, the similarity in the % crystallinity, and the similarity in mass loss values *accounting for enzyme activity* suggest that OLA itself does not increase degradation.

TGA is a useful technique to evaluate the composition of materials. For the 5%, 1%, and OLA-free scaffolds, they were expected to contain 95%, 99%, and 100% PCL respectively. Although the mass loss during TGA for 5% scaffolds was slightly greater than the expected value 95% (**Figure 4.2 (b)**), it was still significantly different than OLA-free, 1% OLA, and untreated PCL. This may be due in part to the encapsulation efficiency for OLA being less than 100%, and that will be examined in the future. Weight loss within the chosen temperature range is associated primarily with loss of PCL [242], although some OLA is also likely to oxidize or degrade away [245]. Most importantly, this data confirms that the 5% OLA scaffolds lost less mass than the 1% OLA and OLA-free scaffolds. This difference is attributed due to higher amount of OLA present in the scaffold.

In order for a synthetic tissue scaffold to augment the natural healing process of the bone, it must support adhesion and proliferation of MSCs. For MSCs, trafficking and migration to an injury site occurs in a very carefully coordinated manner that is not yet fully understood [147, 148, 246]. Once at the site, the cell-cell and cell-ECM interactions significantly influence the capacity of the progenitor cells to differentiate into matrix-producing cell phenotypes [184, 185, 247]. Thus the initial adhesion and proliferation of MSCs is a key requirement for the success of a tissue engineered scaffold for bone regeneration.

In this study, MSCs were cultured on nanofiber scaffolds for up to 7 days in maintenance media (media without osteogenic differentiation factors). The cells were

allowed to adhere and proliferate on the scaffold surfaces. Cell viability on nanofiber scaffolds was measured using MTT assay during the log phase growth (i.e. after 1 and 4 days of culture). This assay measures metabolic levels by detecting the activity of mitochondrial dehydrogenases, though it cannot indicate the task for which cells are expending energy (i.e. cell division, migration, etc.). Our results show that even though the OLA-free scaffolds support highest metabolic activity of MSCs, all scaffolds are clearly capable of supporting viable MSC cultures (**Figure 4.4**). Further, the live cell stain and cell coverage measurements show very strong evidence that the cells are adhering to all the scaffolds. However, there are clear differences in the cell coverage on the scaffolds with different OLA concentrations. These results show that the cell coverage on the scaffolds decreases as the OLA concentration increases. This could be due to individual cells spreading to a lower degree and/or fewer cells populating the scaffolds. For 5% OLA scaffolds, individual cells appear to be less spread than those on 1% OLA and OLA-free scaffolds, and this difference is especially apparent at day 7 (**Figure 4.5**). Further, individual cells on 1% OLA scaffolds displayed a similar spreading morphology as those on OLA-free scaffolds, but the cell density is visibly lower than that on OLA-free scaffolds. Given that fiber diameters for the three scaffolds are very similar, the differences in cell behavior (spreading and colonization) can attributed to the OLA released from within the nanofibers (**Figure 4.6**). The general trend of decreasing metabolic activity with increasing OLA concentration matches well with MTT results. Overall, it appears that the significant differences in cell populations due to OLA are result from a combination of decreased proliferation as well as a lesser degree of cell spreading.

Polymer nanofiber scaffolds offer significant benefits for bone tissue engineering due to their highly featured and porous architecture [34], and the ability to carry bioactive

molecules within the polymer [248]. The key design feature investigated in this work was the inclusion of oleic acid (OLA), a fatty acid that has been linked to increased phenotypic behaviors by osteoblast cell. Fatty acids are a class of biomolecules that have not yet been extensively investigated as a means to enhance mineralization on synthetic scaffolds. The most likely mechanism of action of OLA on osteoblasts is through activation of peroxisome proliferation activator receptors (PPARs) [230, 249]. The activation of the gamma isoform, PPARγ is sufficient to differentiate capable cells into the adipocyte phenotype [250], but the osteogenic influences of PPARs are still unclear. OLA has a low affinity for PPARγ and -δ, and the greatest affinity for PPARα [177], an isoform with a very broad range of functions and has been implicated in mineralization by osteoblast precursor cells [143].

In order to evaluate the effect of OLA on osteogenic differentiation of MSCs, the expression of several key phenotypic markers were investigated. Mineralization was evaluated by measuring ALP activity and calcium deposition on scaffold surface. ALP is a key component of bone matrix vesicles; it cleaves organic phosphate esters, thus potentiating Ca-P crystal nucleation [149, 205, 251]. Pre-osteoblasts typically up-regulate ALP as they differentiate into osteoblasts, and then maturing osteoblasts down-regulate ALP before they either undergo apoptosis or become terminally differentiated osteocytes [39]. As such, it is expected that the statistical significance for the interaction of treatment by time would be highly significant. ALP activity after 1 week of differentiation on all the scaffolds was much lower than that after 2 and 3 weeks of differentiation (**Figure 4.7**). However, the cells on 5% OLA scaffolds exhibited higher levels of ALP activity for the entire duration of culture in osteogenic media, followed by 1% OLA and OLA-free scaffolds. Elevated levels of ALP activity is indicative of

enhanced bone matrix vesicle synthesis by cells on 5% OLA scaffolds as compared to that on other scaffolds.

The ALP expression by pre-osteoblasts and mature osteoblasts leads to deposition of bone mineral matrix on the scaffolds. The mineralization was characterized by measuring the amount of calcium deposited on the scaffold surfaces (**Figure 4.8**). Our results suggest that 5% OLA scaffolds supported highest mineralization. Further, there were insignificant differences in calcium deposition on all the scaffolds for up to 2 weeks of differentiation. This may be due to lower levels of ALP activity. However, there was significant increase in calcium deposited on the scaffolds after 3 weeks of differentiation. Higher levels of ALP activity after 3 weeks of differentiation on 5% OLA scaffolds suggests that the cells on 5% OLA scaffolds would continue deposition of bone mineral matrix at a higher rate than that on other scaffolds.

SEM and EDX can provide valuable information regarding cell colonization and mineralization patterns. By detecting the presence of overlapped Ca and P on the scaffold surface, EDX can make semi-quantitative measurements of surface mineral deposits and demonstrate that they are phases of Ca-P. Spatial elemental mapping with EDX was also used in imaging mode to detect the distribution of Ca and P deposition on scaffold surfaces. EDX elemental map shows large Ca-P aggregates on the scaffold surfaces. In many cases cells were in intimate contact with these aggregates, and non-cellular fibrils (potentially collagen) were clearly visible (**Figure 4.9 (A)**). High magnification EDX elemental maps also confirmed the presence of small Ca-P spherulites that had adsorbed to the nanofiber architecture. In fact, combined SEM/EDX images at high magnification show these spherulites beneath the top-most nanofiber layer (**Figures 4.10 (A, D) red phase**). It should be noted that for all scaffolds, the EDX atomic spectral analysis of mineral deposits on scaffold surfaces indicated presence of

Ca and P with an approximate peak ratio of 1.6 to 1.7 (Ca:P) (**Figures 4.10 (C, F)**), and naturally occurring hydroxyapatite has a Ca:P ratio of 1.66. Precise stoichiometric analysis is difficult with EDX since the scaffolds are coated with gold, and the proximity of the gold and phosphorus peaks in the scans make it difficult to de-convolute the individual signals.

OP and OC are two bone matrix proteins that are differentially regulated by osteoblasts during *de novo* bone matrix production. OP is an acidic phosphoprotein that contains a highly-conserved aspartic acid-rich domain believed to facilitate calcium binding, and it also contains a separate domain capable of binding to integrins [41, 42, 154]. OC contains a calcium-binding glutamic acid sequence, and although it was originally believed to be involved with hydroxyapatite nucleation, it is now believed to be more closely associated with bone tissue remodeling [252]. Both proteins play important roles in bone tissue maintenance, and they contain multiple phosphorylation and sulfation sites that may expose or hide cell-binding domains associated with increased or decreased matrix production, thus their expression by cells is critical for long term success of bone scaffolds. Immunofluorescence images showed cells on all scaffolds had secreted both OC and OP (**Figure 4.13**). OC was deposited on surfaces without discernable differences between scaffolds, whereas OP appeared in greater abundance on 5% OLA scaffolds. This observation was supported by qPCR data which suggested an overall increase in OP expression on 5% OLA scaffolds. The cumulative measure is appropriate because as cells express the OP gene, it will be translated, packaged, and then secreted into the extracellular environment where it can accumulate.

The role of PPARγ in MSC fate processes is becoming clear, and it is regarded as a master regulator for adipocytic differentiation from progenitor cells [145, 253]. However, regulatory roles for PPARα and PPARδ in MSC differentiation are still unclear despite

some preliminary evidence that PPARα/δ agonists enhance bone formation under certain conditions [143, 191]. This work elucidated the differential activation of each of the three PPARs by measuring their respective gene expression levels using qPCR. Quantitatively measuring PPAR gene expression is an accurate assessment of activation because PPAR expression has been inversely related to dose exposure of PPAR agonists to specific isoforms [254]. In other words, as any one PPAR type (α, δ, or γ) is activated by an agonist, its expression may be down-regulated.

The results showed the greatest PPARα expression by cells on OLA-free scaffolds, followed by 1% and then 5% OLA scaffolds (**Figure 4.15**). This indicates that, due to OLA release from 1% and 5% scaffolds, PPARα is being activated at the greatest levels on 5% OLA scaffolds. OLA-free scaffolds also supported the greatest expression of PPARδ, followed by 5% and then 1% scaffolds. The finding that OLA had no significant effect on PPARγ expression was predictable because OLA has and 8-fold lower affinity for PPARγ than for PPARα. Further, OLA is noted to nominally activate PPARγ and efficiently activate PPARα [177, 255]. It is important to note that for both PPARα and PPARδ, the differences in expression levels on 1% and 5% scaffolds was very small (**Figures 4.15 and 4.16**). Yet our previous work showed very large differences in mineralization and ALP activity. To account for this difference, the expression ratios between each of the three PPARs were examined.

Keeping in mind that OLA has an 8-fold greater affinity for PPARα than PPARγ, and that PPARγ is viewed as a master regulator of adipocytic differentiation [231], the expression ratio for α/γ is an important measurement to explain OLA-induced changes in osteoblast behaviors. The overall effect of OLA showed both 1% and 5% scaffolds supporting nearly identical expression ratios (**Figure 4.18**), and both were lower than that for OLA-free scaffolds. This adds additional support to the hypothesis that OLA

released from nanofibers is binding to and activating PPARα at significantly greater levels than PPARγ. A similarly-important observation can be made about the ratio of α/δ expression (**Figure 4.19**), in which the overall effect of OLA led to decreases in expression of PPARα to PPARδ. In this case, there were notable differences between levels on 1% and 5% OLA scaffolds as well as OLA-free scaffolds. Taken together, this may explain for why osteoblast behaviors in this study and our previous one were expressed in greater amounts on 5% OLA than on 1% OLA scaffolds.

A recent study examining nuclear receptor expressions in adipogenic and osteogenic conditions demonstrated that in osteogenic conditions (ie. differentiation by glucocorticoids), PPARα and γ were expressed at nearly equal levels during differentiation in the absence of PPAR agonists [231]. This study, and others examining PPARs and bone also did not examine PPARδ [256], although it is clear here that PPARδ is differentially-expressed. With this in mind, the PPAR expression results here best explain observed differences in osteoblast behaviors when presented as relative ratios of expression. Clearly, OLA released from the PCL nanofibers has altered the expression ratios and increased osteoblast behaviors significantly on 5% OLA scaffolds.

There is one significant concern for a confounding factor influencing the enhanced osteogenic behaviors by cells on 5% OLA scaffolds. Cell coverage measurements (**Figure 4.6**) and calcein images (**Figure 4.5**) showed that by day 7, cells on 5% OLA scaffolds remained very small, with lower cell coverage and observably smaller size. In order to achieve the cuboidal morphology associated with osteoblasts, differentiating progenitor cells may need to remodel their cytoskeletons to a greater degree or more rapidly. RhoA is a Rho-GTPase associated with remodeling of actin filaments, and its expression is necessary for progenitor cells to differentiate into osteoblasts [184, 185]. By showing that RhoA expression was not differentially expressed (**Figure 4.14**) in an

OLA-dependent manner, we ruled out over-expressed RhoA as a possible confounding factor.

In summary, the results present a clear conclusion about the efficacy of infusing OLA into PCL nanofibers for enhancing bone regeneration. The combined SEM/EDX images (**Figures 4.6 and 4.7**) show extensive mineral deposition on all the scaffolds, particularly on 5% OLA scaffolds. This judgment is strongly supported by the results from the Ca and ALP assays which both indicate that mineralization is greatest on 5% OLA scaffolds. Furthermore, von Kossa stains, which stain phosphates, show a dense heterogeneous stain distribution that is associate with bone nodule formation [207]. Finally, densely-deposited non-collagenous bone matrix proteins, notably OP on 5% OLA scaffolds, shows that the mineralization is progressing from small Ca-P spherulite deposits into larger bone nodules. All of these strongly data indicate that 5% OLA supports the greatest *de novo* tissue synthesis.

4.6 Conclusions

This work represents a novel approach of enhancing bone formation on synthetic scaffolds by taking advantage of the simplicity of incorporating stable lipids into polymer nanofibers. This was the first attempt to demonstrate that lipids could differentially affect primary cells in serum-containing media. The fabrication results clearly demonstrated that any differences in cellular response would not derive from the insignificant architectural differences. Cells began to respond to scaffolds with different OLA concentrations beginning on the first day after seeding, as shown with different cell coverage and metabolic activity. After seven days, cells were differentiated by glucocorticoids and the differential response continued through 3 weeks of culture, with 5% OLA scaffolds supporting the greatest levels of osteoblast behaviors and

mineralization. Further, this work demonstrated that two PPAR isoforms – α and δ – were expressed at significantly different levels, and at different ratios with respect to each other and PPARγ. This expression is a suitable surrogate measurement for activation, and thus the likely mechanism of action for increasing osteoblast activities was via PPAR signaling.

4.7 Future work

The most important piece of information to gather in the future will be release data for OLA. Prior to this portion of work being publishable, the release profile must be measured through 28 days – the length of time that cells were cultured on these scaffolds. One attempt was already made for quantifying OLA release with gel chromatography/mass spectroscopy (GC/MS), however the results were partially unusable were excluded from this chapter. However, this is a key piece of data and a second release study will be performed using GC/MS to measure the release at days 1, 4, 7, 14, 21, and 28. Additionally, the encapsulation efficiency of OLA will be measured using GC/MS in order to accurately determine the initial quantities of OLA incorporated into the PCL nanofibers.

The osteoblast behaviors measured in this chapter demonstrated that OLA was effective in enhancing several markers of bone matrix deposition, and that the OLA was likely acting through PPARs. The next step in demonstrating the effectiveness of these PCL-OLA scaffolds is to evaluate their biocompatibility osteoconductivity *in vivo*. Traditionally, this has been done with post-mortem histological analysis of implanted scaffolds. However, new imaging technologies developed over the last decade include the ability to probe for specific proteins and gene transcripts without sacrificing animals, and therefore the same animal can be used for multiple time points in an *in vivo* study.

This, along with post-mortem histological analysis, is an approach which would permit similar gene expression measurements as well as histomorphological evaluation of osteogenesis on PCL-OLA scaffolds.

4.8 References

1. Oest, M.E., et al., *Quantitative assessment of scaffold and growth factor-mediated repair of critically sized bone defects.* J Orthop Res, 2007. **25**(7): p. 941-50.
2. Hartman, O., et al., *Biofunctionalization of electrospun PCL-based scaffolds with perlecan domain IV peptide to create a 3-D pharmacokinetic cancer model.* Biomaterials, 2010. **31**(21): p. 5700-18.
3. Laflamme, C. and M. Rouabhia, *Effect of BMP-2 and BMP-7 homodimers and a mixture of BMP-2/BMP-7 homodimers on osteoblast adhesion and growth following culture on a collagen scaffold.* Biomed Mater, 2008. **3**(1): p. 15008.
4. Basmanav, F., G. Kose, and V. Hasirci, *Sequential growth factor delivery from complexed microspheres for bone tissue engineering.* Biomaterials, 2008. **29**: p. 4195.
5. Hamada, K., et al., *Spatial distribution of mineralized bone matrix produced by marrow mesenchymal stem cells in self-assembling peptide hydrogel scaffold.* J Biomed Mater Res A, 2008. **84**(1): p. 128-36.
6. Hosseinkhani, H., et al., *Bone regeneration on a collagen sponge self-assembled peptide-amphiphile nanofiber hybrid scaffold.* Tissue Eng, 2007. **13**(1): p. 11-9.
7. Lee, J.Y., et al., *Osteoblastic differentiation of human bone marrow stromal cells in self-assembled BMP-2 receptor-binding peptide-amphiphiles.* Biomaterials, 2009. **30**(21): p. 3532-41.
8. Zhang, F., et al., *Sustained BMP signaling in osteoblasts stimulates bone formation by promoting angiogenesis and osteoblast differentiation.* J Bone Miner Res, 2009. **24**(7): p. 1224-33.
9. Zadravec, D., et al., *Ablation of the very-long-chain fatty acid elongase ELOVL3 in mice leads to constrained lipid storage and resistance to diet-induced obesity.* Faseb J, 2010.
10. Mahe, G., et al., *An unfavorable dietary pattern is associated with symptomatic ischemic stroke and carotid atherosclerosis.* J Vasc Surg, 2010.
11. Smit, L.A., A. Baylin, and H. Campos, *Conjugated linoleic acid in adipose tissue and risk of myocardial infarction.* Am J Clin Nutr, 2010. **92**(1): p. 34-40.
12. MacLean, C.H., et al., *Effects of omega-3 fatty acids on cancer risk: a systematic review.* JAMA, 2006. **295**(4): p. 403-15.
13. Leitzmann, M.F., et al., *Dietary intake of n-3 and n-6 fatty acids and the risk of prostate cancer.* Am J Clin Nutr, 2004. **80**(1): p. 204-16.
14. Holmes, M.D., et al., *Association of dietary intake of fat and fatty acids with risk of breast cancer.* JAMA, 1999. **281**(10): p. 914-20.
15. Michalik, L. and W. Wahli, *Peroxisome proliferator-activated receptors: three isotypes for a multitude of functions.* Curr Opin Biotechnol, 1999. **10**(6): p. 564-70.
16. Willson, T., et al., *The PPARs: From Orphan Receptors to Drug Discovery.* Journal of Medicinal Chemistry, 2000. **43**(4): p. 527-550.
17. Jeninga, E.H., et al., *PPAR{gamma} regulates expression of the anti-lipolytic G-protein-coupled receptor 81 (GPR81/Gpr81).* J Biol Chem, 2009.

18. Still, K., et al., *The Peroxisome Proliferator Activator Receptor Alpha/Delta Agonists Linoleic Acid and Bezafibrate Upregulate Osteoblast Differentiation and Induce Periosteal Bone Formation In Vivo.* Calcif Tissue Int, 2008.
19. Jackson, S.M. and L.L. Demer, *Peroxisome proliferator-activated receptor activators modulate the osteoblastic maturation of MC3T3-E1 preosteoblasts.* FEBS Lett, 2000. **471**(1): p. 119-24.
20. Kliewer, S., et al., *Peroxisome proliferator-activated receptors: from genes to physiology.* Recent Prog Horm Res, 2001. **56**: p. 239 - 263.
21. Chan, B., et al., *PPAR agonists modulate human osteoclast formation and activity in vitro.* Bone, 2007. **40**(1): p. 149 - 159.
22. Lin, T.-H., et al., *PPARγ inhibits osteogenesis via the down-regulation of the expression of COX-2 and iNOS in rats.* Bone, 2007. **41**: p. 562-574.
23. Maurin, A.C., et al., *Role of polyunsaturated fatty acids in the inhibitory effect of human adipocytes on osteoblastic proliferation.* Bone, 2002. **31**(1): p. 260-6.
24. Xu, H.E., et al., *Molecular recognition of fatty acids by peroxisome proliferator-activated receptors.* Mol Cell, 1999. **3**(3): p. 397-403.
25. Pirih, F.Q., et al., *Nuclear receptor profile in calvarial bone cells undergoing osteogenic versus adipogenic differentiation.* Journal of Cellular Biochemistry, 2008. **105**(5): p. 1316-1326.
26. Grey, A., et al., *The peroxisome proliferator-activated receptor-gamma agonist rosiglitazone decreases bone formation and bone mineral density in healthy postmenopausal women: a randomized, controlled trial.* J Clin Endocrinol Metab, 2007. **92**(4): p. 1305 - 1310.
27. Lemberger, T., et al., *PPAR tissue distribution and interactions with other hormone-signaling pathways.* Ann N Y Acad Sci, 1996. **804**: p. 231 - 251.
28. Dang, Z. and C.W. Lowik, *The balance between concurrent activation of ERs and PPARs determines daidzein-induced osteogenesis and adipogenesis.* J Bone Miner Res, 2004. **19**(5): p. 853-61.
29. Kawaguchi, H., et al., *Distinct effects of PPARgamma insufficiency on bone marrow cells, osteoblasts, and osteoclastic cells.* J Bone Miner Metab, 2005. **23**(4): p. 275-9.
30. Takada, I. and S. Kato, *[Molecular mechanism of switching adipocyte / osteoblast differentiation through regulation of PPAR-gamma function.].* Clin Calcium, 2008. **18**(5): p. 656-61.
31. Takada, I., et al., *Suppression of PPAR transactivation switches cell fate of bone marrow stem cells from adipocytes into osteoblasts.* Ann N Y Acad Sci, 2007. **1116**: p. 182-95.
32. Guarino, V., et al., *The Influence of Hydroxyapatite Particles on in Vitro Degradation Behaviour of Pcl Based Composite Scaffolds.* Tissue Eng Part A, 2009.
33. Kulkarni, A., et al., *Enzymatic Chain Scission Kinetics of Poly(ε-caprolactone) Monolayers.* Langmuir, 2007. **23**(24): p. 12202-12207.
34. Hoshino, A. and Y. Isono, *Degradation of aliphatic polyester films by commercially available lipases with special reference to rapid and complete degradation of poly(L-lactide) film by lipase PL derived from Alcaligenes sp.* Biodegradation, 2002. **13**(2): p. 141-7.
35. Fregel, R., A. Gonzalez, and V.M. Cabrera, *Improved ethanol precipitation of DNA.* Electrophoresis, 2010. **31**(8): p. 1350-2.
36. Bellows, C.G., S.M. Reimers, and J.N. Heersche, *Expression of mRNAs for type-I collagen, bone sialoprotein, osteocalcin, and osteopontin at different stages of osteoblastic differentiation and their regulation by 1,25 dihydroxyvitamin D3.* Cell Tissue Res, 1999. **297**(2): p. 249-59.

37. Denhardt, D.T. and M. Noda, *Osteopontin expression and function: role in bone remodeling.* J Cell Biochem Suppl, 1998. **30-31**: p. 92-102.
38. Katayama, Y., et al., *Casein kinase 2 phosphorylation of recombinant rat osteopontin enhances adhesion of osteoclasts but not osteoblasts.* J Cell Physiol, 1998. **176**(1): p. 179-87.
39. Khatiwala, C.B., et al., *ECM compliance regulates osteogenesis by influencing MAPK signaling downstream of RhoA and ROCK.* J Bone Miner Res, 2009. **24**(5): p. 886-98.
40. McBeath, R., et al., *Cell shape, cytoskeletal tension, and RhoA regulate stem cell lineage commitment.* Dev Cell, 2004. **6**(4): p. 483-95.
41. Meyers, V.E., et al., *RhoA and cytoskeletal disruption mediate reduced osteoblastogenesis and enhanced adipogenesis of human mesenchymal stem cells in modeled microgravity.* J Bone Miner Res, 2005. **20**(10): p. 1858-66.
42. Gerardo-Nava, J., et al., *Human neural cell interactions with orientated electrospun nanofibers in vitro.* Nanomedicine (Lond), 2009. **4**(1): p. 11-30.
43. Kumbar, S.G., et al., *Electrospun poly(lactic acid-co-glycolic acid) scaffolds for skin tissue engineering.* Biomaterials, 2008. **29**(30): p. 4100-7.
44. Nam, J., et al., *Novel electrospun scaffolds for the molecular analysis of chondrocytes under dynamic compression.* Tissue Eng Part A, 2009. **15**(3): p. 513-23.
45. Grasl, C., et al., *Electrospun polyurethane vascular grafts: In vitro mechanical behavior and endothelial adhesion molecule expression.* J Biomed Mater Res A, 2010. **93**(2): p. 716-23.
46. Badami, A.S., et al., *Effect of fiber diameter on spreading, proliferation, and differentiation of osteoblastic cells on electrospun poly(lactic acid) substrates.* Biomaterials, 2006. **27**(4): p. 596-606.
47. Bashur, C.A., L.A. Dahlgren, and A.S. Goldstein, *Effect of fiber diameter and orientation on fibroblast morphology and proliferation on electrospun poly(D,L-lactic-co-glycolic acid) meshes.* Biomaterials, 2006. **27**(33): p. 5681-8.
48. Bashur, C.A., et al., *Effect of fiber diameter and alignment of electrospun polyurethane meshes on mesenchymal progenitor cells.* Tissue Eng Part A, 2009. **15**(9): p. 2435-45.
49. Chen, M., et al., *Role of fiber diameter in adhesion and proliferation of NIH 3T3 fibroblast on electrospun polycaprolactone scaffolds.* Tissue Eng, 2007. **13**(3): p. 579-87.
50. Persenaire, O., et al., *Mechanisms and kinetics of thermal degradation of poly(epsilon-caprolactone).* Biomacromolecules, 2001. **2**(1): p. 288-94.
51. Zeng, J., et al., *Enzymatic degradation of poly(L-lactide) and poly(epsilon-caprolactone) electrospun fibers.* Macromol Biosci, 2004. **4**(12): p. 1118-25.
52. von Burkersroda, F., L. Schedl, and A. Gopferich, *Why degradable polymers undergo surface erosion or bulk erosion.* Biomaterials, 2002. **23**(21): p. 4221-31.
53. Pitt, C., et al., *Aliphatic polyesters II. The degradation of poly (DL-lactide), poly (epsilon-caprolactone), and their copolymers in vivo.* Biomaterials, 1981. **2**(4): p. 215-220.
54. Pulkkinen, M., et al., *Effects of block length on the enzymatic degradation and erosion of oxazoline linked poly-ε-caprolactone.* European Journal of Pharmaceutical Sciences, 2007. **31**(2): p. 119-128.
55. Prakash, A., et al., *Bilayers as phase transfer agents for nanocrystals prepared in nonpolar solvents.* ACS Nano, 2009. **3**(8): p. 2139-46.

56. Ponte, A.L., et al., *The in vitro migration capacity of human bone marrow mesenchymal stem cells: comparison of chemokine and growth factor chemotactic activities.* Stem Cells, 2007. **25**(7): p. 1737-45.
57. Wang, H.B., et al., *Focal adhesion kinase is involved in mechanosensing during fibroblast migration.* Proc Natl Acad Sci U S A, 2001. **98**(20): p. 11295-300.
58. Brooke, G., et al., *Molecular trafficking mechanisms of multipotent mesenchymal stem cells derived from human bone marrow and placenta.* Stem Cells Dev, 2008. **17**(5): p. 929-40.
59. Chen, C.S., et al., *Geometric control of cell life and death.* Science, 1997. **276**(5317): p. 1425-8.
60. Guarino, V., et al., *Polylactic acid fibre-reinforced polycaprolactone scaffolds for bone tissue engineering.* Biomaterials, 2008. **29**(27): p. 3662-70.
61. Xie, J. and C.-H. Wang, *Electrospun Micro- and Nanofibers for Sustained Delivery of Paclitaxel to Treat C6 Glioma in Vitro.* Pharmaceutical Research, 2003. **23**(8): p. 1817-1826.
62. Musacchio, E., et al., *Effects of unsaturated free fatty acids on adhesion and gene expression of extracellular matrix macromolecules in human osteoblast-like cultures.* Connective Tissue Research, 2007. **48**: p. 34-38.
63. Berger, J. and D. Moller, *The Mechanisms of Action of PPARs.* Annual Review of Medicine, 2002. **53**: p. 409-435.
64. Orimo, H. and T. Shimada, *The role of tissue-nonspecific alkaline phosphatase in the phosphate-induced activation of alkaline phosphatase and mineralization in SaOS-2 human osteoblast-like cells.* Mol Cell Biochem, 2008. **315**(1-2): p. 51-60.
65. Beertsen, W. and T. van den Bos, *Alkaline phosphatase induces the mineralization of sheets of collagen implanted subcutaneously in the rat.* J Clin Invest, 1992. **89**(6): p. 1974-80.
66. Anderson, H.C., et al., *Impaired calcification around matrix vesicles of growth plate and bone in alkaline phosphatase-deficient mice.* Am J Pathol, 2004. **164**(3): p. 841-7.
67. Liu, F., L. Malaval, and J.E. Aubin, *Global amplification polymerase chain reaction reveals novel transitional stages during osteoprogenitor differentiation.* J Cell Sci, 2003. **116**(Pt 9): p. 1787-96.
68. Gordon, J.A., et al., *Bone sialoprotein expression enhances osteoblast differentiation and matrix mineralization in vitro.* Bone, 2007. **41**(3): p. 462-73.
69. Baht, G.S., G.K. Hunter, and H.A. Goldberg, *Bone sialoprotein-collagen interaction promotes hydroxyapatite nucleation.* Matrix Biol, 2008. **27**(7): p. 600-8.
70. Young, M.F., *Bone matrix proteins: their function, regulation, and relationship to osteoporosis.* Osteoporos Int, 2003. **14 Suppl 3**: p. S35-42.
71. Gundberg, C.M., *Matrix proteins.* Osteoporos Int, 2003. **14 Suppl 5**: p. S37-40; discussion S40-2.
72. Hasegawa, T., et al., *The PPARgamma-selective ligand BRL-49653 differentially regulates the fate choices of rat calvaria versus rat bone marrow stromal cell populations.* BMC Dev Biol, 2008. **8**: p. 71.
73. Valmeseda, A., et al., *Opposite regulation of PPAR-a and -g gene expression by both their ligands and retinoic acid in brown adipocytes.* Mol Cell Endocrinol, 1999. **154**: p. 101-109.
74. Kliewer, S.A., et al., *Fatty acids and eicosanoids regulate gene expression through direct interactions with peroxisome proliferator-activated receptors α and γ.* Proceedings of the National Academy of Sciences of the United States of America, 1997. **94**(9): p. 4318-4323.

75. Syversen, U., et al., *Different skeletal effects of the peroxisome proliferator activated receptor (PPAR)alpha agonist fenofibrate and the PPARgamma agonist pioglitazone.* BMC Endocrine Disorders, 2009. **9**(1): p. 10.
76. Venugopal, J., et al., *Electrospun-modified nanofibrous scaffolds for the mineralization of osteoblast cells.* Journal of Biomedical Materials Research Part A, 2007. **85**(2): p. 408-417.

Chapter 5

5.1 Chapter summary

This chapter builds on chapters 3 and 4 by investigating the effects of OLA and HAp on biocompatibility and osteogenesis *in vivo*. The experimental design tested four scaffolds – HAp-free, OLA-free; 3% OLA; 10% HAp; and 3% OLA, 10% HAp. This allowed for the evaluation of each design factor separately and together. For biocompatibility, scaffolds were implanted in paravertebral muscles and then harvested after one or four weeks. They were then stained with hemotoxylin and eosin (H&E) and evaluated for changes in cellular elements and cellular features. For osteogenesis, scaffolds were implanted in calvarial defects and harvested after four weeks. The scaffolds and the adjacent tissue were stained with toluidine blue or hemotoxylin and assayed for tartrate-resistant acidic phosphatase (TRAP) activity. The results showed that all scaffold elicited moderate to severe immune response after one week, and by week four that response had reduced significantly. Bone morphometric analysis showed that both HAp and OLA individually caused enhanced osteoid production in the adjacent bone tissue, and more pre-osteoblasts, osteoblasts, and osteoclasts had populated those scaffold surfaces than control scaffolds (HAp-free, OLA-free). Scaffolds with both HAp and OLA showed the most osteoid in adjacent bone, the most pre-osteoblasts, osteoblasts, and osteoclasts, and then most bone deposition on the implant. Thus although both design factors individually enhance osteogenesis, combining the two design factors together appears to have positive synergy.

5.2 Motivation and Aims

Bone tissue replacements have traditionally been derived from two sources – autograft and allograft. Autografted bone offers a non-immunogenic, biologically-active construct at the expense of tissue at a donor site, and thus availability and donor site pain limit this source's feasibility [6]. Allografted bone tissue is far more abundant than

autografted bone, but immunogenicity and sterility are major concerns, and sterilization procedures such as irradiation or freeze-drying may alter mechanical and biochemical integrity [7, 8]. Synthetic tissue scaffolds offer an attractive option for both availability and sterility, but these are still considered an inferior clinical choice to allograft and autograft because of inferior integration and necrosis related to stress shielding [4, 6, 9]. Thus, synthetic tissue scaffold design strategies over the last decade and more have aimed at making substantial progress in mimicking various features of natural tissue in order to enhance osseointegration [10, 11].

Previous investigations in chapters 3 and 4 have shown that simple modifications to poly(ε-caprolactone) (PCL) nanofiber scaffolds can significantly alter the expression of key osteoblast genes and behaviors. Oleic acid (OLA) is an ω-9 monounsaturated fatty acid that is an agonist for peroxisome proliferator-activator receptors [255], a class of nuclear membrane receptors for which fatty acids are ligands [177]. OLA has been shown to increase key osteoblast behaviors such as alkaline phosphatase (ALP) activity *in vitro* and we have shown evidence of concurrent PPAR activation with ALP up-regulation due to OLA release from nanofiber scaffolds.

Concurrently, including OLA in electrospinning solutions allows for an additional osteogenic design factor – hydroxyapatite (HAp) nanoparticles. OLA acts as a surfactant between the hydrophobic PCL and hydrophilic HAp, thus preventing HAp particle agglomeration and maintaining the scaffold's fibrous morphology. HAp is the major inorganic component of natural bone tissue, and the inclusion of HAp nanoparticles into nanofibrous scaffolds has been shown by our lab and others to moderately increase markers of osteogenesis *in vitro* [32, 175]. However, both design factors have yet to be evaluated *in vivo*. This point is important because most tissue

scaffolds evaluated *in vitro* rely on glucocorticoid-induced osteoblastogenesis which is different from *in vivo* differentiation which occurs by a multitude of soluble signals.

In this chapter, we evaluated the effects of OLA and HAp on *in vivo* biocompatibility and osteogenesis. For biocompatibility, scaffolds were implanted in rat paravertebral muscles and harvested at days 7 and 28, and then they were examined for changes in cellular and tissue characteristics with a hematoxylin and eosin (H&E) stain. For osteogenesis, scaffolds were implanted in critically-sized rat calvarial defects and harvested at day 28. Implant and mineralized tissue analysis were performed using histomorphometric techniques for osteoblasts and osteoclasts.

5.3 Methods

5.3.1 Fabrication and characterization of nanofibrous scaffolds

Scaffold fabrication was performed with electrospinning, which has been previously described. Briefly, poly(ε-caprolactone) (PCL) was dissolved in chloroform at 12% w/w, oleic acid sodium salt was dissolved in methanol at 3% of the weight of PCL, and the two solutions were mixed with a chloroform:methanol ratio of 3:1. For hydroxyapatite (HAp) scaffolds, HAp was mixed into the electrospinning solution at 10% of the solid weight. The solution was electrospun with a blunt-tip 18-gauge catheter at a tip-to-collector distance of 3-3.5", applied voltage of 18-21 kV, and volumetric feed rate of 2.2-2.8 mL/hr, depending on the solution. OLA-free scaffolds were obtained for both Hap-free and 10% HAp scaffolds by soaking the scaffolds in methanol for 24 hours. Scaffold morphology and composition was verified as previously described.

5.3.2 In vivo *Biocompatibility*

Surgeries were performed by a board-certified veterinary surgeon in sterile conditions according to ASTM standard F-763-04 for short-term screening of biomedical implants. 12 male Wistar rats were used for the biocompatibility study in accordance with guidelines developed by NIH Institutional Animal Care and User Committee (IACUC). 6 mm discs of each scaffold were cut with a sterile biopsy punch prior to surgeries, and then sterilized by UV exposure for 30 min and successive washing with deionized water and PBS with an additional 10 min UV exposure between and after the washes. All animals received an analgesic injection of Buprenorphine (0.1ml, 0.005mg) preoperatively and 6 and 24 hours postoperatively. Incision sites and surrounding areas were shaved and disinfected with povidine iodine. 2-3 cm dorsal midline skin incisions were made in the lumbar spine region. For implantation, skin was retracted laterally and four muscle pouches (two cranial and two caudal) were made in the paravertebral muscle on the left and right sides of the spine. The muscle pouch was closed with a single cruciate pattern suture of 5/0 nylon, and the skin then closed with surgical staples. One rat (#3) died approximately 20 hours after surgery, and another rat (#6) exhibited distress for the first 24 hours after surgery but then recovered. All others recovered from surgeries without concern. After 7 and 28 days, 6 of the 12 animals were sacrificed and euthanized with CO_2. Immediately after euthanasia, the implant as well as 1-6 mm of surrounding tissue was removed from the implantation site using a 10 mm biopsy punch and placed in formalin.

For histological analysis, samples were dehydrated in ethanol and embedded in paraffin. Sections were taken from the middle of the implant and stained with hematoxylin and eosin (H&E). A board-certified veterinary histologist then examined the sections for cell and tissue elements. Guidelines described by ATSM standard 981 were used to score cellular elements (polymorphonuclear leukocytes, lymphocytes, plasma

cells, macrophages), cellular changes (giant cells, necrosis, fibrosis), and tissue changes (fat infiltration, foreign material, granuloma).

5.3.3 In vivo *osteogenesis and bone histomorphometry*

Osteogenesis was examined in rat calvarial defects created in the same rats used for biocompatibility studies. Scaffold sterilization and animal handling procedures were the same as in the biocompatibility study. For the surgeries, incision sites were shaved, and a dorsal midline incision was made and the skin was retracted laterally. A 6 mm biopsy punch was used to create calvarial defects in the left and right sides of the rats' skulls and the defect site was rinsed extensively with saline. Sterile 6 mm scaffolds were placed in the defects and the skin was closed over them using 5/0 nylon sutures. When animals were sacrificed for biocompatibility studies as described above, the skulls were harvested and fixed in formalin.

For histological analysis, specimens were kept un-decalcified prior to dehydration. Successive incubation at 4^{o}C in ethanol (70% up to 100%) dehydrated the tissue samples and then they were infiltrated twice for 24 hours (48 hours total) at 4^{o}C in 100 ml destabilized methylmethacrylate (MMA), 14 ml nonylphenyl-polyethyleneglycol acetate (NPG) and 0.33 g anhydrous benzoyl peroxide (BPO) prior to MMA polymerization. Polymerization was initiated at 4^{o}C in 100 ml MMA, 14 ml NPG, 0.55 g BPO and 500 ml N,N dimethyl-p-toluidine 99%. Sectioning was performed on a motorized Leica RM2165 microtome using tungsten-carbide blades. Sections were selected to pass through the middle of implanted nanofiber scaffolds and the histologist ensured that all specimens had the same orientation. For osteoblast analysis, sections were stained with toluidine blue and analyzed at 20x magnification. Osteoclast analysis relied on an enzymatic assay for tartrate-resistant acidic phosphatase (TRAP).

Osteoclast slides were stained with faded hematoxylin for visualization of multinucleated bodies. Each image was subjected to a background subtraction so that the background appeared white for clearer viewing

5.3.4 Statistical analysis

For biocompatibility values, a Mann-Whitney non-parametric test was used to calculate the effect of week, HAp, and OLA on measurements. Significance was defined at the 95% confidence level. Some treatments had a uniform response and all samples contained identical scores, which were incompatible with the Mann-Whitney test. One sample score value was then changed by 0.02 to allow analysis to proceed. Significantly different groups were denoted by the symbol '*'. The sample size for bone histomorphometry measurements was n=1, which does not allow for the application of statistical methods.

5.4 Results

5.4.1 In vivo *Biocompatibility*

In order to assess the differences in the biocompatibility and inflammatory response to osteogenic design factors, scaffolds were implanted into paravertebral muscle spaces according to ASTM standard F-763-04. After 7 or 28 days, the implants were removed and examined histologically for changes in cellular elements and changes (**Table 5.1**). To control for architecture, scaffolds without HAp and leached of OLA were used as negative controls (12-3 leached), and test scaffolds were used to independently evaluate the effects of

Cellular elements		Cellular changes	
Score	*# of elements*	Score	Represents
0	0	0	Absent
1	1-5	1	Minimal
2	6-15	2	Mild
3	16-25	3	Moderate
4	>25	4	Marked

Table 5.1 – Scoring criteria for cellular changes and cellular elements in H&E stained slides

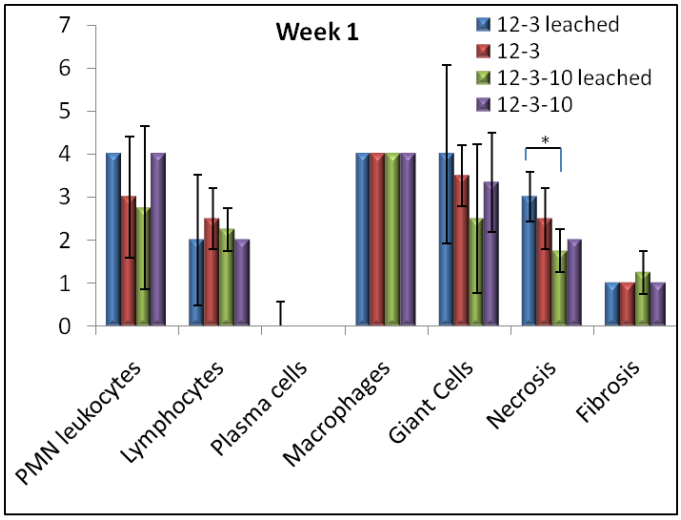

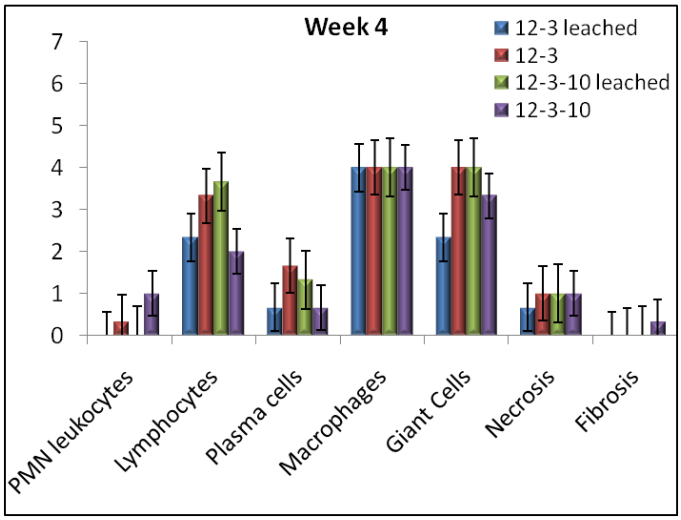

Figure 5.1 – Scores for biocompatibility evaluation for implants, either 1 or 4 weeks post-implantation. Statistically significant ($p \leq 0.05$) point in week 1 is denoted by '*'. PMN refers to polymorphonuclear

HAp (12-3-10 leached) and OLA (12-3) respectively. Scaffolds with both HAp and OLA were used to evaluate any synergistic effects of the two design factors (12-3-10). All implant sites were characterized by localized destruction of the muscle fibers and the formation of fluid-filled spaces immediately adjacent to the scaffolds. There were no discernable morphological differences in tissue response due to scaffold features (ie. HAp and/or OLA).

After seven days, contained large numbers of polymorphonuclear leukocytes (PNMLs), which were identified as primarily eosinophils with a small number of neutrophils also present (**Figure 5.1**). These PMNL were dramatically fewer after 28 days, and plasma cells, which were nearly absent after 7 days, had begun to populate the space near the implant surfaces. Additionally, both necrosis and fibrosis, which were minimal to mild after 7 days, had subsided after 28 days. Statistically, there was only one significant

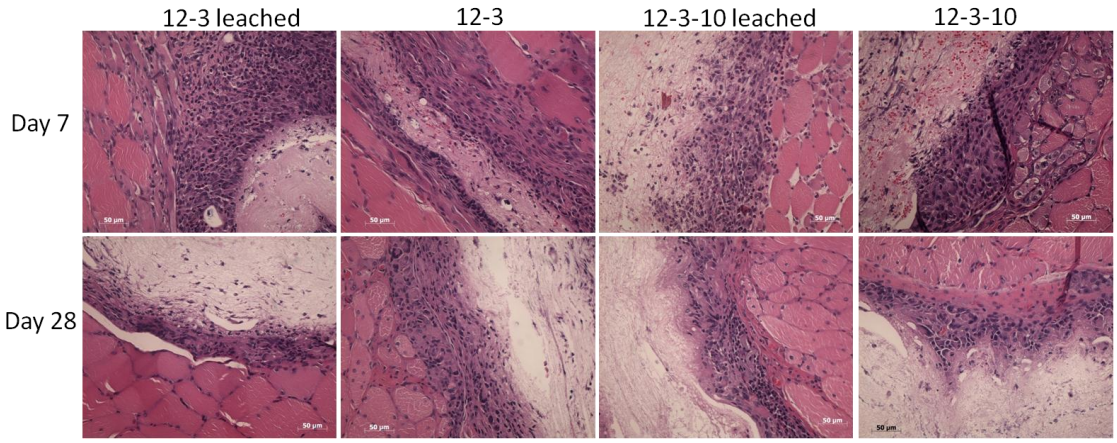

Figure 5.2 – H&E stained implants and the surrounding tissue either 1 or 4 weeks post implantation

difference for all parameters and time-points, and that was the necrosis between 12-3 Leached (OLA-free) and 12-3-10 (10% HAp, OLA-free) scaffolds.

Visually, all the nanofibrous scaffolds appear to permit cellular infiltration. The greatest cellular infiltration at week one occurred on scaffolds with both HAp and OLA (12-3-10) (**Figure 5.2**), which also had a high score – four – of PMNL cells. These PMNLs were identified primarily as eosinophils (brick red cells in all H&E images) with some neutrophils, both of which are immune cells with high mobility and relatively small size (12-17 μm) [257, 258]. Cellular infiltration seems to be less at week four than at week one, as is the score for PMNLs, which also suggests that PMNLs are highly active in infiltrating scaffolds. At week four, cells have still infiltrated scaffolds, and thus some of the other cell phenotypes will also infiltrate the scaffolds.

Finally, tissue necrosis scored between mild and moderate for all scaffolds, with the highest score on HAp-free, OLA-free (12-3 leached) scaffolds. Fibrosis was relatively consistent across all scaffolds, with only a minimal presence. By week four, necrosis had decreased to a minimal level and fibrosis was nearly absent. The changes in necrosis and fibrosis were highly similar for all scaffolds.

5.4.2 In vivo *osteogenesis and bone histomorphometry*

In order to evaluate the osteoconductive action of the two design factors, nanofibrous scaffolds that had been implanted in rat calvarial defects for four weeks were examined histomorphologically for osteoblasts, osteoclasts, and bone or osteoid deposition. Osteoblasts were stained with toluidine blue (**Figure 5.3**), and osteoclasts were stained with hemotoxylin (**Figure 5.4**) and also assayed for TRAP. Staining results were used to analyze the cells and tissue in and around the nanofiber scaffolds. An analysis of the mineralized tissue adjacent to the implants demonstrated several notable differences between scaffolds. First, the percent of bone surface with osteoid (OS/BS %, **Figure 5.5**) was lowest on HAp-free, OLA-free (12-3 leached) scaffolds, then greater on either 10% HAp (12-3-10 leached) or 3% OLA (12-3) scaffolds, and greatest on scaffolds with both 10% HAp and 3% OLA (12-3-10). The same trend was described for two osteoblast measures: the number of osteoblasts lining the bone surface (Ob.S/BS), and the percent of osteoid with osteoblasts adjacent to bone surface (OS(Ob+)/BS). In contrast, the reverse trend was observed for the percent of quiescent surface (QS/BS, or surface with no osteoblast or osteoclast related activity), and for the number of osteoblasts per osteoid surface (N.Ob/OS). Overall, these results indicate that scaffolds with both osteogenic design factors support the greatest neo-mineralization and osteoblast activity on mineralized tissue.

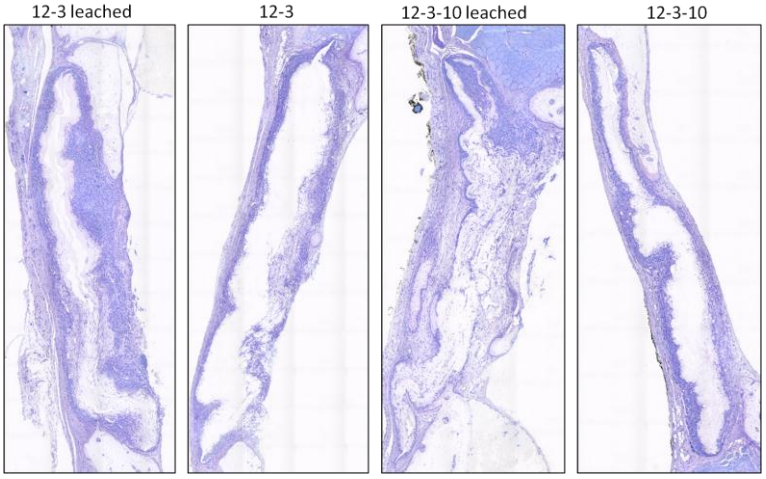

Figure 5.3 – Osteoblasts and implants, 4 weeks post-implantation

Analysis of the implants was performed using the same stains. The histologist noted that cellular infiltration was minimal, but all implant surfaces were heavily covered by cells, and this trend can be seen on any of the stained slides (**Figures 5.3 and 5.4**). Osteoblast, pre-osteoblasts, and osteoclasts were identified with the stains, and all showed the lowest population presence on scaffolds with neither OLA nor HAp (12-3), and the most on scaffolds with both factors, and a milieu on scaffolds with either HAp or OLA (**Figure 5.6**). The percent of bone tissue in the tissue surrounding the implant (BV/TV%) and the bone surface density (BS/TV) showed similar trends (**Figure 5.7**), which were slightly different from the analysis of cells adjacent to the implanted scaffolds. In both cases, scaffolds with HAp (12-3-10 leached and 12-3-10) supported the highest levels of osteoid by both measurements. Overall, osteoblasts, pre-osteoblasts, and osteoclasts responded to

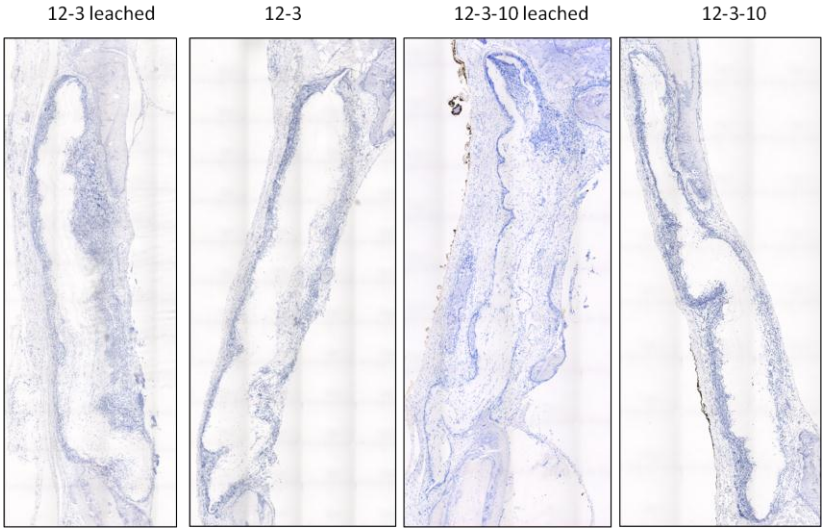

Figure 5.4 – Osteoclasts and implants, 4 weeks post-implantation

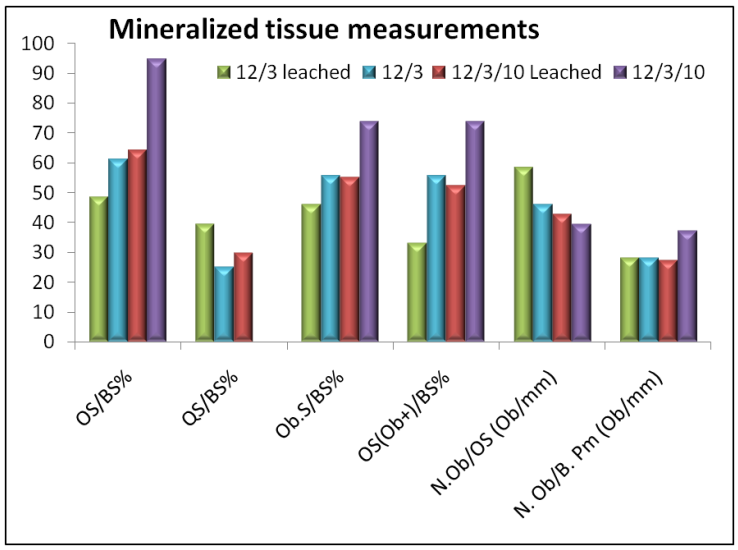

Figure 5.5 – Mineralized tissue measurements of implants, 4 weeks post-implantation

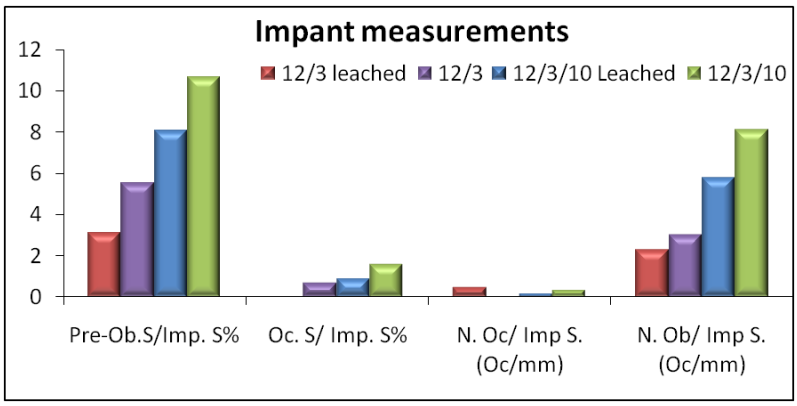

Figure 5.6 – Measurements of the cell types lining the implants

the osteogenic design factors, and the two design factors together resulted in the greatest presence of important bone remodeling cells on the implant surfaces. Based on the amount of osteoid deposited in the tissue adjacent to the implants, HAp induces a greater osteogenic response than OLA.

5.5 Discussion

In order to evaluate the biocompatibility and osteoconduction of nanofiber scaffolds with and without HAp and OLA, the scaffolds were implanted either in paravertebral muscle pouches or calvarial defects. Nanofiber constructs offer an attractive platform for implants for several reasons. As has been demonstrated here, nanofiber scaffolds may carry multiple design factors within the same construct. Additional modifications to these scaffolds, for example growth factor or peptide delivery, may yet be incorporated. Furthermore, the nanofibrous morphology allows water and enzymes a high level of access to the polymer so that it may degrade at a fast enough rate so as to permit osteoid deposition and neo-vascularization throughout the full scaffold volume.

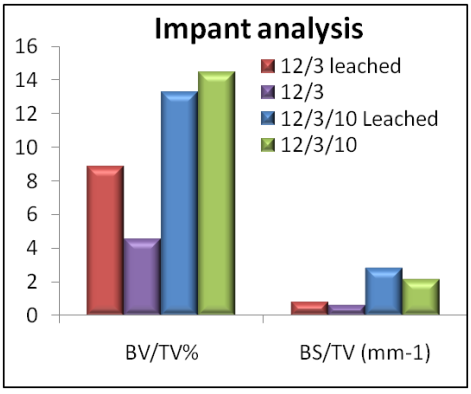

Figure 5.7 – Analysis of tissue deposited directly onto scaffolds

The results demonstrate two important

points regarding the two design factors of interest. First, neither design factor significantly increased the inflammatory response relative to HAp-free, OLA-free scaffolds (**Figure 5.1**). Second, in an osseous environment, the design factors individually and synergistically enhance new osteoid deposition (**Figure 5.5**) and pre-osteoblast, osteoblast, and osteoclast populations (**Figure 5.6**). These two observations are tied together because normal fracture healing involves an inflammatory response, during which immune cells such as granulocytes and macrophages are recruited to the wound to remove microbes and debris before osteoblasts and chondroblasts arrive to begin tissue remodeling [259]. The nearly minimal and absent necrosis and fibrosis, respectively (**Figure 5.1**), at week four is permissive for the tissue remodeling that was observed in calvarial defects after four weeks.

Pre-osteoblasts and osteoblasts have a dissimilar morphology and gene expression profile, with osteoblasts expressing mineralization-associated genes such as alkaline phosphatase and pre-osteoblasts expressing proliferation-related genes [39, 206]. With both osteoblasts and pre-osteoblasts present on scaffolds that have been implanted for four weeks, it is likely that these cells have been recruited from the general cell population. Cell recruitment is a key difference between *in vivo* and *in vitro* culture conditions because *in vitro* culture conditions typically involve only a single cell-seeding event and differentiation by dexamethasone, a glucocorticoid, rather than soluble growth factors [260]. As a result of those two conditions, it is difficult to conceive of a series of *in vitro* events which would permit these two distinct phenotypes to co-exist in large numbers. Further, the balance of matrix deposition by osteoblasts and matrix resorption by osteoclasts dictates the net rate of osteoid and bone formation. However, if there are active osteoclasts within the cell population, dexamethasone down-regulates osteoprotegrin production, thus biasing this balance towards greater osteoclast activity *in*

vitro [261, 262]. These differences are important to keep in mind when comparing the results presented herein with results from *in vitro* cell experiments.

With regards to the two osteogenic design factors, OLA and HAp, there is clear evidence that neither factor substantially increases the inflammatory response or decreases the biocompatibility of the nanofibrous construct (**Figure 5.1**). Scaffolds with HAp nanoparticles also showed the greatest overall support for osteoid formation and bone tissue remodeling, based on the numbers of pre-osteoblast, osteoblast, and osteoclasts (**Figure 5.5 and 5.6**), and the analysis of tissue surrounding the implant (**Figure 5.6 and 5.7**). Although OLA increased the numbers of bone-related cells and new osteoid (**Figure 5.5 and 5.6**), the effect of OLA on bone deposition onto the scaffolds was less clear. OLA slightly increased the percent of bone tissue for HAp scaffolds, but the opposite effect was observed on HAp-free scaffolds (**Figure 5.7**). Taken together this indicates that HAp has a more osteoconductive effect, and that OLA may be synergistically osteogenic in the presence of mineralized scaffolds.

5.6 Conclusions

Scaffolds were fabricated to evaluate the effects of HAp nanoparticles and OLA on biocompatibility and bone formation *in vivo*. The results indicated that neither design factor negatively affected biocompatibility separately or in combination. All scaffolds caused mild to moderate necrosis and the recruitment of PMNLs to the implant site after one week, and both these inflammatory markers were minimal or absent by four weeks. A histomorphological analysis of the cells and tissue on and adjacent to the implants revealed that both factors increase the numbers of bone-related cells. Both factors also increased the new osteoid on mineralized tissue, but only HAp increased the bone volume on the implants.

5.7 Future work

This work on its own shows that both OLA and HAp enhance new osteoid production, with HAp being the more osteogenic of the two design factors. This work combined with chapter 3 which shows only modest gains in ALP due to HAp *in vivo* and decreases in type I collagen expression. The disparity between the *in vivo* and *in vitro* osteogenesis results is an area of research that should be explored. One likely cause for the differences is the differentiation method. *In vitro* osteoblastogenesis is achieved by glucocorticoid treatments, while *in vivo* differentiation is achieved by soluble signals such as bone morphogenic proteins, fibroblast growth factors, WNTs, and hedgehog proteins [263]. Medical imaging technologies such as transcription MRI have been developed to the point of being able to quantify active gene transcription *in vivo* [264, 265]. Changes in osteoblastogenesis markers such as Runx2/Cbfa1, osterix, ALP, Col1, and osteoprotegerin due to HAp in nanofibers should be investigated. For long-term work, osteo-immuno crosstalk is highly complex [44, 45] and likely to change due to these osteogenic design factors. An accurate profile of just a few differential responses *in vivo* would provide valuable insight which can be used to incorporate additional osteogenic design features into bone tissue scaffolds.

5.8 References

1. Lewandrowski, K-U, J D. Gresser, DL Wise and DJ Trantolo, *Bioresorbable bone graft substitutes of different osteoconductivities: a histologic evaluation of osteointegration of poly(propylene glycol-co-fumaric acid)-based cement implants in rats.* Biomaterials, 2000. **21**(8): p. 757-764.
2. Moreau, MF, Y Gallois, M-F Baslé and D Chappard, *Gamma irradiation of human bone allografts alters medullary lipids and releases toxic compounds for osteoblast-like cells.* Biomaterials, 2000. **21**(4): p. 369-376.
3. Akkus, O and CM Rimnac, *Fracture resistance of gamma radiation sterilized cortical bone allografts.* Journal of Orthopaedic Research, 2001. **19**(5): p. 927-934.
4. Salgado, AJ, OP Coutinho and RL Reis, *Bone tissue engineering: state of the art and future trends.* Macromol Biosci, 2004. **4**(8): p. 743-65.
5. Soucacos, PN, EO Johnson and G Babis, *An update on recent advances in bone regeneration.* Injury, 2008. **39 Suppl 2**: p. S1-4.
6. Alves, NM, IB Leonor, HS Azevedo, RL Reis and JF Mano, *Designing biomaterials based on biomineralization of bone.* Journal of Materials Chemistry, 2010. **20**(15): p. 2911-2921.
7. Jang, J-H, O Castano and H-W Kim, *Electrospun materials as potential platforms for bone tissue engineering.* Advanced Drug Delivery Reviews, 2009. **61**(12): p. 1065-1083.
8. Kliewer, SA, SS Sundseth, SA Jones, PJ Brown, GB Wisely, CS Koble, P Devchand*, et al.*, *Fatty acids and eicosanoids regulate gene expression through direct interactions with peroxisome proliferator-activated receptors α and γ.* Proceedings of the National Academy of Sciences of the United States of America, 1997. **94**(9): p. 4318-4323.
9. Xu, HE, MH Lambert, VG Montana, DJ Parks, SG Blanchard, PJ Brown, DD Sternbach*, et al.*, *Molecular recognition of fatty acids by peroxisome proliferator-activated receptors.* Mol Cell, 1999. **3**(3): p. 397-403.
10. Lee, JH, NG Rim, HS Jung and H Shin, *Control of osteogenic differentiation and mineralization of human mesenchymal stem cells on composite nanofibers containing poly[lactic-co-(glycolic acid)] and hydroxyapatite.* Macromol Biosci, 2010. **10**(2): p. 173-82.
11. Wutticharoenmongkol, P, P Pavasant and P Supaphol, *Osteoblastic Phenotype Expression of MC3T3-E1 Cultured on Electrospun Polycaprolactone Fiber Mats Filled with Hydroxyapatite Nanoparticles.* Biomacromolecules, 2007. **8**(8): p. 2602-2610.
12. Wang, X, H Zhao and R Andersson, *Proteomics and leukocytes: an approach to understanding potential molecular mechanisms of inflammatory responses.* J Proteome Res, 2004. **3**(5): p. 921-9.
13. Tachimoto, H, M Ebisawa and BS Bochner, *Cross-talk between integrins and chemokines that influences eosinophil adhesion and migration.* Int Arch Allergy Immunol, 2002. **128 Suppl 1**: p. 18-20.
14. Komatsu, DE and SJ Warden, *The control of fracture healing and its therapeutic targeting: Improving upon nature.* Journal of Cellular Biochemistry, 2010. **109**(2): p. 302-311.
15. Liu, F, L Malaval and JE Aubin, *Global amplification polymerase chain reaction reveals novel transitional stages during osteoprogenitor differentiation.* J Cell Sci, 2003. **116**(Pt 9): p. 1787-96.
16. Kulterer, B, G Friedl, A Jandrositz, F Sanchez-Cabo, A Prokesch, C Paar, M Scheideler*, et al.*, *Gene expression profiling of human mesenchymal stem cells derived from bone marrow during expansion and osteoblast differentiation.* BMC Genomics, 2007. **8**: p. 70.

17. Robling, AG, AB Castillo and CH Turner, *Biomechanical and molecular regulation of bone remodeling.* Annu Rev Biomed Eng, 2006. **8**: p. 455-98.
18. Kim, HJ, H Zhao, H Kitaura, S Bhattacharyya, JA Brewer, LJ Muglia, FP Ross*, et al.*, *Dexamethsone suppresses bone formation via the osteoclast.* Adv Exp Med Biol, 2007. **602**: p. 43-6.
19. Kondo, T, R Kitazawa, A Yamaguchi and S Kitazawa, *Dexamethasone promotes osteoclastogenesis by inhibiting osteoprotegerin through multiple levels.* J Cell Biochem, 2008. **103**(1): p. 335-45.
20. Karsenty, G, HM Kronenberg and C Settembre, *Genetic Control of Bone Formation.* Annu Rev Cell Dev Biol, 2009. **25**: p. 629-648.
21. Liu, CH, Z You, J Ren, YR Kim, K Eikermann-Haerter and PK Liu, *Noninvasive delivery of gene targeting probes to live brains for transcription MRI.* Faseb J, 2008. **22**(4): p. 1193-203.
22. Liu, PK, JB Mandeville, D Guangping, BG Jenkins, YR Kim and CH Liu, *Transcription MRI: a new view of the living brain.* Neuroscientist, 2008. **14**(5): p. 503-20.
23. Lorenzo, J, M Horowitz and Y Choi, *Osteoimmunology: interactions of the bone and immune system.* Endocr Rev, 2008. **29**(4): p. 403-40.
24. Takayanagi, H, *Osteoimmunology: shared mechanisms and crosstalk between the immune and bone systems.* Nat Rev Immunol, 2007. **7**(4): p. 292-304.

Chapter 6

6.1 Chapter Summary

The goal of this chapter was to develop a biodegradable, antimicrobial tissue scaffold that could deliver various antibiotics while providing architecture for tissue regeneration. This study determined the release profile and bactericidal efficacy of rifampicin (RIF) against Gram-positive and Gram-negative bacteria in static-flow conditions. Antibiotic-loaded scaffolds were fabricated by electrospinning poly (ε-caprolactone) (PCL) with RIF so that the mass of RIF was either 9% or 16% of the final solid mass. SEM was used to quantify scaffold morphology based on the fiber diameters measured, and scaffold composition was verified using thermogravimetric analysis (TGA). The release of RIF from scaffolds was measured at hours 1, 4, 8, and 24 by colorimetric assay. In order to determine the bactericidal efficacy, RIF scaffolds and RIF-free scaffolds were placed in either lysogeny or trypticase soy broth and inoculated with either *Pseudomonas aeruginosa* (*PA*) or *Staphylococcus epidermidis* (*SE*), respectively. Each hour for 0-6 hours, aliquots of the medium were removed and filtered through a membrane for counting with fluorescent microscopy. Bacterial growth and extracellular polysaccharide secretion was also examined using SEM on scaffolds after 6 hours of bacterial growth. Results showed that mean fiber diameters were within 200 nm for all three scaffolds, with 9% RIF scaffolds being significantly different than the other two. TGA confirmed that the 9% and 16% RIF scaffolds contained the intended amounts of RIF, and the release profiles for both RIF scaffolds showed significant differences in the mass released. Both profiles exhibited a burst during the first 8 hours, and by 24 hours both scaffolds had stopped releasing RIF. The cumulative release profile for 16% RIF was greater at each time point, and the duration of release was longer than that of 9% RIF scaffolds. Bacterial growth on RIF-loaded scaffolds was hindered compared to control materials. SEM images showed clear differences between bacterial growth on RIF-free

and PCL-RIF scaffolds. Both bacterial species formed dense populations and secreted extracellular polysaccharides (EPS) on the RIF-free scaffolds. *PA* or *SE* exhibited minimal colonization on both RIF scaffolds.

6.2 Motivation and Aims

Major orthopaedic surgeries such as total joint arthroplasty (ie. hip and knee), internal fracture fixation, and spinal fusion require invasive surgeries that are accompanied with the potential for life-threatening infections [266]. Amongst the most popular clinical strategies for combating infection is two-stage re-implantation in which infected tissue is removed along with the implant [130], and antibiotic-loaded cement is often loaded into the vacated space to prevent wound closure [267]. After approximately six weeks of local and systemically administered antibiotics, the patient receives another implant. Thus, a patient would undergo three surgeries and withstand an infection plus powerful antibiotics such as vancomycin or methicillin [122]. Prophylactic measures such as antibiotic implant coatings [268] offer a means to reduce the occurrence and severity of these infections.

Electrospun nanofibers have been effective in delivering biologically-active molecules such as growth factors [269, 270], short peptides [215], and antibiotics [271]. The deposited fibers may form a surface coating on an implant or a stand-alone nanofibrous matrix from which a desired molecule can elute [158]. By releasing these molecules locally, highly-effective concentrations may be achieved while avoiding potentially toxic effects by reducing the overall systemic concentrations. Furthermore, drugs such as gentamicin or vancomycin are ineffective when taken orally, and localized delivery from electrospun nanofibers would avoid intravenous administration.

Staphylococcus Epidermis (*SE*) and *Pseudomonas Aeruginosa* (*PA*) are Gram-positive and Gram-negative microbes, respectively. *SE* is involved with approximately 30% of bacterial colonies in clinical orthopaedic implants [272, 273]. *PA* is the most common non-*staphylococcus* bacterial strain found in clinical orthopaedic infections [273]. Although infection rates are low for closed fractures, up to 60% of all open fractures are infected when the injury occurs [274]. It should be noted that even for the more favorable closed-fracture scenario, prophylactic antibiotic administration has been shown to significantly reduce incidence of infections [275]. Thus, for implantation surgeries, including an antibiotic treatment, even if the risk of infection is low, is likely to help reduce hospital-acquired infections which cost an average of $68,000 per patient [276].

In this chapter, PCL nanofibers were loaded with rifampicin (RIF), an antibiotic that is most effective against Gram-positive bacteria. Scaffolds were loaded with two concentrations of RIF, and the release profile of RIF from PCL nanofibers was measured. Then the bactericidal efficacy of PCL-RIF nanofiber scaffolds was evaluated using a Gram-positive and Gram-negative strain of bacteria – *Staph E.* and *Pseud. A.* respectively – in static conditions.

6.3 MATERIALS AND METHODS

6.3.1 Fabrication & Characterization of Nanofiber Scaffolds

Nanofiber scaffolds were fabricated by electrospinning 80,000 molecular weight PCL polymer (Sigma) solution (12% w/w) with 3% oleic acid sodium salt (Sigma), and 0%, 9% or 16% Rifampicin (RIF). PCL, OLA, and RIF were dissolved in a solvent mixture of 3:1 (volume ratio) chloroform:methanol (Sigma) and loaded into a glass syringe (Hamilton, Gastight 1010). The polymer solution was fed to a blunt-tip catheter

by a syringe pump (Harvard Apparatus) at a rate of 1.8-2.1 mL/hr. A high-voltage power supply (Gamma High Voltage Research, model ES30P-10W/DAM) was used to apply voltage in the range of 18-21 kV to the blunt-tip catheter that was positioned 4-4.5" from the grounded collector plate.

In order to examine the morphology of the nanofiber scaffolds and determine the fiber diameter, they were sputter-coated with 10 nm of gold and imaged under high magnification using a field-emission scanning electron microscope (SEM, JEOL JSM-6500F). Fiber diameters were measured using SEM image analysis software. Ten measurements were made on each scaffold with n_{min}=30 and size distribution histogram was plotted.

Thermal characterization of the nanofiber scaffolds was performed to determine the effect of electrospinning process on polymer crystallinity and thermal stability. Differential scanning calorimetry (DSC, TA Instruments DSC 2920) was used to determine the polymer crystallinity in different nanofiber scaffolds. The scaffolds were heated from 5^{o}C to 120^{o}C at 5^{o}C/min and the crystallinity of a sampled was calculated by the following equation:

$$X_c\% = 100 \times \frac{\Delta H_{m,sampl}}{\Delta H_{m,std}} \quad \text{Equation 6.1}$$

where $\Delta H_{m,sample}$ is the enthalpy of melting of the nanofiber scaffold and $\Delta H_{m,std}$ is the enthalpy of melting of 100% crystalline PCL ($\Delta H_{m,std}$ = 139 J/g) [174].

6.3.2 Rifampicin release from nanofibers

The release profile of rifampicin (RIF) from PCL nanofibers was evaluated at hours 1, 4, 8, and 24. 10 mm discs were cut out using a biopsy punch and then placed in 1mL sterile PBS at 37^{o}C and 100% humidity. At each aforementioned time point, a 200 μL

aliquot of PBS was removed and replaced with 200 μL of fresh PBS. Each aliquot was immediately stored in a -80°C freezer until the completion of the release study. The concentration of antibiotic in each aliquot was measured colorimetrically by subtracting the absorbance at 690 nm from 570 nm. Concentration data points were fitted to the Peppas equation for diffusion-mediated release, which takes the form:

$$\frac{M_t}{M_{tot}} = kt^n \quad \text{(Equation 6.2)}$$

In this equation, t is a time point, M_t, and M_{tot} are the mass released at time, t, and the total mass within the scaffold. This means that M_t/M_{tot} is the percent of antibiotic released at t. The constant k accounts for the ground matrix (polymer nanofibers) and drug (RIF) characteristics, and n is the diffusional exponent [277, 278].

6.3.3 Static bacterial challenge

Scaffolds were placed in 3 mL of lysogeny or trypticase soy broth and inoculated with either *Pseudomonas aeruginosa* (*PA*) or *Staphylococcus epidermidis* (*SE*), respectively. Each hour for 0-6 hours, aliquots of the medium were removed and filtered through a 100nm membrane. Trapped bacteria were then stained with Live/Dead BacLight™ (Invitrogen) stains and counted microscopically. BacLight™ contains SYTO 9 and propidium iodide which stain live and dead bacteria respectively. SYTO 9 is a proprietary stain that gives a fluorescent signal for live bacterial cells. Propidium iodide (PI) is impermeable to intact cell membranes, and live cells will exlude this dye. When bacteria no longer maintain their cell membranes, the PI can diffuse into cells and intercalate DNA. SYTO 9 (ex: 480 nm; em: 550 nm) and PI (ex: 490; em: 635 nm) were visualized at identical locations and the images were used to count live and dead bacteria using ImageJ (NIH). After 6 hours, scaffolds were fixed in 3% glutaraldehyde

and dehydrated in an ethanol wash series. Scaffolds were sputter coated with 7 nm of gold and examined under SEM.

The growth of the population was modeled, with a focus on the exponential population growth phase (**Figure 6.1**). The exponential growth constant, μ, for the population was determined by the microbial growth equation:

$$\frac{dN}{dt} = \mu N \quad \text{(Equation 6.3)}$$

When this equation is integrated over time, *t*, and the terms arranged to solve for μ it takes the form:

$$\mu = \frac{Ln\, N_t - Ln\, N_0}{t - t_0} \quad \text{(Equation 6.4)}$$

where *N* is the number of bacteria, also referred to as the population.

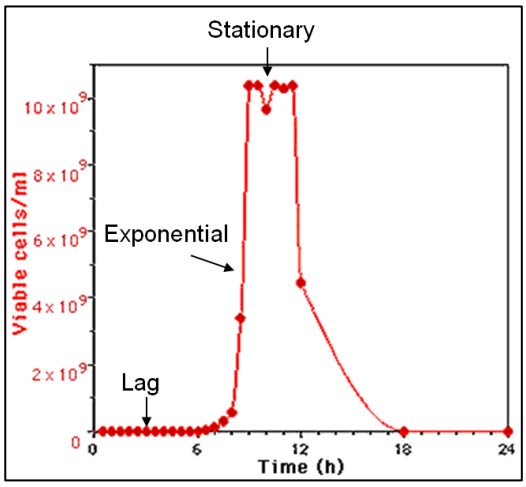

Figure 6.1 – Stages of bacterial population growth and maintenance

6.3.4 Statistical analysis

The scaffold characterization methods evaluating the effects of RIF on fiber diameter and crystallinity were evaluated with t-tests. For the release study, a nonlinear regression was used to fit the constants for equation 1 using a least-squares method. For bacterial growth data, the population values were analyzed using linear regression on a log(10) scale to determine the significance of the effects of hours, RIF, and hours*RIF. Significance was defined at the 95% confidence level. All analysis was performed in Excel as well as in JMP statistics software (SAS).

6.4 RESULTS

6.4.1 Fabrication and Characterization of Nanofiber Scaffolds

All scaffolds were fabricated to contain 3% OLA as a process stabilizer, and RIF-loaded scaffolds were fabricated to have two RIF concentrations – 9% or 16% of the solid scaffold weight. In order to characterize the architecture of the scaffolds, scaffolds were examined under SEM and their fiber diameters were measured. The 9% RIF scaffolds were significantly different from the other two scaffolds, and their measurements showed the narrowest distribution and the smallest mean fiber diameter (**Figure 6.2**). The 16% RIF scaffolds had the flattest distribution of fiber diameters, with quite a few very large fibers, and SEM images reflect this relatively even distribution. Although the mean fiber diameters for RIF-free and 16% RIF scaffolds were statistically similar, their distributions are clearly different. Similarly, the fiber diameters for RIF-free and 10% RIF scaffolds were statistically different, but their fiber diameter distributions were fairly similar except for the occurrence of larger fibers on RIF-free scaffolds.

Differential scanning calorimetry (DSC) results showed that the PCL in RIF-free scaffolds had the highest value of crystallinity (**Figure 6.3**), and a t-test revealed that this difference was significant compared to both RIF scaffolds. The test between 9% and 16% RIF scaffolds was not significantly different.

6.4.2 Rifampicin release from nanofibers

The release of RIF from nanofiber scaffolds was studied by removing small aliquots of media (PBS) at hours 1, 4, 8, and 24. The concentration of the RIF within each aliquot was calculated by generating standard curves and measuring the absorbance at 475 nm. An adjustment accounting for the removed media was used when calculating the

mass released of RIF, and the percent released was fit

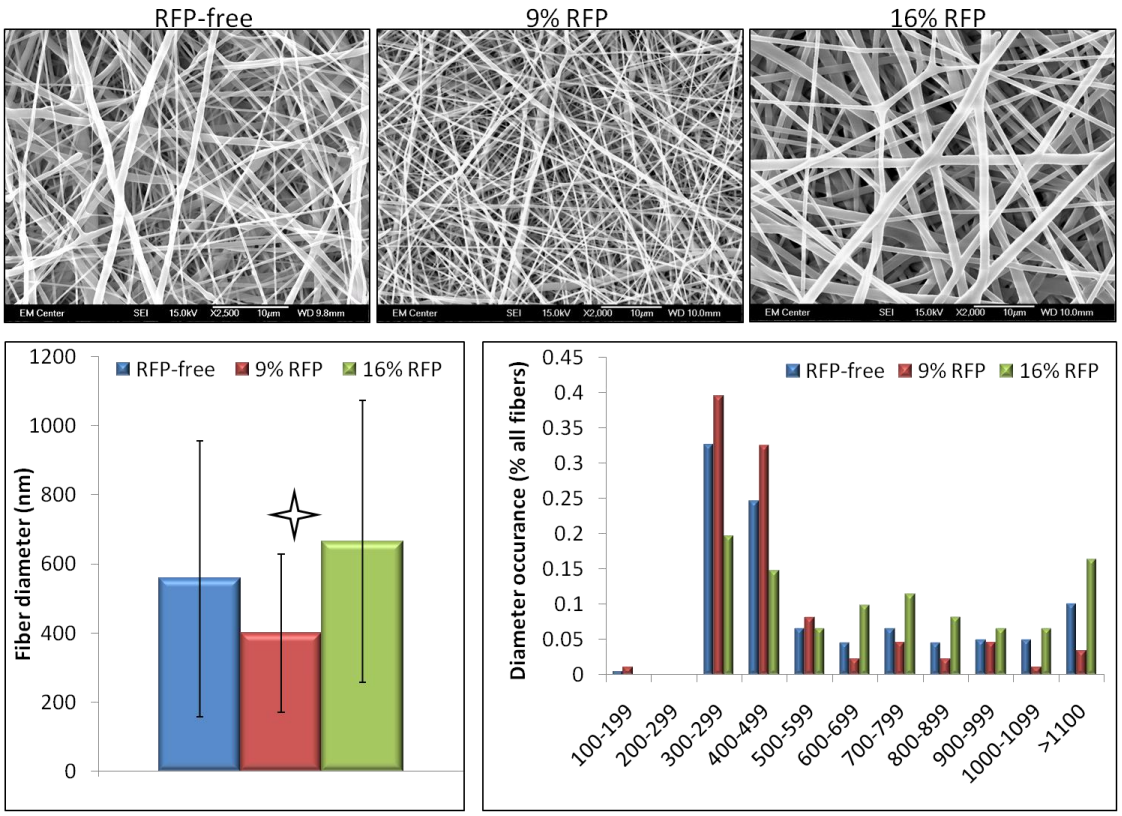

Figure 6.2 – SEM of scaffolds, mean fiber diameters, and fiber diameter histograms. Magnification for RFP-free scaffolds is 2500x, magnification for 9% and 16% RFP scaffolds is 2000x. Scale bar for all SEM images is 10 μm. Star for fiber diameter plot indicates significant difference ($p \leq 0.05$).

to equation 2. The results for percent release (**Figure 6.4 (A)**) showed that both scaffolds initially released a burst of antibiotic and then the release quickly died off. 9% RIF scaffolds released a greater percent of their theoretical loading, and the release occurred more rapidly than 16% scaffolds. The models for both release profiles fit experimentally-measured values very closely for the initial release, which took place during the first 8 hours. Between eight and twenty-four hours, only a small percent of mass was released and the models predicted a much larger zero-order release which did not match the measured trend. The mass release (**Figure 6.4 (B)**) showed that 9% scaffolds released most of the mass very quickly, within the first 4 hours, while 16% scaffolds released most of the mass by 8 hours. The difference in mass released was

clear after just 1 hour and the total mass released by 16% scaffolds was approximately twice the amount released by 9% scaffolds.

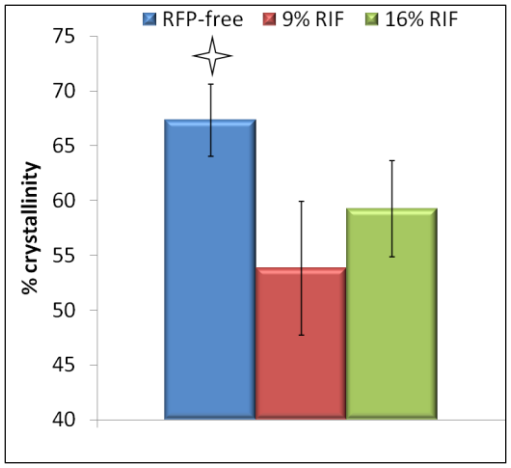

Figure 6.3 – % crystallinity measured by differential scanning calorimetry

6.4.3 Static bacterial challenge

Two strains of bacteria, Gram-negative *Psuedomonas Aeruginosa* (*PA*) and Gram-positive *Staphylococcus Epidermis* (*SE*), were used to determine the inhibitory effect of RIF release on bacterial colony growth. Bacterial colonies were sampled, filtered, and fluorescently stained with a commercially-available kit for microscopic population counting. Because of rapid population growth, a series of different dilutions (**Figure 6.5**) were used to ensure that cell counts were accurate. The live cell images (**Figure 6.6**) show that even with the significantly larger dilution of the aliquots, bacterial growth on RIF-free scaffolds was visibly greater.

% RIF	16%	9%
K	37.8	53.27
n	0.188	0.104

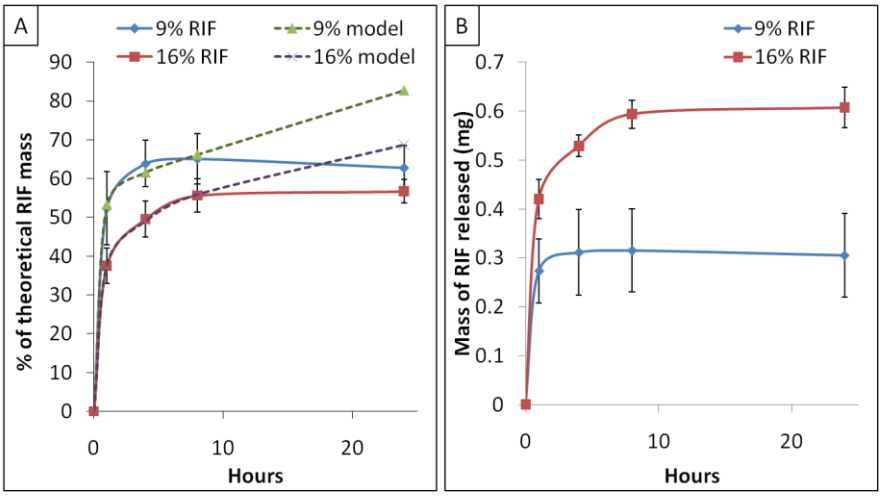

Figure 6.4 - % RIF release for 24 hours with the model parameters, *K* and *n*, for the percent of RIF released from 9% and 16% scaffolds

SE dilutions		*PA* dilutions	
Control	Antibiotic	Control	Antibiotic
10	10	10	10
20	10	20	20
20	20	40	40
20	20	100	40
50	20	200	40
200	20	500	40
500	20	1000	40

Figure 6.5 – Dilutions used for bacterial analysis

The quantification of both bacterial colonies showed strong growth on RIF-free scaffolds, with exponential growth constants (μ) greater than 1 (**Figures 6.7 and 6.8**). For *PA*, the live populations on both RIF scaffolds were nearly constant, with small increases by hour 3 and then decreases back to initial population levels by hour 6. *SE* live cell populations also had only small changes during the 6 hour study. However, 9% and 16% RIF scaffolds caused decreases in their bacterial populations of 70% and 50% respectively.

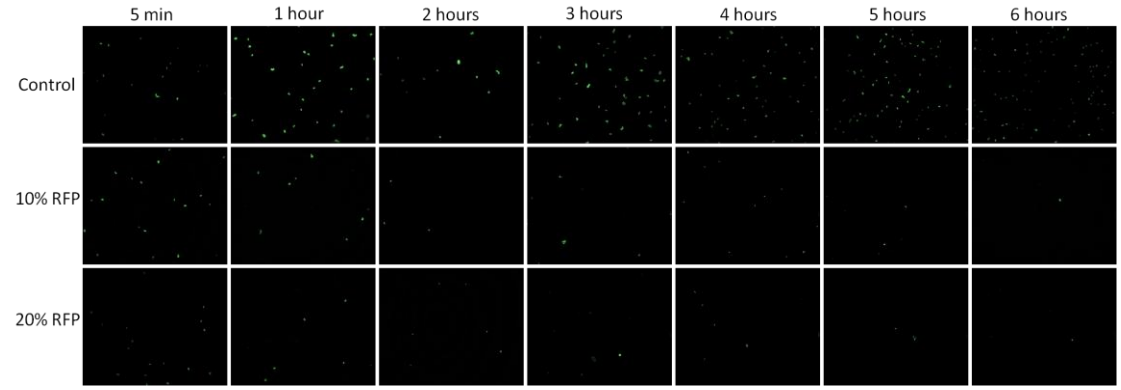

Figure 6.6 – Live bacteria stained by SYTO 9™ at hours 0-6 on RIF-free, 9% RIF, or 16% RIF scaffolds

After 6 hours, scaffolds were removed from the broth and the bacteria were fixed for examination under SEM. The differences observed in population growth were reflected in the SEM images for both *PA* and *SE*. On RIF-free scaffolds, both bacterial strains multiplied prolifically and had populated scaffold surfaces in dense colonies (**Figures 6.9 (A & B) and 6.10 (A & B)**). Differences between the behaviors of the two bacterial strains were also apparent on RIF-free scaffolds, as *SE* laid down extracellular polysaccharide (EPS) in sparingly (**Figure 6.9 (B)**), while *PA* produced abundant EPS and formed biofilms on scaffold surfaces around bacterial colonies (**Figure 6.10 (B)**) and

on the surface. In fact, the EPS produced by *PA* was so thick that it obstructed the view into the interior of the scaffolds over large portions of the surface (**Figure 6.10 (A)**). Both strains also showed up very sparingly on RIF scaffolds. There were no visible differences in bacterial populations between 9% and 16% RIF scaffolds for either bacterial strain. Only an occasional pair of *SE* were observed on either RIF scaffold (**Figures 6.9 (C & D)**) and only one or two bacteria had produced EPS. *PA* also only appeared as an occasional pair on the RIF scaffold surfaces with minimal EPS (**Figures 6.10 (C & D)**). It should be emphasized that for both bacterial strains, the amount of EPS observed was very low.

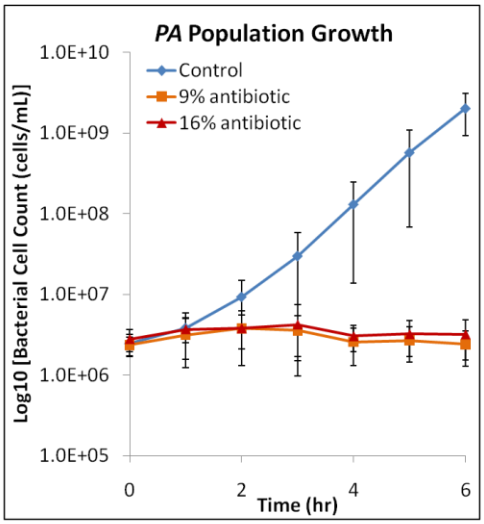

RIF Concentration	0%	9%	16%
Growth Constant	1.34	0.0035	0.023

PA population growth effects

Source	*F-stat*	*p-val*
Hour	58.31	<0.0001
RFP	115.66	<0.0001
Hour*RFP	100.93	<0.0001

Figure 6.7 – Population growth by *pseudomonas aeruginosa*

6.5 DISCUSSION

Nanofiber scaffolds were fabricated to have either 9% or 16% w/w of rifampicin (RIF), an antibiotic with bactericidal action primarily against Gram-positive bacteria [128, 279]. The scaffolds showed morphological differences, and 9% RIF scaffolds had a mean fiber diameter ~150-200 nm smaller than both other scaffolds (**Figure 6.2**). The 9% RIF scaffolds were significantly different from the other two scaffolds, and the differences in fiber diameter distribution were also apparent from the histogram. Further, PCL crystallinity was reduced by adding RIF at both concentrations in a statistically-significant manner (**Figure 6.3**).

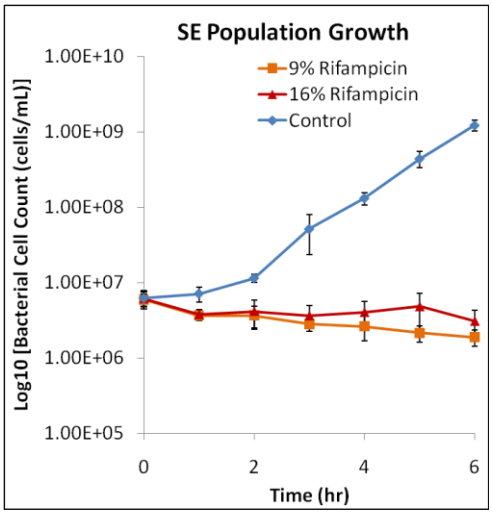

RIF Concentration	0%	9%	16%
Growth Constant	1.17	-0.191	-0.115

SE population growth effects

Source	*F-stat*	*p-val*
Hour	82.06	<0.0001
RFP	269.72	<0.0001
Hour*RFP	160.30	<0.0001

Figure 6.8 – Population growth by *staphylococcus epidermis*

Both of these results are important to keep in mind for PCL-based scaffolds for bone tissue engineering. Architectural considerations affect different cell phenotypes in different manners, and cells with osteoblast and fibroblast phenotypes have demonstrated relative insensitivity to changes in fiber diameters between ~200-800 nm [140] and fiber alignments [280]. Thus, the significant difference in fiber diameter between 9% RIF scaffolds and both other scaffolds is less likely to influence new cell colonization than the release of high local concentrations of RIF. The decrease in crystallinity due to RIF (**Figure 6.3**) may increase the degradation rate because hydrolysis of ester bonds in PCL occurs preferentially in amorphous regions [109, 244]. PCL degradation occurs relatively slowly in the absence of hydrolyzing enzymes [237, 243], and approximating scaffold mass loss with new tissue deposition has been identified as an ideal characteristic of biodegradable scaffolds [281].

The release of RIF from 9% and 16% scaffolds were fit to a diffusion-mediated release model (equation 2) [277]. Multiple iterations of analyses were performed varying *B* between 0% and 50% of the *t=1 hour* release values for either 9% or 16% RIF scaffolds. However, none of the iterations led to a fit of *n* close to 0.45, which is the theoretical value for cylindrical geometries of non-swellable matrices [277]. The exponential variable, *n*, takes the substrate geometry into account and is theoretically

0.45 for cylindrical substrates such as nanofibers. The values calculated by JMP were 0.188 and 0.104 for 16% and 9% RIF scaffolds, respectively. In an attempt to more closely match the theoretical value of 0.45, an offset factor was added into the equation, yielding the form:

$$\frac{M_t}{M_{tot}} = Kt^n + B \quad \text{(Equation 6.4)}$$

This approach did not bring the value of *n* closer to 0.45. In fact, the lowest standard error values for the model were achieved by eliminating this offset factor.

The release profiles for both RIF scaffolds showed a short burst of drug release (**Figure 6.4**), followed by a period of only nominal drug release. This is a common observation in studies of small-molecule release from nano-scale substrates [282]. The model parameters were accurate in fitting a predicted release profile to the initial burst release profile which lasted approximately 8 hours. After that point though, the models for both scaffolds predicted a continued release whereas the measured RIF concentrations indicated that release had ceased. The model for 9% RIF scaffolds would approach an asymptotic value of ~80% release by day 7 while the model for 16% RIF scaffolds would approach 100% release by day 7, which illustrates the differences in models due to changes in the diffusional exponential, *n*. Neither scaffold released 100% of the theoretical RFP mass, which suggests that the encapsulation efficiency for RIF was less than 100%. It should be noted that the % release may also not be 100% of the loaded RIF mass. Therefore, it will be important to measure the encapsulation efficiency and the release efficiency of RIF in the future.

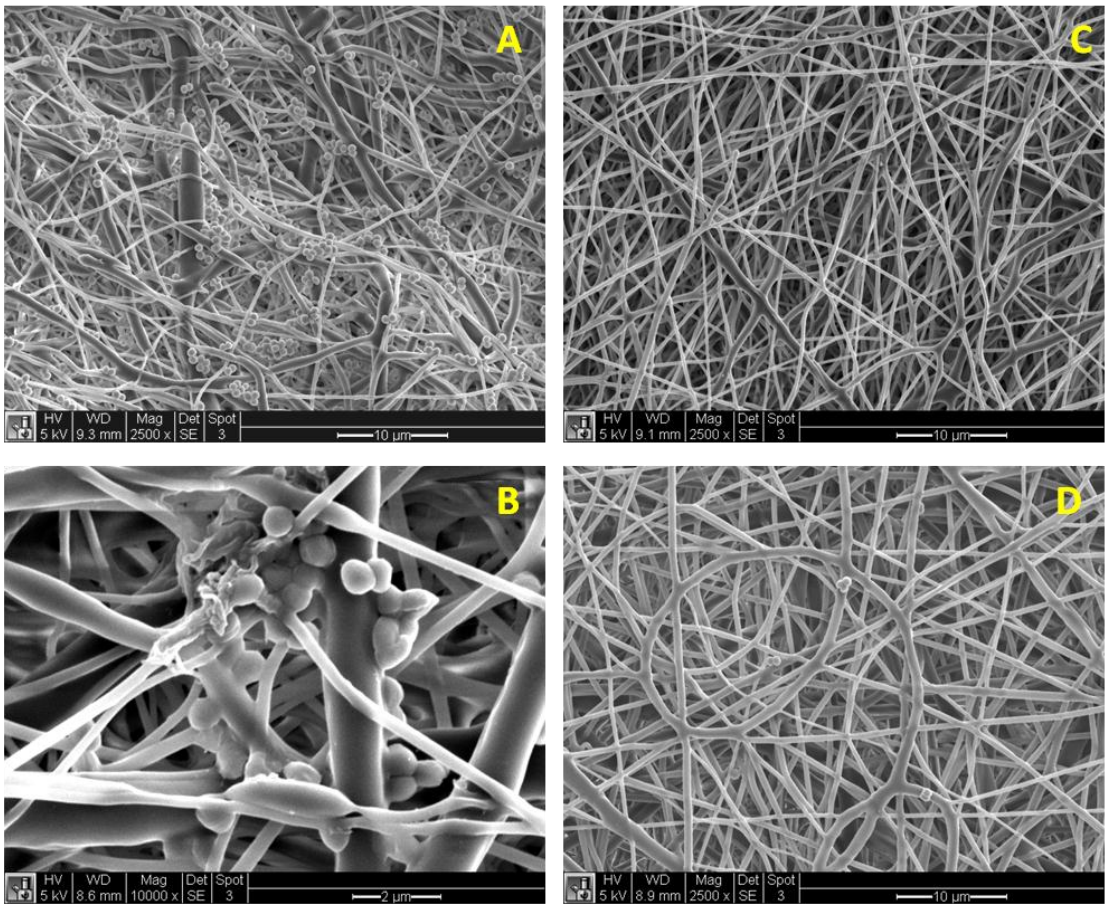

Figure 6.9 – SEM images of *staphylococcus epidermis* on RIF-free (A & B), 9% RIF (C), and 16% RIF (D) scaffolds 6 hours after inoculation. Magnification for A, C, and D is 2500x and scale bar is 10 μm. Magnification for B is 10,000x and scale bar is 2 μm

In order to test the effectiveness of RIF released from nanofibers scaffolds, scaffolds were inoculated with either *staphylococcus epidermis* (*SE*) or *pseudomonas aeruginosa* (*PA*) and the population growth was compared against RIF-free control scaffolds. RIF is viewed with some skepticism clinically because bacteria can develop resistance with a relatively simple mutation in the β subunit of RNA polymerase [129]. Additionally, oral dosage regiments should be increased in frequency because the serum half-life decreases due to increased metabolism rates as liver enzymes are up-regulated in response to the RIF administration. However, RIF is appealing because it can act against bacteria in any state of activity [127].

The results showed a clear inhibition of bacterial population growth through 6 hours in static conditions (**Figures 6.7 and 6.8**). Additionally, SEM images of scaffolds after 6 hours showed that neither *PA* nor *SE* were able to form biofilms on either RIF scaffold, while both strains were able to form biofilms on RIF-free scaffolds (**Figures 6.9 and 6.10**). In particular, *PA* formed thick biofilms on large portions of the scaffold surfaces (**Figure 6.10 (A)**). Interestingly, there did not appear to be any additional benefit with 16% RIF scaffolds over the 9% scaffolds. The static nature of the experimental conditions may explain this observation.

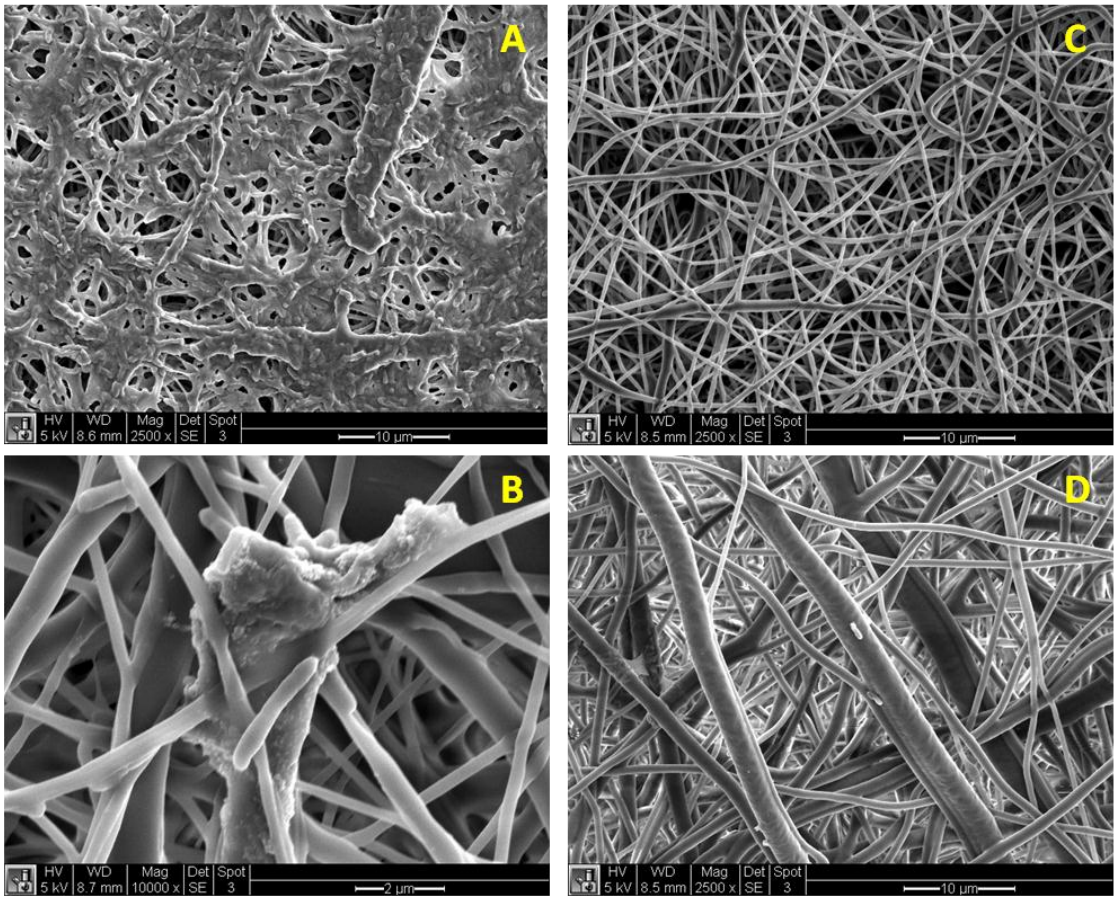

Figure 6.10 – SEM images of *pseudomonas aeruginosa* on RIF-free (A & B), 9% RIF (C), and 16% RIF (D) scaffolds 6 hours after inoculation. Magnification for A, C, and D is 2500x and scale bar is 10 µm. Magnification for B is 10,000x and scale bar is 2 µm

The static conditions permit a cumulative release of RIF without any clearance except for small aliquots removed each hour, but those aliquots represented only a few

percent of the total volume. This is a key detail for interpreting the translation of these scaffolds into clinical settings. The static nature of this *ex vivo* model is appropriate for healing scenarios in which extracellular fluid is cleared slowly. For example, spaces adjacent to cauterized tissues where blood flow is temporarily obstructed would have a slow RIF clearance, and this slow clearance would lead to sustained high RIF concentrations until blood flow was restored. However, highly-dynamic environments such would clear the RIF quickly into the blood stream where it would be metabolized by the liver and gall bladder [283]. Thus, further evaluation in dynamic systems should be pursued to determine the efficacy of scaffolds with 9% or 16% RIF.

6.6 Conclusions

Poly(ε-caprolactone) nanofiber scaffolds were fabricated to include either 9% or 16% w/w rifampicin (RIF), and the RIF release and bactericidal efficacies from the scaffolds were evaluated against RIF-free control scaffolds. There were significant differences between the RIF release profiles, though both scaffolds showed an initial burst release and RIF release did not increase after 8 hours. The concentrations released by both RIF scaffolds into static conditions were sufficient to prevent bacterial colony growth through 6 hours for *PA* and *SE*. Both bacterial strains were able to grow prolifically on RIF-free scaffolds and produce biofilms quickly. These results demonstrate the efficacy of locally-delivered small molecule antibiotics in static conditions, and the same scaffolds will be evaluated in dynamic conditions in the future.

6.7 Future work

There are two areas of RIF release needing attention. First, the measured mass released from both RIF scaffolds was substantially less than 100%, and it is likely that

the encapsulation efficiency is also less than 100%. Thus two separate experiments are currently being prepared in order to measure the encapsulation efficiency. First, thermogravimetric analysis (TGA) can measure the mass of PCL lost, demonstrating the mass or RIF remaining. Colorimetric measurements of re-dissolved scaffolds will provide a second measure of RIF concentration. Similar experiments will be performed for scaffolds after the 7 day release study in order to measure the release efficiency.

Additional experiments examining the efficacy of these RIF scaffolds in dynamic conditions will also be performed. These experiments will be designed to mimic an environment that scaffolds would be exposed to if they were used as a vascular constructs. In that case, a short burst of antibiotics for eight hours may not be sufficient to eliminate robust infections. To address these difficulties, additional antibiotics and release mechanism will be designed into the scaffolds so that release of additional antibiotics can take place following the initial burst of RIF. Finally, the effects of RIF release on primary mammalian cells will also be evaluated. Given the short release profile, the initial 24 hours after seeding is the most important time period to examine.

6.8 References

1. Langer, R. and J.P. Vacanti, *Tissue engineering.* Science, 1993. **260**(5110): p. 920-6.
2. Compston, J.E., *Bone marrow and bone: a functional unit.* J Endocrinol, 2002. **173**(3): p. 387-94.
3. Drosse, I., et al., *Tissue engineering for bone defect healing: an update on a multi-component approach.* Injury, 2008. **39 Suppl 2**: p. S9-20.
4. Soucacos, P.N., E.O. Johnson, and G. Babis, *An update on recent advances in bone regeneration.* Injury, 2008. **39 Suppl 2**: p. S1-4.
5. Mistry, A.S. and A.G. Mikos, *Tissue engineering strategies for bone regeneration.* Adv Biochem Eng Biotechnol, 2005. **94**: p. 1-22.
6. Lewandrowski, K.-U., et al., *Bioresorbable bone graft substitutes of different osteoconductivities: a histologic evaluation of osteointegration of poly(propylene glycol-co-fumaric acid)-based cement implants in rats.* Biomaterials, 2000. **21**(8): p. 757-764.
7. Moreau, M.F., et al., *Gamma irradiation of human bone allografts alters medullary lipids and releases toxic compounds for osteoblast-like cells.* Biomaterials, 2000. **21**(4): p. 369-376.
8. Akkus, O. and C.M. Rimnac, *Fracture resistance of gamma radiation sterilized cortical bone allografts.* Journal of Orthopaedic Research, 2001. **19**(5): p. 927-934.
9. Salgado, A.J., O.P. Coutinho, and R.L. Reis, *Bone tissue engineering: state of the art and future trends.* Macromol Biosci, 2004. **4**(8): p. 743-65.
10. Alves, N.M., et al., *Designing biomaterials based on biomineralization of bone.* Journal of Materials Chemistry, 2010. **20**(15): p. 2911-2921.
11. Jang, J.-H., O. Castano, and H.-W. Kim, *Electrospun materials as potential platforms for bone tissue engineering.* Advanced Drug Delivery Reviews, 2009. **61**(12): p. 1065-1083.
12. Hosseinkhani, H., et al., *Osteogenic differentiation of mesenchymal stem cells in self-assembled peptide-amphiphile nanofibers.* Biomaterials, 2006. **27**(22): p. 4079-4086.
13. Bashur, C.A., L.A. Dahlgren, and A.S. Goldstein, *Effect of fiber diameter and orientation on fibroblast morphology and proliferation on electrospun poly(d,l-lactic-co-glycolic acid) meshes.* Biomaterials, 2006. **27**(33): p. 5681-5688.
14. Hu, J., X. Liu, and P.X. Ma, *Induction of osteoblast differentiation phenotype on poly(l-lactic acid) nanofibrous matrix.* Biomaterials, 2008. **29**(28): p. 3815-3821.
15. Basmanav, F., G.T. Kose, and V. Hasirci, *Sequential growth factor delivery from complexed microspheres for bone tissue engineering.* Biomaterials, 2008. **29**(31): p. 4195-204.
16. Karageorgiou, V., et al., *Porous silk fibroin 3-D scaffolds for delivery of bone morphogenetic protein-2 in vitro and in vivo.* J Biomed Mater Res A, 2006. **78**(2): p. 324-34.
17. Quaglia, F., et al., *Microspheres Made of Poly(ε-caprolactone)-Based Amphiphilic Copolymers: Potential in Sustained Delivery of Proteins.* Macromolecular Bioscience, 2005. **5**(10): p. 945-954.

18. Muller, P., et al., *Calcium phosphate surfaces promote osteogenic differentiation of mesenchymal stem cells.* J Cell Mol Med, 2008. **12**(1): p. 281-91.
19. Kim, I.-Y., et al., *Chitosan and its derivatives for tissue engineering applications.* Biotechnology Advances, 2008. **26**(1): p. 1-21.
20. Shin, M., H. Yoshimoto, and J.P. Vacanti, *In vivo bone tissue engineering using mesenchymal stem cells on a novel electrospun nanofibrous scaffold.* Tissue Eng, 2004. **10**(1-2): p. 33-41.
21. Kurtz, S., et al., *Prevalence of Primary and Revision Total Hip and Knee Arthroplasty in the United States From 1990 Through 2002.* J Bone Joint Surg Am, 2005. **87**(7): p. 1487-1497.
22. Langer, R. and J.P. Vacanti, *Tissue Engineering.* Science, 1993. **260**(5110): p. 920-926.
23. Jeys, L.M., et al., *Endoprosthetic Reconstruction for the Treatment of Musculoskeletal Tumors of the Appendicular Skeleton and Pelvis.* J Bone Joint Surg Am, 2008. **90**(6): p. 1265-1271.
24. Schuckert, K.H., S. Jopp, and S.H. Teoh, *Mandibular Defect Reconstruction Using Three-Dimensional Polycaprolactone Scaffold in Combination with Platelet-Rich Plasma and Recombinant Human Bone Morphogenetic Protein-2: De Novo Synthesis of Bone in a Single Case.* Tissue Eng Part A, 2008.
25. Arthur, A., A. Zannettino, and S. Gronthos, *The therapeutic applications of multipotential mesenchymal/stromal stem cells in skeletal tissue repair.* Journal of Cellular Physiology, 2008. **9999**(9999): p. n/a.
26. Ishaug, S.L., et al., *Bone formation by three-dimensional stromal osteoblast culture in biodegradable polymer scaffolds.* Journal of Biomedical Materials Research Part A, 1997. **36**(1): p. 17-28.
27. Yoshimoto, H., et al., *A biodegradable nanofiber scaffold by electrospinning and its potential for bone tissue engineering.* Biomaterials, 2003. **24**(12): p. 2077-2082.
28. Tiedeman, J.J., et al., *The role of a composite, demineralized bone matrix and bone marrow in the treatment of osseous defects.* Orthopedics, 1995. **8**: p. 1153-1158.
29. Rougraff, B.T. and T.J. Kling, *Treatment of active unicameral bone cysts with percutaneous injection of demineralized bone matrix and autogenous bone marrow.* J Bone Joint Surg Am, 2002. **84-A**(6): p. 921-9.
30. Ban, S., et al., *Effect of electrochemically deposited apatite coating on bonding of bone to the HA-G-Ti composite and titanium.* Journal of Biomedical Materials Research Part A, 1997. **36**(1): p. 9-15.
31. Shin, H., S. Jo, and A.G. Mikos, *Biomimetic materials for tissue engineering.* Biomaterials, 2003. **24**(24): p. 4353-4364.
32. Wutticharoenmongkol, P., P. Pavasant, and P. Supaphol, *Osteoblastic Phenotype Expression of MC3T3-E1 Cultured on Electrospun Polycaprolactone Fiber Mats Filled with Hydroxyapatite Nanoparticles.* Biomacromolecules, 2007. **8**(8): p. 2602-2610.

33. Venugopal, J., et al., *Interaction of Cells and Nanofiber Scaffolds in Tissue Engineering.* Journal of Biomedical Materials Research Part B: Applied Biomaterials, 2008. **84B**(1): p. 34-48.
34. Guarino, V., et al., *Polylactic acid fibre-reinforced polycaprolactone scaffolds for bone tissue engineering.* Biomaterials, 2008. **29**(27): p. 3662-70.
35. Park, S.-H. and *e. al*, *Effect of hydroxyapatite-coated nanofibrous membrane on the responses of human periodontal ligament fibroblast.* Journal of the Ceramic Society of Japan, 2008. **116**(1349): p. 31-35.
36. Ramay, H.R. and M. Zhang, *Biphasic calcium phosphate nanocomposite porous scaffolds for load-bearing bone tissue engineering.* Biomaterials, 2004. **25**(21): p. 5171-80.
37. Zhang, P., et al., *In vivo mineralization and osteogenesis of nanocomposite scaffold of poly(lactide-co-glycolide) and hydroxyapatite surface-grafted with poly(l-lactide).* Biomaterials, 2008.
38. Kim, H.-W., H.-H. Lee, and J.C. Knowles, *Electrospinning biomedical nanocomposite fibers of hydroxyapaite/poly(lactic acid) for bone regeneration.* Journal of Biomedical Materials Research Part A, 2006. **79A**(3): p. 643-649.
39. Liu, F., L. Malaval, and J.E. Aubin, *Global amplification polymerase chain reaction reveals novel transitional stages during osteoprogenitor differentiation.* J Cell Sci, 2003. **116**(Pt 9): p. 1787-96.
40. Sikavitsas, V.I., J.S. Temenoff, and A.G. Mikos, *Biomaterials and bone mechanotransduction.* Biomaterials, 2001. **22**(19): p. 2581-93.
41. Gordon, J.A., et al., *Bone sialoprotein expression enhances osteoblast differentiation and matrix mineralization in vitro.* Bone, 2007. **41**(3): p. 462-73.
42. Baht, G.S., G.K. Hunter, and H.A. Goldberg, *Bone sialoprotein-collagen interaction promotes hydroxyapatite nucleation.* Matrix Biol, 2008. **27**(7): p. 600-8.
43. Nam, J. and *e. al*, *Improved cellular infiltration in electrospun fiber via engineered porosity.* Tissue Engineering, 2007. **13**(9): p. 2249-2257.
44. Lorenzo, J., M. Horowitz, and Y. Choi, *Osteoimmunology: interactions of the bone and immune system.* Endocr Rev, 2008. **29**(4): p. 403-40.
45. Takayanagi, H., *Osteoimmunology: shared mechanisms and crosstalk between the immune and bone systems.* Nat Rev Immunol, 2007. **7**(4): p. 292-304.
46. Ferrari, S.L., et al., *A role for N-cadherin in the development of the differentiated osteoblastic phenotype.* J Bone Miner Res, 2000. **15**(2): p. 198-208.
47. Kii, I., et al., *Cell-cell interaction mediated by cadherin-11 directly regulates the differentiation of mesenchymal cells into the cells of the osteo-lineage and the chondro-lineage.* J Bone Miner Res, 2004. **19**(11): p. 1840-9.
48. Wu, L.N., B.R. Genge, and R.E. Wuthier, *Analysis and molecular modeling of the formation, structure, and activity of the phosphatidylserine-calcium-phosphate complex associated with biomineralization.* J Biol Chem, 2008. **283**(7): p. 3827-38.

49. Genge, B.R., L.N. Wu, and R.E. Wuthier, *In vitro modeling of matrix vesicle nucleation: synergistic stimulation of mineral formation by annexin A5 and phosphatidylserine.* J Biol Chem, 2007. **282**(36): p. 26035-45.
50. Hunter, G.K. and H.A. Goldberg, *Nucleation of hydroxyapatite by bone sialoprotein.* Proc Natl Acad Sci U S A, 1993. **90**(18): p. 8562-5.
51. Taller, A., et al., *Specific adsorption of osteopontin and synthetic polypeptides to calcium oxalate monohydrate crystals.* Biophys J, 2007. **93**(5): p. 1768-77.
52. Chen, M. and *e. al*, *Role of Fiber Diameter in Adhesion and Proliferation of NIH 3T3 Fibroblast on Electrospun Polycaprolactone Scaffolds.* Tissue Engineering, 2007. **13**(3): p. 579-587.
53. Haynesworth, S., et al., *Characterization of cells with osteogenic potential from human marrow.* Bone, 1992. **13**: p. 81-88.
54. Prockop, D., *Marrow stromal cells as stem cells for nonhematopoietic tissues.* Science, 1997. **276**: p. 71-74.
55. Altman, G.H., et al., *Cell differentiation by mechanical stress.* Faseb J, 2002. **16**(2): p. 270-2.
56. Caplan, A., et al., *Mesenchymal stem cells and tissue repair. In: Jackson, D.W., ed. The Anterior Cruciate Ligament: Current and Future Concepts*. 1993, New York: Raven Press.
57. Wall, M.E., S.H. Bernacki, and E.G. Loboa, *Effects of serial passaging on the adipogenic and osteogenic differentiation potential of adipose-derived human mesenchymal stem cells.* Tissue Eng, 2007. **13**(6): p. 1291-8.
58. Beresford, J.N., et al., *Evidence for an inverse relationship between the differentiation of adipocytic and osteogenic cells in rat marrow stromal cell cultures.* J Cell Sci, 1992. **102 (Pt 2)**: p. 341-51.
59. Seshi, B., S. Kumar, and D. Sellers, *Human bone marrow stromal cell: coexpression of markers specific for multiple mesenchymal cell lineages.* Blood Cells Mol Dis, 2000. **26**(3): p. 234-46.
60. Bianco, P. and P. Gehron Robey, *Marrow stromal stem cells.* J Clin Invest, 2000. **105**(12): p. 1663-8.
61. Marletta, G., et al., *Improved osteogenic differentiation of human marrow stromal cells cultured on ion-induced chemically structured poly-[epsilon]-caprolactone.* Biomaterials, 2007. **28**(6): p. 1132-1140.
62. Li, W.-J., et al., *Multilineage differentiation of human mesenchymal stem cells in a three-dimensional nanofibrous scaffold.* Biomaterials, 2005. **26**(25): p. 5158-5166.
63. Holt, S.E., J.W. Shay, and W.E. Wright, *Refining the telomere-telomerase hypothesis of aging and cancer.* Nat Biotechnol, 1996. **14**(7): p. 836-9.
64. Miura, M., et al., *Accumulated chromosomal instability in murine bone marrow mesenchymal stem cells leads to malignant transformation.* Stem Cells, 2006. **24**(4): p. 1095-103.
65. Popat, K.C., et al., *Decreased Staphylococcus epidermis adhesion and increased osteoblast functionality on antibiotic-loaded titania nanotubes.* Biomaterials, 2007. **28**(32): p. 4880-4888.
66. Schwartz, Z. and B. Boyan, *Underlying Mechanisms at the Bone-Biomaterial Interface.* Journal of Cellular Biochemistry, 1994. **56**: p. 340-347.

67. Dee, K.C. and R. Bizios, *Mini Review: Proactive Biomaterials and Bone Tissue Engineering.* Biotechnology and Bioengineering, 1996. **50**: p. 438-442.
68. Engel, E., et al., *Nanotechnology in regenerative medicine: the materials side.* Trends in Biotechnology, 2008. **26**(1): p. 39-47.
69. Murugan, R. and S. Ramakrishna, *Design strategies of tissue engineering scaffolds with controlled fiber orientation.* Tissue Eng, 2007. **13**(8): p. 1845-66.
70. Wainwright, S., et al., *Mechanical Design in Organisms*. 2 ed. 1982: Princeton University Press.
71. Schnell, E., et al., *Guidance of glial cell migration and axonal growth on electrospun nanofibers of poly-ε-caprolactone and a collagen/poly-ε-caprolactone blend.* Biomaterials, 2007. **28**(19): p. 3012-3025.
72. Horii, A., et al., *Biological designer self-assembling Peptide nanofiber scaffolds significantly enhance osteoblast proliferation, differentiation and 3-D migration.* PLoS ONE, 2007. **2**(2): p. e190.
73. Dersch, R., et al., *Electrospinning of Nanofibres: Towards New Techniques, Functions, And Applications.* Australian Journal of Chemistry, 2007. **60**: p. 719-728.
74. Sill, T.J. and H.A. von Recum, *Electrospinning: Applications in drug delivery and tissue engineering.* Biomaterials, 2008. **In Press, Corrected Proof**.
75. Theron, S.A., E. Zussman, and A.L. Yarin, *Experimental investigation of the governing parameters in the electrospinning of polymer solutions.* Polymer, 2004. **45**(6): p. 2017-2030.
76. Moroni, L., et al., *Fiber diameter and texture of electrospun PEOT/PBT scaffolds influence human mesenchymal stem cell proliferation and morphology, and the release of incorporated compounds.* Biomaterials, 2006. **27**(28): p. 4911-4922.
77. Price, R.L., et al., *Selective bone cell adhesion on formulations containing carbon nanofibers.* Biomaterials, 2003. **24**(11): p. 1877-87.
78. Teo, W.E. and S. Ramakrishna, *A review on electrospinning design and nanofibre assemblies.* Nanotechnology, 2006. **17**: p. R89-R106.
79. Kim, G. and W. Kim, *Highly porous 3D nanofiber scaffold using an electrospinning technique.* Journal of Biomedical Materials Research Part B: Applied Biomaterials, 2007. **81B**(1): p. 104-110.
80. Rutledge, G.C. and S.V. Fridrikh, *Formation of fibers by electrospinning.* Advanced Drug Delivery Reviews, 2007. **59**(14): p. 1384-1391.
81. Thomas, V., et al., *Mechano-morphological studies of aligned nanofibrous scaffolds of polycaprolactone fabricated by electrospinning.* Journal of Biomaterials Science -- Polymer Edition, 2006. **17**(9): p. 969-984.
82. Chen, J.-P., G.-Y. Chang, and J.-K. Chen, *Electrospun collagen/chitosan nanofibrous membrane as wound dressing.* Colloids and Surfaces A, 2008. **313-314**: p. 183-188.
83. Zhang, D. and J. Chang, *Patterning of Electrospun Fibers Using Electroconductive Templates.* Advanced Materials, 2007. **19**(21): p. 3664-3667.

84. Ramakrishna, S., et al., *An Introduction to Electrospinning and Nanofibers*. 2005, Singapore: World Scientific Publishing Co. Pte. Ltd. 382.
85. Choi, J.S., et al., *Effect of organosoluble salts on the nanofibrous structure of electrospun poly(3-hydroxybutyrate-co-3-hydroxyvalerate).* International Journal of Biological Macromolecules, 2004. **34**(4): p. 249-256.
86. Bolgen, N., et al., *In vitro and in vivo degradation of non-woven materials made of poly(ε-caprolactone) nanofibers prepared by electrospinning under different conditions.* Journal of Biomaterials Science -- Polymer Edition, 2005. **16**(12): p. 1537-1555.
87. Popat, K.C., et al., *Osteogenic differentiation of marrow stromal cells cultured on nanoporous alumina surfaces.* Journal of Biomedical Materials Research Part A, 2007. **80A**(4): p. 955-964.
88. Sangsanoh, P., et al., *In Vitro Biocompatibility of Schwann Cells on Surfaces of Biocompatible Polymeric Electrospun Fibrous and Solution-Cast Film Scaffolds.* Biomacromolecules, 2007. **8**(5): p. 1587-1594.
89. Corey, J.M. and *e. al*, *Aligned electrospun nanofibers specify the direction of dorsal root ganglia neurite growth.* Journal of Biomedical Materials Research Part A, 2007. **83a**(3): p. 636-645.
90. Chua, K.-N., et al., *Stable immobilization of rat hepatocyte spheroids on galactosylated nanofiber scaffold.* Biomaterials, 2005. **26**(15): p. 2537-2547.
91. Farokhzad, O.C. and R. Langer, *Impact of nanotechnology on drug delivery.* ACS Nano, 2009. **3**(1): p. 16-20.
92. Youan, B.B., *Impact of nanoscience and nanotechnology on controlled drug delivery.* Nanomed, 2008. **3**(4): p. 401-6.
93. Zeng, J., et al., *Biodegradable electrospun fibers for drug delivery.* Journal of Controlled Release, 2003. **92**(3): p. 227-231.
94. Xie, J., R.S. Tan, and C.-H. Wang, *Biodegradable microparticles and fiber fabrics for sustained delivery of cisplatin to treat C6 glioma in vitro.* Journal of Biomedical Materials Research Part A, 2008. **85A**(4): p. 897-908.
95. Fujiyama, J., et al., *Cisplatin incorporated in microspheres: development and fundamental studies for its clinical application.* Journal of Controlled Release, 2003. **89**: p. 397-408.
96. Farokhzad, O.C., J.M. Karp, and R. Langer, *Nanoparticle-aptamer bioconjugates for cancer targeting.* Expert Opin Drug Deliv, 2006. **3**(3): p. 311-24.
97. Sharman, W.M., J.E. van Lier, and C.M. Allen, *Targeted photodynamic therapy via receptor mediated delivery systems.* Adv Drug Deliv Rev, 2004. **56**(1): p. 53-76.
98. Luo, Y. and G.D. Prestwich, *Cancer-targeted polymeric drugs.* Curr Cancer Drug Targets, 2002. **2**(3): p. 209-26.
99. Arifin, D.Y., L.Y. Lee, and C.H. Wang, *Mathematical modeling and simulation of drug release from microspheres: Implications to drug delivery systems.* Adv Drug Deliv Rev, 2006. **58**(12-13): p. 1274-325.
100. Tzafriri, A.R., *Mathematical modeling of diffusion-mediated release from bulk degrading matrices.* J Control Release, 2000. **63**(1-2): p. 69-79.

101. Anderson, D.G., J.A. Burdick, and R. Langer, *Materials science. Smart biomaterials.* Science, 2004. **305**(5692): p. 1923-4.
102. Kopecek, J., *Smart and genetically engineered biomaterials and drug delivery systems.* Eur J Pharm Sci, 2003. **20**(1): p. 1-16.
103. Furth, M.E., A. Atala, and M.E. Van Dyke, *Smart biomaterials design for tissue engineering and regenerative medicine.* Biomaterials, 2007. **28**(34): p. 5068-73.
104. Whang, K., T.K. Goldstick, and K.E. Healy, *A biodegradable polymer scaffold for delivery of osteotropic factors.* Biomaterials, 2000. **21**(24): p. 2545-2551.
105. Ma, P.X., *Biomimetic materials for tissue engineering.* Advanced Drug Delivery Reviews, 2008. **60**(2): p. 184-198.
106. Bolgen, N. and *e. al*, *In vivo performance of antibiotic embedded electrospun PCL membranes for prevention of abdominal adhesions.* Journal of Biomedical Materials Research Part B: Applied Biomaterials, 2007. **81b**(2): p. 530-543.
107. Tauro, J.R. and R.A. Gemeinhart, *Matrix Metalloprotease Triggered Delivery of Cancer Chemotherapeutics from Hydrogel Matrixes.* Bioconjugate Chem., 2005. **16**(5): p. 1133-1139.
108. Sinha, V.R., et al., *Poly-ε-caprolactone microspheres and nanospheres: an overview.* International Journal of Pharmaceutics, 2004. **278**(1): p. 1-23.
109. Pulkkinen, M., et al., *Effects of block length on the enzymatic degradation and erosion of oxazoline linked poly-ε-caprolactone.* European Journal of Pharmaceutical Sciences, 2007. **31**(2): p. 119-128.
110. Kulkarni, A., et al., *Enzymatic Chain Scission Kinetics of Poly(ε-caprolactone) Monolayers.* Langmuir, 2007. **23**(24): p. 12202-12207.
111. von Burkersroda, F., L. Schedl, and A. Gopferich, *Why degradable polymers undergo surface erosion or bulk erosion.* Biomaterials, 2002. **23**(21): p. 4221-31.
112. Biondi, M., et al., *Controlled drug delivery in tissue engineering.* Advanced Drug Delivery Reviews, 2008. **60**(2): p. 229-242.
113. Charlier, A., B. Leclerc, and G. Couarraze, *Release of mifepristone from biodegradable matrices: experimental and theoretical evaluations.* Int J Pharm, 2000. **200**(1): p. 115-20.
114. Berchane, N.S., et al., *Effect of mean diameter and polydispersity of PLG microspheres on drug release: experiment and theory.* Int J Pharm, 2007. **337**(1-2): p. 118-26.
115. Arifin, D.Y., L.Y. Lee, and C.-H. Wang, *Mathematical modeling and simulation of drug release from microspheres: Implications to drug delivery systems.* Advanced Drug Delivery Reviews, 2006. **58**(12-13): p. 1274-1325.
116. Higuchi, T., *Mechanism of Sustained-Action Medication.* Journal of Pharmaceutical Sciences, 1963. **52**(12): p. 1145-1149.
117. Coccoli, V., et al., *Engineering of poly(epsilon-caprolactone) microcarriers to modulate protein encapsulation capability and release kinetic.* J Mater Sci Mater Med, 2008. **19**(4): p. 1703-11.

118. Berkland, C., K. Kim, and D.W. Pack, *PLG microsphere size controls drug release rate through several competing factors.* Pharm Res, 2003. **20**(7): p. 1055-62.
119. Zilberman, M. and J.J. Elsner, *Antibiotic-eluting medical devices for various applications.* J Control Release, 2008. **130**(3): p. 202-15.
120. Coviello, V. and M.R. Stevens, *Contemporary concepts in the treatment of chronic osteomyelitis.* Oral Maxillofac Surg Clin North Am, 2007. **19**(4): p. 523-34, vi.
121. Schmidmaier, G., et al., *Prophylaxis and treatment of implant-related infections by antibiotic-coated implants: a review.* Injury, 2006. **37 Suppl 2**: p. S105-12.
122. Klevens, R.M., et al., *Invasive methicillin-resistant Staphylococcus aureus infections in the United States.* JAMA, 2007. **298**(15): p. 1763-71.
123. Lucke, M., et al., *Systemic versus local application of gentamicin in prophylaxis of implant-related osteomyelitis in a rat model.* Bone, 2005. **36**(5): p. 770-8.
124. Rohrbaugh, T.M., et al., *Absorption of oral aminoglycosides following bone marrow transplantation.* Cancer, 1984. **53**(7): p. 1502-6.
125. Shakil, S., et al., *Aminoglycosides versus bacteria – a description of the action, resistance mechanism, and nosocomial battleground.* J. Biomed. Sci., 2005. **15**: p. 5-14.
126. Saad, E.I., et al., *Role of oxidative stress and nitric oxide in the protective effects of alpha-lipoic acid and aminoguanidine against isoniazid-rifampicin-induced hepatotoxicity in rats.* Food Chem Toxicol, 2010.
127. Frippiat, F., F. Meunier, and G. Derue, *Place of newer quinolones and rifampicin in the treatment of Gram-positive bone and joint infections.* J Antimicrob Chemother, 2004. **54**(6): p. 1158; author reply 1159.
128. Pohlod, D.J., L.D. Saravolatz, and M.M. Somerville, *In-vitro susceptibility of gram-positive cocci to LY146032 teicoplanin, sodium fusidate, vancomycin, and rifampicin.* J Antimicrob Chemother, 1987. **20**(2): p. 197-202.
129. Tupin, A., et al., *Resistance to rifampicin: at the crossroads between ecological, genomic and medical concerns.* Int J Antimicrob Agents, 2010. **35**(6): p. 519-23.
130. Mont, M., B. Waldman, and D.S. Hungerford, *Evaluation of preoperative cultures before second-stage reimplantation of a total knee prosthesis complicated by infection: A comparison-group study.* Journal of Bone and Joint Surgery, 2000. **82**: p. 1552-1557.
131. Smith, A.W., *Biofilms and antibiotic therapy: is there a role for combating bacterial resistance by the use of novel drug delivery systems?* Adv Drug Deliv Rev, 2005. **57**(10): p. 1539-50.
132. Prockop, D.J., *Marrow stromal cells as stem cells for nonhematopoietic tissues.* Science, 1997. **276**(5309): p. 71-4.
133. Young, R.G., et al., *Use of mesenchymal stem cells in a collagen matrix for Achilles tendon repair.* J Orthop Res, 1998. **16**(4): p. 406-13.
134. Bianco, P., et al., *Bone marrow stromal stem cells: nature, biology, and potential applications.* Stem Cells, 2001. **19**(3): p. 180-92.

135. Yoshimoto, H., et al., *A biodegradable nanofiber scaffold by electrospinning and its potential for bone tissue engineering.* Biomaterials, 2003. **24**(12): p. 2077-82.
136. Michalik, L. and W. Wahli, *Peroxisome proliferator-activated receptors: three isotypes for a multitude of functions.* Curr Opin Biotechnol, 1999. **10**(6): p. 564-70.
137. Shin, H., et al., *Modulation of differentiation and mineralization of marrow stromal cells cultured on biomimetic hydrogels modified with Arg-Gly-Asp containing peptides.* J Biomed Mater Res A, 2004. **69**(3): p. 535-43.
138. Bancroft, G.N., et al., *Fluid flow increases mineralized matrix deposition in 3D perfusion culture of marrow stromal osteoblasts in a dose-dependent manner.* Proc Natl Acad Sci U S A, 2002. **99**(20): p. 12600-5.
139. Chen, M., et al., *Role of fiber diameter in adhesion and proliferation of NIH 3T3 fibroblast on electrospun polycaprolactone scaffolds.* Tissue Eng, 2007. **13**(3): p. 579-87.
140. Bashur, C.A., L.A. Dahlgren, and A.S. Goldstein, *Effect of fiber diameter and orientation on fibroblast morphology and proliferation on electrospun poly(D,L-lactic-co-glycolic acid) meshes.* Biomaterials, 2006. **27**(33): p. 5681-8.
141. Bashur, C.A., et al., *Effect of fiber diameter and alignment of electrospun polyurethane meshes on mesenchymal progenitor cells.* Tissue Eng Part A, 2009. **15**(9): p. 2435-45.
142. Jackson, S. and L. Demer, *Peroxisome proliferator-activated receptor activators modulate the osteoblastic maturation of MC3T3-E1 preosteoblasts.* FEBS Lett, 2000. **471**(1): p. 119 - 124.
143. Still, K., et al., *The Peroxisome Proliferator Activator Receptor Alpha/Delta Agonists Linoleic Acid and Bezafibrate Upregulate Osteoblast Differentiation and Induce Periosteal Bone Formation In Vivo.* Calcif Tissue Int, 2008.
144. Kawaguchi, H., et al., *Distinct effects of PPARgamma insufficiency on bone marrow cells, osteoblasts, and osteoclastic cells.* J Bone Miner Metab, 2005. **23**(4): p. 275-9.
145. Lin, T.-H., et al., *PPARγ inhibits osteogenesis via the down-regulation of the expression of COX-2 and iNOS in rats.* Bone, 2007. **41**: p. 562-574.
146. Moerman, E., et al., *Aging activates adipogenic and suppresses osteogenic programs in mesenchymal marrow stroma/stem cells: the role of PPAR-gamma2 transcription factor and TGF-beta/BMP signaling pathways.* Aging Cell, 2004. **3**: p. 379.
147. Brooke, G., et al., *Molecular trafficking mechanisms of multipotent mesenchymal stem cells derived from human bone marrow and placenta.* Stem Cells Dev, 2008. **17**(5): p. 929-40.
148. Ponte, A.L., et al., *The in vitro migration capacity of human bone marrow mesenchymal stem cells: comparison of chemokine and growth factor chemotactic activities.* Stem Cells, 2007. **25**(7): p. 1737-45.
149. Anderson, H.C., et al., *Impaired calcification around matrix vesicles of growth plate and bone in alkaline phosphatase-deficient mice.* Am J Pathol, 2004. **164**(3): p. 841-7.

150. Heinemann, C., et al., *Novel textile chitosan scaffolds promote spreading, proliferation, and differentiation of osteoblasts.* Biomacromolecules, 2008. **9**(10): p. 2913-20.
151. Damsky, C.H., *Extracellular matrix-integrin interactions in osteoblast function and tissue remodeling.* Bone, 1999. **25**(1): p. 95-6.
152. Sodek, J., et al., *Novel functions of the matricellular proteins osteopontin and osteonectin/SPARC.* Connect Tissue Res, 2002. **43**(2-3): p. 308-19.
153. McKee, M.D. and A. Nanci, *Osteopontin: an interfacial extracellular matrix protein in mineralized tissues.* Connect Tissue Res, 1996. **35**(1-4): p. 197-205.
154. Young, M.F., *Bone matrix proteins: their function, regulation, and relationship to osteoporosis.* Osteoporos Int, 2003. **14 Suppl 3**: p. S35-42.
155. Young, M.F., et al., *Structure, expression, and regulation of the major noncollagenous matrix proteins of bone.* Clin Orthop Relat Res, 1992(281): p. 275-94.
156. Robey, P.G., et al., *Structure and molecular regulation of bone matrix proteins.* J Bone Miner Res, 1993. **8 Suppl 2**: p. S483-7.
157. Koh, H.S., et al., *Enhancement of neurite outgrowth using nano-structured scaffolds coupled with laminin.* Biomaterials, 2008. **29**(26): p. 3574-82.
158. Sill, T.J. and H.A. von Recum, *Electrospinning: applications in drug delivery and tissue engineering.* Biomaterials, 2008. **29**(13): p. 1989-2006.
159. Johnson, M.R., et al., *Sustained release of BMP-2 in a lipid-based microtube vehicle.* Acta Biomater, 2009. **5**(1): p. 23-8.
160. Laflamme, C. and M. Rouabhia, *Effect of BMP-2 and BMP-7 homodimers and a mixture of BMP-2/BMP-7 homodimers on osteoblast adhesion and growth following culture on a collagen scaffold.* Biomed Mater, 2008. **3**(1): p. 15008.
161. Laurencin, C.T., et al., *Poly(lactide-co-glycolide)/hydroxyapatite delivery of BMP-2-producing cells: a regional gene therapy approach to bone regeneration.* Biomaterials, 2001. **22**(11): p. 1271-7.
162. Lee, J.Y., et al., *Osteoblastic differentiation of human bone marrow stromal cells in self-assembled BMP-2 receptor-binding peptide-amphiphiles.* Biomaterials, 2009. **30**(21): p. 3532-41.
163. Olivares-Navarrete, R., et al., *Integrin alpha2beta1 plays a critical role in osteoblast response to micron-scale surface structure and surface energy of titanium substrates.* Proc Natl Acad Sci U S A, 2008. **105**(41): p. 15767-72.
164. Marletta, G., et al., *The effect of irradiation modification and RGD sequence adsorption on the response of human osteoblasts to polycaprolactone.* Biomaterials, 2005. **26**(23): p. 4793-804.
165. Palmer, L.C., et al., *Biomimetic systems for hydroxyapatite mineralization inspired by bone and enamel.* Chem Rev, 2008. **108**(11): p. 4754-83.
166. Nikolov, S. and D. Raabe, *Hierarchical modeling of the elastic properties of bone at submicron scales: the role of extrafibrillar mineralization.* Biophys J, 2008. **94**(11): p. 4220-32.

167. Norman, J., et al., *Micromechanical properties of human trabecular bone: a hierarchical investigation using nanoindentation.* J Biomed Mater Res A, 2008. **87**(1): p. 196-202.
168. McCreadie, B.R., et al., *Hierarchical structure of bone and micro-computed tomography.* Adv Exp Med Biol, 2001. **496**: p. 67-83.
169. White, D.J., et al., *The collagen receptor subfamily of the integrins.* Int J Biochem Cell Biol, 2004. **36**(8): p. 1405-10.
170. Denhardt, D.T. and M. Noda, *Osteopontin expression and function: role in bone remodeling.* J Cell Biochem Suppl, 1998. **30-31**: p. 92-102.
171. Kazanecki, C.C., D.J. Uzwiak, and D.T. Denhardt, *Control of osteopontin signaling and function by post-translational phosphorylation and protein folding.* J Cell Biochem, 2007. **102**(4): p. 912-24.
172. Cui, W. and *e. al*, *In situ growth of hydroxyapatite within electrospun poly(DL-lactide) fibers.* Journal of Biomedical Materials Research Part A, 2007. **82A**(4): p. 831-841.
173. Fang, B., et al., *Proliferation and osteoblastic differentiation of human bone marrow stromal cells on hydroxyapatite/bacterial cellulose nanocomposite scaffolds.* Tissue Eng Part A, 2009. **15**(5): p. 1091-8.
174. Guarino, V., et al., *The Influence of Hydroxyapatite Particles on in Vitro Degradation Behaviour of Pcl Based Composite Scaffolds.* Tissue Eng Part A, 2009.
175. Lee, J.H., et al., *Control of osteogenic differentiation and mineralization of human mesenchymal stem cells on composite nanofibers containing poly[lactic-co-(glycolic acid)] and hydroxyapatite.* Macromol Biosci, 2010. **10**(2): p. 173-82.
176. Mei, F., et al., *Improved Biological Characteristics of Poly(L-Lactic Acid) Electrospun Membrane by Incorporation of Multiwalled Carbon Nanotubes/Hydroxyapatite Nanoparticles.* Biomacromolecules, 2007. **8**(12): p. 3729-3735.
177. Xu, H.E., et al., *Molecular recognition of fatty acids by peroxisome proliferator-activated receptors.* Mol Cell, 1999. **3**(3): p. 397-403.
178. Berger, J. and D. Moller, *The mechanisms of action of PPARs.* Annu Rev Med, 2002. **53**: p. 409 - 435.
179. Lecka-Czernik, B. and L.J. Suva, *Resolving the Two "Bony" Faces of PPAR-gamma.* PPAR Res, 2006. **2006**: p. 27489.
180. Syversen, U., et al., *PPAR-Alpha Agonists Increase Bone Mineral Density in Female Rats.* Abstract at ASBMR 25th Annual Meeting, 2003.
181. Ruckh, T.T., et al., *Osteogenic Differentiation of Bone Marrow Stromal Cells on Poly(epsilon-caprolactone) Nanofiber Scaffolds.* Acta Biomater, 2010.
182. Fregel, R., A. Gonzalez, and V.M. Cabrera, *Improved ethanol precipitation of DNA.* Electrophoresis, 2010. **31**(8): p. 1350-2.
183. Khatiwala, C.B., et al., *ECM compliance regulates osteogenesis by influencing MAPK signaling downstream of RhoA and ROCK.* J Bone Miner Res, 2009. **24**(5): p. 886-98.

184. McBeath, R., et al., *Cell shape, cytoskeletal tension, and RhoA regulate stem cell lineage commitment.* Dev Cell, 2004. **6**(4): p. 483-95.
185. Meyers, V.E., et al., *RhoA and cytoskeletal disruption mediate reduced osteoblastogenesis and enhanced adipogenesis of human mesenchymal stem cells in modeled microgravity.* J Bone Miner Res, 2005. **20**(10): p. 1858-66.
186. Salih, E., et al., *Protein kinases of cultured osteoblasts: selectivity for the extracellular matrix proteins of bone and their catalytic competence for osteopontin.* J Bone Miner Res, 1996. **11**(10): p. 1461-73.
187. Katayama, Y., et al., *Casein kinase 2 phosphorylation of recombinant rat osteopontin enhances adhesion of osteoclasts but not osteoblasts.* J Cell Physiol, 1998. **176**(1): p. 179-87.
188. Wang, J., et al., *Expression of bone microsomal casein kinase II, bone sialoprotein, and osteopontin during the repair of calvarial defects.* Bone, 1998. **22**(6): p. 621-8.
189. Bellows, C.G., S.M. Reimers, and J.N. Heersche, *Expression of mRNAs for type-I collagen, bone sialoprotein, osteocalcin, and osteopontin at different stages of osteoblastic differentiation and their regulation by 1,25 dihydroxyvitamin D3.* Cell Tissue Res, 1999. **297**(2): p. 249-59.
190. Gupta, D., et al., *Nanostructured biocomposite substrates by electrospinning and electrospraying for the mineralization of osteoblasts.* Biomaterials, 2009. **30**(11): p. 2085-94.
191. Jackson, S.M. and L.L. Demer, *Peroxisome proliferator-activated receptor activators modulate the osteoblastic maturation of MC3T3-E1 preosteoblasts.* FEBS Lett, 2000. **471**(1): p. 119-24.
192. de Jong, D.S., et al., *Identification of novel regulators associated with early-phase osteoblast differentiation.* J Bone Miner Res, 2004. **19**(6): p. 947-58.
193. Badami, A.S., et al., *Effect of fiber diameter on spreading, proliferation, and differentiation of osteoblastic cells on electrospun poly(lactic acid) substrates.* Biomaterials, 2006. **27**(4): p. 596-606.
194. Tsiridis, E., N. Upadhyay, and P. Giannoudis, *Molecular aspects of fracture healing: which are the important molecules?* Injury, 2007. **38 Suppl 1**: p. S11-25.
195. Chen, L., et al., *Insulin-like growth factor 2 (IGF2) potentiates BMP9-induced osteogenic differentiation and bone formation.* J Bone Miner Res, 2010.
196. Sundelacruz, S. and D.L. Kaplan, *Stem cell- and scaffold-based tissue engineering approaches to osteochondral regenerative medicine.* Semin Cell Dev Biol, 2009. **20**(6): p. 646-55.
197. Ekholm, E.C., et al., *Expression of extracellular matrix genes: transforming growth factor (TGF)-beta1 and ras in tibial fracture healing of lathyritic rats.* Bone, 2000. **27**(4): p. 551-7.
198. Hirakawa, K., et al., *Localization of the mRNA for bone matrix proteins during fracture healing as determined by in situ hybridization.* J Bone Miner Res, 1994. **9**(10): p. 1551-7.

199. Schuckert, K.H., S. Jopp, and S.H. Teoh, *Mandibular defect reconstruction using three-dimensional polycaprolactone scaffold in combination with platelet-rich plasma and recombinant human bone morphogenetic protein-2: de novo synthesis of bone in a single case.* Tissue Eng Part A, 2009. **15**(3): p. 493-9.
200. Thorwarth, M., et al., *Expression of bone matrix proteins during de novo bone formation using a bovine collagen and platelet-rich plasma (prp)--an immunohistochemical analysis.* Biomaterials, 2005. **26**(15): p. 2575-84.
201. Kosaki, N., et al., *Impaired bone fracture healing in matrix metalloproteinase-13 deficient mice.* Biochem Biophys Res Commun, 2007. **354**(4): p. 846-51.
202. Weiss, S., et al., *Systemic regulation of angiogenesis and matrix degradation in bone regeneration--distraction osteogenesis compared to rigid fracture healing.* Bone, 2005. **37**(6): p. 781-90.
203. Henle, P., G. Zimmermann, and S. Weiss, *Matrix metalloproteinases and failed fracture healing.* Bone, 2005. **37**(6): p. 791-8.
204. Coleman, J.E., *Structure and mechanism of alkaline phosphatase.* Annu Rev Biophys Biomol Struct, 1992. **21**: p. 441-83.
205. Orimo, H. and T. Shimada, *The role of tissue-nonspecific alkaline phosphatase in the phosphate-induced activation of alkaline phosphatase and mineralization in SaOS-2 human osteoblast-like cells.* Mol Cell Biochem, 2008. **315**(1-2): p. 51-60.
206. Kulterer, B., et al., *Gene expression profiling of human mesenchymal stem cells derived from bone marrow during expansion and osteoblast differentiation.* BMC Genomics, 2007. **8**: p. 70.
207. Venugopal, J., et al., *Electrospun-modified nanofibrous scaffolds for the mineralization of osteoblast cells.* Journal of Biomedical Materials Research Part A, 2007. **85**(2): p. 408-417.
208. Qin, C., O. Baba, and W.T. Butler, *Post-translational modifications of sibling proteins and their roles in osteogenesis and dentinogenesis.* Crit Rev Oral Biol Med, 2004. **15**(3): p. 126-36.
209. Keykhosravani, M., et al., *Comprehensive identification of post-translational modifications of rat bone osteopontin by mass spectrometry.* Biochemistry, 2005. **44**(18): p. 6990-7003.
210. Yoshida, T., M.F. Clark, and P.H. Stern, *The small GTPase RhoA is crucial for MC3T3-E1 osteoblastic cell survival.* J Cell Biochem, 2009. **106**(5): p. 896-902.
211. Chan, M.C., et al., *A novel regulatory mechanism of the bone morphogenetic protein (BMP) signaling pathway involving the carboxyl-terminal tail domain of BMP type II receptor.* Mol Cell Biol, 2007. **27**(16): p. 5776-89.
212. Zambuzzi, W.F., et al., *On the road to understanding of the osteoblast adhesion: cytoskeleton organization is rearranged by distinct signaling pathways.* J Cell Biochem, 2009. **108**(1): p. 134-44.
213. Fromigue, O., et al., *RhoA GTPase inactivation by statins induces osteosarcoma cell apoptosis by inhibiting p42/p44-MAPKs-Bcl-2 signaling*

independently of BMP-2 and cell differentiation. Cell Death Differ, 2006. **13**(11): p. 1845-56.
214. Oest, M.E., et al., *Quantitative assessment of scaffold and growth factor-mediated repair of critically sized bone defects.* J Orthop Res, 2007. **25**(7): p. 941-50.
215. Hartman, O., et al., *Biofunctionalization of electrospun PCL-based scaffolds with perlecan domain IV peptide to create a 3-D pharmacokinetic cancer model.* Biomaterials, 2010. **31**(21): p. 5700-18.
216. Basmanav, F., G. Kose, and V. Hasirci, *Sequential growth factor delivery from complexed microspheres for bone tissue engineering.* Biomaterials, 2008. **29**: p. 4195.
217. Hamada, K., et al., *Spatial distribution of mineralized bone matrix produced by marrow mesenchymal stem cells in self-assembling peptide hydrogel scaffold.* J Biomed Mater Res A, 2008. **84**(1): p. 128-36.
218. Hosseinkhani, H., et al., *Bone regeneration on a collagen sponge self-assembled peptide-amphiphile nanofiber hybrid scaffold.* Tissue Eng, 2007. **13**(1): p. 11-9.
219. Zhang, F., et al., *Sustained BMP signaling in osteoblasts stimulates bone formation by promoting angiogenesis and osteoblast differentiation.* J Bone Miner Res, 2009. **24**(7): p. 1224-33.
220. Zadravec, D., et al., *Ablation of the very-long-chain fatty acid elongase ELOVL3 in mice leads to constrained lipid storage and resistance to diet-induced obesity.* Faseb J, 2010.
221. Mahe, G., et al., *An unfavorable dietary pattern is associated with symptomatic ischemic stroke and carotid atherosclerosis.* J Vasc Surg, 2010.
222. Smit, L.A., A. Baylin, and H. Campos, *Conjugated linoleic acid in adipose tissue and risk of myocardial infarction.* Am J Clin Nutr, 2010. **92**(1): p. 34-40.
223. MacLean, C.H., et al., *Effects of omega-3 fatty acids on cancer risk: a systematic review.* JAMA, 2006. **295**(4): p. 403-15.
224. Leitzmann, M.F., et al., *Dietary intake of n-3 and n-6 fatty acids and the risk of prostate cancer.* Am J Clin Nutr, 2004. **80**(1): p. 204-16.
225. Holmes, M.D., et al., *Association of dietary intake of fat and fatty acids with risk of breast cancer.* JAMA, 1999. **281**(10): p. 914-20.
226. Willson, T., et al., *The PPARs: From Orphan Receptors to Drug Discovery.* Journal of Medicinal Chemistry, 2000. **43**(4): p. 527-550.
227. Jeninga, E.H., et al., *PPAR{gamma} regulates expression of the anti-lipolytic G-protein-coupled receptor 81 (GPR81/Gpr81).* J Biol Chem, 2009.
228. Kliewer, S., et al., *Peroxisome proliferator-activated receptors: from genes to physiology.* Recent Prog Horm Res, 2001. **56**: p. 239 - 263.
229. Chan, B., et al., *PPAR agonists modulate human osteoclast formation and activity in vitro.* Bone, 2007. **40**(1): p. 149 - 159.
230. Maurin, A.C., et al., *Role of polyunsaturated fatty acids in the inhibitory effect of human adipocytes on osteoblastic proliferation.* Bone, 2002. **31**(1): p. 260-6.

231. Pirih, F.Q., et al., *Nuclear receptor profile in calvarial bone cells undergoing osteogenic versus adipogenic differentiation.* Journal of Cellular Biochemistry, 2008. **105**(5): p. 1316-1326.
232. Grey, A., et al., *The peroxisome proliferator-activated receptor-gamma agonist rosiglitazone decreases bone formation and bone mineral density in healthy postmenopausal women: a randomized, controlled trial.* J Clin Endocrinol Metab, 2007. **92**(4): p. 1305 - 1310.
233. Lemberger, T., et al., *PPAR tissue distribution and interactions with other hormone-signaling pathways.* Ann N Y Acad Sci, 1996. **804**: p. 231 - 251.
234. Dang, Z. and C.W. Lowik, *The balance between concurrent activation of ERs and PPARs determines daidzein-induced osteogenesis and adipogenesis.* J Bone Miner Res, 2004. **19**(5): p. 853-61.
235. Takada, I. and S. Kato, *[Molecular mechanism of switching adipocyte / osteoblast differentiation through regulation of PPAR-gamma function.].* Clin Calcium, 2008. **18**(5): p. 656-61.
236. Takada, I., et al., *Suppression of PPAR transactivation switches cell fate of bone marrow stem cells from adipocytes into osteoblasts.* Ann N Y Acad Sci, 2007. **1116**: p. 182-95.
237. Hoshino, A. and Y. Isono, *Degradation of aliphatic polyester films by commercially available lipases with special reference to rapid and complete degradation of poly(L-lactide) film by lipase PL derived from Alcaligenes sp.* Biodegradation, 2002. **13**(2): p. 141-7.
238. Gerardo-Nava, J., et al., *Human neural cell interactions with orientated electrospun nanofibers in vitro.* Nanomedicine (Lond), 2009. **4**(1): p. 11-30.
239. Kumbar, S.G., et al., *Electrospun poly(lactic acid-co-glycolic acid) scaffolds for skin tissue engineering.* Biomaterials, 2008. **29**(30): p. 4100-7.
240. Nam, J., et al., *Novel electrospun scaffolds for the molecular analysis of chondrocytes under dynamic compression.* Tissue Eng Part A, 2009. **15**(3): p. 513-23.
241. Grasl, C., et al., *Electrospun polyurethane vascular grafts: In vitro mechanical behavior and endothelial adhesion molecule expression.* J Biomed Mater Res A, 2010. **93**(2): p. 716-23.
242. Persenaire, O., et al., *Mechanisms and kinetics of thermal degradation of poly(epsilon-caprolactone).* Biomacromolecules, 2001. **2**(1): p. 288-94.
243. Zeng, J., et al., *Enzymatic degradation of poly(L-lactide) and poly(epsilon-caprolactone) electrospun fibers.* Macromol Biosci, 2004. **4**(12): p. 1118-25.
244. Pitt, C., et al., *Aliphatic polyesters II. The degradation of poly (DL-lactide), poly (epsilon-caprolactone), and their copolymers in vivo.* Biomaterials, 1981. **2**(4): p. 215-220.
245. Prakash, A., et al., *Bilayers as phase transfer agents for nanocrystals prepared in nonpolar solvents.* ACS Nano, 2009. **3**(8): p. 2139-46.
246. Wang, H.B., et al., *Focal adhesion kinase is involved in mechanosensing during fibroblast migration.* Proc Natl Acad Sci U S A, 2001. **98**(20): p. 11295-300.
247. Chen, C.S., et al., *Geometric control of cell life and death.* Science, 1997. **276**(5317): p. 1425-8.

248. Xie, J. and C.-H. Wang, *Electrospun Micro- and Nanofibers for Sustained Delivery of Paclitaxel to Treat C6 Glioma in Vitro.* Pharmaceutical Research, 2003. **23**(8): p. 1817-1826.
249. Musacchio, E., et al., *Effects of unsaturated free fatty acids on adhesion and gene expression of extracellular matrix macromolecules in human osteoblast-like cultures.* Connective Tissue Research, 2007. **48**: p. 34-38.
250. Berger, J. and D. Moller, *The Mechanisms of Action of PPARs.* Annual Review of Medicine, 2002. **53**: p. 409-435.
251. Beertsen, W. and T. van den Bos, *Alkaline phosphatase induces the mineralization of sheets of collagen implanted subcutaneously in the rat.* J Clin Invest, 1992. **89**(6): p. 1974-80.
252. Gundberg, C.M., *Matrix proteins.* Osteoporos Int, 2003. **14 Suppl 5**: p. S37-40; discussion S40-2.
253. Hasegawa, T., et al., *The PPARgamma-selective ligand BRL-49653 differentially regulates the fate choices of rat calvaria versus rat bone marrow stromal cell populations.* BMC Dev Biol, 2008. **8**: p. 71.
254. Valmeseda, A., et al., *Opposite regulation of PPAR-a and -g gene expression by both their ligands and retinoic acid in brown adipocytes.* Mol Cell Endocrinol, 1999. **154**: p. 101-109.
255. Kliewer, S.A., et al., *Fatty acids and eicosanoids regulate gene expression through direct interactions with peroxisome proliferator-activated receptors α and γ.* Proceedings of the National Academy of Sciences of the United States of America, 1997. **94**(9): p. 4318-4323.
256. Syversen, U., et al., *Different skeletal effects of the peroxisome proliferator activated receptor (PPAR)alpha agonist fenofibrate and the PPARgamma agonist pioglitazone.* BMC Endocrine Disorders, 2009. **9**(1): p. 10.
257. Wang, X., H. Zhao, and R. Andersson, *Proteomics and leukocytes: an approach to understanding potential molecular mechanisms of inflammatory responses.* J Proteome Res, 2004. **3**(5): p. 921-9.
258. Tachimoto, H., M. Ebisawa, and B.S. Bochner, *Cross-talk between integrins and chemokines that influences eosinophil adhesion and migration.* Int Arch Allergy Immunol, 2002. **128 Suppl 1**: p. 18-20.
259. Komatsu, D.E. and S.J. Warden, *The control of fracture healing and its therapeutic targeting: Improving upon nature.* Journal of Cellular Biochemistry, 2010. **109**(2): p. 302-311.
260. Robling, A.G., A.B. Castillo, and C.H. Turner, *Biomechanical and molecular regulation of bone remodeling.* Annu Rev Biomed Eng, 2006. **8**: p. 455-98.
261. Kim, H.J., et al., *Dexamethsone suppresses bone formation via the osteoclast.* Adv Exp Med Biol, 2007. **602**: p. 43-6.
262. Kondo, T., et al., *Dexamethasone promotes osteoclastogenesis by inhibiting osteoprotegerin through multiple levels.* J Cell Biochem, 2008. **103**(1): p. 335-45.
263. Karsenty, G., H.M. Kronenberg, and C. Settembre, *Genetic Control of Bone Formation.* Annu Rev Cell Dev Biol, 2009. **25**: p. 629-648.

264. Liu, C.H., et al., *Noninvasive delivery of gene targeting probes to live brains for transcription MRI.* Faseb J, 2008. **22**(4): p. 1193-203.
265. Liu, P.K., et al., *Transcription MRI: a new view of the living brain.* Neuroscientist, 2008. **14**(5): p. 503-20.
266. Bozic, K.J. and M.D. Ries, *The impact of infection after total hip arthroplasty on hospital and surgeon resource utilization.* J Bone Joint Surg Am, 2005. **87**(8): p. 1746-51.
267. Shi, Z., et al., *Antibacterial and mechanical properties of bone cement impregnated with chitosan nanoparticles.* Biomaterials, 2006. **27**(11): p. 2440-9.
268. Nablo, B.J., et al., *Inhibition of implant-associated infections via nitric oxide release.* Biomaterials, 2005. **26**(34): p. 6984-90.
269. Choi, J.S., K.W. Leong, and H.S. Yoo, *In vivo wound healing of diabetic ulcers using electrospun nanofibers immobilized with human epidermal growth factor (EGF).* Biomaterials, 2008. **29**(5): p. 587-96.
270. Schneider, A., et al., *Biofunctionalized electrospun silk mats as a topical bioactive dressing for accelerated wound healing.* Acta Biomater, 2009. **5**(7): p. 2570-8.
271. Kim, K., et al., *Incorporation and controlled release of a hydrophilic antibiotic using poly(lactide-co-glycolide)-based electrospun nanofibrous scaffolds.* J Control Release, 2004. **98**(1): p. 47-56.
272. Lee, J.H., et al., *Microfluidic Approach to Create 3D Tissue Models for Biofilm-Related Infection of Orthopaedic Implants.* Tissue Eng Part C Methods, 2010.
273. Campoccia, D., L. Montanaro, and C.R. Arciola, *The significance of infection related to orthopedic devices and issues of antibiotic resistance.* Biomaterials, 2006. **27**(11): p. 2331-9.
274. Harris, L.G. and R.G. Richards, *Staphylococci and implant surfaces: a review.* Injury, 2006. **37 Suppl 2**: p. S3-14.
275. Gillespie, W.J. and G.H. Walenkamp, *Antibiotic prophylaxis for surgery for proximal femoral and other closed long bone fractures.* Cochrane Database Syst Rev, 2010. **3**: p. CD000244.
276. Chu, V.H., et al., *Staphylococcus aureus bacteremia in patients with prosthetic devices: costs and outcomes.* Am J Med, 2005. **118**(12): p. 1416.
277. Ritger, P. and N.A. Peppas, *A simple equation for description of solute release I. Fickian and non-Fickian release from non-swellable devices in the form of slabs, spheres, and cylinders or discs.* Journal of Controlled Release, 1987. **5**: p. 23-36.
278. Sinclair, G. and N. Peppas, *Analysis of non-Fickian transport in polymers using simplified exponential expressions.* Journal of Membrane Science, 1984. **17**: p. 329-331.
279. Lavicky, J., et al., *The effects of peptidoglycan, a pyrogenic constituent of gram-positive microorganisms, on the pharmacokinetics of rifampicin.* Toxicon, 1988. **26**(3): p. 293-300.

280. Ma, J., X. He, and E. Jabbari, *Osteogenic Differentiation of Marrow Stromal Cells on Random and Aligned Electrospun Poly(L: -lactide) Nanofibers.* Ann Biomed Eng, 2010.
281. Ishaug, S.L., et al., *Bone formation by three-dimensional stromal osteoblast culture in biodegradable polymer scaffolds.* J Biomed Mater Res, 1997. **36**(1): p. 17-28.
282. Venugopal, J., et al., *Continuous nanostructures for the controlled release of drugs.* Curr Pharm Des, 2009. **15**(15): p. 1799-808.
283. Liu, L., et al., *Radiosynthesis and bioimaging of the tuberculosis chemotherapeutics isoniazid, rifampicin and pyrazinamide in baboons.* J Med Chem, 2010. **53**(7): p. 2882-91.

Chapter 7

7.1 Conclusions

This work aimed to develop poly(ε-caprolactone) nanofiber scaffolds with osteogenic design factors incorporated into the fibers, and also for localized antibiotic delivery. The two design factors, oleic acid (OLA) and hydroxyapatite (HAp), represented soluble and insoluble signals, respectively, which elicited differential responses from marrow stromal cells (MSCs). *In vitro*, OLA appeared to inhibit cell spreading and metabolic activity in maintenance conditions while it increased osteogenic phenotypic behaviors. Additionally, OLA differentially affected the expression of two peroxisome proliferator-activator receptors (PPARs) which have been associated with osteoblastogenesis. HAp also differentially affected osteoblast behaviors, but in a less-clear manner. Although alkaline phosphatase was slightly increased, two other key genes, osteopontin and type I collagen, were down-regulated *in vitro*. However, *in vivo* HAp incorporation into PCL nanofiber scaffolds proved to be a strong enhancer of bone formation in calvarial defects, while OLA showed some positive synergy with HAp as an osteogenic factor. Finally, the release of a small-molecule antibiotic, rifampicin (RIF) was effective against both Gram-positive and Gram-negative bacterial strains separately and in static culture conditions. The release profiles for RIF-eluting scaffolds showed a fast burst release of RIF with a cessation by 24 hours. This burst effect provides a strong motivation for materials engineering by incorporating additional antibiotics with slower release mechanisms.

Future work will be focused on profiling the release of OLA from nanofibers scaffolds, understanding the manner with which cells interpret mineralization in their extracellular environment, and further developing and evaluating antibiotic delivery from these nanofiber scaffolds.